Theses & Dissertations   Graduate Studies

Winter 12-20-2019

Synthesis and Characterization of Long Acting Darunavir Prodrugs

Mary Banoub

Synthesis and Characterization of Long Acting Darunavir Prodrugs

By

Mary Girgis Banoub

A Dissertation

Presented to the Faculty of the
University of Nebraska Graduate College
in Partial Fulfillment of the Requirements for the
Degree of Doctor of Philosophy

Pharmacology and Experimental Neuroscience
Graduate Program

Under the Supervision of Doctor Howard E. Gendelman

University of Nebraska Medical Center
Omaha, Nebraska

August, 2019

Supervisory Committee:

Benson Edagwa, Ph.D.   Larisa Poluektova, Ph.D.

JoEllyn McMillan, Ph.D.   Jered C. Garrison, Ph.D.

R. Lee Mosley, Ph.D.

Synthesis and Characterization of Long-Acting Darunavir Prodrugs

Mary G. Banoub, Ph.D.

University of Nebraska Medical Center, 2019

Supervisor: Howard E. Gendelman, M.D.

Patient adherence is critical for ART success to ensure adequate viral suppression, therefore, long-acting antiretrovirals are soon replacing current daily regimens. In recent years, two drugs were successfully transformed into long-acting injectables; CAB LA and RPV LA. These long-acting nanoformulations made it possible to abandon the daily pill burden, instead approximately a bimonthly injection of both drugs is enough to suppress and maintain viral load suppression. Our laboratory has been instrumental in transforming FDA-approved and experimental-HIV medications into long-acting slow effective release drugs, also known as LASER ART. LASER ART consists of slow drug metabolism and high permeability and retention inside cellular reservoirs eventually increasing the apparent life of the drugs. In this work, we apply LASER strategies to darunavir, a protease inhibitor (PI). DRV is a preferred PI due to its potency against wild type HIV as well as many mutant resistant viral strains. Among other drugs from its class, DRV is considered to have the highest genetic barrier to HIV mutations. To transform DRV into a LASER DRV, we chemically modified DRV to a prodrug, an inactive form of the drug, by conjugation of different lengths of fatty acids/lipids; M1DRV and M2DRV. These prodrugs were encased in amphiphilic polymer, NM1DRV and NM2DRV, to increase nanoparticles stability and permeability across cell membranes. The prodrug nanoformulations improved uptake, retention, release and antiretroviral

activities in macrophages and T cells. Pharmacokinetics studies in mice affirmed the advantage of the modifications in extending the apparent half life of DRV in animal models. Long-acting DRV offers the option of a long-acting PI that does not require a booster to maintain high concentrations in plasma, blood, and tissues. Therefore, DRV prodrugs nanoformulations can eliminate heavy pill burden and reduce drug-drug interactions that are prominent with PI boosters such as ritonavir and cobicistat.

Acknowledgments

First I sincerely thank my supervisor and mentor, Dr. Howard E. Gendelman. Thank you for being so very patient with me and for always making the time to meet with me to discuss my projects and progress. I learned so much from you as a leader, scientist and an individual. Thank you for your encouragements and the immense support you gave me. Also, I'm beyond grateful for you being extremely understanding as my personal life was unfolding from death in the family to my wedding right around my comprehensive exam. You were absolutely supportive and understanding and I truly feel blessed and honored to have been a part of Dr. Gendelman's team. You are an exceptional supervisor and a fatherly figure for me in Omaha.

I also would like to thank Dr. Benson Edagwa, who has been an amazing teacher for me throughout my education here in Omaha. Thank you for your patience and generosity with your time to teach me so much about chemistry and all the different prodrug syntheses. I'm exceedingly grateful for your mentorship and friendship. I would like to also thank Dr. JoEllyn McMillan for all her valuable advices and help with my project, my animal experiment designs and mass spectrometry analyses. And on top of that, thank you for making everything runs smoothly in lab and taking care of any issues us students may have. I would like to thank the rest of my exceptional committee members; Drs. Larisa Poluektova, Lee Mosley, and Jered Garrison for all your advices and feedback for my project. I'm truly appreciative of you keeping me on track and focused throughout my education here. You are very generous with your time, valuable advices and even resources and I'm sincerely grateful for your constructive feedbacks, directions and continual support.

I thank my coworkers for being an amazing lab family. When I first came to Omaha, I did not know anyone but you all provided a second home for me in lab. I truly enjoyed

working with you and knowing you. My life here in Omaha was not just about work and school but also friendships and even mentorships. Thank you for being so patient with me on my bad days, for your encouragements and for your enormous help as I began to work on my projects and had countless questions. I especially would like to thank Drs. Aditya Bade, Nagsen Gautam, Prasanta Dash, Zhiyi Lin along with Bhagya Laxmi Dyavar Shetty, Melinda Wojtkiewicz, Hang Su, Denise Cobb, Ted Kocher, Diana Palandri for their help with my animal experiments and mass spectrometry samples' processing, methods and analysis. I also would like to thank the rest of my phenomenal lab family from current, past members and summer students; Drs. Bhavesh Kevediya, Tian Zhou, Dongwei Guo, Nathan Smith, Brady Sillman, James Hilaire, Christopher Woldstad, Dhirender Singh along with Tanmay Kulkarni, Dhruvkumar Soni, Brendan Otteman, Insiya Mukadam, Yoni Herskovitz, Mahmudul Hasan, Marwa Mohamed, Leticia Montgomery, Andrew Nguyen, Daniel Stein, and Evan. Thank you all for your help, advices, snacks, laughter and friendship. I am blessed to have joined a lab where I can meet so many hard working scientists like you with high ethics and integrity. I learned so much from you and I wholeheartedly wish you all the best.

I also would like to thank the administrative office at the PEN department especially Reed Felderman, Lana Reichardt, Theresa Grutel and Robin Taylor. You make our lives, as students, a ton easier with your support, assistance and even reminders. I am thankful for everything you have done and still do.

I would like to acknowledge my church family in Omaha for being loving and inclusive as soon as they learned of my presence in Omaha. I'm beyond thankful for every one of you, especially Father Rofael's family, who had helped me so much with many car rides after my car accident in the first month I moved here. I am grateful for each one of you who were there for me when you had your own things going on; you were so selfless and giving and I honestly learned true service from you all.

I would like to thank my loving family. I am beyond blessed to have an amazing, supportive and God loving family. I thank my dad, Dr. Girgis Banoub for all his continual love, support and friendship. I wish I took after him more when it came to resilience and hard work - you don't quit and don't know the meaning of defeat. Thank you and mom for all your sacrifices for our family especially how much you sacrificed for my brothers and I to come to the United States. I look up to you and pray for you everyday. I thank my awesome momma, Manal Banoub. Thank you for all your love and support and above all thank you for all your prayers. I am forever grateful for you and can't wait until you give your future grandkids the love and support you showed my brothers and me. I also would like to thank my two amazing and kind-hearted brothers; Kerolus and Mina Banoub for their love and true friendship. Also, my cousins Marmar Ishak, Verna Mikhail and Lorraine Fam, my sister-in-law Anna Banoub and my auntie Nousa Gadallah for all the trouble they went through and their selfless love and support in planning my wedding in NJ during a time when I was busiest in UNMC.

Lastly but certainly not least, I want to thank my husband, Michael Baskharon. Thank you for being my amazing second half and best friend. I am so grateful to have met someone so pure, awesome and God loving like you. Thank you for being so generous and committed to our marriage even with the long distance. I appreciate you taking so many days off of work to come and check on me when I wasn't able to travel. Thank you for everything. You are simply amazing and I thank God everyday for you.

Mary Banoub

Table of Contents

Table of Figures

List of Abbreviations

^{13}C-NMR	Carbon nuclear magnetic resonance
^{1}H-NMR	Proton nuclear magnetic resonance
3TC	(−)-L-2′,3′-dideoxy-3′-thiacytidine; lamivudine
ABC	Abacavir
ACN	Acetonitrile
ADME	Absorption distribution metabolism excretion
AIDS	Acquired immunodeficiency syndrome
ART	Antiretroviral therapy
AZT	Azidothymidine
CAB	Cabotegravir
cART	Combination antiretroviral therapy
CCK-8	Cell counting kit-8
DAB	3,3'-diaminobenzidine
DCM	Dichloromethane
DEA	Diethylamine
DLS	Dynamic light scattering
DMEM	Dulbecco's modified eagle medium
DMF	Dimethylformamide
DMSO	Dimethyl sulfoxide
DRV	Darunavir
DRV/r	Ritonavir-boosted darunavir
DTG	Dolutegravir
EC_{50}	Half maximal effective concentration
ESI-MS	Electrospray ionization mass spectrometry

Et$_3$N	Triethylamine
Et$_3$SiH	Triethylsilane
FA	Folic acid
FDA	Food and Drug Administration
FTC	2',3'-dideoxy-5-fluoro-3'-thiacytidine; emtricitabine
FTIR	Fourier-transform infrared
HCl	Hydrochloric acid
HIV-1	Human immunodeficiency virus 1
HPLC	High performance liquid chromatography
HSC	Hematopoietic stem cell
IM	intramuscular
IP	intraperitoneal
IS	internal standard
KS	Kaposi's sarcoma
LA	Long-acting
LASER ART	Long-acting slow effective release antiretroviral therapy
LPV	Lopinavir
LPV/r	Ritonavir-boosted lopinavir
MABC	Myristoylated abacavir
MCSF	Macrophage colony stimulating factor
MDM	Monocyte-derived macrophages
MeOH	Methanol
MOI	Multiplicity of infection
MTT	3-(4,5-dimethylthiazol-2-yl)-2,5-diphenyltetrazolium bromide
NaOH	Sodium hydroxide
NMABC	Nanoformulated MABC

NNRTI	Non-nucleoside reverse transcriptase inhibitor
NRTI	Nucleoside reverse transcriptase inhibitor
NSG	NOD/SCID/IL2Rγc$^{-/-}$
P407	Poloxamer 407
PBS	Phosphate buffered saline
PCR	Polymerase chain reaction
PD	Pharmacodynamics
PDI	Polydispersity index
PEG	Polyethylene glycol
PFA	paraformaldehyde
PI	Protease inhibitor
PK	Pharmacokinetics
PrEP	Pre-exposure prophylaxis
RPV	Rilpivirine
RT	Reverse transcriptase
RTV	Ritonavir
SEM	Scanning electron microscopy
SEM	Standard error of the mean
TDF	Tenofovir disoproxil
TEM	Transmission electron microscopy
THF	Tetrahydrofuran
TMSCl	Trimethylsilyl chloride
UPLC-MS/MS	Ultraperformance liquid chromatography tandem mass spectrometry
UV/Vis	dual-wavelength ultraviolet/visible light detection
XRD	X-ray diffraction

Chapter 1: Overview

Introduction

Human immunodeficiency virus type one (HIV-1) causes a chronic incurable infection. If not treated, viral replication progresses to the acquired immune deficiency syndrome (AIDS) where the patient commonly develops a plethora of coinfections that when left untreated lead to death[1]. Clinical cases of AIDS were documented as early as 1981[2]. Early in the epidemic, AIDS principally affected previously healthy homosexual men[2]. These cases revealed that virus progression was characterized by many opportunistic infections such as *Pneumocystis carinii* pneumonia*, Mycobacterium avium*, herpes simplex virus, mucosal candidiasis cryptosporidiosis, Kaposi's sarcoma (KS), and many types of lymphomas[2]. The already known KS was a malignant and slow-growing tumor in the lower extremities[2]. However, AIDS-related KS was found in 20 cases where the Kaposi's skin lesions were multifocal and disseminated to various body parts including the lymph nodes and visceral organs[2]. Thus, upon initial discovery, infections signaled a definite death sentence with no available treatment[2]. However, with the development of antiretroviral therapy (ART), the disease was controlled and treatment confers a good prognosis[3]. Indeed, patients are now able to lead healthy normal lives with reasonably normal lifespans conditioned by strict adherence to ART medications[4]. As of 2016, 36.7 million people are infected with HIV worldwide[5]. HIV infection is transmitted through unsafe/unprotected sex, use and sharing of needles for drugs, blood transfusions, and men who have sex with men[6]. In 1985, HIV was molecularly cloned and sequenced leading to the development of diagnostic tests and later determinations of viral load and antiretroviral drug (ARV) resistance tests[6]. Each and all were used to measure infection and monitor patients' response to medications[6].

Symptoms of a primary HIV infection may start within 4-10 weeks post infection and resemble normal flu symptoms; fever, joint pain, sore throat and swollen lymph nodes in addition to skin rashes[5]. Once infection progresses, additional symptoms develop which can continue for years and include fever and fatigue, diarrhea, weight loss, oral thrush, shingles, and persistent generalized lymphadenopathy[5]. Lymph node biopsies taken from HIV-1 infected patients show florid follicular hyperplasia, mixed follicular hyperplasia, follicular involution, or lymphocyte depletion patterns[5]. Co-infections contribute dramatically to the morbidity and fatality of HIV – common co-infections include but are not limited to tuberculosis, cryptococcosis, hepatitis B virus, hepatitis C virus, and malaria[1]. Several serological tests that include ELISA with confirmatory Western blots can confirm infection[7]. However, polymerase-chain-reaction (PCR) have emerged as a sensitive and specific test for HIV-1 diagnosis and confirmatory tests[5]. PCR can also determine the viral load and be used to monitor the efficacy of therapeutic regimens[5, 8]. HIV exhibits latency within the host genome shielding the virus from recognition and clearance by the immune system[9]. These viral reservoirs represent the main obstacle for curing HIV completely. The virus can be suppressed by ART, however no available treatment to eradicate the virus has been realized, except by transplantation of stem cells with a mutant *CCR5* gene as in the case for the Berlin patient[10]. In this overview we briefly examine HIV-1 viral life cycle, available antiretroviral treatments and its limitations that eventually led to the development of long-acting (LA) ART strategies.

Structure of HIV-1

HIV-1 was first isolated in 1983 starting a journey of intensive research on the virus infection and treatment to this current day[6]. The virus belongs to the Retroviridae family and Lentivirus genus. It is an enveloped retrovirus containing 2 copies of positive

sense single-stranded RNA. There are two types of HIV; HIV-1 and HIV-2. The two subtypes are similar in structure however differ in their origin, prevalence, infectivity, and virulence. HIV-1 is more virulent and higher in infectivity than HIV-2 and frequently causes more disease of the CNS as well as more spread throughout the world[11]. HIV-1 originated from chimpanzees and HIV-2 from the sooty mangabey. The former is the main culprit of AIDS in the United States and worldwide, while the latter is more common in Western and Central Africa[11].

Enveloped RNA viruses possess specific vital proteins that must be able to perform certain functions to preserve the virus' life and infectivity[12]. These proteins enable the genomic condensation of the virus into an RNA-protein complex into a protein shell enclosed by a lipid membrane, also known as the viral envelope[12] that recognizes host cellular receptors such as the gp120 and CCR5 in T-cells in the case of HIV-1[12]. Retroviruses replicate through a DNA intermediate, flanked by two long terminal repeats containing a promoter required to synthesize genomic and regulatory RNAs[13]. The promoter is located towards the 3' end of the RNA sequence. The main HIV-1 viral genes found in the reverse transcribed virus DNA are *gag*, *pol*, *pro*, and *env*[11, 12]. These genes encode for proteins with specific functions (Fig 1.1). These include the *gag* gene which encodes for the main structural proteins such as matrix, capsid and nucleoproteins represented in p24, p7, p6 (core), and p17 (matrix)[11, 12]. *Pol* genes encode for vital enzymes responsible of viral DNA formation and integration into the host genome; reverse transcriptase, RNase H, and integrase[11]. *Pro* genes encode the viral protease that mediates proteolytic cleavage of polyproteins resulting from encoding by *gag* and *pol*[11]. *Env* encodes essential glycoproteins and transmembrane proteins responsible for host cell recognition and interaction leading ultimately to fusion and entry of the viral particle into the host cell, these are gp120 and gp41[11, 12]. Once transformed into the viral DNA, the long terminal repeats (LTRs) represent a main characteristic of

these viruses[13]. LTRs consist of three elements; U3, R, and U5. The 5' and 3' LTRs play different roles in the virus survival where the first functions as viral promoter and the second as transcription termination site[13]. The virus genome also encodes for accessory genes such as tat, rev, vpr, vpu, vif, and nef[11]. These genes encode for proteins Tat, Rev, Vpr, Vpu, Vif, and Nef that are implicated in facilitating viral replication and generation of new infectious virions to continue the infectious cylce[11]. Briefly, Tat protein enhances viral genes expression and Rev facilitates and ensures the correct transport of viral mRNA and genomic RNA from the nucleus after transcription to the cytoplasm for translation and/or packaging into new viral particles[11, 14]. Vpr has a critical role in halting the cell cycle at G2 and Vpu has important roles in the release of newly formed viral particles[11]. Vif enhances virions' infectivity, where Nef is implicated in cellular signal transduction and CD4 down regulation allowing for virions' budding during late replication stages where mature infectious virions are released from a replicating host cell[9, 11].

HIV-1 life cycle

The HIV replication cycle consists mainly of 7 stages. These are binding, uncoating, transcription, integration of viral DNA into host genome, protein synthesis, assembly and budding of new HIV particles[11] (Fig 1.2). HIV viral particles, 100 nm, have a lipoprotein membrane decorated with trimers of glycoprotein heterodimer complex of external surface receptor gp120 and transmembrane gp41 bound together noncovalently and represent the first responsible keys for infections[11, 15]. In the first stages of the viral cycle, the surface receptor gp120 binds to CD4 on the target cell. Because the two glycoproteins, heterodimers, gp120 and gp41 are not bound covalently, gp120 has a tendency to shed and fall off spontaneously and can be detected in the serum and lymphatic tissue of HIV patients[11]. Initial binding of gp120 to CD4's Phe43 residue

promotes structural changes in the viral Env allowing coreceptor binding (CCR5 or CXCR4 depending on tropism) to the V3 loop[16]. This interaction initiates membrane fusion facilitated by gp41, which inserts its fusogenic hydrophobic peptide located at the amino terminus of the receptor into the membrane ultimately causing fusion of the two membranes together through six-helix bundle formation[11, 14, 16] and allowing for the subsequent entry of the infecting capsid. Upon membrane fusion and entry, the virus particle uncoats into the target cell's cytoplasm releasing the infectious viral RNA and other vital proteins[14].

Once inside the cell, the viral enzyme reverse transcribes the viral RNA at the minus-strand polymerization into a RNA/DNA hybrid double helix through the enzyme's ribonuclease H active site[11, 14]. Ribonuclease H then degrades and breaks down the RNA strand of the hybrid helix and proceeds to complete a complementary DNA strand to form a double helix DNA through its polymerase active site forming the pre-integration complex (PIC)[13, 14, 17]. The proviral DNA is then cleaved at each 3' end to create sticky ends and is transported into the host nucleus where it is integrated into the host genome by the action of the integrase[13]. Post integration shifts HIV-1 replication to late phase[14]. Upon cellular activation, the transcription of proviral DNA into mRNA takes place from U3 promoter within the upstream LTR and produces regulatory HIV-1 proteins such as Tat and Rev[11, 14]. Tat protein recruits enhancer transcription factor b (P-TEFb) that binds to the transactivation response element (TAR site) of the viral RNA[11, 14, 17]. Similarly, Rev enhances transcription of longer RNA transcripts leading to expression of structural and enzymatic genes enhancing formation of mature virions[11].

Long mRNA is transported to the cytoplasm where it is translated into structural and other viral proteins for the assembly of new virions. Translation leads to formation of proteins resulting from pol and gag genes form the nucleus of the virus where proteins encoded by the env form the viral envelope with its glycoproteins[9, 11]. New virions require

the assembly of two identical viral RNA strands with other vital viral proteins for replication encapsulated inside core proteins forming the viral capsid[11]. Assembly takes place by the arrangements of multifunctional polyprotein precursors; Gag, Gag-Pol, and Env[18]. Specifically Gag precursor (Pr55) plays a critical role in assembly of HIV-1 particle because of its many interactions with other subunits such as RNA and lipids thus incorporates the major components to form a functional virus[18]. Following the capsid assembly, the immature viral capsid particle migrates to the cell surface where Gag Pol polyproteins are cleaved by the HIV protease into their active final forms[11, 18-20]. Upon cleavage and activation by HIV-1 protease mature virions are unleashed and cause a highly reproductive infection in cells that meet their entry/fusion requirements[11]. After activation by the viral protease, these viral particles bud through the host membrane taking a part of it to form their new envelope taking on phospholipids and cholesterol from the host cell membrane[11]. This is done to improve its own infectivity, as the virus has eventually evolved to acquire and incorporate host cell membrane proteins on its surface improving its adhesion to target cells. These proteins may include HLA class I and II proteins and ICAM-1 adhesion proteins[11].

In T-lymphocytes, new viral particles bud in the extracellular space where, in monocytes and macrophages the virions first collect in intracellular vaculoes and then are released[11, 18]. Three types of filaments known as intermediate filaments, actin, and microtubules make up the cell's cytoskeleton where their main function is to support cell movement, division, and transport of the organelles in the cytoplasm[21]. HIV-1 uses the cell cytoskeleton to ease its entry and infection into cells and during cell-to-cell transmission using virological synapses. Transmission of HIV-1 from cell-to-cell was found to be 100–18000 times more efficient than in cell-free infection[21]. This is because cell-to-cell transfer has many advantages to the virus such as dodging of the virus to neutralizing antibodies, speeding diffusion time to new cells, and increasing viral fusion

by the action of virological synapses that work to concentrate virus and its entry receptors[21].

HIV-1 interaction with host immunity

Virus isolation led to the identification of CD4 T cells as the main viral target[6]. Infection occurs through CD4 cell surface receptors[6, 17]. CD4, a 58 kDa monomeric glycoprotein is expressed on surfaces of circulating T-lymphocytes and precursors in the bone marrow and thymus, monocytes/macrophages, eosinophils, dendritic cells, and microglia[11]. This discovery introduced the knowledge of CD4+ T-cell depletion as a result of HIV infection, which directly led to monitoring of CD4 cell counts clinically to follow up with HIV+ patients as well as check on their response to the different ART treatments[9, 11]. It was not until mid-1990s that the specific co-receptors/chemokine receptors on the CD4 cells were finally identified; CXC-chemokine receptor 4 (CXCR4) in the case of T/X4-tropic HIV-1 and CC-chemokine receptor 5 (CCR5) in the case of M/R5-tropic HIV-1[9, 11]. CXCR4 chemokine is found expressed on a plethora of cells including T-lymphocytes and CCR5 is found on antigen presenting cells and activated T-lymphocytes[11]. Deletion mutations of CCR5 offered resistance to R5-tropic HIV[6]. The host cell was found to contain many viral restriction factors such as tripartite motif-containing 5α (TRIM5 α), APOBEC3G, SAMHD1 and tetherin, however all these factors are also counteracted and inhibited by HIV antagonists Vif, Vpx, and Vpu[14, 19].

Immune cells possess innate defense mechanisms in attempts to fight off the virus, however these defenses are not enough to prevent HIV-1 infection. Eventually HIV infects CD4 T cells as activated CD4 T cells are the most susceptible to infection, however not all CD4 T cells are depleted[22]. Upon infection of CD4+ T cells with HIV-1 the cells produce IFN-β and IL-1β leading to pyroptosis with the help of IFI16 DNA detector which eventually leads to the formation of the inflammasome[23]. Many HIV non-

permissive CD4 T cells perform cellular suicid by pyroptosis, mediated by caspase-1[24].
HIV infection in quiescent CD4 T cells in the lymph nodes led to an accumulation of
incomplete dysfunctional reverse transcripts[24]. These transcripts are detected by cellular
DNA IFI16, which leads to formation of the inflammasomes, eventually activating
caspase-1 leading to cells depletion[22, 24]. HIV viral replicates inside lymph nodes 5-10
higher than peripheral blood[22]. Although CD4 T cells are known to be cellular viral
reservoirs and the most cell types being affected by the infection, they may not be the
first cells infected. HIV infection in rhesus macaques (having similar histologic
anatomical genital tracts of humans) through the intravaginal route crossed the
cervicovaginal mucosa within an hour infecting first the intraepithelial DC that later are
found in draining lymph nodes within 18 hours of inoculation[25]. DCs are antigen
presenting cells found in all tissues and specifically lymphoid tissues. In humans,
dendritic cells in the vaginal tissues/foreskin epithelium are the CD1a^{+} intraepithelial DC
also known as Langerhans cells (LC) an immature MHC II positive and CD+ DC in the
stratified squamous epithelia[25, 26]. Upon activation by a pathogen, these cells migrate to
the draining lymph nodes in durations range from minutes to hours depending on
species and pathogen[25]. Hence, these cells and others in the female reproductive tract
enhance the initial spread of HIV infection[27]. The vaginal CD1a+ LCs endocytose HIV-1
virions, migrate from the epithelium, and pass the virions to CD4+ T cells [26]. Transferring
nonproductive virus in the LC has viral advantage because it enables the bypassing of
topical antiviral drugs while these cells spread the virus to lymphatic CD+ T cells[26].

Immune cells; plasmacytoid dendritic cells (pDCs), monocyte-derived DC, MDM,
and CD+ T cells utilize sensing defense mechanisms to sense exogenous and
endogenous virus[23]. pDCs were found less susceptible to HIV-1 infection where infection
was detected at low levels both *in vivo* and *in vitro*[23]. The low infectivity and thus
protection of these cells is most likely connected to the high levels of IFN-α produced in

response to HIV-1 RNA binding to TLR7 in early endosomes where the virus is contained after endocytosis[23]. However pDCs are unable to function as efficient APCs when crossing exogenous viral particles since they are considered procurators of mature DCs[23] and hence require activation that is separate from signals that would induce type I IFN production. High levels of type I IFNs are seen in HIV-1 patients, which finally led to suggesting that pDCs contribute to the viral-driven immunopathogenesis[23]. In MDMs, sensing and infection with HIV-1 is dependent on the viral capsid function in binding to the cell's cyclophilin A (CypA), which modulated the capsid uncoating and subsequent viral replication[23, 28]. Sensing of the cells by CypA depends on their detection of viral DNA synthesis. In human cells, interaction of host cell's CypA with the viral capsid protein enhances infection[28]. In infected MDMs, breaking of the tight interactions leads to production of type I IFN and suppression of viral replication[23]. Natural killer (NK) cells eliminate infected cells making them vital in fending off the immune system. They differ from the cytotoxic T-lymphocytes in their ability in responding to infected cells in the absence of prior exposure thus they play a critical role taking the initiative to eliminate virus during early stages before the adaptive immunity has kicked into gear. Studies showed that natural killer cells control the virus through the function of KIRs (Killer Immunoglobulin-like receptors)[6, 29].

HIV-1 Latency

HIV-1 infection leads to productive replicative infection as well as latent infection where the virus essentially forms a reversible nonproductive infection with the ability to replicate functionally yet transcription is latent/silent[30]. Latency is established directly after infection necessitating the regular administration of suppressive antiretrovirals to inhibit the rebound and activation of the latent virus[30]. Two kinetically different latent reservoirs have recently been identified represented in different memory CD4 T-cell

subsets[30]. T-cell infection starts when naive CD4 T-cells become activated by the interaction with antigen presenting cells (APCs) such as dendritic cells and macrophages where the APCs present T-cells with HIV antigens. In response, the now-activated T cells proliferate and differentiate into several subsets; the effector T cell subsets such as Th1, Th2, and Th17 the effector subsets and regulatory T-cells[30]. A fraction of these effector cells survive and transform into resting memory CD4 T-cells that migrate to the lymphoid tissue functioning as ready-guards against the same antigen enhancing future immune responses[30]. These cells can generate secondary effector cells upon recognizing the antigen again. Characteristics such as their small size, low RNA levels, and absence of activation markers such as CD69, CD25, and HLA-DR make it possible to differentiate between resting and activated cells[30].

Latency can take place using two main methods of infection. The first is infection during deactivation where virus infects an effector cell that later differentiates and reverts to resting memory cell generating the common route of latency or a second method through the direct infection of resting cells where these cells can be naive or memory cells[30]. While it takes place, infection of resting CD4 T-cells is difficult due to the low expression of CCR5 co-receptor slowing viral fusion, cytoskeletal barriers, low levels of deoxynucleoside triphosphates (dNTPs), and poor nuclear import and integration with host genome. In vivo, infection in resting cells is aided by high levels cytokine/chemokine in lymphoid tissues leading to generation of latent virus in these cells[30]. Homeostatic proliferation of latent infected cells induced by homeostatic cytokines like IL-7 and IL-15 is a key factor in survival of these secret viral storage cells[30]. Research is still ongoing to determine the exact route of establishing latency.

Mechanisms that aid the occurrence of latency include but are not limited to transcriptional interference, unavailability of certain transcription, post-transcriptional and elongation factors, certain chromatin modifications, and low Tat activity[30]. Studies have

shown latent provirus in resting CD4 T-cells integrated within highly expressed transcriptional gene regions, which may lead to transcriptional interference and contribute to latency[30]. Low levels of certain transcription factors such as NF-κB and NFAT or mutation in the binding sites of these factors were shown to contribute to the onset of latency in the quiescent T-cells[30]. Scarcity of certain elongation factors such as P-TEFb in memory cells were also shown to contribute to latency[30]. Furthermore, many factors may contribute to progression of HIV, some of these are; an impaired innate and/or adaptive immune responses, polyclonal B-cell activation, increased T-cell turnover and decreased thymic activity, short lifespan of central memory CD4+ T cells, breakdown of mucosal barriers leading to infection and immune activation, increasingly dysfunctional T cells that mimic an activated phenotype, and high levels of proinflammatory cytokines and chemokines[31]. To study these factors, investigating elite controllers (ECs), long-term nonprogressors (LTNPs), and viremic nonprogressors (VNPs) become an essential tool to understanding their contribution to HIV progression[31]. Microarray gene-expression analysis on jejunal biopsies of three groups, ART-naive HIV-1 seropositive individuals, HIV-1 seronegative, and LTNPs showed that gene-expression profiles differ between groups. Compared to uninfected individuals, HIV-1 seropositive individuals showed upregulation of 369 genes whereas LTNPs showed upregulation of only 150 genes. In addition, some genes implicated in activation of lymphocytes and inflammation, such as RANTES (major CCR5 ligand) which was downregulated in the LTNP group and upregulated in the HIV-1 seropositive individuals compared to the control seronegative group. Seropositive individuals were found to have upregulated cell cycling-related genes such as CCNA2 and MCM4 as well as genes related to growth and cell adhesion[31]. However, both seropositive and LTNP groups showed induced immune response genes such as IFITM1 and OAS2 involved in the

interferon pathway, cell surface receptors such as PD-1, leukocyte immunoglobulin receptor, and B2, and Eotaxin and MCP-1 involved in chemotaxis[31].

Treatments

Antiretrovirals

In response to the devastating epidemic, major efforts from governments, public institutions, and pharmaceutical companies yielded approximately 30 anti-HIV drugs, antiretroviral therapies (ART) that are still used[32]. US Food and Drug Administration (FDA) approved many drugs that target five different stages of the virus[32, 33]. These are nucleoside reverse transcriptase inhibitors (lamivudine, abacavir, tenofovir and emtricitabine) and non-nucleoside reverse transcriptase inhibitors (rilpivirine and efavirenz) that inhibit the reverse transcriptase where the former function as analogues of nucelosides/nucleotides causing chain termination and the latter inhibit the reverse transcriptase and both ultimately inhibit reverse transcription of the viral RNA[32, 33]. Integrase inhibitors (raltegravir, dolutegravir and cabotegravir) inhibit viral DNA integration into host genome[33]. Protease inhibitors (such as atazanavir, saquinavir, amprenavir and darunavir) inhibit the viral protease that is responsible for maturation of HIV-1 entailed in the cleavage of the polyproteins[32, 33]. Fusion inhibitors (enfuviritide), and entry inhibitors (maraviroc)[32, 33] are less used in regimens however are promising alternatives. In the absence of an effective ART therapy, CD4 cell counts fall to below 200 cells per microliter causing HIV-positive individuals to eventually progress to AIDS within 10 years and become very susceptible to a plethora of opportunistic infections[5, 34]. Many complications and coinfections arise from AIDS such as tuberculosis, candidiasis, cryptosporidiosis, Kaposi's sarcoma, and many other neurological AIDS-related complications[5]. In a meta-analysis, Poorolajal et al estimated that most AIDS patients on HAART have survival expectancy for more than 10 years when starting regimens with

the onset of the disease which is significant compared to only 2 years of life from the onset of the disease in those who do not receive HAART[34]. Viral exposure to subtherapeutic drug levels due to lack of adherence leads to development of drug resistance mutations which represents a major setback for current ART[33, 35].

The first drug to be used in HIV ART is the anticancer drug azidothymidine (AZT)[6]. The drug was able to suppress the virus by blocking the reverse transcription of viral RNA into DNA[6]. As a result, major decline in death and HIV-associated infections rates were achieved. However, due to the high mutation rate of the virus, resistance against AZT quickly aroused forcing scientists to go back to the drawing board to develop new drugs. A decade later, it was discovered that these drugs may be combined into the combinational ART therapy (cART) of 3 drugs to limit resistance, increase viral suppression, and enable lower doses of each drugs to avoid specific drug toxicities[6]. In addition, many studies showed that combination of two nucleoside reverse transcriptase inhibitors (NRTIs) combined with a protease inhibitor showed superior therapeutic effects and reduced mortality[6]. Development of cART decreased AIDS related deaths by almost 50% between 2005 and 2016[22]. In South Africa, life expectancy of HIV-1 patients increased by 11 years[6]. Adhering effective antiretroviral regimens, patients who reach a CD4 count more than 500 are expected to have normal life span expectancy and lead a healthy life[5]. Mother-to-infant HIV transmission was thought unpreventable until the ACTG076/ANRS 024 study in 1994 showed that the administration of AZT during ante- and intra-partum periods provided significant reduction in newborn viral acquisition paving the way to Pre-Exposure Prophylaxis (PrEP)-directed research.

To tackle preventive regimens, tenofovir disoproxil fumarate was investigated for use as a prophylaxis drug to prevent or decrease HIV-1 transmission in prone individuals. Initially, a Caprisa 004 trial in South Africa studied the effect of the drug as vaginal gel applied before and after sexual intercourse and the results were promising

showing reduction in HIV acquisition by 54% where results were affected by the individuals adherence to the treatments[6, 36]. Additionally, the iPrEX trial looked into prophylaxis effects of a once daily oral emtricitabine and tenovofir disoproxil fumarate in the population of men and transgender women who have sex with men showing a reduction of 44% in viral infection[6, 37, 38]. In another study involving 9 different countries, 1763 serodiscordant sexually active couples were enrolled where one partner was HIV-1 positive and the other is negative. The study investigated the prophylaxis effect of antiretroviral therapy to limit HIV-1 transmission between serodiscordant couples. The study showed that early initiation of ART reduced sexual transmission of the virus and the onset of clinical events by 96%, where suppression was due to suppressed virus levels in the genital secretions[39]. More clinical trials such as Partners PrEP and TDF2 studies showed more than 60% efficacy in HIV reduction when tenofovir tablets or Truvada (tenofovir and emtricitabine combined) were given to heterosexual couples prone to HIV transmission[38, 40, 41]. Currently, Truvada shows a leading role in reducing HIV-1 acquisition in different populations of sexual exposure and HIV high risk individuals[42, 43]. Truvada has good safety profiles in kidneys and bones and pregnancy cases[42].

HIV broad neutralizing antibodies (bnAb)

Neutralizing antibodies (nAbs) are targeted against viral epitopes to fight infectious disease[44]. Antibodies have been extensively used in infectious disease prevention and treatment such as measles, hepatitis A and B, tetanus, varicella, rabies, and cases of cytomegalovirus, parvovirus B19 and enterovirus[45]. BnAbs are antibodies targeted to conserved viral structures, the envelope protein (Env) and its different epitopes/structures[46]. In turn, viruses evolved to protect their Env trimer from neutralizing antibodies by mutations or masking its epitopes employing a glycan shield [47]. BnAbs can

also recruit effector cells response to apparent infection[47]. These antibodies are often characterized by long half-lives[48] and increase in potency and neutralization characteristics with time with viral exposure[49]. Newly engineered antibodies; bi-specific mAbs and dual-affinity re-targeting (DART) proteins can recruit effector cells as well as recognize HIV-1 Env epitopes[50]. A few of these bnAbs are 3BNC117, VRC01, N6-LS, and VRC07-LS that target CD4 binding site (CD4bs); 10-1074 and PGT121 that bind to the V3 loop; PGDM1400, PG9, and PG16 that target the V1/V2 loop; PGT151 that targets gp120-gp41 interface; 10E8V-LS that target the membrane-proximal region; and finally glycan-dependent SF12 and VRC-PG05 that bind to glycans on the center of the 'silent face' of gp120. Many of these are progressing to early clinical trials[46, 48, 50-52].

BnAbs are produced from B cells surviving in spleen and lymph node germinal centers and are characterized by having one or more unique features that set them apart from other antibodies; long antibody combining regions heavy chain third complementarity-determining regions (HCDR3), high somatic mutations, and autoreactivity to some self-antigens[53, 54]. While, these unique features contribute significantly to the breadth and efficacy of bnAbs, they down regulate their own production due to immune intolerance[54]. For these reasons, bnAbs production could be increased in individuals with a certain autoimmune disease where many antibodies are frequently made by avoiding immune responses via defective immune tolerance. In a chronic HIV-1 patient that is also diagnosed with systemic lupus erythematosus (SLE), the patient was found to be able to control the virus[53]. Hence, the immune system response to the development and maturation of effective bnAbs presents a considerable limitation to their use in vaccination and treatments where other medications may need to be administered to dampen the immune responses against production of bnAbs. This explains the delay in the production of bnAbs since their production is correlated with the high viral loads in plasma also this could be a result of the slow antigen-dependent

maturation process these bnAbs have to go through where the antibodies also undergo many somatic mutations[51, 55, 56].

Moreover, bnAbs were shown to be prophylactic against viral challenges in animal models. Administering 10-1074 or 3BNC117 showed prophylaxis against intrarectal $SHIV_{AD8EO}$ challenge in rhesus monkeys[57]. The antibodies were administered a day before viral infection and showed inhibition of virus in all animal treated. Gautam et al. showed that modifying antibodies by introducing two amino acid mutations referred to as LS (M428L and N434S); 3BNC117-LS of 10-1074-LS, were able to increase their half-lives and confer further protection against repeated viral challenge in monkeys for a longer duration than the native antibodies did [58]. To simplify future bnAb regimens while increasing their breadth and potency, Xu et al. designed a trispecific bnAb that contained V1V2, MPER, and CD4bs binding sites[59]. The first two bind the virus/virus-infected cells and the CD4bs domain binds and recruits killer T lymphocytes to elicit additional immune responses[59]. The trispecific bnAbs were tested against a large panel of viruses (208 different viruses) where 4 resistant viruses were found in the case of VRC01/PGDM1400-10E8v4 and only one resistance with N6/PGDM1400-10E8v4. The individual parental bnAbs showed neutralization efficiency but not as potent and efficient as when combined in the trispecific bnAbs designs. Furthermore, in attempts to improve antibodies binding to the neonatal Fc receptor to ultimately extend their half-lives and confer further protection, a mutation to CD4bs-targeting bnAb, VRC01 and N6, was incorporated. When tested in rhesus macaques, mutated parenteral VRC01 showed longer half-life than mutated N6. The same results were paralleled when the animals were treated with the trispecific bnAbs that incorporated the mutations to VRC01 and N6 reflecting the half-lives of 7.4 and 4.8 days, respectively [59]. The study reflects the significance of engineering bnAbs with multispecificity and mutations to increase their breadth, potency and circulation time.

Gaudinski et al. recently concluded a phase 1 open-label clinical trial testing the monoclonal antibody VRC01LS. VRC01LS is a modified version of VRC01. The modification is a mutation in two amino acids that render the antibody with a longer half-life by increasing its binding to neonatal Fc receptor [60]. The trial confirmed the safety of the antibody with only a few cases of mild adverse effects and showed the advantage of modifying the antibody to extend its half-life, which enables it to stay in circulation four-fold longer than the native form in healthy volunteers. Study participants' sera were tested for their antibodies neutralization activity using standardized assays against three Env-psudoviral strains confirming that VRC01LS still retained its neutralizing activity in serum 36 weeks after injection into the patients [60]. Also, sera were tested for resistant antibodies to VRC01LS confirming the safety of the antibodies in evading an autoimmune response. In another clinical study, 10-1074 was tested for safety in 14 healthy and 19 HIV-1 infected volunteers. Antibody infusion on day zero, followed by a period of 24 weeks follow up deemed the antibody tolerated in all participants with half-lives of 24 and 12.8 days in non-infected and infected participants, respectively [61]. The shorter antibody half-life in infected individuals points to the presence of viral targets that are being neutralized by the antibody administered leading to clearance of the complex[61].

In another phase II clinical study, the efficacy of 3BNC117 against HIV-1 was evaluated in infected volunteers who were on ART for a year where ART was stopped for analytical treatment interruptions. The study enrolled participants with viral strains sensitive to the antibody and administered antibody infusions every 2-3 weeks. Two infusions of 3BNC117 (30 mg/kg) succeeded in viral inhibition for a period ranging from 5-9 weeks, where four infusions were able to maintain viral delay for up to 19 weeks [62]. However, in more than 50% of the participants, viral escape was detected where resistant strains had emerged. Therefore, a downside of using a single antibody for

treatment is the rise of resistant viral strains that may have been a pre-existing minority or de-novo generated from the virus turnover[61], thus current studies are steering towards the path of combinational antibodies to circumvent the viral escape dilemma.

Mendoza et al. used both 3BNC117 and 10-1074 in a combinational therapy in a phase 1b clinical trial where the antibodies (30 mg/kg each) were administered in 3 different doses to HIV-1 infected individuals during and after ART treatment interruption [63]. The antibodies had half-lives of 17.6 and 23.2 days for 3BNC117 and 10-1074, respectively. Antibody combination was administered at weeks 0,3, and 6 and ART were completely interrupted two days post the first antibodies infusion. Over 80% of the participants (9 out of 11) showed viral suppression for 15 weeks, and the rest had rebounded by 5-7 weeks [63]. Taken together, the studies confirm the positive antiviral effects of bnAbs in human subjects. Moreover, the role of bnAbs in vaccines was tested in the most recent human clinical trial for HIV vaccine in a phase I clinical trial (IAVI W001) testing the BG505 SOSIP.664 gp140 candidate administered via intramuscular injection. The vaccine consists of glycosylated HIV-1 envelope glycoprotein trimers containing disulfide bonds to stabilize gp120 and gp41 domains resembling the actual virus envelope, a three-pronged spike[64]. Previous studies in infected animals showed the vaccine is capable of inducing B cells to produce bnAbs neutralizing the virus[64].

Pathways to viral eradications

Although no readily available cure has been developed for HIV, stem cell transplant-based therapy has been shown to be a promise for a permanent cure. This was demonstrated and confirmed in only one case thus far where the patient, the Berlin patient has been cured. The Berlin patient has shown persistent aviraemia and prolonged viral suppression even in the absence of ART following stem cells transplantation from a donor that had a CCR5 mutation, rendering the recipient resistant

to new HIV viral infections [10]. Initially, the Berlin patient received the transplantation to treat his acute myeloid leukemia. The donor had homozygous 32-bp deletion in the CCR5 allele rendering CCR5 receptor ineffective in aiding HIV-entry as its co-receptor and enabling the first known HIV cure to go down in history [6, 10].

One approach for viral eradication explored the ability of combination ART (cART) to inhibit reservoir formation if administered during acute infections/primary infection[65]. Although, initial results were promising where studies showed post-treatment controllers controlled viremia after halting therapy, the probability of controlling the virus at 24-month post-halting early treatment intervention was found to be approximately 15%[66]. One case that confirmed early ART treatment insufficiency for eradication is the Mississippi Child. The baby was administered antiretrovirals as soon after birth by 30 hours and treatment was halted after 18 months where remission lasted for 27 month before rebound[67]. No signs of acute retroviral syndrome were observed but her plasma viral load was at 16,750 copies/mL which dropped to 2,658 copies/mL within 72 hours of antiretroviral therapy with an increase in CD4+ T cells by 43% [67]. Moreover, early treatment is difficult strategy to establish due to difficulty assessing infection onset.

Another strategy for eradication explored the shock and kill method that utilizes latent reversal agents (LRA)[65] like histone deacetylase (HDAC), a most common LRA. The approach is based on shock/activation of HIV from latent cells to be recognized and killed by the immune system and administered antiretrovirals[68]. The treatment has various limitations that include lack of targeting to cellular reservoirs[68], which may lead to the need of an increased dose increasing the risk of toxicities[65]. Another limitation is the necessary need of a potent combination of LRA to effectively penetrate the tissues and activate reservoirs in order to achieve eradication[69]. The lacking efficacy of this approach was seen in clinical settings where LRAs were administered to HIV-infected patients who were on ART. The treatment showed activation of virus seen in the elevating levels of

HIV RNA in CD4 T cells and plasma without change in latent cells frequency[69]. Various strategies were explored to cure HIV by activation, making the latent virus susceptible to cytopathic effects and immune responses, however a complete long-term solution has yet to be attained[30]. Of these strategies, histone deacetylase (HDAC) inhibitors were explored however elimination of latent reservoirs was not achieved because of remaining viral transcription due to survival-cellular mechanisms where the cells did not die promoting further infection[70].

A study investigated the effect of administering latency inducers (LARs) to assess if combination therapy may decrease reservoir maintenance using the shock and kill strategy. A combination of inducers; vorinostat, I-BET151, and α, were administered after multiple tri-mix bnAbs treatments, caused 57% of mice to maintain viremia suppression compared to 10% of the mice showing non-rebound in the groups where only antibodies were given or antibodies plus one inducer [71]. Since the latent reservoirs represent unbreakable barrier to viral eradication, Borducchi et al. tested the extent of the shock and kill-strategy using combination of bnAb treatment with an immune system activator to decrease/eliminate the viral reservoirs. Indian rhesus monkeys were infected intrarectally with SHIV-SF162P3 and were administered ART cocktail subcutaneously (tenofovir disoproxil fumarate, emtricitabine, dolutegravir) starting from 1-130 weeks post-infection. The combination group received oral doses of GS-9620 (TLR7 A agonist) and intravenous infusions of PGT121 (V3 glycan-dependent bnAb). A period of antibody washout was followed by ART termination on day 130 [72]. By week 120, no virus was detected in the treatment or control groups (including groups that were treated with either drugs; PGT121 or GS-9620). To measure viral rebound from reservoirs, the group monitored plasma viral loads for 196 days after ART discontinuation. As a result, groups that received either GS-9620 or PGT121 alone had rebounded with a percentage of 91% or 82% of animals. However, in the group that was treated with both only 55% of the

animals showed a rebound, highlighting the significance of immune system activation to sharpen the antiviral effects of both bnAbs and antiretroviral therapy. The study showed promising results using a triple-strategy therapy on HIV-1 administering a combination of ART, bnAb, and LRA. The study is a proof-of-concept that HIV-1 eradication strategy is possible if the right strategies are combined and utilized together.

In the recent decade, gene editing has been explored as a promising tool to eradicate latent HIV-1 from resting memory T cells to eventually allow for therapy termination. DNA sequence targeted CRISPR/Cas9 genome editing of HIV-1 provirus has been explored to eradicate transcriptionally latent virus that is not affected by therapy[70]. The biggest obstacle to gene editing is the viral diversity, which requires multiple sites' targeting in the viral genome. An additional obstacle is the possible off-target effects in host genome. CRISPR/Cas9 consists of Cas9 endonuclease, which causes a double strand break at a specific virus sequence. This is guided by a 20 nucleotides long guide RNA. CRISPR/Cas9 was used to target the LTRs of the provirus using a single gRNA where some reports showed 8.5 kb provirus excision[70]. Moreover, it was noted recently from post treatment controllers' data that there's a correlation between the viral copies and the efficacy of CRISPR/Cas9[70]. Notably, Dash et al. were able to show viral elimination in 33% of humanized mice treated with long-acting slow effective release ART (LASER ART) and CRISPR/Cas9 targeting the LTRs and Gag genes of the provirus[73]. Elimination of virus in this fraction of humanized mice was only possible with the initial administration of LASER ART, which restricted viral infection to very low levels followed by the administration of CRISPR/Cas9 to excise the remaining latent virus. These mice showed elimination of competent HIV-1 in blood and tissues confirmed by nested and digital-droplet PCR and RNAscope assays[73]. The study is a proof-of-concept of complete eradication of the virus from previously infected animals.

Long-Acting Slow Effective Release Antiretroviral Therapies (LASER ART)

The many obstacles to an HIV-1 cure necessitate the improvement of current ART. ART is the most critical aspect known to date to suppress HIV-1 where HIV-1 patient can live a longer lifespan leading a fulfilling life. Nevertheless, the daily doses of ART create a pill burden on HIV-1 patients, and hence, regimen adherence is found to be an issue in the HIV-1 population. In recent years, pharmaceutical companies and researchers invested efforts into transforming the current daily ART into a long-acting (LA) ART that may be dosed monthly or bimonthly[74, 75]. However, current LA ART approaches depend on whether these drugs can be nanoformulated and possessing certain physiochemical characteristics such as poor water solubility and high potency[76]. Nevertheless, many ART are highly water-soluble with low potency like many NRTIs. To overcome these many limitations, prodrug and nanoformulation strategies as well as targeting and harnessing the macrophage depot system were combined and were shown to significantly improve the current antiretroviral therapies by transforming native drugs into long-acting slow effective release ART (LASER ART)[77] (Fig 1.3). LASER ART utilizes prodrugs as well as nanoformulation strategies to improve current drugs transforming them into LA regimens. Specifically, these LASER ARTs are characterized by poor water-solubility, slow drug dissolution, increased bioavailability, extended apparent half-life and decreased off-target toxicities ultimately improving pharmacokinetic and pharmacodynamic profiles [75, 77, 78]. LASER ART strategies improved on many relevant and current HIV-1 drugs such as lamivudine, emtricitabine, dolutegravir, cabotegravir, abacavir, and rilpivirine to date[75, 78-82].

Briefly, modifications to parent drugs were explored to alter physicochemical characteristics of the drugs making them more hydrophobic hence improving their uptake in addition to their retention inside HIV-1 cellular reservoirs[77, 79]. Prodrug

strategies are used to improve drug's absorption, distribution, metabolism and excretion profiles (ADME) of many drugs and can be exploited to improve aqueous solubility, hydrophobicity, permeability, half-life and many other factors that affect the drug's pharmacokinetics and potency[83, 84]. Modifying DTG and CAB, integrase inhibitors, with 14-carbon fatty acid chains by covalent ester bonds yielded more hydrophobic and lipophilic drugs that were able to maintain high drug potency. These modified drugs were coined as MDTG and MCAB. These drugs showed superior pharmacokinetic and pharmacodynamic profiles as newly developed prodrug nanoformulations over the control treatments[75, 78]. In HIV-1 infected human-reconstituted peripheral blood lymphocytes (PBL) reconstituted $NOD/SCID/IL2R\gamma c^{-/-}$ (NSG) mice, NMCAB treatment showed viral restriction in terms of reduction in plasma viral RNA and DNA levels by more than one log in magnitude and in tissues by more than 3 $logs_{10}$ in magnitude when compared to HIV-1 positive and GSK's CAB LA controls. Furthermore, in preliminary PK in rhesus macaques MCAB had a more superior PK profile when compared to GSK's CAB LAP as evident in the increase in half-life ($t_{1/2}$) by 2-4 folds [75, 85].

Moreover, LASER ART was utilized to improve many current NRTIs. NRTIs are the backbone of many ART regimens where common regimens would include two NRTIs and an integrase inhibitor, NNRTI, or a protease inhibitor. Modifying the hydrophilic lamivudine (3TC) with a myristic acid after blocking the drug's amine group to avoid side products yielded M3TC[79]. This modification decreased the drug's aqueous solubility and improved its protein binding. Previously, 3TC could not be nanoformulated with polymers due to its high aqueous solubility but upon modification of the drug to M3TC, nanoformulation with P407 through high pressure homogenization was plausible and yielded stable nanoformulations[79]. Compared to free 3TC, M3TC showed high uptake and retention levels inside monocyte-derived macrophages (MDM). Once inside the cells these nanoparticles were stored in late and recycling endosomes where viral

replication/reservoirs were suggested to reside in macrophages. Inside the cells, different esterases such as (lysosomal acid lipase, phospholipase, and acetylhydrolase) can cleave the ester bond releasing 3TC and myristic acid where 3TC is free to be phosphorylated into the active moiety. Moreover, myristic acid, the modifying moiety, may have additional antiviral by inhibiting N-myristoyltransferase (NMT) that is responsible for the myristolyation of different capsid proteins. Administration of M3TC nanoformulation in BALB/cJ mice showed improved PK profiles with increase in 3TC plasma levels 10 days post treatment compared to undetected 3TC levels from native 3TC beyond 8 hours post treatment. Similarly, modification of another NRTI, abacavir, with myristic acid as in the case in M3TC yielded a more hydrophobic drug that can be formulated with P407 with comparable antiretroviral potency as ABC[80]. More recently our laboratory has combined long-acting and ProTides strategies to further improve ABC by delivering slow effective release of monophosphorylated abacavir into cells and tissues[86]. LASER ART utilizes many strategies used in currently used contraceptives and antipsychotic drugs to synthesize long-acting ART that may in the near future be available in clinical settings where these LA regimens will be dosed less frequently and ultimately improve patient-drug adherence [77, 87]. Hence our lab extends the LASER ART strategies to many different ART classes such as protease inhibitors such as darunavir.

Darunavir (DRV)

Darunavir, DRV, also known as TMC114 is a nonpeptidic peptidomimetic protease inhibitor that was approved by the FDA in 2006 as a twice-daily RTV-boosted regimen for treatment-experience patients and was later approved for once daily dose [88-92]. DRV is effective against wild-type HIV-1 and a wide range of multidrug-resistant strains making DRV a preferred HIV PI treatment in pregnant women, pediatrics, HIV-2, and HCV co-infection[93]. DRV binds to the viral protease inhibiting its function to cleave

precursor proteins, the gag-pol polyproteins, of newly formed viral particles leading to a halt in the virus cycle and ultimate viral turnover [94-96].

Protease inhibitors are considered a cornerstone in the treatment of HIV and hence are found in most of the first line HIV treatments for adults and adolescents[97]. In a study investigating PIs' mechanisms, Hayashi et al. showed that DRV not only inhibits the enzyme's activity but also inhibits its dimerization. DRV can bind to viral proteases preventing their dimerization while conventional drugs such as saquinavir only inhibit the proteolytic activity of the protease and not the dimerization[98]. The drug molecule has high affinity for the viral protease's active site forming a stable complex with it, which explains the drug's antiretroviral activity even in the presence of resistance-associated mutations[96]. The reported binding affinity of DRV to wild-type HIV-1 protease is K_d 4.5 x 10^{-12} mol/L and decreases by a factor of 13.3 to 6.0 x 10^{-11} mol/L when binding to multidrug-resistance HIV-1 protease[89]. With mutant proteases however, DRV still bound more efficiently that first-generation PIs. DRV is similar in structure to the first-generation PI amprenavir, however DRV binds to multidrug resistant (MDR) HIV-1 protease 33 fold more tightly than amprenavir[89].

In vitro antiviral activity revealed the EC_{50} to range from 1-5 nmol/L and EC_{90} from 2.7-12 nmol/L in HIV-1/2 infected cells such as MT-4, peripheral blood mononuclear cells (PBMCs) and macrophages[89]. In structure and binding studies, it was found DRV forms 11 hydrogen bond interactions and 4 water-mediated ones with a typical viral protease however several mutations can lead to inhibition of dimerization due to separation in the flaps and hence affect the binding of DRV with the viral proteases[99]. One such mutation is the $PR_{P51-D25N}$ which is resistant to DRV. The mutation leads to lower affinity to DRV and dimer dissociation. Mutant protease binds DRV in a perpendicular manner to its original binding conformation with only 2 hydrogen interactions and 2 water-mediated bonds[99]. Three different viral mutations must exist to

have negative impact against DRV. In vitro experiments showed lower resistance development to DRV when compared to other protease inhibitors such as amprenavir, nelfinavir, and lopinavir. Clinical and observational studies also reported that resistance associated mutations to DRV was rare in both naive and experience ART-individuals. Two recent retrospective studies further showed that PI RAM is very rare with ritonavir (RTV) boosted darunavir (DRV/r) treatment and that mutations are more common in the ART-experienced compared to the naive-ART patients. DRV is an effective drug with a high genetic barrier enabling it to remain effective against PI-resistant isolates. In an analytical study assessing prevalence of DRV mutations from 2010 to 2017, it was found that DRV RAM were maintained at low levels in the samples being analyzed resulting in high drug susceptibility[88]. In a sample of 60,760 HIV-1 patients, 91.7% showed no DRV RAM in 2010 and remaining high in 2017 by 95.8%. The study showed that all drugs compared; darunavir, atazanaivr, and lopinavir fared equally well when tested in samples that demonstrated phenotypic susceptibility to the PI being analyzed in the study. However when the three drugs were compared in a sample of 4,799 that showed phenotypic resistance to one or more PIs the results toppled and showed leading susceptibility to DRV by 73.3%, followed by 41.5% for atazanavir, and 46.0% for lopinavir when assessed in 2010. When revisited in 2017, the susceptibility had remained the same for all three drugs; DRV by 70.7%, atazanavir by 53.7% and 48.8% for lopinavir [88].

DRV is a highly plasma protein-bound drug and more specifically bound to 1-acid glycoprotein. Elimination time of boosted DRV is around 15 hours and is eliminated in feces (79.5%) and urine (14%). The drug is detected in the CSF unbound (90%) and is detected more with boosted twice-daily doses (600/100) over once-daily dose (800/100). In many Phase III trials, the PI has been shown to treat naive and non-naive patients for HIV suppression when used with other drug combinations. ARTEMIS, a 192-week phase

III study compared two different regimens consisting of TDF and FTC with either DRV/r or LPV/r. At the end of the 192 weeks, DRV/r regimen was found to be more statistically superior over the LPV/r regimen. Adverse events with DRV/r were fewer than with LPV/r as well as diarrhea treatment (grade 2-4) was significantly less with the DRV/r treatment [96]. Phase II clinical study ARIEL assessed safety of DRV/r in ART-experienced pediatric patients showing no resistance to the drug over a period of 48 weeks leading to lowering the age of ART-experienced children to 3 years highlighting the drug's safety due to its high genetic barrier. The patients were monitored for normal growth and virology responses [100]. In a study to estimate the cost of DRV/r regimen as a first-line therapy for HIV-1, it was found that for 96-week treatment period the cost would be $87,680. DRV/r cost more than RAL or ATV/r regimen needed for the same treatment period, RAL regimen being the lowest in cost [101]. A recent study found that a dual regimen consisting of a boosted DRV and lamivudine (3TC) had effectiveness similar to a triple therapy consisting of the boosted drug administered with two different nucleoside reverse transcriptase inhibitors [102]. Boosted DRV is also given in combination with emtricitabine and tenofovir in a recommended and approved regimen in the Europe, Canada, and the US [88]. Symtuza[R] is the first PI-based single-tablet regimen containing DRV boosted by cobicistat in combination of two NRTIs emtricitabine and tenofovir AF used in treatment of both ART-naive/experiences adults [103]. HIV is still an ongoing global epidemic where an average of 37 million people living with HIV with 1.8 million of new HIV infection that took place in 2016 and an estimated of a million death AIDS-related in the same year [22].

Protease inhibitors target HIV proteases efficiently but they are known for their poor oral bioavailability. The poor bioavailability is a result of oxidation/biotransformation by cytochrome P450 3A4 (CYP3A4) in gut and liver (human small intestinal enterocytes and hepatocytes) in addition to the high P-glycoprotein efflux transporters on the apical surface of intestinal enterocytes that pump the drug out of the gut wall back in the

intestinal lumen; all contributing to major loss of active drug during first-pass metabolism [104]. PIs are all CYP3A4 substrates hence administering a PI booster/CYP3A4 inhibitor increases level of active drug available. Ritonavir and cobicistat are both CYP3A inhibitors ultimately acting as a PK enhancer for many protease inhibitors. A recent in vitro study confirmed the similarities between both enhancers referring to them as high potent inhibitors of CYP3A and weak inhibitors of other CYP enzymes with high IC50 (two orders of magnitude). Both drugs enhance absorption of the PIs by inhibition of Pg-p efflux. Ritonavir was initially administered as a PI in 1996 for treatment of HIV-1 however because of its required high dose of 600 mg twice a day and its side effects it was soon used as an enhancer of PIs instead. As a PK enhancer, RTV dose is lowered to 100 mg once a day and hence is well-tolerated and dramatically increases half-life and bioavailability of the coadministered PI[105]. DRV's low oral bioavailability 37% is enhanced up to 82% in the presence of RTV boost [106]. Similarly, cobicistat is a PK enhancer that was approved by the FDA. The drug acts only as booster due to inhibition of CYP3A4 and P-glycoprotein transporters from binding the PI substrates. Its boosting effect is comparable to RTV. Cobicistat is a potent and more specific inhibitor of CYP3A and has no effect on other CYP enzymes while RTV is known to inhibit beyond CYP3A4; (2C19, 2C8, 2D6, and 2E1) and induces CYP1A2, CYP2B6, CYP2C9 and CYP2C19 and uridine 5'-diphospho-glucuronosyltransferase [104, 105]. Substituting RTV with cobicistat may be favorable to avoid RTV-side effects such as alterations in lipid metabolism, gastrointestinal issues, and many drug-drug interactions. However switching regimen from ritonavir to cobicistat may not be appropriate with drugs that have a narrow therapeutic index[104, 105]. On the other hand, in certain cases of co-infection boosters may cause additional drug interactions leading to severe side effects. Few cases showed that drug-drug interactions between ritonavir and a corticosteroid, digoxin, caused a severe toxicity in HIV-1 positive patients[107]. Moreover, due to the associated co-infections that

accompany HIV-1, drug-drug interactions are to be expected between the different drug regimens targeting different diseases. Potential drug interactions were found between HIV protease inhibitors and the 3D antiviral regimens prescribed for HCV reflecting significant reduction in DRV concentration and many other boosted-PIs post HCV treatment[108-111]. HCV medications; elbasvir and grazoprevir (potent inhibitors of NS5A and NS3/4A, respectively) were found to have increased exposure when coadministered with ritonavir or ritonavir-boosted PI making boosted-PI-inclusive HIV treatment undesirable for HCV/HIV co-infected patients [112]. Similarly, co-infection with TB and its subsequent treatment with rifampicin was found to show dramatic decreases in PI concentrations administered hence PI dose increase would be essential to achieve the same PI effect in co-infection absence. This happens due to the combined effect of the booster ritonavir and rifampicin eventually negatively affecting DRV bioavailability [113]. Pretreatment of PXR/CYP3A4-humanized mice with rifampicin lowered the intestinal permeability for DRV by 50% compared to the untreated controls suggesting the importance of a different dosage route for DRV in HIV+ patients with TB co-infection [114]. Since alcohol consumption is prevalent in the HIV+ population, a study showed ethanol negatively affects apparent half-life of RTV-boosted DRV and speeds its degradation and metabolism in the liver but not for DRV alone [115]. As previously mentioned, RTV induces and inhibits beyond CYP3A4 leading to switching of booster to cobicistat, being a more specific CYP3A4 inhibitor with less drug-drug interactions. However, while RTV causes more interactions with co-medications both boosters may cause drug-drug interactions with medications like with dihydrocodeine, pethidine, phenprocoumon, warfarin, duloxetine, sertraline, nateglidine and many contraceptives such as oestradiol and norethisterone[116]. In a cobicistat boosted-DRV/DTG regimen, cobicistat coadministered with triamcinolone (glucocorticoid to treat greater trochanteric pain syndrome and other rheumatic disorders) in a HIV+ patient lead to clearance inhibition of

triamcinolone leading to exogenous glucocorticoid excess and ultimately adrenal suppression making this HIV+ regimen problematic and requiring instant re-evaluation [117]. Attempts were made to eliminate the need for CYP3A inhibitors/PI boosters preventing resistance and drug interactions. One such group did so by encapsulating darunavir in solid lipid nanoparticles engrafted with certain peptides to increase uptake in CD4+ cells specifically. Uptake of the DRV NLS via caveole-dependent endocytosis in Caco-2 cells was reported to be 4-fold over the DRV suspension control. Particle uptake was confirmed by confocal microscopy of Molt-4 cells (containing the CD4 receptors). Desai et al. also showed improved the drug's bioavailability in rats increasing the C_{max} by 2.68-fold when using the peptide decorated darunavir SLN compared to the regular drug suspension upon oral administration at a dose of 40 mg/kg [106]. Inugala et al. attempted improving dissolution and oral bioavailability of DRV through the development of solid self-nanoemulsifying drug delivery system [118]. Using their delivery system composed of Capmul MCM C8 and surfactants such as Tween 90 and Transcutol, the team improved the dissolution rate of DRV by 3 times greater mean dissolution rate when compared to the free drug in vitro. In vivo, PK in Wistar rats showed enhanced peak drug concentration at 1 hour of 3.7 ug/mL for the solid self-nanoemulsifying DRV as compared to 1.57 ug/mL on the pure DRV treatment arm however concentrations were undetectable by 24 hours [118]. Half-life of both treatments was 6.41 and 9.91 hours for pure DRV and solid self-nanoemulsifying DRV. Therefore, to ultimately eliminate boosters would be the best scenario for individuals taking ART therapy hence this would eliminate many side effects and complications[119]. Hence modifying drugs into prodrugs may obliterate the need for a booster, which can decrease many side effects and circumvent many negative drug-drug interactions that accompany the various co-infections that accompany HIV-1 infection.

Protease inhibitors are infamous for their short half-life, low plasma levels, poor cell penetration, and low oral bioavailability [120, 121]. Chronic administration of PIs may also lead to complications such as hyperlipidemia, insulin resistance, and bone density loss [121]. This led to further research where prodrug strategies were explored to improve the ADME properties of these drugs [121-124]. However most previous modifications were directed towards improving solubility and the overall oral bioavailability of the drugs. These modifications were directed to the hydroxyl groups on the various PIs and many were specifically targeted on hydroxyl groups existing in the pharmacophore region of the drugs [121, 124-127]. As a result many of these prodrugs resulted in a marked loss of antiviral activity or only exhibited comparable half-lives to that of parent drugs [120, 126, 127].

Hostetler et al. modified PI at the C-terminal valine with a phospholipid (DPPE) to produce phospholipid prodrug to improve its plasma levels and extend drug's half-lives. Reducing rapid elimination of PI can extend tissue exposure time to these drugs These modifications improved penetration into the cell membrane because of the lipid chains inserting into the cell membrane facilitating entry of the drug. However, the modification yielded a prodrug that only extended the drug's half-life from 0.04h to 0.299h after one dose in rats showing modest improvements [120]. Modifying saquinavir with myristic or oleic acids yielded highly stable prodrugs with decreased IC50 and long hydrolysis half-lives of more than a month. Similarly, modifying indinavir with oleic acid yielded a stable prodrug with a hydrolysis half-life of 24 days. However modifying indinavir with myristic on C-8 hydroxyl group yielded a produrg that only showed 3-fold decrease in efficacy [123, 127]. This is critical to note because same modification when targeted to the internal hydroxyl group on C-14 yielded a highly stable prodrug with more than 400-folds increases in the IC50. By the same token, carbamate modifications on the internal hydroxyl group on indinavir, nelfinavir and saquinavir yielded stable prodrugs that showed significant increase in the IC50 with increments ranging from 400 to more than

5200-folds [126]. It's suggested that the significant changes in potency due to the hydroxyl group's role in peptidomimetic noncleavable transition state responsible for the drug's activity against the viral protease therefore blocking that group interferes with drug interactions with the enzyme [126]. On the other hand, ester modifications to the internal hydroxyl groups of these PIs yielded prodrugs with IC50 increases by only 1- to 26-fold which could be due to the reversible and labile nature of ester bonds making the prodrugs hydrolysable to the parent active moiety. Hence, utilizing this knowledge and these strategies we can synthesize DRV prodrugs that may show extended half-lives without sacrificing potency. Development of long-acting stable DRV prodrug nanoformulations could potentially lead to infrequent drug administration and improve drug cell penetrance and tissue biodistribution. To this day, no long-acting injectables of protease inhibitors are available.
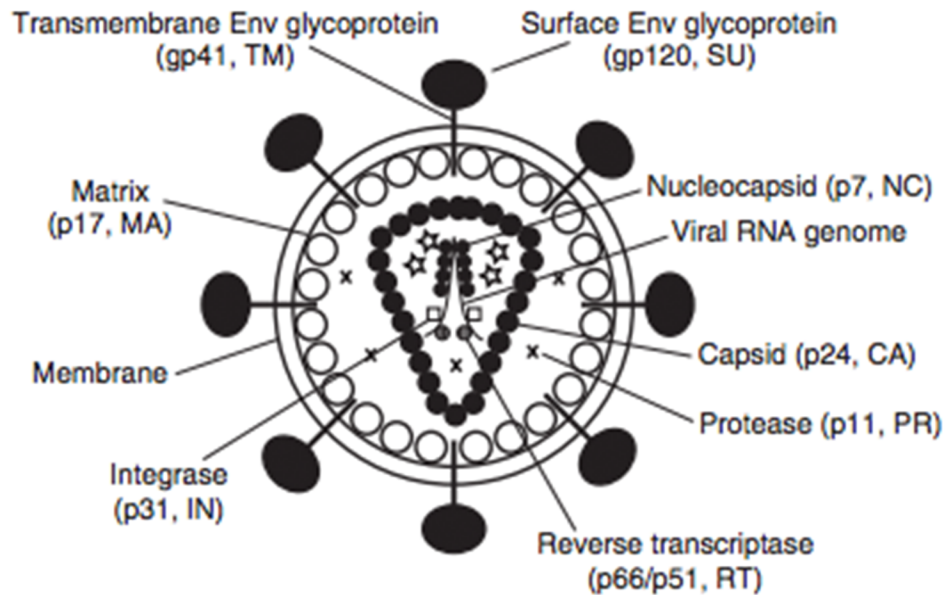
Figures

Figure 1. 1 HIV-1 Structure*

Outer HIV-1 membrane is decorated with surface and transmembrane envelope glycoproteins such as gp120 and gp 41 that are the main keys responsible for viral attachment to CD4 for entry and fusion into host cell. Viral matrix includes the viral proteins and capsid. The capsid is composed of p24 antigens and encases the nucleocapsid proteins complexed with two positive sense RNAs and other proteins for transcription initiation and integrations such as reverse transcriptase and integrase.

*Adapted with permission from Catherine S. Adamson and Eric O. Freed: Human Immunodeficiency Virus Type 1 Assembly, Release, and Maturation. Advances in Pharmacology (2007) pp. 347-387. (Copyright Elsevier)
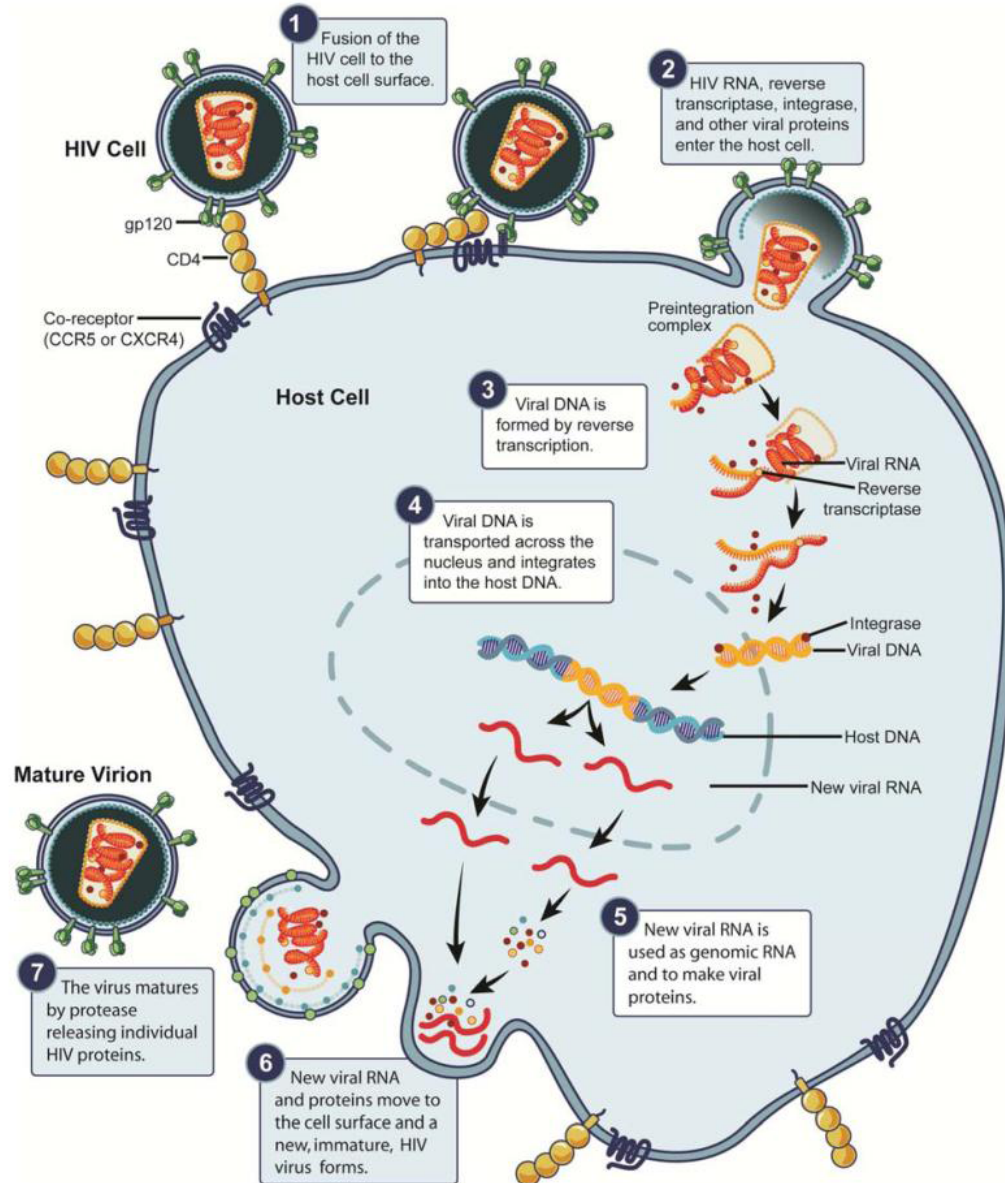
Figure 1. 2 HIV-1 Life Cycle[φ]

Briefly, viral cycle starts with entry of the virus (1) through the binding of CD4 on the host cells and coreceptor (CXCR4 or CCR5). Upon entry the virus uncoats (2) and empties its contents from viral RNA and initiating proteins inside host cell. Viral RNA is then (3) reverse transcribed into the viral DNA and transported into the nucleus where it is integrated (4) into the host genome by the action of integrase. New viral mRNA is produced and translated in the cytoplasm producing new viral proteins (5). New viral genomic RNA and proteins move to cell surface to assemble (6) and bud from the cell where the final maturation (7) takes place through the action of the viral protease.

Figure 1. 3 LASER ART[Σ]

(A) Schematic illustrates the main difference between regular NanoART and the recently coined LASERT ART defined in the hydrophobic and lipophilic modifications to the native drug followed by the nanoformulations techniques used in NanoART. (B) Prodrug strategy allows the conjugation of a reversible promoity to the parent drug, which increases drug's hydrophobicity and lipophilicity. This improves drug permeability inside cells where the promoity is eventually cleaved through the action of esterases to release the free drug where it can induce its therapeutic effect.

Chapter 2: Synthesis and Characterization of Long-Acting Darunavir Prodrugs

Abstract

Antiretroviral therapy (ART) has improved the quality of life in patients infected with HIV-1. However, viral suppression at anatomical sites of infection remains a formidable task. This is further complicated by adverse side effects and poor adherence to lifelong therapy that leads to emergence of drug resistant viral strains. Thus, the need for cellular and tissue targeted ART delivery platforms with potential for less frequent dosing cannot be overstated. Herein, we describe two long-acting prodrug formulations of darunavir (DRV), a potent protease inhibitor and component of HIV-1 treatment regimen. Two classes of DRV prodrugs; M1DRV and M2DRV were synthesized and stabilized into long-acting slow effective release (LASER) aqueous nanosuspensions designated NM1DRV and NM2DRV, respectively. NM2DRV was found to exhibit enhanced intracellular prodrug levels with sustained retention and efficacy for 30 days compared to drug washout within hours for native DRV formulation (NDRV) and 15 days for NM1DRV following single treatment of monocyte derived macrophages (MDM) and CD4+ T cells at equivalent drug concentrations. Pharmacokinetics of NM1DRV and NM2DRV administered to mice demonstrated sustained drug levels in blood and tissues with higher concentrations of the prodrugs observed for 30 days. These data, taken together, support the idea that extended release of DRV with sustained antiretroviral responses could be realized through lipophilic prodrug formulations.
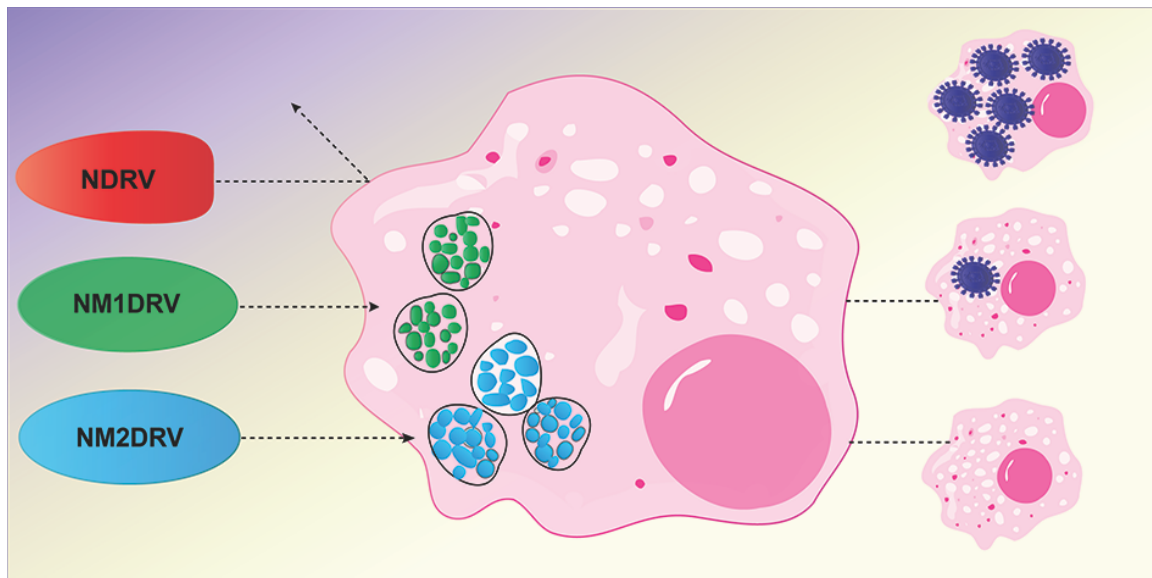
Graphic 1: Nanoformulation of native drug, DRV, does not achieve high uptake into cells resulting in HIV-1 infection in antiretroviral efficacy studies. Modified DRV nanoformulations, M1DRV and M2DRV, show higher uptake and retention inside cells leading to viral inhibition. M2DRV shows longer and higher retention inside MDM resulting in longer sustained antiretroviral activities.

Introduction

While antiretroviral therapy has revolutionized human immunodeficiency virus type one (HIV-1), treatment and preventative drug regimens require strict adherence to daily dosing. With substantive extensions in longevity and quality of life, ART still remains associated with a number of adverse drug reactions, poor compliance and drug resistance[128-130]. Comorbid events include stigma of infection, depression and other neuropsychiatric disorders associated with or without substance abuse. These all negatively affect regimen adherence[131, 132]. These events ultimately lead to the emergence of virus drug resistance mutations[133]. Moreover, associated acquired opportunistic infections and drug-drug interactions commonly emerge[134, 135]. These affect clinical outcomes such as viral transmission and disease progression impeding ART virologic suppression goals set by United Nations Programme on HIV and AIDS (UNAIDS) and the US national HIV/AIDS strategic plan[136-139]. Such complications have set the stage for the development of long-acting (LA) ART[77, 140-142].

Recent surveys support an immediate need for LA ART for HIV-1 infected patients including those who would prefer the ease of extended release regimens compared to taking daily pills[141]. Thus currently in development are monthly injectables of cabotegravir and rilpivirine (CAB and RPV) for treatment and prevention of viral infection[140, 143]. These suffer limitations that include large injection volumes, injection site reactions and restricted access to tissue compartment sites of viral replication[75, 140, 143]. Moreover, most antiretroviral drugs (ARVs) used in combination therapy have either poor physicochemical properties or require high doses limiting their potential reformulation into long-acting therapies. To overcome such obstacles we transformed ARVs into lipophilic and hydrophobic prodrugs in our laboratory[75, 78-80, 86]. These long-acting slow effective release ART (LASER ART) are surfactant stabilized nanocrystals with enhanced drug loading and tissue penetrance properties. Indeed, each of our LASER ART formulations were designed to facilitate rapid diffusion across physiological barriers allowing sustained therapeutic drug concentrations at sites of viral replication[75, 78-80, 86, 144]. With these advances established, we now describe the development of two LA DRV prodrug formulations with extended apparent drug half-lives and improved antiretroviral activities.

DRV is a second-generation unnatural peptidomimetic PI used in combination ART for treatment of HIV-1 infection[89, 102]. Compared to other approved PIs, DRV has a higher genetic barrier to resistance with potent antiviral activity against multidrug resistant viral strains[93]. However, limitations of DRV use include its short half-life and restricted access to cellular and tissue reservoirs of infection. Moreover, DRV and other PIs require high doses and pharmacokinetic boosting agents increasing the potential for secondary toxicities[121]. Thus, there is an immediate need to develop improved means for delivery of these medicines. One strategy is utilizing prodrugs to extend the half-life and biodistribution of the agent. While such prodrug approaches were previously explored in

attempts to improve ADME, none have yet to be applied to the generation of reservoir targeted LA DRV[121-124]. Prior efforts included, but were not limited to, carrier-mediated drug delivery approaches that incorporate amino acids to minimize p-glycoprotein efflux and mitigate first pass metabolism[121, 145]. Notably, extensive prodrug efforts have previously led to development and approval of fosamprenavir, a phosphorylated water-soluble prodrug of amprenavir[125]. Various fatty ester prodrugs of indinavir and saquinavir have been described but are significantly less potent compared to the parent drugs[122]. Overall, the reported prodrug and formulation approaches sought to improve aqueous solubility of native drugs and the few lipophilic ester modifications made had proven limitations[120, 122, 123]. Specifically, PI prodrug designs were exclusively focused on modifications of the free hydroxyl group and such attempts have resulted in a marked loss of antiviral activity with comparable half-lives to that of parent drugs[120, 126, 127]. Thus, LA delivery systems for PIs have remained elusive. Based on extensive prior works from our laboratory on LASER ART platforms we sought to transform DRV into LA nanoparticles. We reasoned that conversion of DRV into prodrugs was not only feasible and economical but also a much faster strategy for overcoming ADME and formulation challenges associated with the parent drug. Lipophilic **M1DRV** and **M2DRV** ester prodrugs were created by covalent linkage of hydrolysable fatty acid promoieties to functional groups present in the parent drug. These chemical modifications improved physicochemical properties of the modified compounds compared to the parent drug, thereby enabling transformation of DRV into LA nanosuspensions with improved intracellular and tissue drug accumulation and sustained antiretroviral activities (Figure 2.1).

Experimental Section

Reagents

Darunavir (DRV) was purchased from Boc Sciences (Shirley, NY). Anhydrous pyridine, dichloromethane (CH_2Cl_2), chloroform ($CHCl_3$), dimethyl sulfoxide (DMSO), *N,N*-dimethylformamide (DMF), deuterated chloroform ($CDCl_3$), triethylamine (Et_3N), diethyl ether, tetrahydrofuran (THF), triethylsilane (Et_3SiH), pluronic F127 (P407), 4-dimethylaminopyridine (DMAP), stearoyl chloride, myristoyl chloride, zinc chloride, paraformaldehyde (PFA), sodium iodide (NaI), sodium hydride (NaH), potassium iodide (KI), hexanes, ethyl acetate, ciprofloxacin, 3-(4,5-dimethylthiazol-2-yl)-2,5-diphenyltetrazolium bromide (MTT), and 3,3′-diaminobenzidine (DAB) were purchased from Sigma-Aldrich (St. Louis, MO). Benzyl chloroformate was purchased from MilliporeSigma (Burlington, MA). Live/Dead Fixable Green Dead Cell Stain Kits were purchased from Thermo Fisher Scientific (Waltham, MA). LC-MS grade methanol, acetonitrile, LC-MS-grade water, cell culture grade water (endotoxin-free), gentamicin, ammonium formate, bovine serum albumin (BSA), TRIzol reagent and Triton X-100 were purchased from Fisher Scientific (Hampton, NH). Palladium, 10% on activated carbon, was purchased from STREM Inc. (Newburyport, MA). All chemical synthesis reactions were performed under a dry argon atmosphere. Flash column chromatography was performed on 32-63 μm flash silica gels from SiliCycle Inc. (Quebec, Canada). Reactions were monitored by thin-layered chromatography on precoated silica plates (250 μm, F-254 from SiliCycle Inc.). The compounds were visualized by UV fluorescence or stained with potassium permanganate. Heat-inactivated pooled human serum was purchased from Innovative Biologics (Herndon, VA). Dulbecco's Modification of Eagle's Medium (DMEM) was purchased from Corning Life Sciences (Tewksbury, MA). CEM CD4+ T cells were obtained from the National Institute of Health. Monoclonal mouse anti-human HIV-1p24 (clone Kal-1), monoclonal mouse anti-human leukocyte antigen

(HLA-DP/DQ/DR; clone CR3/43), and the polymer-based HRP-conjugated anti-mouse EnVision+ secondary were purchased from Dako (Carpinteria, CA). Alexa Fluor 700 mouse anti-human CD3, FITC mouse anti-human CD45, APC mouse anti-human CD4, BV421 mouse anti-human CD8, PE mouse anti-human CD14, APC mouse anti-human CD4 and PE-Cy5 mouse anti-human CD19 from BD Biosciences (San Jose, CA).

Methods

Prodrug synthesis and physicochemical characterization

To synthesize M1DRV, DRV (0.5 g, 0.9130 mmol, 1 equivalent) was dried from anhydrous toluene (20 mL), dissolved in anhydrous THF (10 mL), cooled to -78°C, followed by slow addition of NaH (0.07303 g, 1.826 mmol, 2 equivalents) and allowed to stir for 15 minutes under an argon atmosphere. A solution of iodomethyl tetradecanoate (0.58121 g, 1.3694 mmol, 1.5 equivalents) was prepared as previously described[146] and added to the precooled DRV solution. The reaction mixture was gradually warmed to room temperature and stirred for 48h after which M1DRV was isolated by silica column chromatography purification using 2:1 ethyl acetate-hexanes to form a colorless powder (84% yield). ^{1}H NMR (500 MHz, CDCl$_3$): 7.59 (br, 2H), 7.17-7.35 (m, 6H), 6.66-6.78 (m, 1H), 5.67 (dd, J = 20.5, 4.9 Hz, 1H), 5.55 (dd, J = 32.9, 5.8 Hz, 1H), 5.25-5.40 (m, 1H), 4.88-5.22 (m, 2H), 4.73 (br, 1H), 4.12-4.23 (m, 1H), 3.63-4.10 (m, 3H), 3.45-3.59 (m, 1H), 3.36 (app. d, J = 11.4 Hz, 1H), 2.80-3.20 (m, 4H), 2.63-2.75 (m, 1H), 2.60 (t, J = 12.5 Hz, 1H), 2.25-2.45 (m, 2H), 1.85-1.97 (m, 1H), 1.50-1.74 (m, 4H), 1.20-1.40 (m, 20H), 0.80-1.05(m, 9H). ^{13}C NMR (125 MHz, CDCl$_3$): δ 173.1, 155.1, 137.7, 129.6, 129.2, 128.3, 126.4, 113.9, 112.3, 109.4, 81.7, 73.5, 73.4, 73.3, 71.4, 69.6, 58.9, 53.7, 45.3, 36.3, 34.2, 33.6, 31.8, 29.6, 29.5, 29.4, 29.3, 29.2, 29.1, 29.0, 26.9, 25.9, 24.6, 22.6, 20.3, 20.2, 20.1, 19.9, 14.1. MS-ES+ (m/z): calcd. for C$_{42}$H$_{65}$N$_3$O$_9$S, 787.44 (100%), 788.45 (45.4%), 789.45 (10.1%); found, 811.05 [M+Na+]. M2DRV was

synthesized in a three-step process that involved protection of the primary amine in the parent drug using a carbobenzoxy (Cbz) group, coupling to stearoyl chloride and a final Cbz deprotection to yield the desired product as a colorless powder. Specifically, DRV (1.0 g, 1.8256 mmol, 1 eq.) was dried from anhydrous pyridine (10 mL) and dissolved in a mixture of anhydrous THF (10 mL) and DMF (10 mL) under an argon atmosphere. The reaction mixture was cooled to 0°C, followed by drop wise addition of Et₃N (254 µL, 1.8256 mmol, 1 eq.) then benzyl chloroformate (388 µL, 2.7389 mmol, 1.5 eq.) and left to stir for 48h under protection from light. The desired protected Cbz-DRV was isolated by silica column chromatography purification eluting with 1:1 ethyl acetate-hexanes. The Cbz-DRV was dissolved in 15 mL of DMF and cooled to 0°C followed by addition of 1.5 equivalents of 4-dimethylaminopyridine and 2 equivalents of Et₃N. The mixture was stirred for 15 minutes after which 1.5 equivalents of stearoyl chloride were added and warmed to 45°C over 24h. The formed Cbz-M2DRV was isolated by column chromatography and subjected to catalytic hydrogenolysis using 10% palladium on activated carbon and 20 equivalents of Et₃SiH in a mixture of methanol and chloroform (1:1) solvents. After reaction completion, the mixture was filtered through a pad of celite to remove carbon followed by further purification by column chromatography eluting with a mixture of 2:1 ethyl acetate-hexanes to isolate M2DRV as a colorless powder. ^{1}H NMR (500 MHz, CDCl₃): 7.58 (d, J = 8.3 Hz, 2H), 7.18-7.34 (m, 7H), 6.70 (d, J = 4.8 Hz, 2H), 5.65 (d, J = 4.8 Hz, 1H), 5.17 (br, 1H), 5.10 (d, J = 9.0 Hz, 1H), 5.02 (dd, J = 13.9, 6.9 Hz, 1H), 4.21-4.39 (m, 1H), 3.98 (t, J = 7.8 Hz, 1H), 3.82 (t, J = 7.6 Hz, 1H), 3.76 (app. t, J = 7.7 Hz, 1H), 3.67 (dd, J = 15.8, 8.9 Hz, 1H), 3.53 (dd, 1H J = 14.8, 5.3 Hz, 1H), 3.11 (app. d, J = 10.7 Hz, 1H), 2.93-3.09 (m, 2H), 2.82-2.92 (m, 1H), 2.65-2.79 (m, 2H), 2.22-2.40 (m, 2H), 1.93 (app. t, J = 6.3 Hz, 1H), 1.50-1.70 (m, 6H), 1.20-1.38 (m, 28H), 0.81-0.95 (m, 9H). ^{13}C NMR (125 MHz, CDCl₃): δ 173.3, 155.1, 150.7, 137.4, 129.5, 129.2, 128.4, 126.7, 126.6, 113.9, 109.3, 73.9, 73.3, 70.8, 69.6, 57.7, 53.5, 49.3, 45.4, 36.9,

34.2, 31.8, 29.7, 29.6, 29.5, 29.4, 29.3, 29.2, 29.1, 26.8, 25.7, 24.6, 22.6, 20.2, 20.2, 19.9, 14.1. MS-ES+ (m/z): calcd. for $C_{45}H_{71}N_3O_8S$, 813.50 (100%), 814.50 (48.7%), 815.50 (11.6%); found, 837.14 [M+Na+]. Nuclear magnetic resonance (^{1}H-NMR and ^{13}C-NMR) spectra were recorded on a Varian Unity/Inova-500 NB (500 MHz; Varian Medical Systems Inc., Palo Alto, CA, USA. Fourier Transform Infrared Spectroscopy (FTIR) was performed on a Spectrum Two FT-IR spectrometer (PerkinElmer,Waltham, MA, USA). LC-MS quadrupole infusion was performed on a Waters TQD (Boston, MA) to confirm the desired molecular ion peaks of M1DRV and M2DRV. Solubilities of DRV, M1DRV, and M2DRV were determined in water. Briefly, homogeneous saturated solutions of each compound were mixed at room temperature for 24 hours and centrifuged at 17,000 x g for 10 minutes to pellet insoluble drug. The amount of drug in the supernatants was quantified by multiple reaction monitoring (MRM) on a liquid chromatography tandem mass spectrometry (LC-MS/MS) system comprised of an Waters ACQUITY ultra-performance liquid chromatography (UPLC) system (Waters, Milford, MA) coupled to a triple quadrupole mass spectrometer with electrospray ionization (ESI) source (Waters Xevo TQ-XS).

Prodrugs stability in different pH
Prodrugs' stabilities were evaluated in different pH of 1, 7 and 11. Stocks of M1DRV or M2DRV with concentrations of 1-2 mg/mL were prepared in MeOH. For stability in acidic pH (pH 1) the drugs were incubated separately in a solution of pH adjusted 0.1 M HCl. Similarly, drugs were incubated in pH adjusted 0.1 M NaOH (pH 11) to test stability in basic environments. Finally, incubation in water (pH 7) determined stability in neutral pH. Triplicate samples of both prodrugs were kept on a shaker either at room temperature (25°C) or incubated at 37°C. Aliquots were collected from the samples at different time points; 8, 24, 72, 120, 168, and 336 hours. Samples were stored at -80°C until drug quantitation where the samples were dried using a speed vacuum, then the pellets were

dissolved in 100 µL MeOH. Drug concentrations/stabilities were determined from samples using Waters Alliance e2695 HPLC Separations Module.

Prodrugs stability and cleavage profiles in plasma
To evaluate plasma stability of M1DRV and M2DRV, 100 µL of plasma samples from mouse or rat were spiked with 1 µM M1DRV or M2DRV. Free prodrugs stocks were prepared in dimethyl sulfoxide (DMSO). Triplicate samples were kept on a shaker at 37°C. At various time points (0, 2, 6, 24, and 48), 1 mL of MeOH was added to each tube and vortexed for 3 minutes to stop enzymatic cleavage, then stored at -80°C until drug quantitation. Negative controls were used to normalize for non-specific binding. Specifically, 100 µL ice cold plasma was added to 1mL MeOH followed by addition of the prodrugs. Additional negative controls were prepared using heat-inactivated plasma to determine whether drug hydrolysis was due to enzymatic activity or non-enzymatic hydrolysis. At various time points, 1mL MeOH was added to the samples. Samples were then vortexed for 3 minutes and centrifuged at 15,000 g for 15 minutes. For UPLC-MS/MS sample prep to quantify prodrugs, 40 µL of supernatant was added to 10 µL of internal standard (IS) and 50 µL of 75% MeOH. For DRV quantitation, 50 µL of sample was added to 10 µL of IS and 40 µL of water. Samples were vortexed and plated for UPLC-MS/MS analyses.

Nanoformulations of DRV, M1DRV and NM2DRV
Poloxamer 407 (P407) coated DRV (NDRV), M1DRV (NM1DRV) and M2DRV (NM2DRV) nanoformulations were produced by high-pressure homogenization (Avestin EmulsiFlex-C3; Avestin Inc, Ottawa, ON, Canada). Briefly, each compound (1% w/v) was premixed in a P407 solution (0.5% w/v in PBS) for 16h at room temperature followed by homogenization at 20,000 psi at 0°C until the desired particle size was achieved (150 – 450 nm). Particle size, polydispersity index (PDI), and zeta potential were determined by dynamic light scattering (DLS) on a Malvern Nano-ZS

(Worcestershire, UK). Drug nanoparticles were diluted in water and triplicate measurements were observed and recorded over 10 weeks to determine particles' stabilities for the translational potential of these nanoparticles in terms of shipping and storage. For animal studies, the different nanoformulations were concentrated using differential centrifugation to allow for small injection volumes during *in vivo* studies. Formulations were centrifuged and pelleted at 5,000 x g for 5 minutes. Supernatants were transferred to a new centrifuge tube and centrifuged at 20,000 x g for 20 minutes. Finally, supernatant was discarded and both pellets were suspended in a total of approximately 500 µL of PBS. Drug content in the concentrated formulations was quantified using HPLC and known standards ranging from 0 – 50 µg/mL. Nanoparticle morphologies were analyzed by FEI Tecnai G2 Spirit transmission electron microscopy (TEM) (Hillsboro, OR) using negative staining. Small volume (10 µL) of diluted nanoformulation (1 mg/mL) was applied on a formavar/silicone monoxide coated 200 mesh copper grid. Grid was left 2-5 minutes to absorb the nanoparticles. Excess sample was dried carefully using a clean filter paper and allowed to dry for 2 minutes. Pipet a drop of Nanovan negative stain on the grid and allow to stain for no longer than a minute while shielding the sample using a filter paper tent to minimize any air contaminants. Blot excess stain and allow grid to dry before viewing under TEM.

Cytotoxicity and cell viability

Effects of NDRV, NM1DRV, and NM2DRV on cell viability were assessed in human monocyte-derived macrophages (MDM) and CEM-SS CD4+ T cells. Briefly, human monocytes were isolated by leukapheresis (from HIV-1/2 and HBV seronegative donors) and purified by current centrifugal elutriation[147]. Cell were then cultured for 7-10 days in 96-well culture plates (80,000 cells/well) with Dulbecco's Modified Eagles Media (DMEM) supplemented with 10% heat-inactivated pooled human serum, 1,000 U/ml of macrophage colony stimulating factor, 1% glutamine, 10 µg/mL ciprofloxacin, and

50 µg/mL gentamicin in a 37°C in a 5% CO_2 incubator[148-150]. A stock solution of each drug nanoformulation was serially diluted in DMEM to produce drug concentrations ranging from 50-400 µM. Cells were treated for 24 hours, washed and incubated with 200 µL/well 3-(4,5-dimethylthiazol-2-yl)-2,5-diphenyltetrazolium bromide (MTT) solution (5 mg/mL) for 45 minutes. Upon MTT removal, 200 µL/well of DMSO was added and absorbance measured at 490 nm on a SpectraMax M3 plate reader with SoftMax Pro 6.2 software (San Jose, CA). Samples' absorbances were normalized to that of non-treated controls. For CEM-SS CD4+ T cell studies, the cells were seeded on round bottom 96-well culture plates at a density of 80,000 cells/mL per well in Roswell Park Memorial Institute (RPMI) media with 10% fetal bovine serum (FBS), 1% penicillin, and 1% streptomycin and treated with each nanoformulation as described for MDM. After 24 hours, cells were centrifuged at 650 x g, dispersed in PBS, centrifuged again at 650 x g, and resuspended in PBS. Excitation dye (0.1 µL) (Molecular Probes, Live/Dead Fixable Green Dead Cell Stain Kits) was added to each well. Cells were excited at 488nm and the percent dead cells determined by flow cytometery.

Evaluation of drug potency (EC50)

To evaluate drug potency, MDMs were seeded on round bottom 96-well culture plates (80,000 cells/well) and exposed to DRV, NM1DRV or NM2DRV containing media at concentrations ranging from 0.0005 nM-50 µM in tenfold dilution increments for 60 min and replaced with drug-containing HIV-1$_{ADA}$ media at a multiplicity of infection (MOI) of 0.1 infectious particles per cell. After 4 hours, infection medium was removed, and the cells were incubated an additional 10 days in the presence of the same concentration of drug prior to infection. Half media changes were done every other day. After 10 days of infection, culture media was collected for measures of HIV-1 reverse transcriptase (RT) activity[148-150]. For CEM-SS CD4+ T cells studies, the cells were cultured in suspension in 96 well plates, spun at 650 x g and re-dispersed in 100µL drug-containing media. After

60 minutes, cells were challenged with HIV-1$_{NL4-3-eGFP}$ at a MOI of 0.1 by spin-inoculation followed by incubation in drug-containing media for 2 hours. Cells were kept at 37°C in a 5% CO_2 incubator for 12 hours, after which media containing drug and FBS was added. Twenty-four hours post infection, all cells were washed twice with PBS to remove extracellular virus and drug-containing media was replaced with medium containing the same drug concentration prior to infection. Every other day, cells were centrifuged at 650 x g and resuspended in fresh drug-containing medium. Ten days post HIV-1 challenge; supernatants were collected for RT activity measurements. Antiretroviral activities were further confirmed using flow cytometry in the case of CEM-SS CD4+ T cells studies infection with the HIV-1$_{NL4-3-eGFP.}$ The EC$_{50}$ was calculated using sigmoidal 4-point logarithmic regression from RT activity using GraphPad Prism v7 (San Diego, CA).

Cell drug uptake and retention
MDM were cultured on 12-well culture plates and treated with media containing 100µM of NDRV, NM1DRV or NM2DRV [148-150]. At 2, 4 and 8 hours post treatment, media was removed and adherent cells were washed twice with PBS then scraped into 1mL PBS. Cells were counted on an Invitrogen Countess Automated Cell Counter (Carlsbad, CA), pelleted by centrifugation at 956 x g for 8 minutes. The cell pellets were reconstituted and sonicated in 100 µL methanol for 5 minutes followed by centrifugation at 20,817 x g for 5 min. For CD4+ T cell experiments, CEM-SS cell line was used[151, 152]. The cells were plated on to poly-L-lysine pre-coated cell culture plates that make it possible for them to adhere and uptake experiment was done following the same steps performed for MDM. For drug retention studies, MDM were treated for 8 hours then washed with PBS and maintained in media with half-media changes every other day until collection days. In collection days, media were collected and cells were washed with PBS then scraped and collected in PBS for drug analysis. Intracellular and supernatant drug content were analyzed using a Waters Alliance e2695 HPLC Separations Module and a Waters

Acquity H-class UPLC with a Waters Acquity QDa detector (Waters, Milford, MA). For HPLC quantitation, a Kinetex 5 µm C18 column (150 × 4.6 mm) (Torrance, CA) was used for separation using mobile phases of 55% 10 mM ammonium formate, pH 3.0/45% ACN, 80% ACN/20% 10 mM ammonium formate pH 3.0, and 90% MeOH/10% water for DRV, M1DRV, and M2DRV, respectively, with a flow rate of 1.0 mL/min and UV detection at 265 nm. For UPLC quantitation using a Waters Acquity QDa detector, an ACQUITY UPLC® BEH Shield RP18 1.7 µm analytical column (2.1mm×100mm, Waters Corp.) was used for separation using mobile phase of 60% MeOH/40% 7.5 mM ammonium formate pH 3.0 at a flow rate of 0.25 mL/min using a mass range of 50 – 600 Da and cone voltage of 12. Transmission electron microscopy (TEM) was used to image the morphology of MDM-loaded with the different drug nanoparticles. Cells were loaded with the different nanoparticles for 4 hours then washed twice with PBS. Cells were collected in PBS, centrifuged, fixed in 2% paraformaldehyde (PFA) and kept at 4°C until TEM processing.

Antiretroviral activities

To assess long-term antiretroviral efficacy, MDM were treated for 8 hours with 100 µM NDRV, NM1DRV or NM2DRV as previously described for uptake studies. After treatment, cells were washed twice with PBS and cultured in fresh media without drug followed by half-media changes every other day. At 5-day intervals from days 1 to 30 after treatment, cells were challenged with HIV-1$_{ADA}$ at a MOI of 0.1 for 16 hours. After infection, HIV-1$_{ADA}$ media was removed, cells were washed with PBS and replaced with fresh media without drug. Ten days after viral challenge culture media were analyzed for RT activity, while adherent MDM were fixed with 2% PFA and assessed for HIV-1p24 protein expression by immunocytochemistry[148-150].

Pilot NDRV, NM1DRV and NM2DRV pharmacokinetics (PK)
Male BALB/cJ mice (25 g) (Jackson Labs, Bar Harbor, ME, USA) were administered a single 50 mg/kg DRV-equivalent dose of NDRV, NM1DRV and NM2DRV intramuscularly (IM) into the caudal thigh muscle to determine PK over a month-long study to assess drug bioavailability in plasma and blood and drugs' distribution into the different tissues. Heparinized tubes were used for blood collection to obtain plasma and blood samples at days 1, 7, 14, 21, and 28 from treated mice. Tissues were collected at time points 7, 14, and 28 of the study and stored at -80°C until drug analysis. Plasma, blood and tissue samples were analyzed by LC-MS/MS to determine parent and prodrug levels.

Pharmacokinetics of NM1DRV and NM2DRV in CYP3A humanized mice
To assess the effect of an RTV boost with the modified DRVs, PK studies were done in mice with human CYP3A enzymes responsible for DRV's metabolism. Mice models used for these studies are the PXR/CAR/CYP3A4/7 tADMET (Taconic Biosciences, Inc) and PXR/CAR/CYP3A/NOG (hCYP3A-NOG developed and characterized in[153]). Only NM1DRV, with and without boost, was tested PXR/CAR/CYP3A4/7 model due to the limited number of animals. However, both NM1DRV and NM2DRV, with and without boost, were evaluated in the hCYP3A-NOG model. The humanized mice were administered 50 mg/kg DRV-equivalent dose of NM1DRV or NM2DRV intramuscularly. RTV-boosted groups were given IM boost injections of RTV nanoformulation (NRTV) on days 0, 7 and 14 of the study. Similar to the BALB/cJ PK studies, plasma and blood samples were collected in heparinized tubes on days 1, 7, 14 and 21. Tissues were collected at the end of the study and stored at -80°C until drug analysis. Plasma, blood and tissue samples were analyzed by LC-MS/MS to determine parent and prodrug levels as well as the effect of the boost on drugs' bioavailability. NRTV used for boosting was formulated and characterized as previously described[154]. Briefly 1% (w/v) RTV was suspended in a solution of 0.2% (w/v) P407 in 15 mL solution of 10 mM HEPES buffer

(pH 7.8) and was left to stir at room temperature overnight. The premix was homogenized using high-pressure homogenization (Avestin EmulsiFlex-C3; Avestin Inc, Ottawa, ON, Canada) at a pressure between 15,0000 – 20,000 psi at 0°C until the desired particle size was achieved. After homogenization, the nansuspension was differentially centrifuged as for the DRV formulations and diluted in PBS. Particle size, polydispersity index (PDI), and zeta potential were determined by dynamic light scattering (DLS) on a Malvern Zetasizer Nano-ZS (Worcestershire, UK).

NDRV, NM1DRV and NM2DRV pharmacodynamics (PD)

In a pre exposure prophylaxis (PrEP) PD study, drugs nanoformulations' antiretroviral activities to protect from viral infection were evaluated in NSG (NOD/scid-IL-2Rγc^{null}) mice-reconstituted with CD34+ human hematopoietic stem cells at birth. Before treatment, mice were assessed for human CD45+, CD3+, CD4+, CD8+, and CD14+ lymphocytes by flow cytometry to confirm the integrity of the model. Mice were administered a single 50 mg/kg DRV-equivalent dose of NDRV, NM1DRV or NM2DRV IM. One week post drug treatment, mice were challenged with 2 x 10^4 $TCID_{50}$ of HIV-1$_{ADA}$ (100-200 µL) by an intraperitoneal injection. Plasma samples were collected one week after infection for viral load determination. At the end of the study, viral loads were determined in plasma and HIV-1 gag RNA levels in the collected spleens were measured by reverse transcription polymerase chain reaction (RT-PCR) to further assess the antiretroviral efficacy of the treatments[78]. Plasma and tissues (lymph nodes, liver, lungs, kidneys, gut and bone marrow) were collected for plasma drug quantitation by LC-MS/MS, human T cell counts, viral load and HIV-1 p24 expression.

Drug quantitation by LC-MS/MS

Briefly, 25 uL of blood samples from mice were immediately mixed with 1 ml ice-cold ACN, and spiked with internal standard (a fourteen carbon fatty-acid modified dolutegravir prodrug (MDTG)[78] and d3-dolutegravir (DTG-D$_3$) at 500 ng/ml each, final

concentration of 50 ng/ml). Samples were then vortexed, and centrifuged at 17,000 x g for 10 minutes. The resulting supernatants were dried under vacuum, reconstituted in 100 μL, and injected for separate LC/MS/MS analysis. For DRV analysis, 45 µL supernatant was mixed with 30 µL of H_2O and for prodrug analysis 35 µL supernatant was mixed with 35 µL of 85% MeOH. Finally 10 µL of samples were injected for separate drug and prodrug LC/MS/MS analyses. Blood and plasma standards were extracted at a final concentration of 0.5-500 ng/mL. For tissue sample preparation, approximately 20-100 mg of spleen, lymph nodes, and liver were weighed and homogenized in 5–20x dilutions of 90% MeOH. 100 µl of the homogenates were mixed with the same internal standards as blood, vortexed, and centrifuged. Supernatant were collected for LC/MS/MS analysis. For DRV analysis, 60 µL of supernatant was mixed with 40 µL of 50% MeOH and for prodrug analysis, 60 µL supernatant was mixed with 40 µL of 85% MeOH before LC/MS/MS analyses. Tissue standards were extracted at a final concentration of 0.5-500 ng/mL. DRV and prodrugs were quantified by injection onto a LC/MS/MS consisting of a Waters ACQUITY H class UPLC coupled to a Waters Xevo TQ-Smicro mass spectrometer (Waters Corp., Milford, MA, USA) with an ESI source in positive mode. Analyte separation was achieved on an ACQUITY UPLC® BEH C18 1.7 µm analytical column (2.1mm×50mm, Waters Corp.). Mobile phase A was composed of 7.5mM ammonium formate in water (MS grade, Fisher), pH adjusted to 3.0 with formic acid (MS grade, Fisher). Mobile phase B was 100% methanol (MS grade, Fisher). For the prodrugs, the isocratic program was held at 20% A for 10 minutes with the flow rate at 0.28 mL/min. For DRV, the isocratic program was held at 40% A for 4.5 minutes. To wash the column, the percentage was decreased to 5% A, held for another minute and then ramped back for equilibration to 40% A for 2 minutes. The flow rate was 0.25 mL/min. On the mass spectrometer, the MRM transitions, cone voltage and collision energy were optimized by direct infusion of each drug and internal standard. Transitions

for DRV were 548.00 < 112.81 m/z for quantification, while transitions 548.00< 68.89 m/z and 548.00 < 392.2 m/z were used for identity confirmation. Internal standard (DTG-d_3) was monitored at 422.84 < 129.94 m/z. Dwell time was 20 msec for each transition. Transitions for M1DRV were 758.4 < 155.93, 758.4 < 112.89 m/z and 758.4 < 602.33 m/z for quantification and identification respectively. Transitions for M2DRV were 814.52 < 155.93, 814.52 < 240.97 m/z and 814.52 < 658.44 m/z for quantification and identification respectively. The internal standard (MDTG) was monitored at a MRM transition 616.27 < 126.95 m/z. Dwell time was 25 msec for each transition.

Study Approvals

All animal studies were approved by the University of Nebraska Medical Center Institutional Animal Care and Use Committee in accordance with the standards incorporated in the Guide for the Care and Use of Laboratory Animals (National Research Council of the National Academies, 2011). Human blood cells were isolated by leukapheresis from HIV-1/2 and hepatitis seronegative donors and were deemed exempt from approval by the Institutional Review Board of UNMC.

Statistics

All data sets are presented as mean ± standard error of the mean (SEM). *In vitro* studies were performed using three biological replicates (n=3). *In vivo* studies included a minimum of 5 animals per group (n=5). For comparisons of two groups, Student's t test (two-tailed) was used. For comparison between multiple groups, one-way ANOVA with Bonferroni correction was performed. For studies with multiple time points, two-way ANOVA and Bonferroni's post hoc tests for multiple comparisons were performed. Results with $P < 0.05$ were considered significant. All data were graphed and analyzed using GraphPad Prism 7.0 software (La Jolla, CA).

Results

Synthesis and characterization of M1DRV and M2DRV

First, we synthesized DRV ester prodrugs by either derivatizing the amine (M1DRV) or hydroxyl (M2DRV) functional groups in the parent drug (Fig 2.12) using fatty acids of variable carbon chain length to form lipophilic compounds with high chemical yields after column chromatography purification (Figures 2.2 and 2.3). The chemical structures were confirmed by proton (^{1}H) and carbon (^{13}C) nuclear magnetic resonance (NMR) spectroscopy (Fig 2.4, 2.5, 2.6, and 2.7). Specifically, broad peaks at 0.9 and 1.26 ppm in the ^{1}H NMR spectra of both prodrugs correspond to the terminal methyl and methylene protons of the fatty esters (Fig 2.4 and 2.6). Additional peaks from the carbonyl groups at 173 ppm and aliphatic carbon atoms from the fatty acids (14.1 and 29.3 ppm) in the ^{13}C-NMR spectra further confirmed M1DRV and M2DRV prodrug synthesis (Fig 2.5 and 2.7). Further prodrug characterization by Fourier transform infrared (FTIR) spectroscopy showed absorption bands at 2917, 2915 and 2848 cm^{-1} representing asymmetric and symmetric C-H stretches in the long chain fatty acids (Fig 2.8 and 2.9). Infusion of each prodrug into a Waters Xevo TQ-Smicro triple quadrupole tandem mass spectrometer showed the desired molecular ion peaks at 811.05 [M+Na+] and 837.14 [M+Na+], for M1DRV and M2DRV, respectively (Fig 2.10 and 2.11). The water solubility of the prodrugs was at 212 ng/mL (M1DRV) and 130 ng/mL (M2DRV) compared to 150 ug/mL for the parent drug (Fig 2.13). The 700-fold decrease in aqueous solubility for the two prodrugs confirmed their hydrophobicity as conferred by the lipid conjugates. Prodrugs' stability was measured in different pH at 25 and 37°C where M1DRV showed most stability in pH 7 in both temperatures (Fig 2.14). Similarly M2DRV showed stability in pH 7 and also pH 1 for both temperatures (Fig 2.15). The stability of the prodrugs was determined in plasma of mice and rats. Incubation of the prodrugs in plasma resulted in a decline in prodrug concentrations by more than 45 %

over 24 h (Fig 2.16 and Fig 2.17). In both plasma matrices, M1DRV and M2DRV concentrations declined over time and levels of DRV cleaving from the prodrugs were detected at increasing concentrations. Parallel studies in heat inactivated plasmas showed no decrease in prodrug concentrations or formation of DRV indicating that the compounds are activated enzymatically through ester bond cleavage (Fig 2.18).

Formulation and Characterization of NM1DRV and NM2DRV
Poloxamer 407 (P407) stabilized native drug (NDRV) and prodrug nanoparticles (NM1DRV and NM2DRV) were produced by high-pressure homogenization with drug encapsulation efficiencies of 57, 74 and 85% for NDRV, NM1DRV and NM2DRV, respectively. The NDRV, NM1DRV and NM2DRV nanoparticles exhibited uniform particle sizes of 384 ± 10, 322 ± 7 and 149 ± 2 nm, narrow polydispersity indices (PDI) of 0.27 ± 0.01, 0.26 ± 0.01 and 0.28 ± 0.01, and zeta potentials of -7.78 ± 0.36, -7.03 ± 0.02, and -1.74 ± 0.09 mV, respectively, and remained stable at 4°, 25° and 37°C for 13 weeks (Fig 2.19, 2.20, 2.21). Notably, concentrated formulations for animal injections remained stable for 17 weeks at 4°C (Fig 2.22 and 2.23). Nanoparticle morphologies were examined by transmission electron microscopy (TEM). NDRV and NM2DRV exhibited uniform rod-shaped morphologies, while NM1DRV showed spherical/globular morphologies (Fig 2.24), all with diameters in the nanometer range (150 – 450 nm). Physicochemical and particle stabilities supported further preclinical development of the prodrug formulations.

Cytotoxicity and efficacy of NM1DRV and NM2DRV
Toxicity of the prodrug nanoformulations in MDM was assessed by 3-(4,5-dimethylthiazol-2-yl)-2,5-diphenyltetrazolium bromide (MTT) assay for mitochondrial function. Similarly, toxicity of the different drug nanoformulations was determined in CEM CD4+ T cells by MTT as well as Live/Dead Fixable Dead Cell Stain Kits. No adverse effects on cell vitality were observed in MDM (Fig. 2.25) or CEM-SS CD4+ T cells (Fig

2.26) after 24h of incubation with concentrations up to 400 µM of drug nanoformulations. Given the hydrophobic nature of the two prodrugs, homogenous nanosuspensions of the prodrug with enhanced apparent aqueous solubility were employed for efficacy studies. The amine modified ester prodrug formulation of DRV (NM1DRV) demonstrated comparable antiretroviral activity to native DRV formulation in human MDM and CEM CD4+ T cells. Modification of the hydroxyl functional group in DRV to form NM2DRV nanoparticles resulted in a 10-fold loss in activity. Nevertheless, the half maximal effective concentration (EC_{50}) of NM2DRV against HIV-1_{ADA} in MDM and CD4+ T cells was in the nanomolar range and the formulation exhibited long-term efficacy when compared to native drug or M1DRV formulations. EC_{50} values of the free DRV and M1DRV in MDM were 20.3 and 26.2 nM respectively. However, because of the hydrophobic nature of M2DRV, the drug was precipitating in media therefore it was necessary to nanoformulate M2DRV to form a suspension that was capable of cell penetration highlighting the significance of the nanoformulations. The EC_{50} values for NDRV, NM1DRV and NM2DRV in MDM were 20.5, 19.1 and 260 nM (Fig 2.27), respectively. Efficacies of free drugs were also measured in CEM-SS CD4+ T cells where EC_{50} of DRV and MDRV values were 1.5 and 2.6 nM, respectively. Similarly EC_{50} of the nanoformulations were assessed; NDRV (1.48 nM) and NM1DRV (0.97 nM) exhibited comparable activity in CEM-SS CD4+ T cells, while NM2DRV (18.7 nM) showed decreased activity compared to native DRV formulation (Fig 2.28). The observed antiviral activities for NM1DRV and NM2DRV are likely linked to improved cellular drug uptake and variable prodrug activation rates in HIV target cells. However, unlike M1DRV that hydrolyzes back to DRV inside cells, M2DRV was found to be hydrolytically stable, suggesting a probability that the prodrug could be intrinsically active. Overall, these data suggest that both prodrug formulations could facilitate long-lasting antiretroviral efficacy.

Uptake of NM1DRV and NM2DRV in MDM and CD4+ T cells

Long acting stable DRV prodrug nanoformulations could affect drug cell penetrance and tissue biodistribution. We therefore evaluated DRV nanoparticle interactions using both MDM and CEM-SS CD4+ T cells. These were measured in parallel studies after a single exposure to equivalent concentrations of drug formulations followed by quantitation of cellular concentrations of native drug and prodrugs. Both NM1DRV and NM2DRV were readily taken up in MDM, with concentrations increasing to peak levels at 24 hours (Fig 2.29). At 24 hours, intracellular drug concentrations were 126 nmol/10^6 cells and 74 nmol/10^6 cells for NM1DRV and NM2DRV, respectively, more than 500-fold higher than NDRV uptake. Intracellular drug levels remained less than 0.4 nmol/10^6 cells over 24 hours after NDRV treatment. The amount of DRV formed from M1DRV was 2.8 nmol/10^6 cells at 24h, a >8-fold significant enhancement compared to peak drug levels after NDRV treatment (0.31 nmol/10^6 cells). Levels of DRV cleaving from M1DRV intracellularly were significantly more than levels of DRV from NDRV at all time points ($^{\wedge\wedge\wedge\wedge}P < 0.0001$) (Fig 2.29). Similarly, levels of M1DRV were higher than M2DRV levels at all time points (****$P < 0.0001$). Moreover, DRV formation from M2DRV was consistently at the limit of detection, suggesting that the prodrug was protected against intracellular hydrolysis. Similarly, drug uptake performed in CEM-SS CD4+ T cells was rapid for NM1DRV and NM2DRV. Intracellular peak drug levels for NM1DRV and NM2DRV treatments were 71 and 49 nmol/10^6 cells, respectively (Figure 2.30). Levels of M1DRV were higher than M2DRV intracellularly at 8 hours (***$P = 0.0007$) and 24 hours (****$P < 0.0001$). In contrast, NDRV treatment did not produce detectable cell drug concentrations at any time point. Taken together, these findings demonstrate formulation stability and rapid prodrug uptake in HIV-1 target cells. Intracellular nanoparticle uptake was further confirmed by TEM (Fig 2.31). After 4-hours of treatment, both NM1DRV and NM2DRV demonstrated significant nanoparticle accumulation in macrophages

compared to NDRV. The electron micrograph images corroborate our prior findings on nanoformulated antiretroviral drug trafficking and storage in endosomal compartments[79, 155].

Retention and antiretroviral activities of NM1DRV and NM2DRV

M1DRV and M2DRV prodrugs were retained within macrophages for 14 and 31 days, respectively, further suggesting their extended release potential (Fig 2.32). Prodrug levels retained by MDM fell to 0.10 nmol/10^6 cells at two weeks for NM1DRV, while NM2DRV treatment exhibited prodrug concentrations of 25.5 nmol/0^6 cells at day 31 (Fig 2.32). Levels of M2DRV retained were significantly higher than M1DRV levels from 1- to 4- weeks of the retention study (P < 0.0001). However, drug from NDRV was not detected in MDM within hours of treatment. Drug released from MDM into culture media showed a burst release followed by rapid decline of M1DRV compared to low but steady concentrations of M2DRV during the 31-day observation period (Fig 2.33), presumably due to slow intracellular dissolution of NM2DRV nanoparticles. Overall, these data sets suggest that transformation of DRV into lipophilic prodrugs could facilitate creation of long-acting and slow-release formulations for efficient intracellular drug delivery. To assess long term intracellular antiretroviral responses, MDM were treated with NDRV, NM1DRV or NM2DRV at equimolar concentrations for 8 h, followed by drug washout and HIV-1$_{ADA}$ challenge at five-day intervals for a period of 1 to 30 days. In cells treated with NM2DRV no HIV reverse transcriptase (RT) activity was detected during the 30-day observation period (Fig 2.34). In contrast, viral breakthrough, as determined by RT activity, was observed at days 5 and 20 after treatment with NDRV and NM1DRV, respectively. Cross validation with HIV-1p24 antigen staining paralleled RT results, demonstrating complete viral inhibition for up to 30 days after a single exposure of MDM to NM2DRV and up to 15 days after a single dose of NM1DRV (Fig 2.35). These findings

demonstrate that NM1DRV and NM2DRV nanoparticles could potentially sustain therapeutic drug concentrations at cellular sites of infection.

Pharmacokinetics of NM1DRV and NM2DRV over a month

To affirm the idea that MDM and CD4+ T cell targeted lipophilic prodrug nanoformulations would achieve sustained drug levels in plasma and tissues, a preliminary pharmacokinetic study was performed in BALB/cJ male mice using 50 mg/kg DRV equivalents for all treatments. In the pilot study, plasma drug bioavailability and tissue distribution was assessed over 1 month. Plasma DRV levels from NDRV treatment group fell below the EC_{50} levels of the drug (55 ng/mL) after day 1 post injection where concentration fell rapidly from 77.2 ng/mL at day 1 to 8.7 ng/mL at day 3 and undetected at the end of the study (Fig 2.36). Similarly, plasma DRV levels cleaving from NM2DRV treatment fell below EC_{50} of the drug after 3 days post injection. DRV levels from NM2DRV treatment fell below 10 ng/mL after day 3, however DRV concentrations remained detectable at the end of the study at concentrations of 5.4 ng/mL. However, plasma DRV levels were highest from NM1DRV treatment group showing DRV levels above the EC_{50} for one-week post injection (Fig 2.36). DRV levels from NM1DRV were significantly higher than DRV levels from NM2DRV (P < 0.0001). DRV plasma levels from NM1DRV showed gradual decrease until day 29; 308.5, 107.7, 62.6, 20.4, 11.1, and 5.1 ng/mL. Moreover, blood DRV levels were assessed to determine drug depots in circulation where drug levels from NDRV fell from 116.9 ng/mL at day 1 to zero at the remaining time points. Notably, high prodrug levels were detected in the blood of these animals for NM1DRV and NM2DRV, reflecting high drug depot in circulation (Fig 2.36). NM2DRV showed highest prodrug levels in blood sustained until the end of the study at 67.7 ng/mL whereas for NM1DRV 2.1 ng/mL of prodrug was detected at day 28. DRV cleaving from NM2DRV in blood was not detected beyond day 1 (13.2 ng/mL) whereas higher DRV levels were detected from NM1DRV (Fig 2.36).

Similarly, high prodrug levels were detected in tissues; liver, spleen, and lymph nodes for both drug nanoformulation treatments (Fig 2.37 and 2.38). NM2DRV reflected higher prodrug concentrations in all three tissues especially in lymph nodes. DRV cleaving from the prodrug nanformulations was not detected in spleen or lymph nodes (Fig 2.38). In livers, DRV levels cleaving from NM1DRV were 23.7, 6.5 and 5.1 ng/g for animals sacrificed at 1, 2, and 4 weeks whereas DRV cleaving from NM2DRV was below 4 ng/g for all time points (Fig 2.37). DRV levels cleaving from NM1DRV in the liver tissues were significantly higher than those measured from NDRV and NM2DRV at the different time points (****$P < 0.0001$, ***$P = 0.0004$ and *$P = 0.0104$). More specifically, DRV from NM1DRV was highest in livers at one week indicating that the drug is cleaving faster by the esterase function than in the case of NM2DRV. Detection of high prodrugs in the case of both NM1DRV and NM2DRV confirms that the prodrugs distribute efficiently in the different tissues however they are not hydrolyzed at the same speed as concluded from the liver-DRV data (Figure 2.37).

Pharmacokinetics of NM1DRV and NM2DRV in CYP3A humanized mice
To slow down metabolism of DRV, the drug is normally administered with a CYP3A4 inhibitor, ritonavir or cobicistat. Therefore, to assess the modification effect on the drug's metabolism and need for a CYP3A4 inhibitor, appropriate humanized mice were used. This experiment was also done to enhance and boost DRV levels since in previous BALB PK, DRV levels in tissues were not detected except in the liver. The models used to test the significant of a booster carry the CYP3A4 human gene and the human transcription factors responsible for its expression; primarily pregnane X receptor (PXR) and the constitutive androstane receptor (CAR)[153, 156, 157]. Specifically, the mice models used are the PXR/CAR/CYP3A4/7 tADMET (Taconic Biosciences, Inc) and PXR/CAR/CYP3A/NOG (hCYP3A-NOG developed and characterized in [153]). The models are of different backgrounds, C57BL/6 and NOG mice, respectively, however both mice

models carry the human CYP3A4 gene. The mice were administered a single 50 mg/kg DRV equivalents doses for NM1DRV and NM2DRV, with or without repeated NRTV doses (50 mg RTV/kg). PK in the tADMET model comparing the RTV-boosted NM1DRV with the unboosted NM1DRV in humanized and control mice showed similar PK profiles to the previously mentioned BALB/cJ study. Significance of RTV boost was seen in DRV plasma levels cleaving from NM1DRV treatment at the first time point, one day post injection, in both humanized and control mice when compared to unboosted NM1DRV ($^\wedge\wedge\wedge$P = 0.0009 and **P = 0.0016) (Fig 2.39). High levels of M1DRV were detected in blood in both boosted and unboosted groups confirming a high drug depot in circulation (Fig 2.39). Interestingly, tissue M1DRV levels were significantly higher than levels in BALB/cJ mice. In BALB/cJ mice, M1DRV levels in liver start at 226.9, 63.9, and 14.8 ng/g for 1, 2, and 4 weeks, respectively (Fig 2.37). On the other hand, in humanized and B6 control mice, M1DRV levels in liver at 3 weeks ranged between 78.6 to 142.9 ng/g reflecting the significance of different mice models (Fig 2.40). The remaining tissues, spleen and lymph nodes, showed significantly higher M1DRV levels in all groups without a significant RTV effect (Fig 2.40). In hCYP3A-NOG mouse model, RTV-boosted NM1DRV and NM2DRV are tested similarly to the experimental design for the tADMET. The mice showed RTV-enhanced plasma DRV levels cleaving from both groups, NM1DRV and NM2DRV, only at day 1 post injection (Fig. 2.41) ($^\wedge\wedge\wedge\wedge$P < 0.0001 and **P = 0.0028) however the raw numbers of DRV cleaving from the boosted prodrugs were higher than the unboosted ones. In this mouse model also, blood prodrug levels were dramatically high in all groups, boosted and unboosted (Fig 2.41). Similarly, high prodrug levels were detected in the livers, spleens, and lymph nodes of these mice (Fig 2.42) for both with higher prodrug levels from NM2DRV as seen in BALB/cJ PK. Notably, in animal models, tADMET and hCYP3A-NOG, DRV levels were detected for the first time in the spleens of the mice (Fig 2.40 and 2.42). This is significant because in normal

BALB/cJ, DRV was only detected in the livers. From this study we can conclude that boosting by RTV may have an effect with these modified DRV drugs however, further studies are necessary to confirm such an observation.

Pharmacodynamics of NM1DRV and NM2DRV

Initial screening to assess prevention and efficacy of the prodrug nanoformulations in a PrEP study using CD34+ HSC humanized mice failed to show protection against the virus. Plasma viral loads (Fig 2.43) showed viral breakthrough in all treatment groups a week after infection/two weeks after treatment. In addition, HIV-1 gag RNA and DNA levels in the collected spleens measured by RT-PCR further confirming infection in all groups (Fig 2.43).

Pharmacokinetics of NM1DRV and NM2DRV

Since the daily dose of DRV for humans is 600 mg twice or 800 mg once boosted with a pharmacokinetic enhancer, PK was repeated in BALB/cJ mice using a higher dose 100 mg/kg DRV equivalents which corresponds to 488 mg in human dose to assess if higher DRV cleaving from prodrugs could be detected in tissues[88, 89]. Specifically, mice were administered a single intramuscular injection of NDRV, NM1DRV, or NM2DRV at 100 mg/kg DRV equivalents. M1DRV and M2DRV nanoformulations provided high and sustained prodrug concentrations in plasma. M1DRV concentrations in plasma were 1297.7 ng/mL at day 1 and declined to 5.6 ng/mL at day 14. Plasma DRV levels cleaving from NM1DRV treatment was significantly higher than that of NM2DRV and NDRV (****P < 0.0001 and *P = 0.0438) at 1 and 2 weeks post injections (Fig 2.44). Plasma M2DRV concentrations at day 28 were 252.4 ng/mL (Fig 2.44). Similarly, M1DRV concentrations in blood were 826 ng/mL at day 1 and declined to 5.3 ng/mL at day 28. M2DRV blood concentrations were 2890.2 ng/mL at day 1 and declined to 120.1 ng/mL by day 28 (Fig 2.44). Prodrug levels from NM2DRV were significantly higher than those from NM1DRV in the blood of these mice one-day as well as one-week post injection (<<<<P < 0.0001

and <<P = 0.0085). At day 28, levels of DRV generated from hydrolysis of M1DRV and M2DRV in plasma were 2.2 and 8.4 ng/mL, respectively. In contrast, DRV levels after NDRV treatment fell below the limit of quantitation within a day (Fig 2.44). Notably, spleen (8216.5 ng/g ± 1745.2), liver (1516.8 ng/g ± 217.2), lymph nodes (26848.7 ng/g ± 15689.5) (^^P = 0.0074 higher levels of prodrugs from NM2DRV compared to NM1DRV in lymph nodes), and brain (12.2 ng/g ± 3.5) exhibited high prodrug concentrations at day 28 (Fig 2.46) after NM2DRV treatment while NM1DRV displayed prodrug concentrations of 55.9 ng/g ± 11.7, 11.1 ng/g ± 2.3 and 42.7 ng/g ± 6.7 in the spleen, liver and lymph nodes, respectively, with detectable DRV levels at day 28. At the end of four weeks post injections, DRV levels cleaving from NM2DRV in lymph nodes and spleens were significantly higher than those detected from NM1DRV and NDRV treatments (****P < .0001 and *P = 0.0237). In contrast, NDRV treatment displayed low drug levels in tissues at early and late time points whether with the low (50 mg/kg) or high (100 mg/kg) doses (Fig 2.37 and 2.45). High prodrug levels in tissues compared to plasma are suggestive of tissue drug depots for controlled and sustained release into blood and other restricted sites of infection.

Discussion

Antiretroviral therapy has revolutionized HIV-1 treatment and enabled millions of patients to lead a normal life. These regimens however require strict adherence in order to remain effective and adequately suppress viral loads. Daily dosages of ART cause adverse drug reactions that may yield poor outcomes such as associated anemia, lipodystrophy, skin rashes, bone homeostasis impairment and reduction of bone mineral density, toxicities to liver, heart, and skeletal muscle among others[128-130]. In addition, a plethora of other factors like stigma, depression, bipolar spectrum disorder, posttraumatic stress disorder and substance abuse, common between HIV-1 patients, can negatively and significantly affect adherence[131, 132]. These may lead to avoidance of

the prescribed daily regimens giving rise to emergence of drug resistance mutations[133]. Moreover, many HIV-1 patients suffer co-infections of associated opportunistic infections like herpes zoster, herpes simplex, hepatitis B/C viruses, tuberculosis and toxoplasma further increasing the risk of drug-drug interactions and their associated side effects [134, 135]. All these factors ultimately lead to patterns of non-adherence to the oral regimens as evident in the frequency of missed doses [136]. Therefore a paradigm shift towards long-acting injectable ART formulations and delivery devices are being explored to lower organ-specific and systemic toxicities and potentially improve the lifestyle of patients by lessening the burden of pill fatigue. Hence improving on the current ART therapy available for HIV-1 patients becomes a critical matter to study [158].

LA formulations could potentially have a significant impact on HIV treatment and prevention strategies [84, 140, 142]. In a survey of 400 HIV-1 individuals, 73% expressed their interest in long-acting injectable therapy [141]. Despite ongoing efforts and documented benefits from long-acting agents in other chronic disease conditions, only two long-acting ARV nanosuspensions containing water insoluble rilpivirine (RPV LA) and cabotegravir (CAB LA) have successfully progressed into clinical trials[76, 159-162]. It is worth noting that the design and selection of an agent for a LA injectable formulation requires compounds with high potency and appropriate physicochemical features since there are limitations for the volume that can be administered in a single injection [163]. Both CAB and RPV are hydrophobic and potent compounds that require doses of less than 100 mg/day, making them suitable candidates for extended release aqueous nanosuspensions. However, these injectables are confounded by high injection volumes, injection site reactions and limited access of native drugs to cellular and tissue reservoirs of infection[74, 75, 164]. Protease inhibitors are infamous for their short half-life, low plasma levels, poor cell penetration, and low oral bioavailability[120, 121]. Chronic administration of PIs may lead to complications such as hyperlipidemia, insulin resistance, and bone density loss[121]. Since

darunavir and most protease inhibitors are hydrophobic, attempts have been made to enhance drug targeting and metabolic stability through nanoformulation of parent compounds[106, 165]. However, native drug formulations exhibited limited improvement in drug biodistribution and PK parameters. Darunavir was also found to be incompatible lipid-based nanoparticles due to poor formulation stability [166].

Others have explored prodrug strategies to improve ADME properties of PIs [121-124]. Such attempts have either resulted in a marked loss of antiviral activity or exhibited comparable half-lives to that of parent drugs [120, 126, 127]. Thus, the realization of long-acting delivery systems for PI has remained elusive for decades. Our laboratory has previously demonstrated extension of apparent half-lives of hydrophilic and hydrophobic ARVs through synthesis and creation of lipophilic antiretroviral prodrug nanocrystals coined as LASER ART[77, 79, 80, 86]. LASER ART enabled slow release and activation of prodrugs within cellular and tissue reservoirs of infection after parenteral administration [75, 78]. We therefore sought to transform DRV into LASER ART nanocrystals. We reasoned that conversion of DRV into prodrugs was not only feasible and economical but also a much faster strategy for overcoming ADME and formulation challenges associated with the parent drug. We herein describe the development of two long-acting DRV prodrug formulations with extended in vitro antiretroviral activities and improved drug half-lives.

To transform DRV into a LASER DRV, we successfully synthesized two hydrophobic and lipophilic prodrugs M1DRV and M2DRV. M1DRV was synthesized through conjugation of DRV with a tetradecanoade iodomethyl linker through a hemiaminal bond on the amine of the aniline ring. To our knowledge, this modification has not been explored for protease inhibitors. The second prodrug, M2DRV followed an ester modification to the internal hydroxyl group of the drug by the conjugation of a stearoyl chloride after the protection of the amine to avoid side product. Both of the resulting

modifications increased the hydrophobicity of the drug by approximately 700-fold as evident by the decreased aqueous solubility of the prodrugs compared to the parent drug. In mice plasma, hydrolysis half-life for both drugs were < 20 hours. After characterization, the prodrugs were developed into stable poloxamer stabilized nanosuspensions of the prodrugs using high pressure homogenization, top down technologies used in all of our LASER ART nanocrystal preparations as well as in other pharmaceutical LA injectable products [75, 160, 162, 167]. Nanoformulating the prodrugs with amphiphilic P407 stabilized and prevented particles' aggregation [77]. Nanofromulations offer a suitable vehicle for poorly water-soluble drugs and making them accessible to their targets. The hydrophobic prodrugs interact with the hydrophobic polymer core yielding a homogenous stable polymer coated nanocrystals; NM1DRV and NM2DRV. Treatment with prodrugs' nanofromulations yielded lower EC_{50} values when compared to free drugs highlighting the importance of nanoformulations in case of highly hydrophobic drugs. These efficacy studies confirmed the prodrugs maintained an inhibitory effect against the virus. The amine modified ester prodrug formulation of DRV (NM1DRV) demonstrated comparable EC_{50} to native DRV in human MDM and CEM-SS CD4+ T cells. This is notable since previous studies with ester prodrugs of PIs in similar cell lines demonstrated diminished potency when compared to native drugs. However, modification of the hydroxyl functional group in DRV to form NM2DRV nanocrystals resulted in a 10-fold loss in potency. Nevertheless, EC_{50} of NM2DRV against HIV-1 in MDM and CEM-SS CD4+ T cells was in the nanomolar range and exhibited long-term efficacy when compared to native drug or M1DRV nanoformulations. The observed antiviral activity for NM1DRV and NM2DRV formulations is likely linked to improved cellular drug uptake. However, unlike M1DRV that hydrolyses back to DRV, M2DRV was found to be hydrolytically stable, suggesting that the prodrug is predominantly responsible for efficacy. Prodrugs are generally pharmacologically inactive compounds

that require enzymatic or chemical hydrolysis to produce the corresponding active parent drugs [83, 168, 169]. The observed efficacy data sets for NM2DRV were surprising in the context of previous studies that demonstrated an almost complete loss in antiviral activity when the secondary hydroxyl group in PIs was irreversibly blocked from interacting with the catalytic site of HIV protease [127]. Therefore, future studies will be required to elucidate association of M2DRV with the viral enzyme. Development of long-acting stable DRV prodrug nanoformulations could potentially lead to infrequent drug administration and improve drug cell penetrance and tissue biodistribution.

Ideal LA ARV formulations should be potent, safe, scalable, and stable to deliver therapeutic concentrations of active agents at infection sites. Given HIV-1 has been shown to infect and replicate in macrophages and CD4+ T cells [170-172], optimal drug delivery strategies should target ART to these cell subsets and other tissue reservoirs of infection where conventional therapies and parent drug formulations have limited access [172]. We have previously shown that macrophages can serve as drug depots [173, 174] and play a pivotal role in nanoparticle trafficking and dissemination to CD4+ T cells and tissues [78, 154, 175, 176]. We have also shown that macrophage targeting prolongs drug half-life to improve efficacy and pharmacokinetic profiles [75, 78]. NM1DRV and NM2DRV were rapidly taken up by MDM and CD4+ T cells compared to NDRV. Of significance, the presence of high intracellular prodrug concentrations had no negative effect on cell viability. It has previously been demonstrated that the presence of therapeutic drug concentrations in plasma after administration of native ART formulations does not reflect cellular and tissue levels presumably due to limited drug access to restricted sites of viral growth [75, 78]. The previous data sets suggest that transformation of DRV into lipophilic prodrugs could enable creation of long-acting and slow-release formulation with improved cell-permeation profiles. Consequently, these prodrug nanoformulations were retained in macrophages for 2 weeks and a month for NM1DRV and NM2DRV,

respectively. The prodrug formulations exhibited superior antiretroviral activity compared to native drug formulation. Notably, viral inhibition paralleled cell retention studies. Viral inhibition was maintained for up to 15 and 30 days after treatment with NM1DRV and NM2DRV, respectively, compared to only 5 days with NDRV. The antiviral activity exerted by NM1DRV and NM2DRV is likely linked to improved cellular drug uptake as evident from the uptake, retention and release studies. The ability of NM2DRV to protect MDM from HIV-1 infection for extended periods of time is a significant step towards transforming DRV into long-acting cell targeted formulations that could be used in combination with other long-acting ART for HIV-1 treatment.

Previous attempts to further improve on the first DRV prodrugs yielded into M3DRV and M4DRV. M3DRV was modified on the internal hydroxyl group through an ester bond similar to M2DRV however the main difference was a succinic linker between the drug and a 14-carbon fatty acid chain (Figure 2.47). The purpose of this was to tackle the problem faced with M2DRV slow hydrolysis inside cells and its low potency compared to DRV. The linker connects to the drug through an ester bond and itself contain another ester bond to the fatty acid, which we posited would speed the hydrolysis back to the parent drug. As expected, Ec_{50} values of the new prodrug in MDM showed enhancements over NM2DRV values; 172.4 nM for M3DRV compared to 260 nM for NM2DRV (Fig 2.48). In CEM CD4+ T cells, NM3DRV (14.4 nM) showed better yet comparable EC_{50} values to NM2DRV (18.7 nM) (Fig 2.49). EC_{50} studies for both M2DRV and M3DRV confirmed the importance of nanoformulating highly hydrophobic prodrugs to make them more soluble accessible to the cells. Uptake and retention studies of NM3DRV in MDM showed comparable uptake and retention levels to NM1DRV and NM2DRV with retention closely resembling NM2DRV until day 30 after one-time treatment (100 µM) on day 0 (Fig 2.50 and 2.51). However, similar to M2DRV, M3DRV nanoformulation treatment in cells showed minimal to no hydrolysis; DRV was not being

cleaved from the prodrug (Fig 2.50 and 2.51). In retention studies, DRV cleaving from NM3DRV remained below 0.2 ug/million cells until day 15 and remained undetectable until the end of the study at day 30 (2.46) (Fig 2.51). Uptake in CEM CD4+ T cells showed lower uptake for M3DRV from NM3DRV treatment when compared to prodrugs' concentrations detected from NM1DRV and NM2DRV over a 24hr uptake (Fig 2.52). Antiretroviral activities of NM3DRV in infected MDMs failed to show a long sustained protection up to 30 days as in the case of NM2DRV. Viral breakthrough could be seen at day 20 (Fig 2.53). However the study will be confirmed in another study where NM1DRV and NM2DRV will be included to further confirm the results and to rule out contamination since the control group seemed to show viral breakthrough by day 30. Even though, NM3DRV showed promising results in *in vitro* characterization, it performed poorly in PK studies in BALB/cJ mice where DRV cleaving from the prodrug was lower than 14 ng/mL at all time points in plasma (Fig 2.54). Plasma drug levels were gradually decreased starting from 13.8 ng/mL at the first time point where we usually see a burst release of DRV cleaving from the previous prodrugs; NM1DRV and NM2DRV. In tissues, DRV cleaving from NM3DRV resembled NDRV treatments and was only detected in lymph nodes with concentrations of 3.5 ng/g (data not shown). Therefore NM3DRV was not used in further studies. M4DRV resembled a similar modification as M1DRV where the aniline's amine was derivatized (Fig 2.55). The amine was modified through a carbamate bond with a 14-carbon fatty acid chain with a phenyl linker in attempts to make the drug stay longer in circulation and cleave in higher concentrations however because of the stability of the carbamate modifications, PK results were poor and showed significant low plasma DRV concentrations for all time points; 7.4, 2.2, 1.4 and 0 for 1, 3, 7 and 14 days (Fig 2.56). Therefore *in vitro* and *in vivo* characterization of NM1DRV and NM2DRV shows more promising grounds for these drugs to be moved into future studies and used as controls for future DRV prodrugs.

Finally, NM1DRV and NM2DRV exhibited superior PK profiles in BALB/c mice over NDRV, which was reflected in higher DRV and prodrug levels in plasma and blood of treated mice as well as significantly high drug biodistribution in tissues. NDRV treated mice showed no detectable DRV levels in plasma or blood beyond a day. Plasma DRV levels cleaving from both NM1DRV and NM2DRV were detected until day 28 of the PK after intramuscular injection on day 0. Moreover, M2DRV was detected in the brain tissues at day 28 which is significant because protease inhibitors have limited to no access through the blood brain barrier and show poor brain penetration preventing protease inhibitors from accessing major viral sanctuary sites [121, 127]. High prodrug levels in blood and tissue reflect the formation of drug depots in these mice achieving a long-acting DRV. Moreover PK studies using the CYP3A humanized mice to assess the effect of RTV boost revealed there is no major effect on plasma DRV levels except in the first time point. Moreover, RTV boosting effect was not seen in DRV concentrations in tissues however M2DRV levels in liver and spleens showed significant increases when boosted. Previous study in our laboratory utilized the hCYP3A-NOG mouse model to look at the RTV boosting effect with NDRV (50 mg/kg DRV-equivalents) (data unpublished). Similarly, the study revealed that RTV showed improvement only on day 1 after injection, however DRV drug levels were entirely undetectable by day 3 for all groups; for male and female mice (data not shown). DRV levels from NDRV followed similar patterns seeing in the mentioned BALB/cJ PK studies where highest concentrations are found in day 1 and rapidly drop to undetectable limits by the first week. In a different study using the same hCYP3A-NOG model to study the CYP3A-mediated ATV metabolism, RTV was found to enhance plasma and tissue ATV concentrations by 2.7-fold in the humanized CYP3A model as compared to only a 1.9-fold increase in the control background mouse model highlighting the importance of using the right mouse model to study protease inhibitors as well as the effect of a boost

[153]. Collectively these studies failed to see RTV boost with either parent drug nanoformulation or prodrug nanoformulation. This could point to the use of unsuitable mouse model for these studies. On the other hand, these studies could also be confirmatory of the significance of the different modifications to DRV, which could eventually reverse the need for a pharmacokinetic enhancer lessening the pill burden on HIV-1 patients.

NM1DRV and NM2DRV failed to inhibit viral infection in infected mice in the PrEP study. This could be explained in terms of the low dose (50 mg/kg) where 160 mg/kg would more closely resemble the human dose for DRV in mice. Moreover, protease inhibitors are not favorable in pre-exposure prophylaxis regimens due to the nature of the drug where it is critical job lies in inhibiting chronic infection post virus integration[177]. Drugs used in PrEP are usually NRTIs (such as TDF, 3TC, or FTC) as well as integrase inhibitors because of their ability to prevent viral integration into host genome[177, 178]. Future studies will investigate the antiretroviral efficacy of these prodrugs in infected animals in post exposure studies in combination with other integrase inhibitors and/or nucleoside reverse transcriptase inhibitors. Overall, M1DRV and M2DRV show great potential for long-acting protease inhibitors. Further modifications utilizing different fatty acid chains and spacers might yield a prodrug with further superior PK profiles to ultimately achieve a monthly or bimonthly long-acting DRV for treatment-experienced patient.

Conclusions and future directions

In summary, hydrophobic DRV prodrugs, M1DRV and M2DRV were synthesized by modification of the aniline's amine and the hydroxyl group, respectively. The prodrugs were successfully characterized. NM2DRV (130 ng/mL) was found to be significantly more hydrophobic than NM1DRV (212 ng/mL). The drugs were nanoformulated and characterized *in vitro*. EC50 studies confirmed that both drugs maintained antiretroviral

activities against the virus, however only M1DRV showed comparable potency to DRV whereas M2DRV showed a decrease in potency by more than 10-fold. Viability studies confirmed that drug concentrations ranging from 50-400 µM were not toxic and did not reflect a decrease in cells' viability (macrophages and T cells). Uptake studies in both macrophages and T cells showed a high uptake of prodrugs over 24 hours uptake with DRV detected from NM1DRV treatment. Moreover, retention studies in macrophages showed that M1DRV is retained for 15 days whereas M2DRV is retained for 30 days after a one-time loading treatment of 100 µM for both prodrug nanoformulations. Long-term antiretroviral activities mirrored the retention studies where viral inhibition was maintained for days 15 and 30 for NM1DRV and NM2DRV, respectively, as confirmed by RT assay and P24 staining. NDRV (nanoformulated DRV) showed complete viral inhibition protection on day 1, however viral breakthrough was detected by day 5. Even though NM2DRV showed a decrease in potency, it reflected the longest protection against the virus and this is because of the higher retention of the M2DRV inside the macrophages compared to M1DRV.

Based on the current pharmacokinetics (PK) of NM1DRV and NM2DRV, it's concluded that both prodrugs cleave in plasma and distribute highly in blood and tissues. From the studies, it is clear that NM1DRV cleaves faster as seen at earlier time points in plasma DRV concentrations as well as the DRV levels in livers at day 7 which were highest compared to all other time points and the different treatments injected. Once intramuscular dose of NM1DRV (50 mg/kg DRV equivalents) is equivalent to around 244 mg DRV/day for a human dose. DRV plasma levels cleaving from NM1DRV seems to remain above the EC50 (55 ng/mL) of the drug for a week. This is paralleled with the highest DRV concentrations found in livers from the NM1DRV treatment compared to consistently low DRV cleaving from NM2DRV at all time points in tissues. It is therefore concluded that NM2DRV cleaves at a slower rate than NM1DRV based on the low

plasma DRV levels detected over 28 days as well as low DRV levels cleaving from NM2DRV in the different tissues; liver, spleen, and lymph nodes. However, a much bigger prodrug depot is found in the plasma, blood, and tissues of mice treated with NM2DRV compared to mice treated with NM1DRV on day 28 which further confirms the faster hydrolysis rate of NM1DRV in plasma and tissues. Notably, M2DRV was detected in the brains of the mice in the higher dose PK (once IM dose of 100 mg/kg DRV equivalents). This could be due to the higher lipophilicity of M2DRV leading to increased permeability through the blood brain barrier and distribution in the brains.

Futures studies on NM1DRV include a dose-finding PK in mice or rats to find the appropriate dose for a long-acting effect. Because of the high dosing of DRV (twice a day 600 mg or once 800 mg) PK is needed to determine the right dose to explore the long-acting aspects of the drug as well as its antiviral efficacy *in vivo*. A human dose 800 mg/day is converted to 160 mg/kg DRV equivalents mouse dose, based on allometric scaling that depends on the body surface area. However, a dose of 160 mg/kg is considered small because it only counts for once-daily dose hence to convert to an initial long-acting dose it may be multiplied by a factor of 5 yielding into 800 mg/kg, based on previous studies in our laboratory on long acting DTG, CAB or RPV[75, 78]. We will perform dose-finding PK study in rats since they have a bigger muscle mass, which may allow for a slow dissolution of the drug from the injection site leading to a long-acting effect for NM1DRV. Ultimately our goal is to find the right dose and appropriate animal model to achieve DRV plasma IC90 levels (200 ng/mL). When the correct dose is determined and the PK profile is determined, a post-exposure prophylaxis (PEP) pharmacodynamics (PD) will be conducted to determine the in vivo antiviral efficacy of NM1DRV in infected animals. NM1DRV will be injected soon after infection is confirmed in NSG (NOD/scid-IL-2Rγcnull) mice-reconstituted with CD34+ human hematopoietic stem cells. Viral loads will be determined based on the PK profile timing where DRV levels cleaving from

NM1DRV are above IC90 of the drug. For NM2DRV, PK design may be different to accommodate the slow hydrolysis of the drug as well as the high biodistribution in the different tissues as well as plasma and blood. We may also switch to rats as a rodent model because of their bigger muscle mass for injections. Initially, we will perform a long term PK (2-3 months long) to determine the hydrolysis rate of NM2DRV at different time points for plasma as well as in the different tissues. Finding out when the drug depots start cleaving back into DRV will be essential for future PEP PD studies. Once the long term PK profile for NM2DRV is determined we may perform a different PK administering multiple/repeating doses of NM2DRV to determine how many doses of NM2DRV are needed to build up and achieve the IC90 and IC50 of DRV. We may also include NM1DRV as a control in the repeating-doses PK to highlight the importance of the experimental design with the different prodrugs. When the right PK design is figured out for both DRV prodrug nanoformulations, parallel PK studies in hCYP3A/NOG mice and control NOGs will be performed to test the significance of a pharmacokinetic booster (ritonavir) when administered with NM1DRV and NM2DRV. This experiment will also highlight the difference, if any, in DRV metabolism rate in the case of mouse CYP3A or human CYP3A.

To further explore and develop LA DRVs, future prodrug strategies will include the synthesis of less stable drugs that can be cleaved faster by esterases *in vivo*. Future DRV prodrugs syntheses will include different linkers between the fatty acid and DRV to aid in propelling the fatty acid away. In the case of M2DRV, the long fatty acid chain was conjugated to the internal hydroxyl group, which may have caused folding of the drug in a way where the ester bond is concealed avoiding activation by esterases. To overcome this in future studies, bulky groups containing phenyl linkers between the fatty acid chain and the drug such as aminoacyl phosphorocholoridates linkers may be utilized. When using aminoacyl phosphorocholoridates linkers we can avoid the solubility increase for

future DRV prodrugs by the conjugation of long-chain fatty acids and shielding the polar groups on the phosphates like in the case of NRTI ProTides[86] from our laboratory. Moreover, since M2DRV does not cleave fast enough, we can attempt the conjugation of considerably short linkers/fatty acid chains on the hydroxyl functional group in hopes of speeding up activation by esterases since with the long fatty acid chain, the molecule was most likely too hindered and inaccessible for activation. Additionally, future modifications would target the aniline's amine since previous modification, M1DRV, showed comparable EC50 values to DRV. Therefore further modifications to the same group may guarantee the maintenance of potency. Since M1DRV seems to be cleaving faster than M2DRV we will attempt the conjugation of longer fatty acid chains (C18 or C22) to slow the prodrug hydrolysis while guaranteeing that the bond is accessible by esterases. Furthermore, future perspectives will include the implementation of the GO/NO GO guidelines from our laboratory. These entail that based on prodrug characterizations and their corresponding in vitro characterization; we can determine whether more time and efforts should be invested into the newly synthesized prodrug. These guidelines will be based on significant values and cutoff values from the different studies' results. These studies include but are not limited to prodrug's solubility, LogP, stability in different pH, hydrolysis in plasma, potency, cytotoxicity, and uptake.

In summary, amine and alcohol ester lipophilic prodrugs of darunavir were successfully synthesized and stabilized into long-acting slow effective release aqueous nanosuspensions. NM2DRV was found to exhibit enhanced intracellular prodrug levels with sustained retention and efficacy. Pharmacokinetics tests of NM1DRV and NM2DRV administered in mice demonstrated sustained drug levels in blood and tissues with higher concentrations of the prodrugs observed over 28 days. These data, taken together, support the idea that tissue and cell targeted lipophilic prodrugs could facilitate

transformation of DRV into long-acting sustained release formulations with improved antiretroviral activities.

Figures
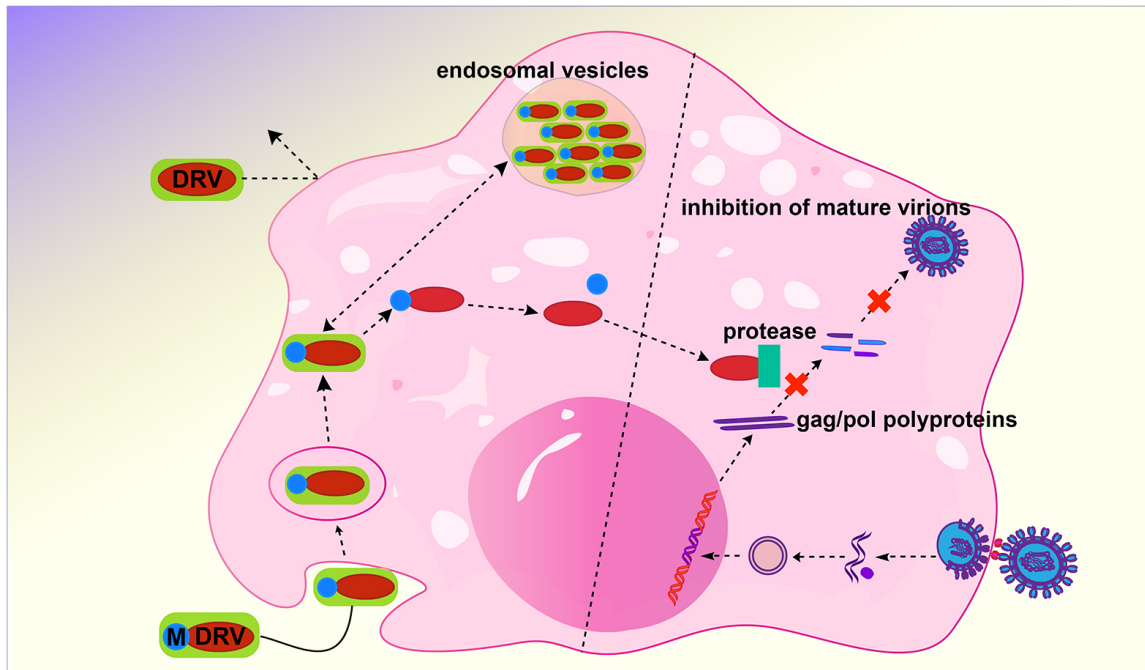
Figure 2. 1 Modification of DRV advantage

Modification of DRV into hydrophobic lipophilic prodrugs MDRV enhances the uptake of the modified drugs and their retention profiles. The modification's effect is seen in the antiretroviral efficacy of the prodrugs. The prodrugs nanoformulation is capable of viral inhibition up to 30 days post treatment. Nanoformulated DRV (NDRV) passes through the cells' membrane however it seems to be soon effluxed based on the very low uptake concentrations after treatment with equivalent concentrations. Modified DRV drugs can lead to the creation of long-acting darunavir nanoformulation for clinical settings.
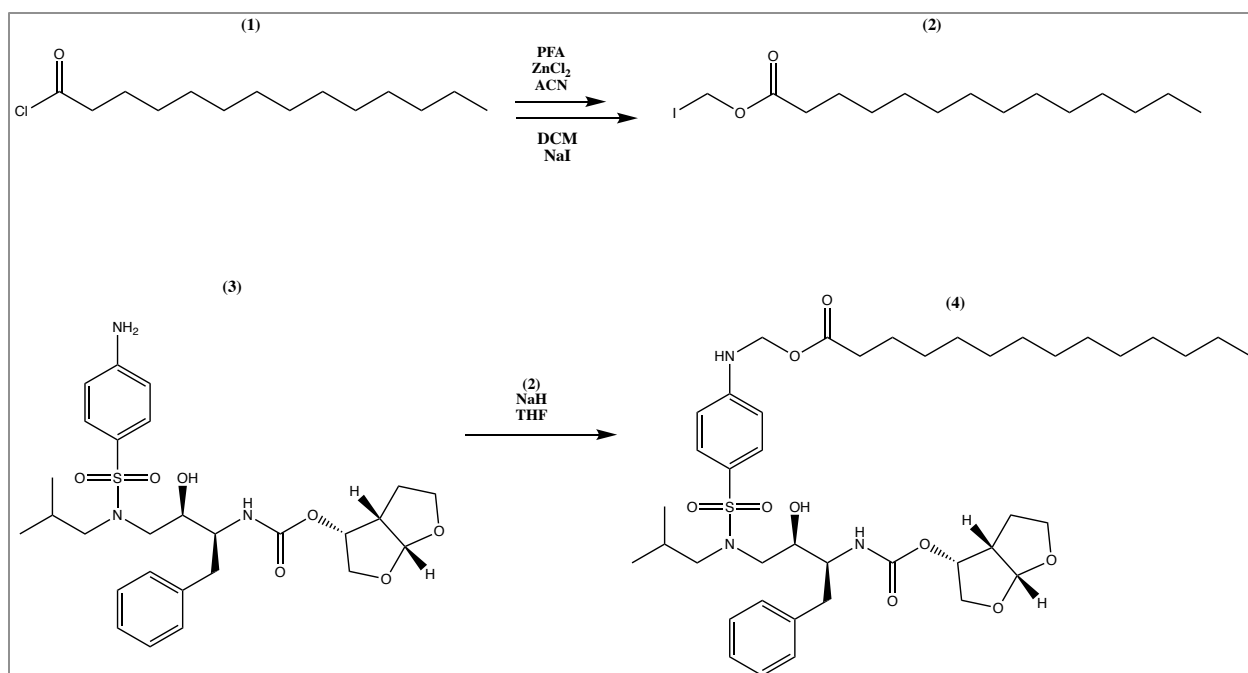
Figure 2. 2 M1DRV synthesis scheme

Myristoyl chloride is first used to synthesize iodomethyl tetradecanoate linker used for direct conjugation on DRV in the presence of sodium hydride and THF to yield M1DRV, an amine modified DRV through a hemiaminal bond.
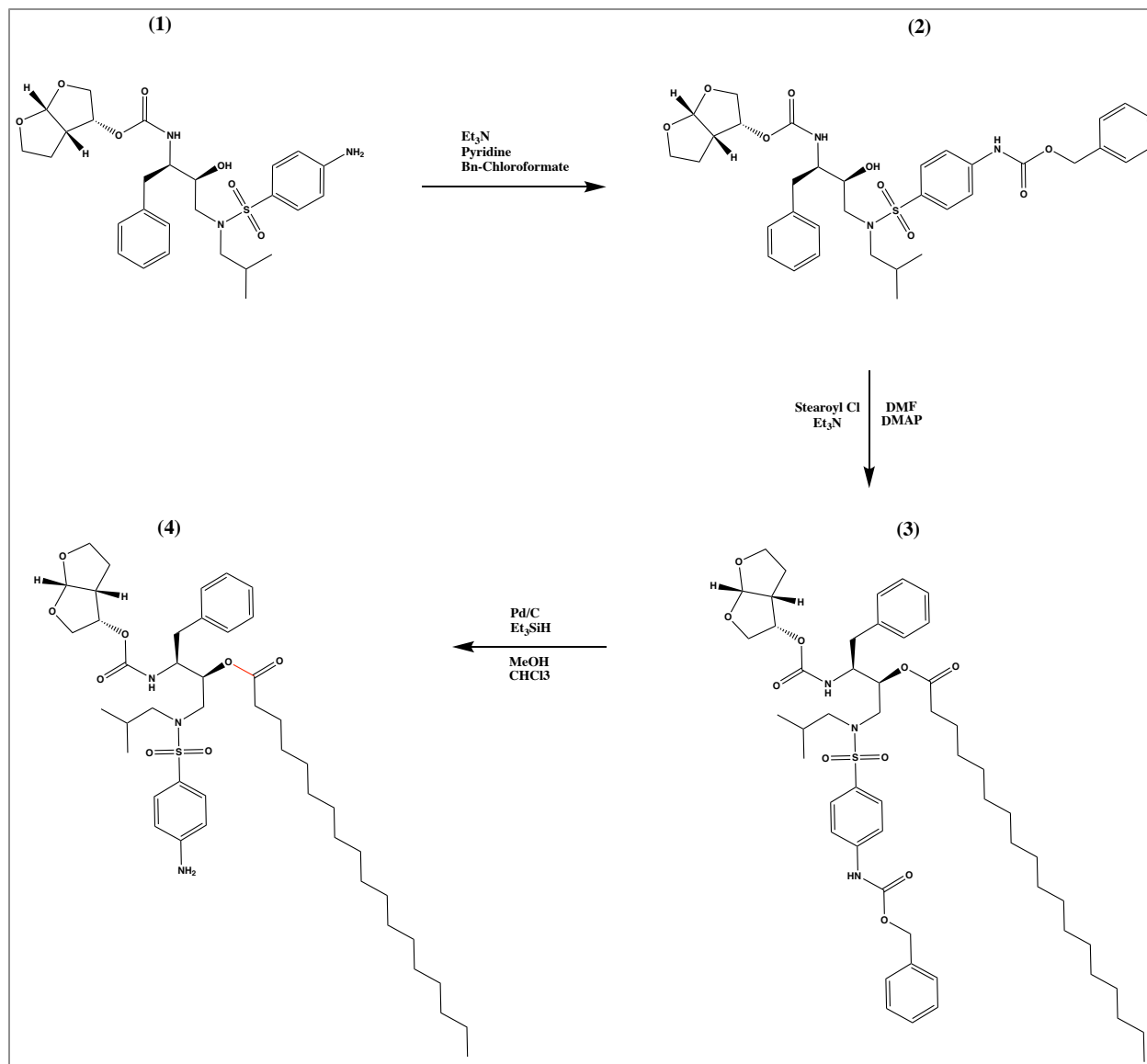
Figure 2. 3 M2DRV synthesis scheme

DRV (1) is first reacting with benzyl chloroformate in a Cbz protection to shield the amine group, Cbz-DRV (2) and prevent side products while modifying the hydroxyl group of DRV. (2) is conjugated to 18-carbon fatty acid (stearoyl chloride) to yield Cbz-M2DRV (3). Cbz-M2DRV is subjected to catalytic hydrogenolysis using palladium on activated carbon and Et_3SiH to deprotect the amine of the aniline yielding the final product; M2DRV.
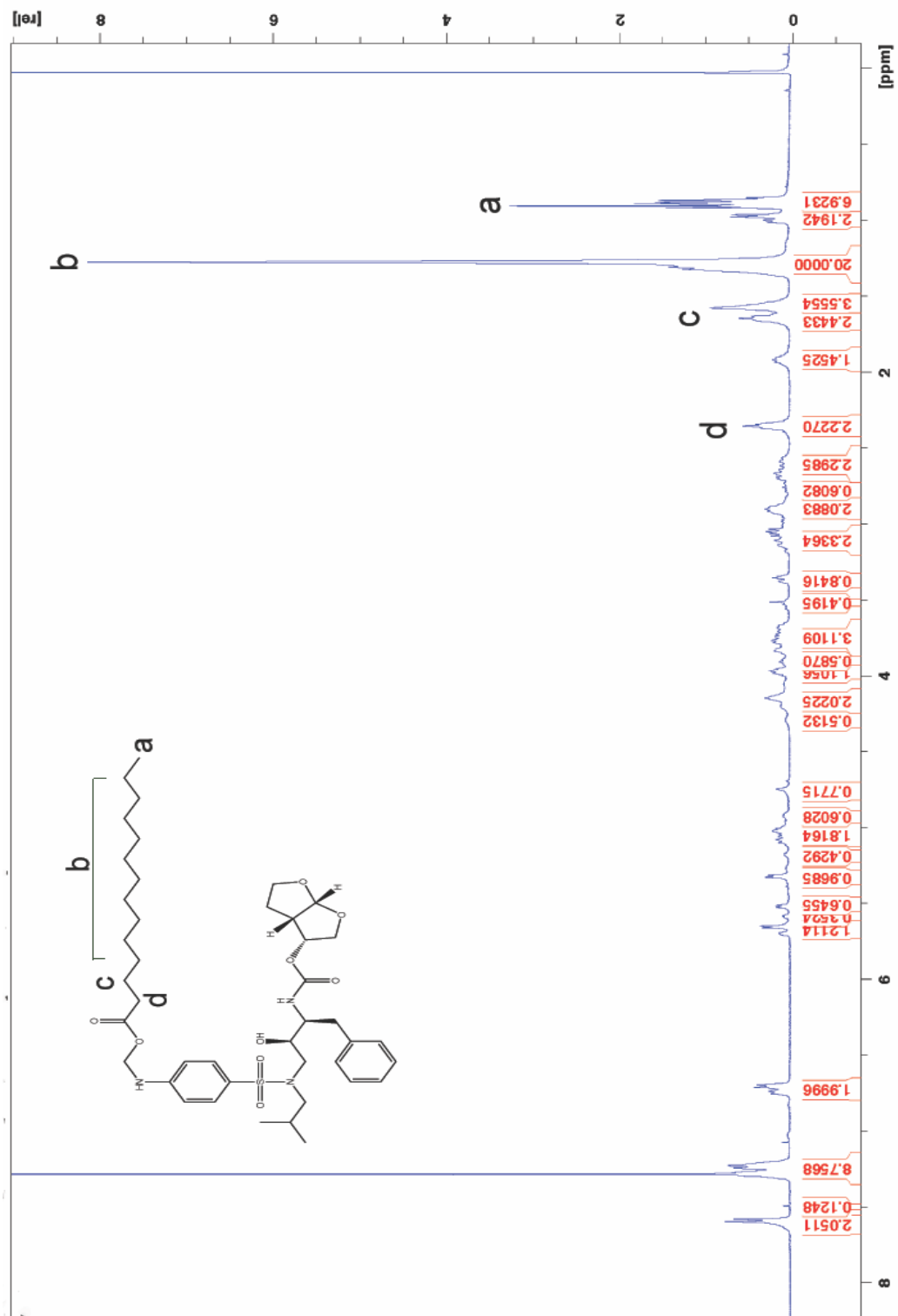
Figure 2. 4 ^{1}H NMR Characterization of M1DRV

^{1}H NMR spectrum reflects the additional terminal methyl (0.9 ppm) and methylene (1.26 ppm) protons of the fatty esters.
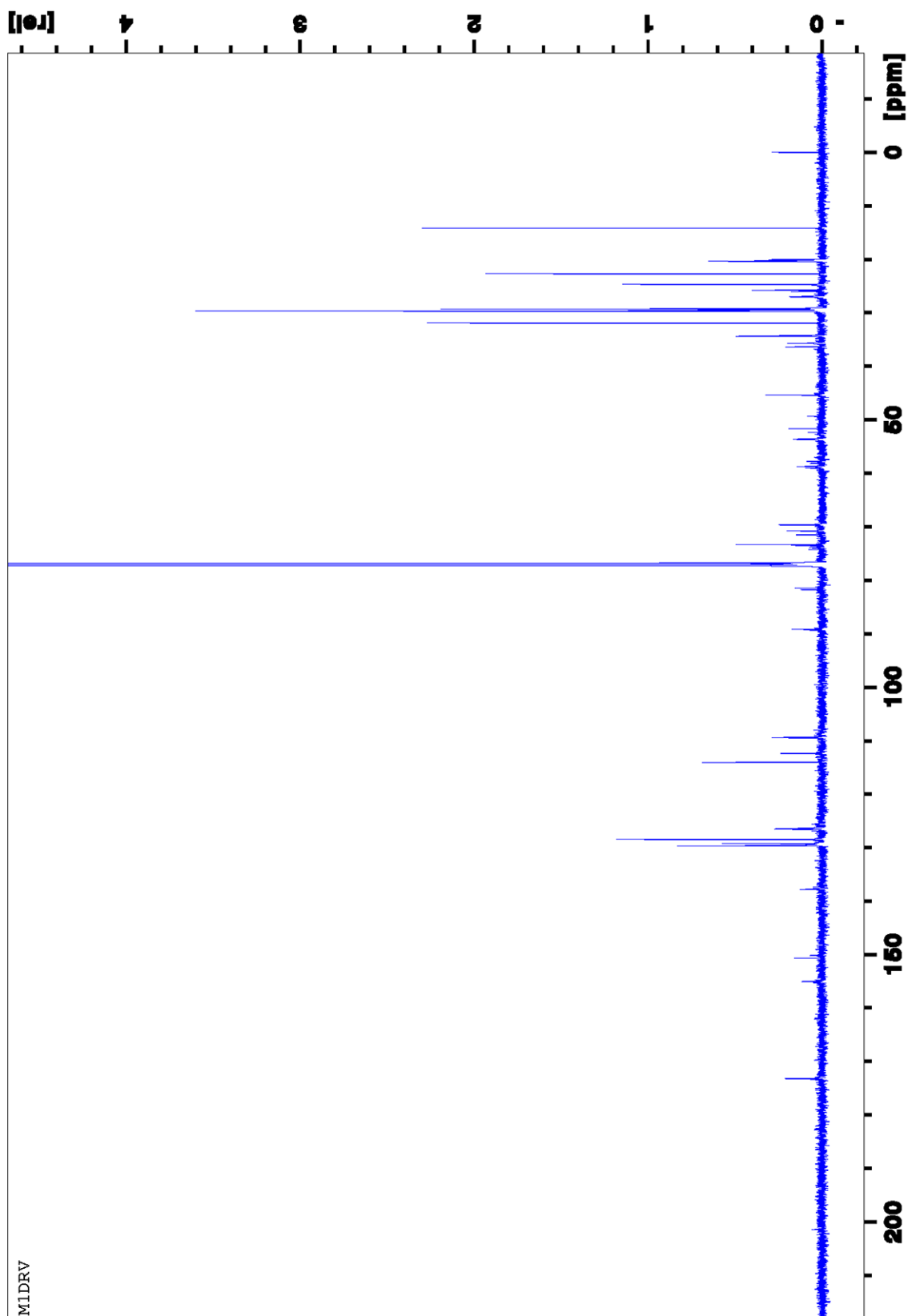
Figure 2. 5 ^{13}C NMR Characterization of M2DRV

^{13}C NMR spectrum shows the addition of carbon peaks corresponding to the carbonyl groups at 173 ppm and aliphatic carbon atoms from the fatty acids where the methyl carbon is at 14.1 ppm and the methylene carbons at 29.3 ppm.
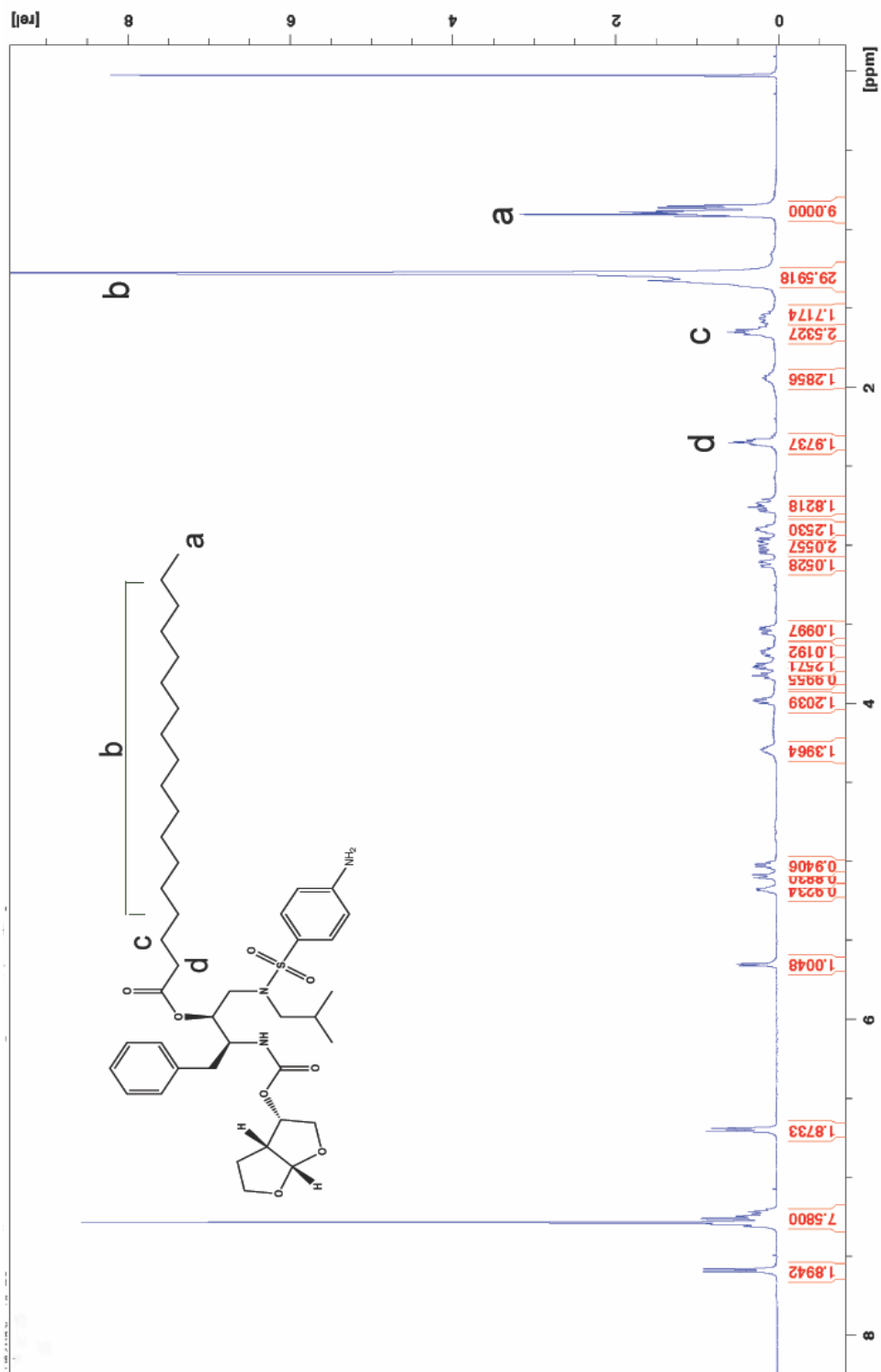
Figure 2. 6 ^{1}H NMR Characterization of M2DRV

^{1}H NMR spectrum reflects the additional terminal methyl (0.9 ppm) and methylene (1.26 ppm) protons of the fatty esters.
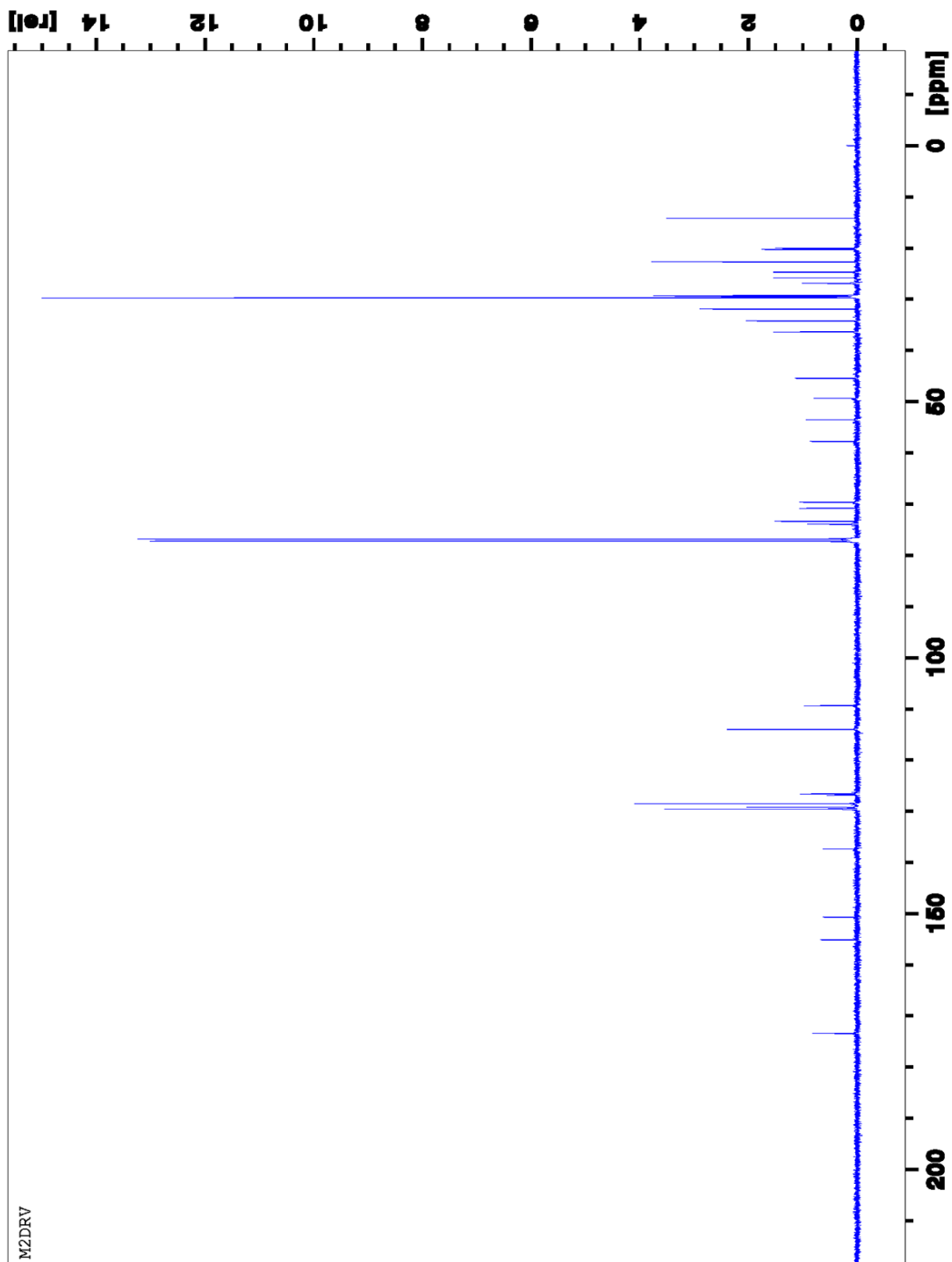
Figure 2. 7 ^{13}C NMR Characterization of M2DRV

^{13}C NMR spectrum shows the addition of carbon peaks corresponding to the carbonyl groups at 173 ppm and aliphatic carbon atoms from the fatty acids where the methyl carbon is at 14.1 ppm and the methylene carbons at 29.3 ppm.
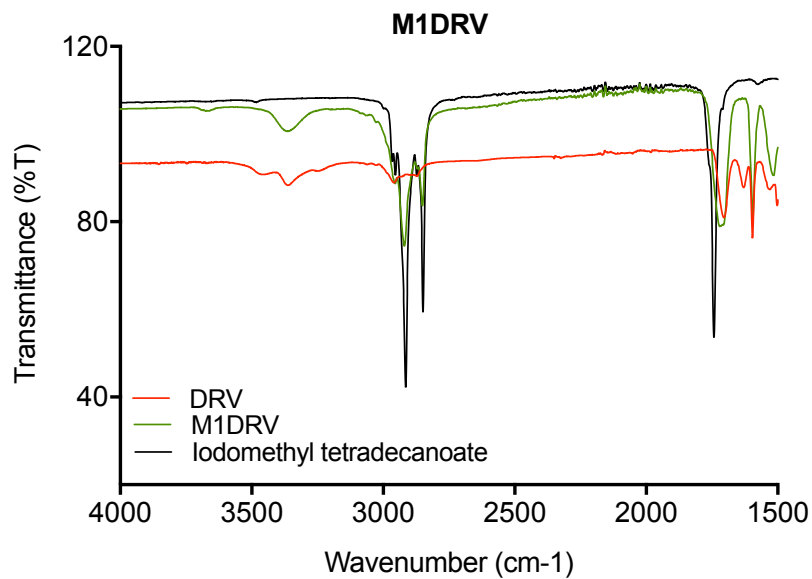
Figure 2. 8 FTIR characterization of M1DRV

Absorption bands at 2917, 2915 and 2848 cm^{-1} represent asymmetric and symmetric C-H stretches in the long chain fatty acids.
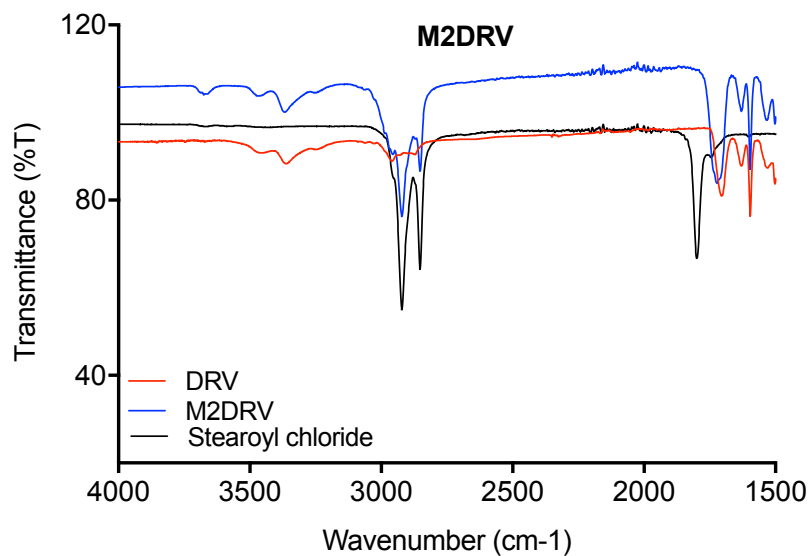
Figure 2. 9 FTIR characterization of M2DRV

Absorption bands at 2917, 2915 and 2848 cm^{-1} represent asymmetric and symmetric C-H stretches in the long chain fatty acids.
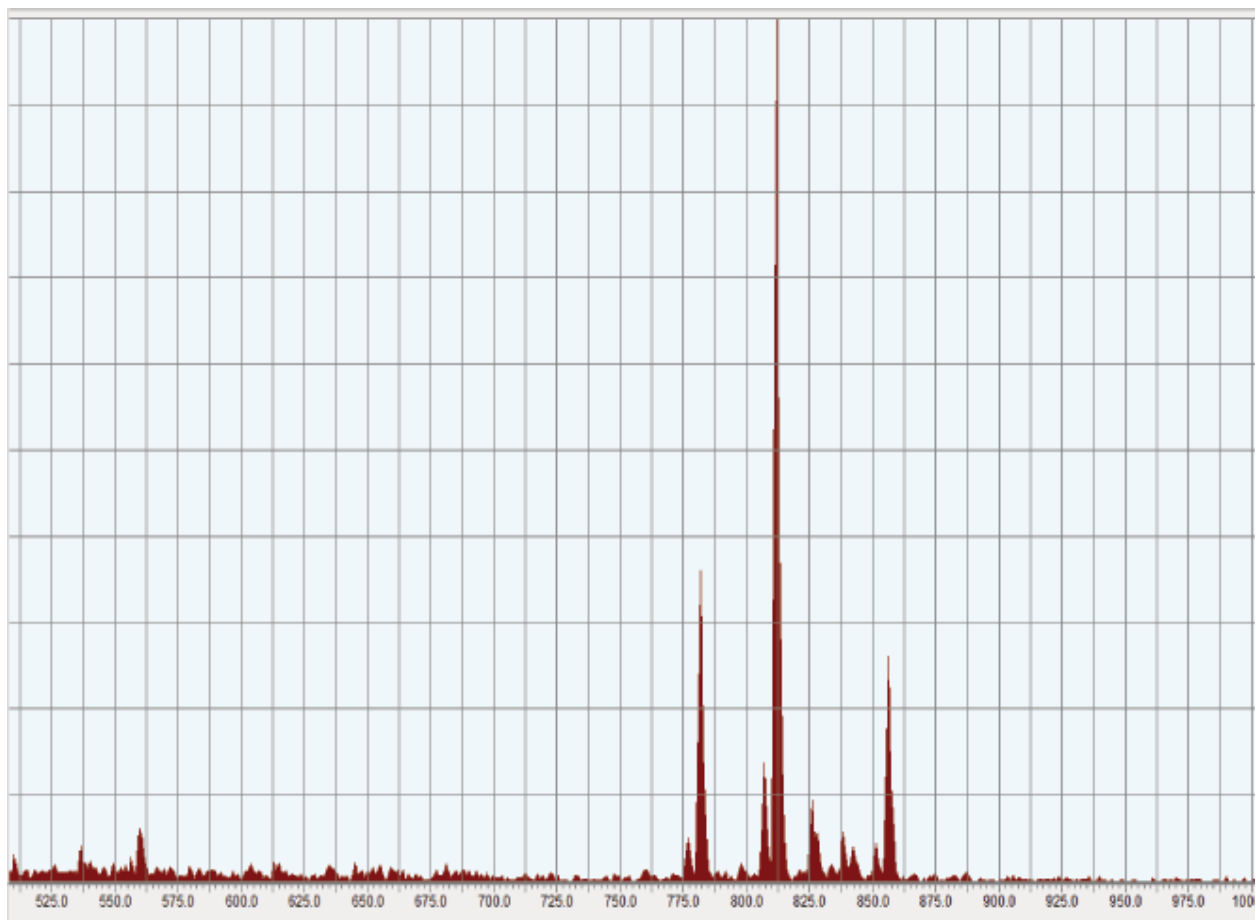
Figure 2. 10 Characterization of M1DRV

Infusion into a Waters Xevo TQ-S micro mass spectrometer confirmed the desired molecular ion peaks at 811.05 [M+Na+].
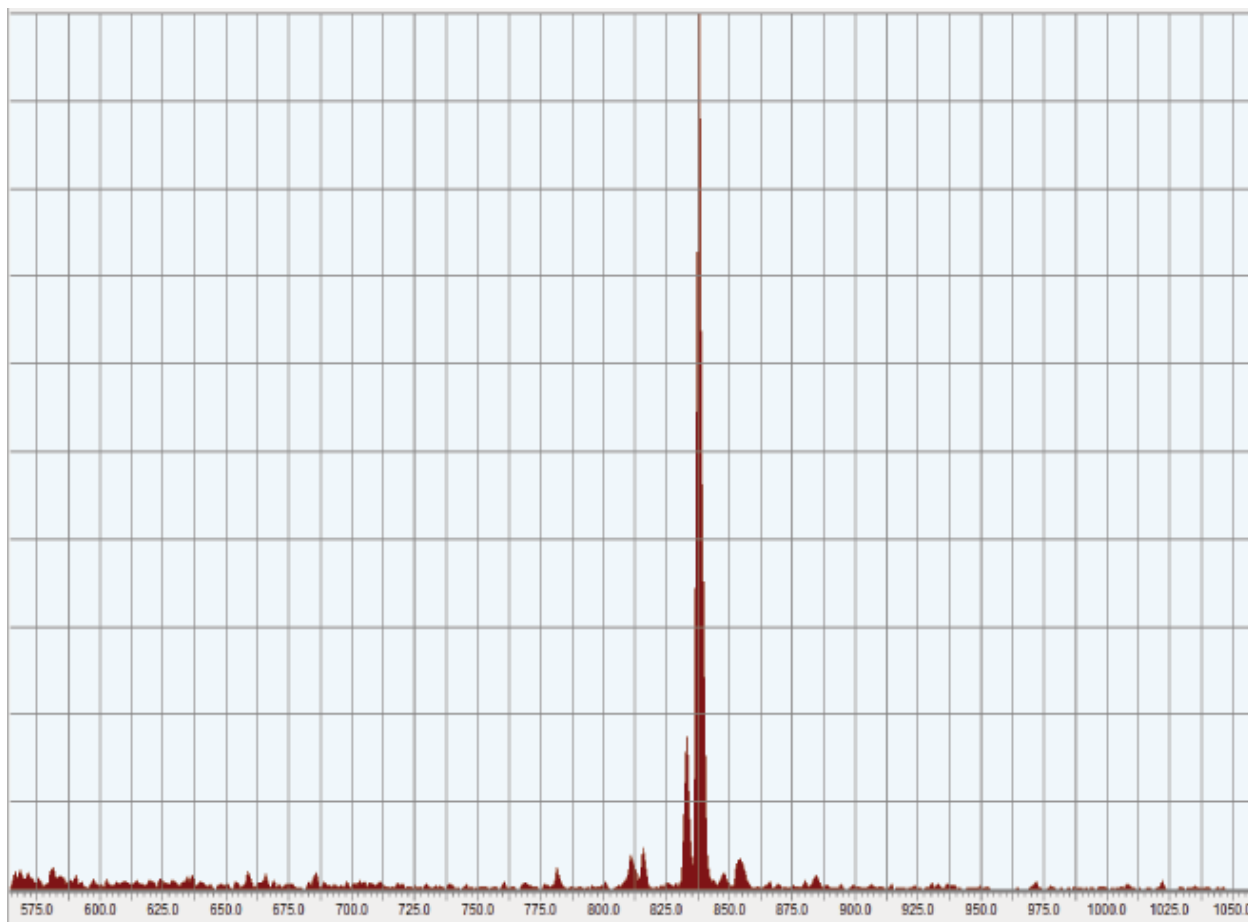
Figure 2. 11 Characterization of M2DRV

Infusion into a Waters Xevo TQ-S micro mass spectrometer confirmed the desired molecular ion peaks at 837.14 [M+Na+].
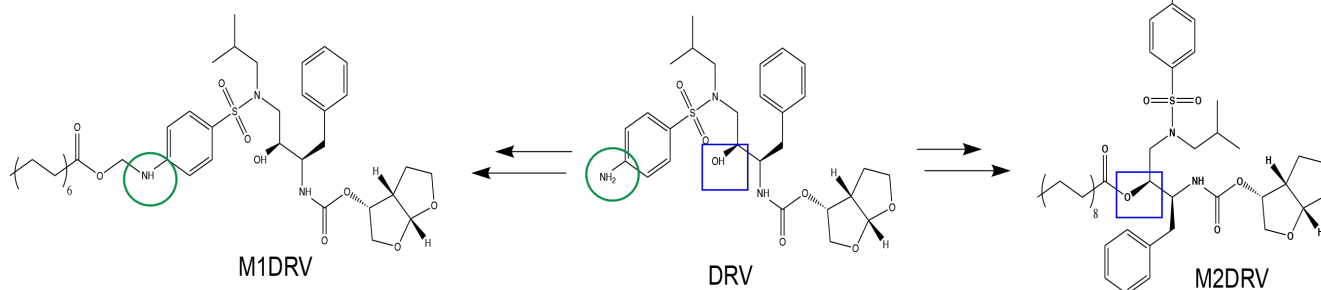
Figure 2. 12 DRV modifications

DRV was modified on the aniline amine group to yield M1DRV – a modification that was rarely explored for PIs. In addition, DRV was modified using the internal hydroxyl group – that has previously been modified in other protease inhibitors to improve ADME profiles.
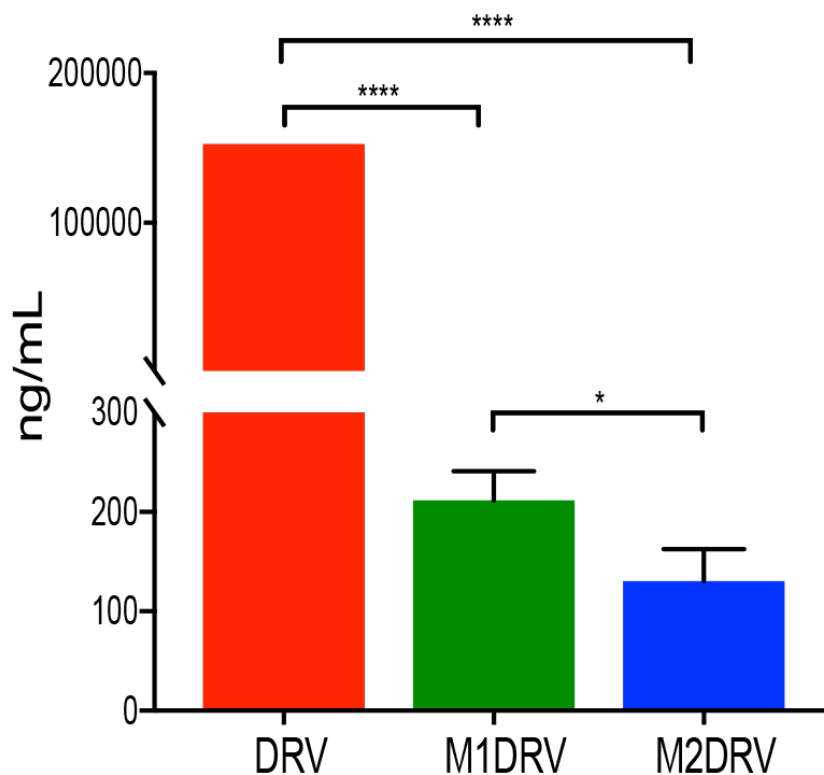
Figure 2. 13 Prodrugs' aqueous hydrophobicity

Aqueous solubility demonstrated enhancement in prodrug hydrophobicity (****$P<0.0001$ for DRV compared to M1DRV or M2DRV, *P=0.0258 for M1DRV vs. M2DRV.
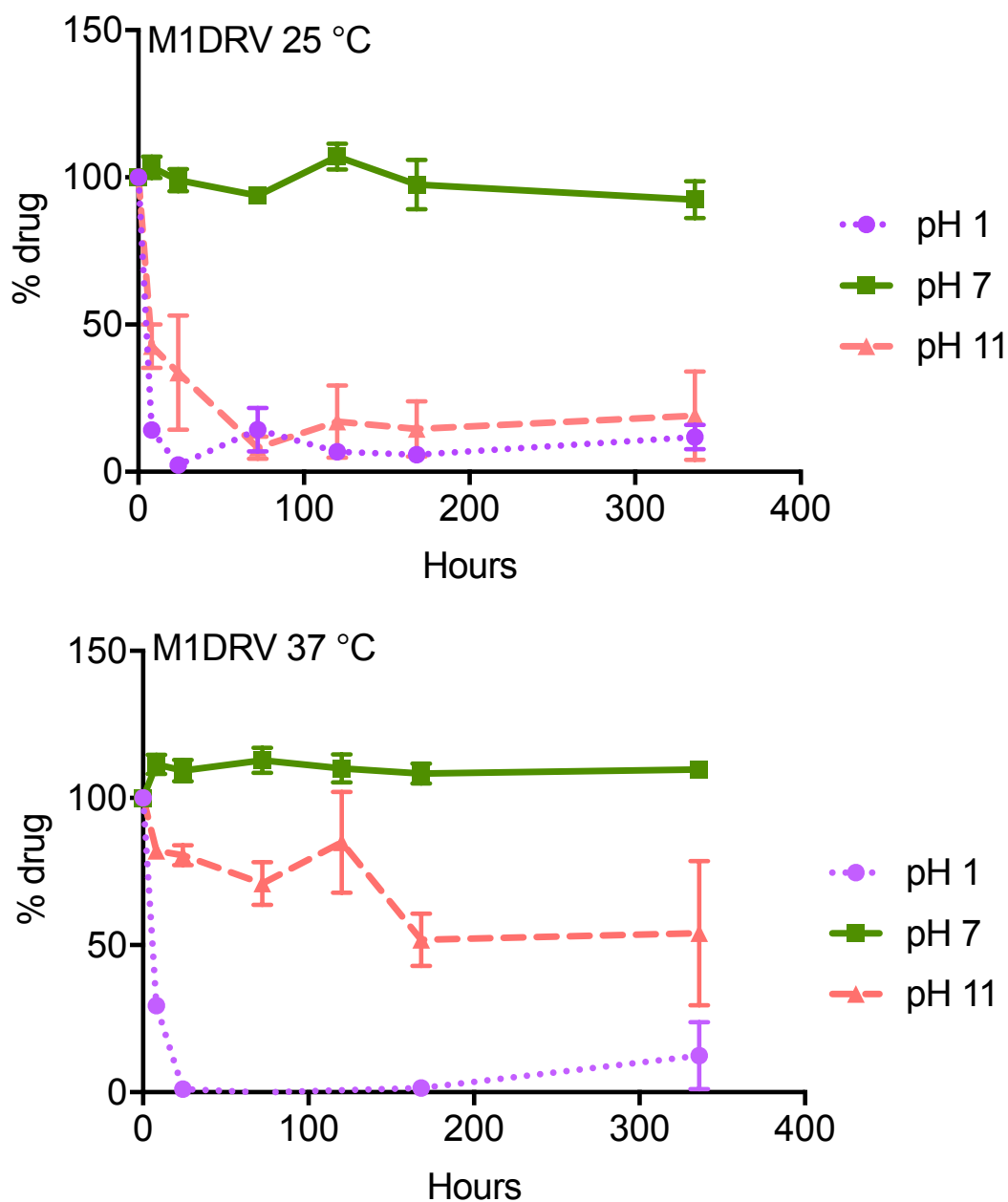
Figure 2. 14 M1DRV stability in different pH

The drug was chemically stable at pH 7 at different temperatures. Prodrugs' stability was evaluated in different pH; 1, 7 and 11. Stocks of M1DRV with concentrations of 1-2 mg/mL were prepared in MeOH. For stability in acidic pH (pH 1) the drugs were incubated separately in a solution of pH adjusted .1 M HCl. Similarly, drugs were incubated in pH adjusted .1 NaOH (pH 11) to test stability in basic environments. Finally, incubation in water (pH 7) determined stability in neutral pH. Triplicate samples of both prodrugs were kept on a shaker either at room temperature (25°C) or incubated at 37°C. Aliquots were collected from the samples at different time points; 8, 24, 72, 120, 168, and 336 hours. Samples were dried under vacuum and quantified by HPLC. The prodrugs were formulated using PBS.
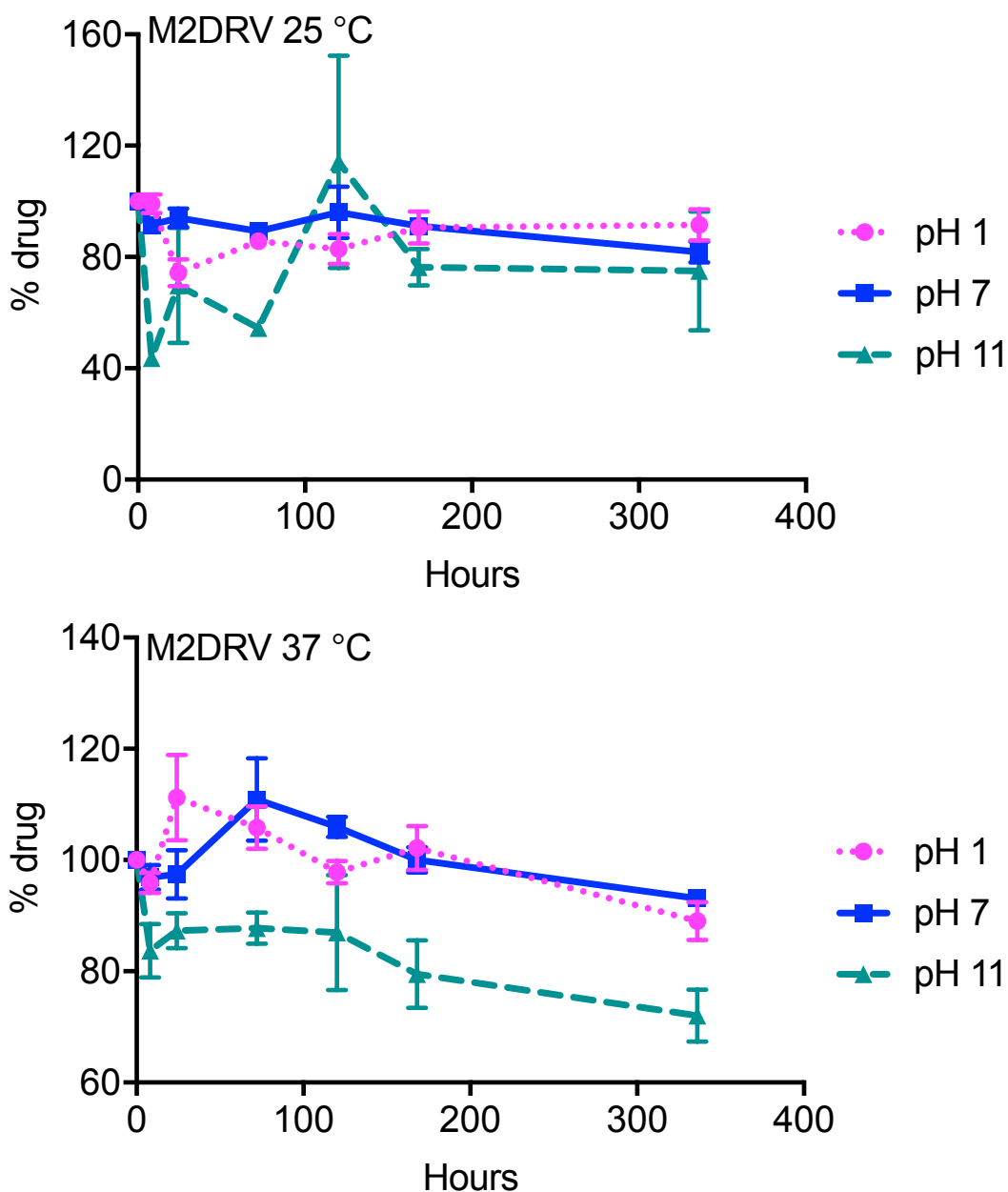
Figure 2. 15 M2DRV stability in different pH

The drug was mostly chemically stable at pH 7 as well as pH 1 at the different temperatures. Prodrugs' stability was evaluated in different pH; 1, 7 and 11. Stocks of M2DRV with concentrations of 1-2 mg/mL were prepared in MeOH. For stability in acidic pH (pH 1) the drugs were incubated separately in a solution of pH adjusted .1 M HCl. Similarly, drugs were incubated in pH adjusted .1 NaOH (pH 11) to test stability in basic environments. Finally, incubation in water (pH 7) determined stability in neutral pH. Triplicate samples of both prodrugs were kept on a shaker either at room temperature (25°C) or incubated at 37°C. Aliquots were collected from the samples at different time points; 8, 24, 72, 120, 168, and 336 hours. Samples were dried under vacuum and quantified by HPLC. The prodrugs were formulated using PBS.
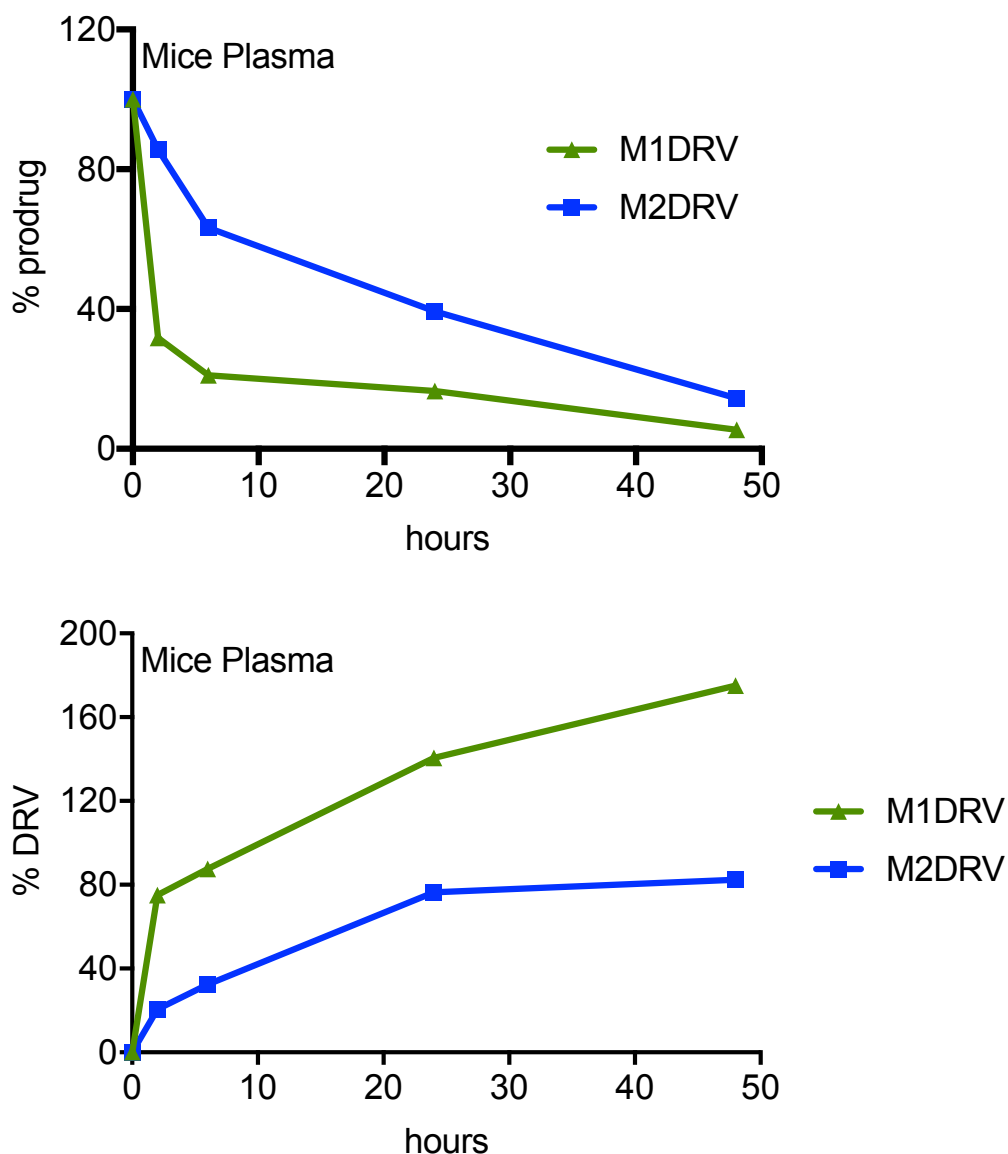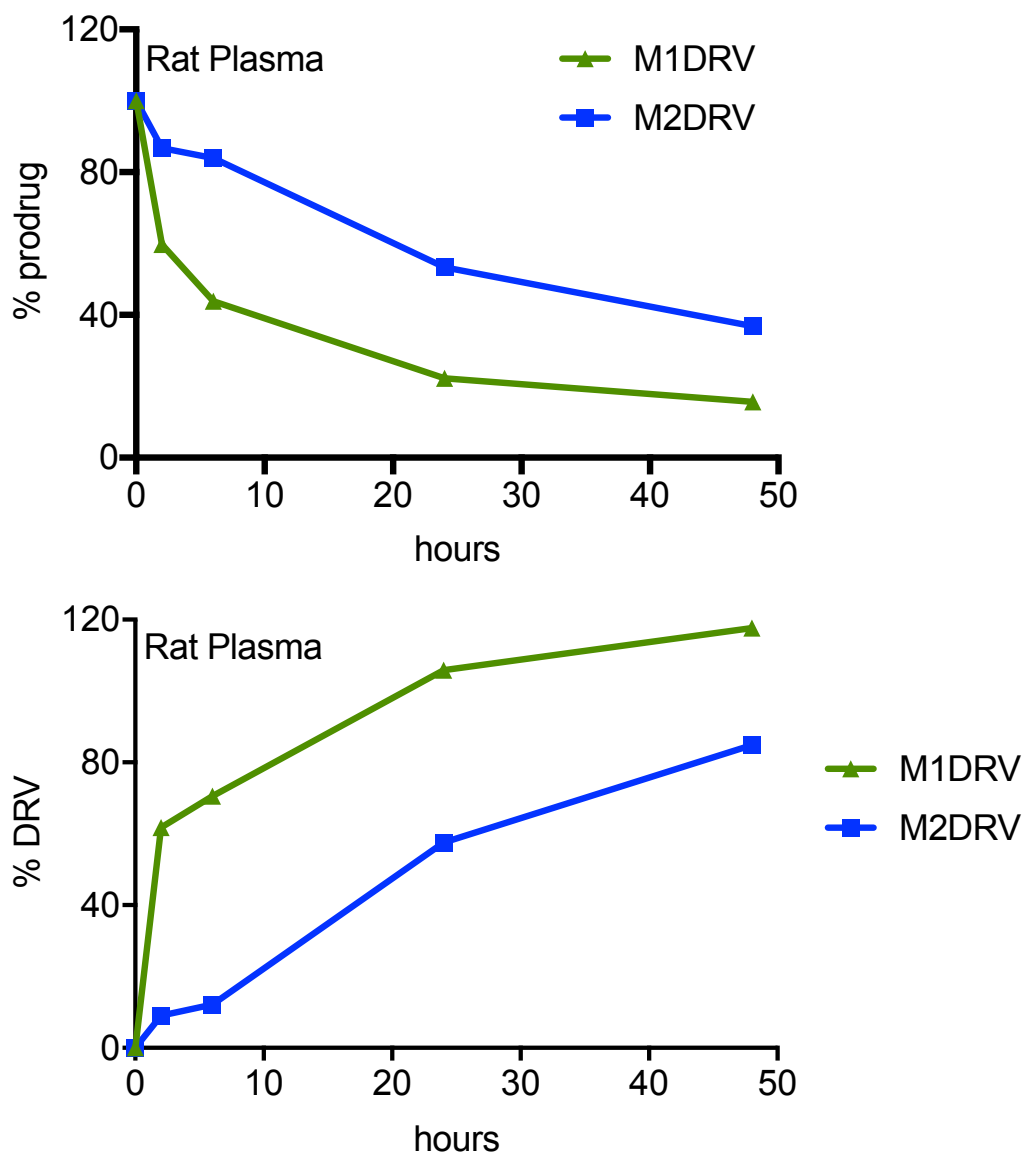
Figure 2. 16 M1DRV and M2DRV hydrolysis in mice plasma

Hydrolysis of M1DRV and M2DRV in plasma over 48 hours at 37°C demonstrating enzymatic degradation of the prodrugs over time. To evaluate plasma stability of M1DRV and M2DRV, 100 µL plasma samples from mouse were spiked with 1 µM M1DRV or M2DRV. Triplicate samples were kept on a shaker at 37°C. At various time points (0, 2, 6, 24, and 48), 1 mL of MeOH was added to each tube and vortexed for 3 minutes to stop enzymatic cleavage, then stored at -80°C until drug quantitation. Negative controls were used to normalize for non-specific binding. 100 µL ice cold plasma was added to 1mL MeOH followed by addition of the prodrugs. At various time points, 1mL MeOH was added to the samples and drug was quantified by HPLC. Incubation of the prodrugs in plasma resulted in a decline in prodrug concentrations by more than 45 % over 24 h. Data are expressed as mean ± SEM for n=3 samples per group.
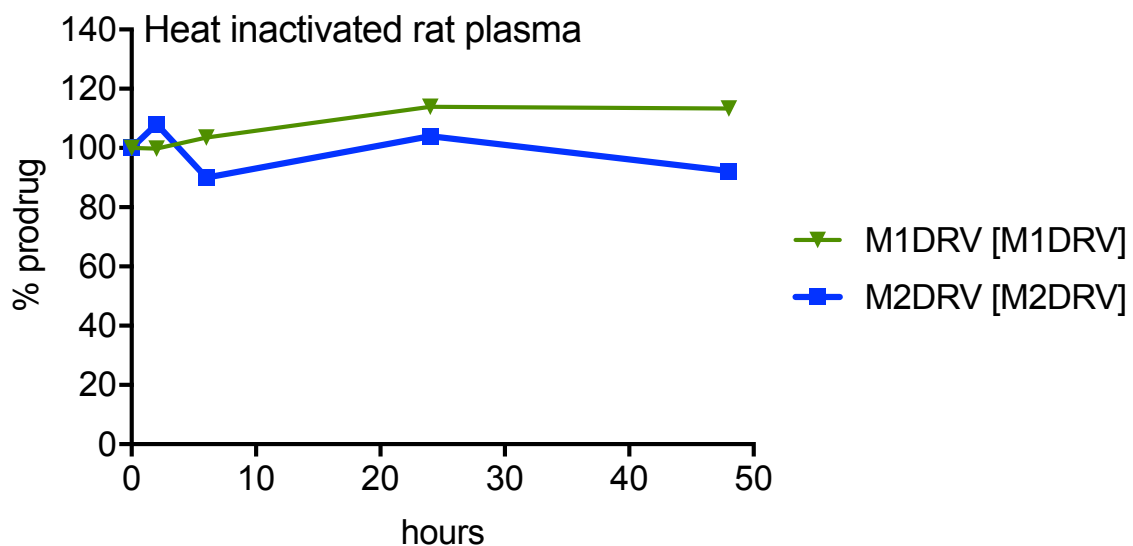
Figure 2. 17 M1DRV and M2DRV hydrolysis in rat plasma

Hydrolysis of M1DRV and M2DRV in plasma over 48 hours at 37°C demonstrating enzymatic degradation of the prodrugs over time. To evaluate plasma stability of M1DRV and M2DRV, 100 µL plasma samples from rat were spiked with 1 µM M1DRV or M2DRV. Triplicate samples were kept on a shaker at 37°C. At various time points (0, 2, 6, 24, and 48), 1 mL of MeOH was added to each tube and vortexed for 3 minutes to stop enzymatic cleavage, then stored at -80°C until drug quantitation. Negative controls were used to normalize for non-specific binding. 100 µL ice cold plasma was added to 1mL MeOH followed by addition of the prodrugs. At various time points, 1mL MeOH was added to the samples and drug was quantified by HPLC. Incubation of the prodrugs in plasma resulted in a decline in prodrug concentrations by more than 45 % over 24 h. Data are expressed as mean ± SEM for n=3 samples per group.

Figure 2. 18 M1DRV and M2DRV hydrolysis in heat inactivated rat plasma

The prodrugs are fairly stable in heat-inactivated plasma confirming their hydrolysis through enzymatic activity. Negative controls were prepared using heat-inactivated plasma to determine whether drug hydrolysis was due to enzymatic activity or non-enzymatic hydrolysis. 100 µL plasma samples from rat were spiked with 1 µM M1DRV or M2DRV. Triplicate samples were kept on a shaker at 37°C. At various time points (0, 2, 6, 24, and 48), 1 mL of MeOH was added to each tube and vortexed for 3 minutes, then stored at -80°C until drug quantitation. Negative controls were used to normalize for non-specific binding. 100 µL ice cold plasma was added to 1mL MeOH followed by addition of the prodrugs. At various time points, 1mL MeOH was added to the samples and drug was quantified by HPLC.
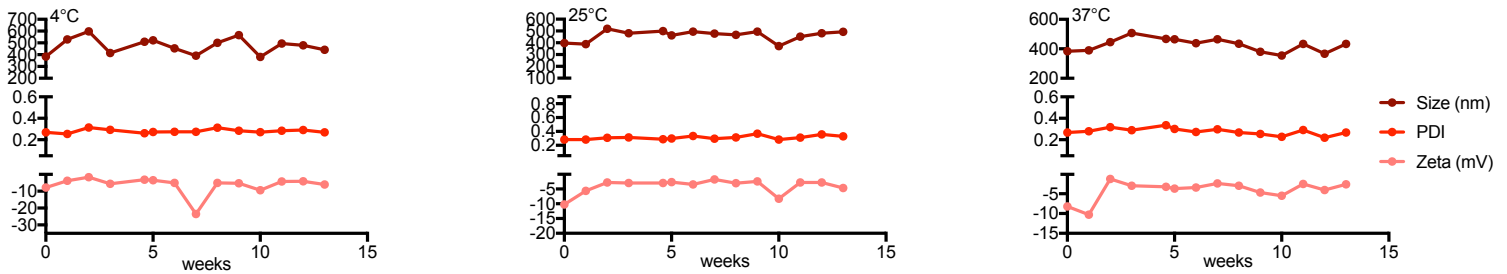
Figure 2. 19 NDRV stability

DRV nanoformulation (NDRV) stability measurements were observed over 13 weeks at different temperatures. Stability with monitored using dynamic light scattering (DLS).
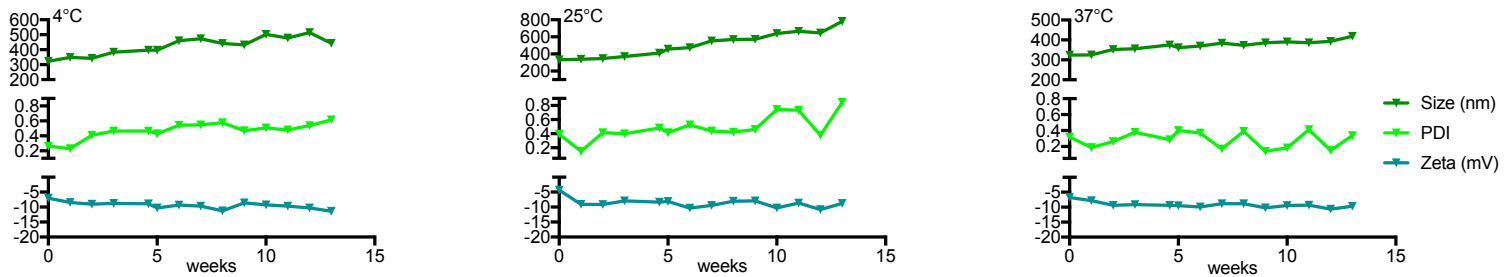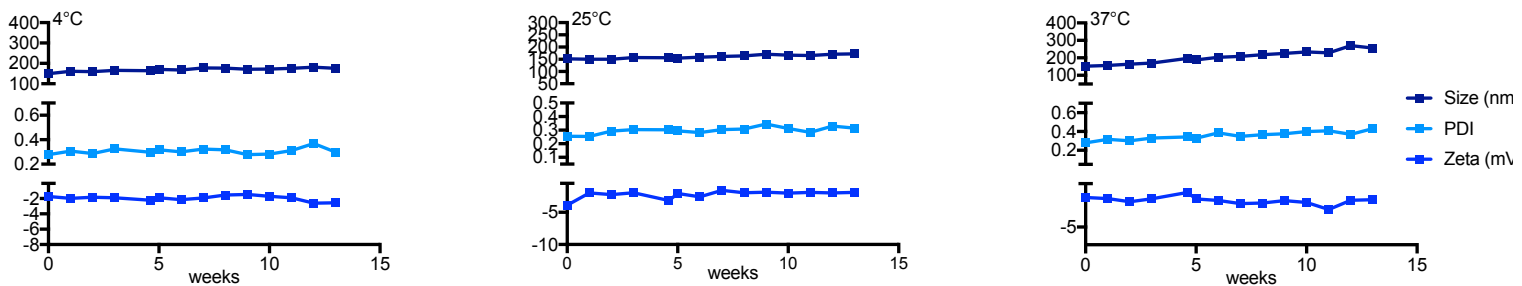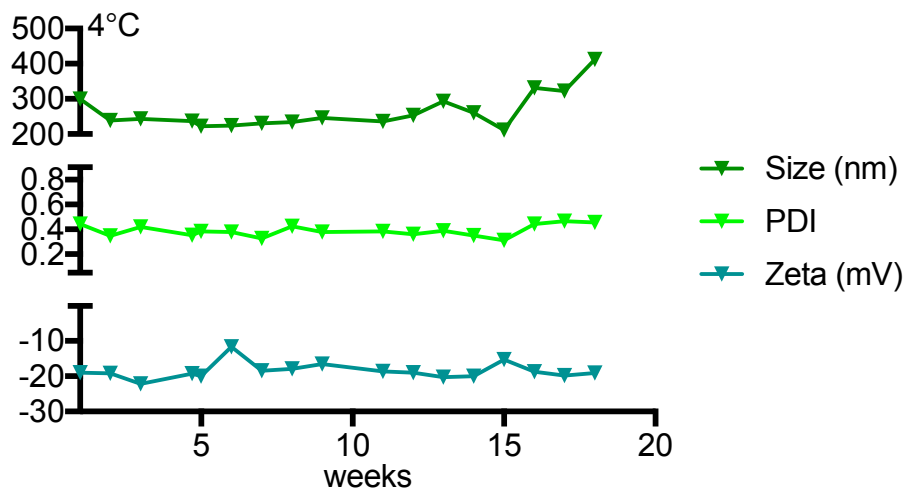

Figure 2. 20 NM1DRV stability

M1DRV nanoformulation (NM1DRV) stability measurements were observed over 13 weeks at different temperatures. Stability with monitored using dynamic light scattering (DLS).

Figure 2. 21 NM2DRV stability

M2DRV nanoformulation (NM2DRV) stability measurements were observed over 13 weeks at different temperatures. Stability with monitored using dynamic light scattering (DLS).

Figure 2. 22 NM1DRV stability (PK formulation)

NM1DRV stability measurements over 18 weeks from concentrated formulations used for PK dosing. Diluted NM1DRV were concentrated using differential centrifugation. First the nanoformulation was pelleted at 5,000 x g for 5 minutes. Then supernatant was transferred to a new centrifuge tube and centrifuged at 20,000 x g for 20 minutes. Supernatant was discarded and both pellets were suspended in a total of approximately 500 µL of PBS.
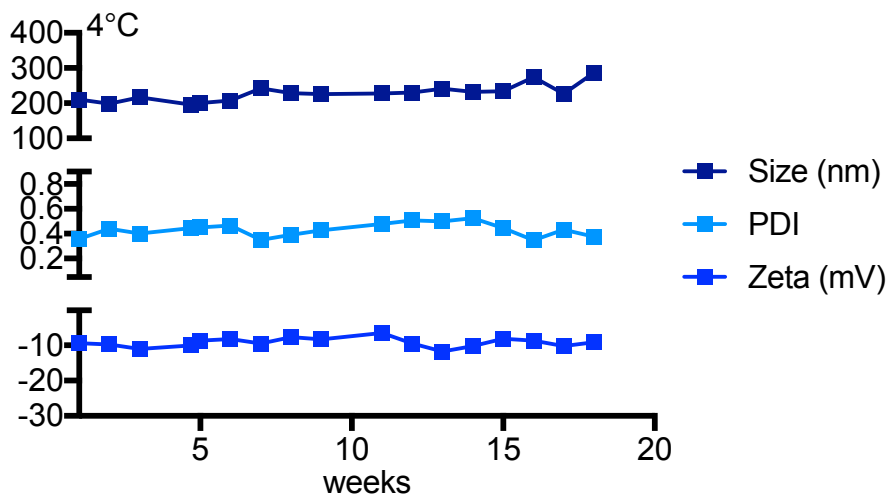

Figure 2. 23 NM2DRV stability (PK formulation)

NM2DRV stability measurements over 18 weeks from concentrated formulations used for PK dosing. Diluted NM2DRV were concentrated using differential centrifugation. First the nanoformulation was pelleted at 5,000 x g for 5 minutes. Then supernatant was transferred to a new centrifuge tube and centrifuged at 20,000 x g for 20 minutes. Supernatant was discarded and both pellets were suspended in a total of approximately 500 µL of PBS.
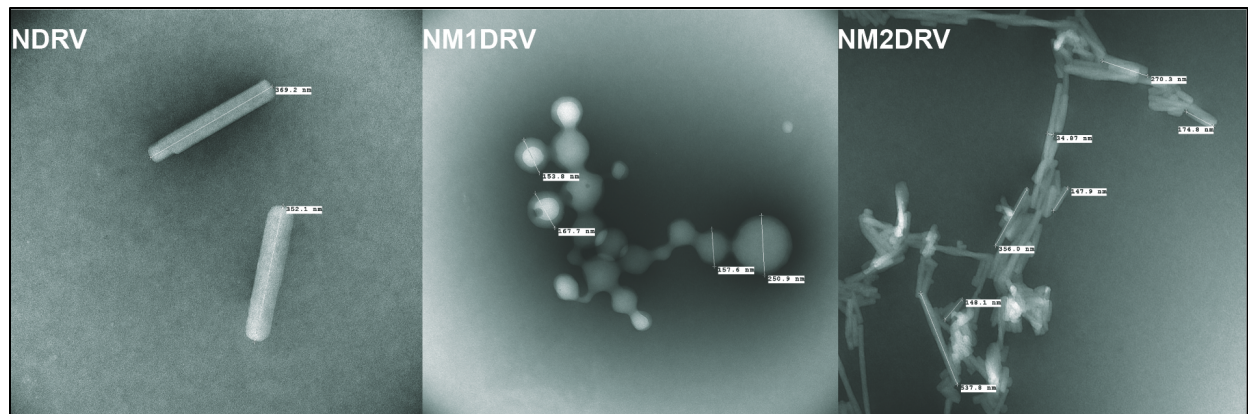
Figure 2. 24 Transmission electron microscopy of the formulations

NDRV and NM2DRV were rod-shaped, while NM1DRV exhibited globular morphologies. The three formulations have diameters in the nanometer range. Nanoparticle morphologies were analyzed by TEM using negative staining. Small volume (10 µL) of diluted nanoformulation (1 mg/mL) was applied on a formavar/silicone monoxide coated 200 mesh copper grid. Grid was left 2-5 minutes to absorb the nanoparticles. Excess sample was dried carefully using a clean filter paper and allowed to dry for 2 minutes. Pipet a drop of Nanovan negative stain on the grid and allow to stain for no longer than a minute while shielding the sample using a filter paper tent to minimize any air contaminants. Blot excess stain and allow grid to dry before viewing under TEM.
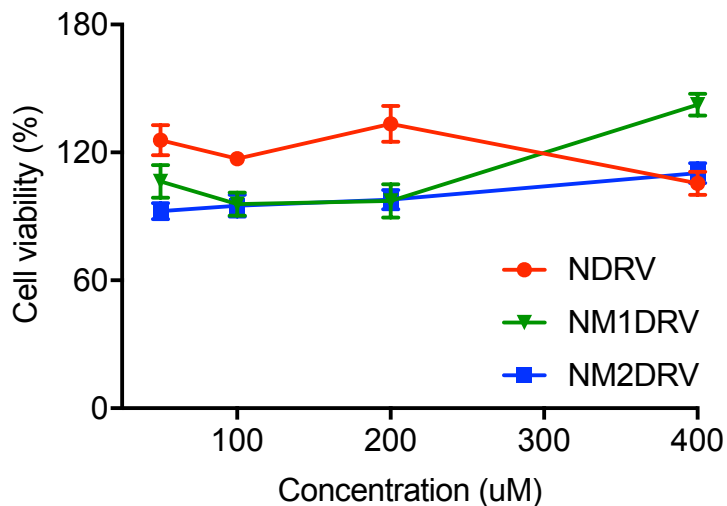
Figure 2. 25 Cytotoxicity of NDRV, NM1DRV and NM2DRV in MDM

Cytotoxicity of NDRV, NM1DRV and NM2DRV in MDM assayed by MTT. A stock solution of each drug nanoformulation was serially diluted in DMEM to produce drug concentrations ranging from 50-400 μM. Cells were treated for 24 hours, washed and incubated with 200 μL/well 3-(4,5-dimethylthiazol-2-yl)-2,5-diphenyltetrazolium bromide (MTT) solution (5 mg/mL) for 45 minutes. Upon MTT removal, 200 μL/well of DMSO was added and absorbance measured at 490 nm on a SpectraMax M3 plate reader. Data are expressed as mean ± SEM for n=3 samples per group.
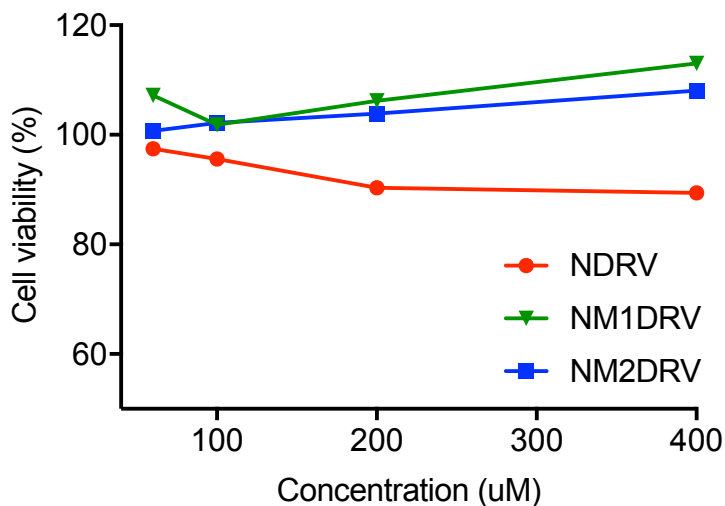

Figure 2. 26 Cytotoxicity of NDRV, NM1DRV and NM2DRV in CEM-SS CD+ T cells

Cytotoxicity of NDRV, NM1DRV and NM2DRV in CEM CD4+ T cells assayed by Live/Dead Fixable Dead Cell Stain Kits. A stock solution of each drug nanoformulation was serially diluted in RPMI media to produce drug concentrations ranging from 50-400 μM. After 24 hours, cells were centrifuged at 650 x g, dispersed in PBS, centrifuged again at 650 x g, and resuspended in PBS. Excitation dye (0.1 μL) (Molecular Probes, Live/Dead Fixable Green Dead Cell Stain Kits) was added to each well. Cells were excited at 488nm and the percent dead cells determined by flow cytometery. Data are expressed as mean ± SEM for n=3 samples per group.
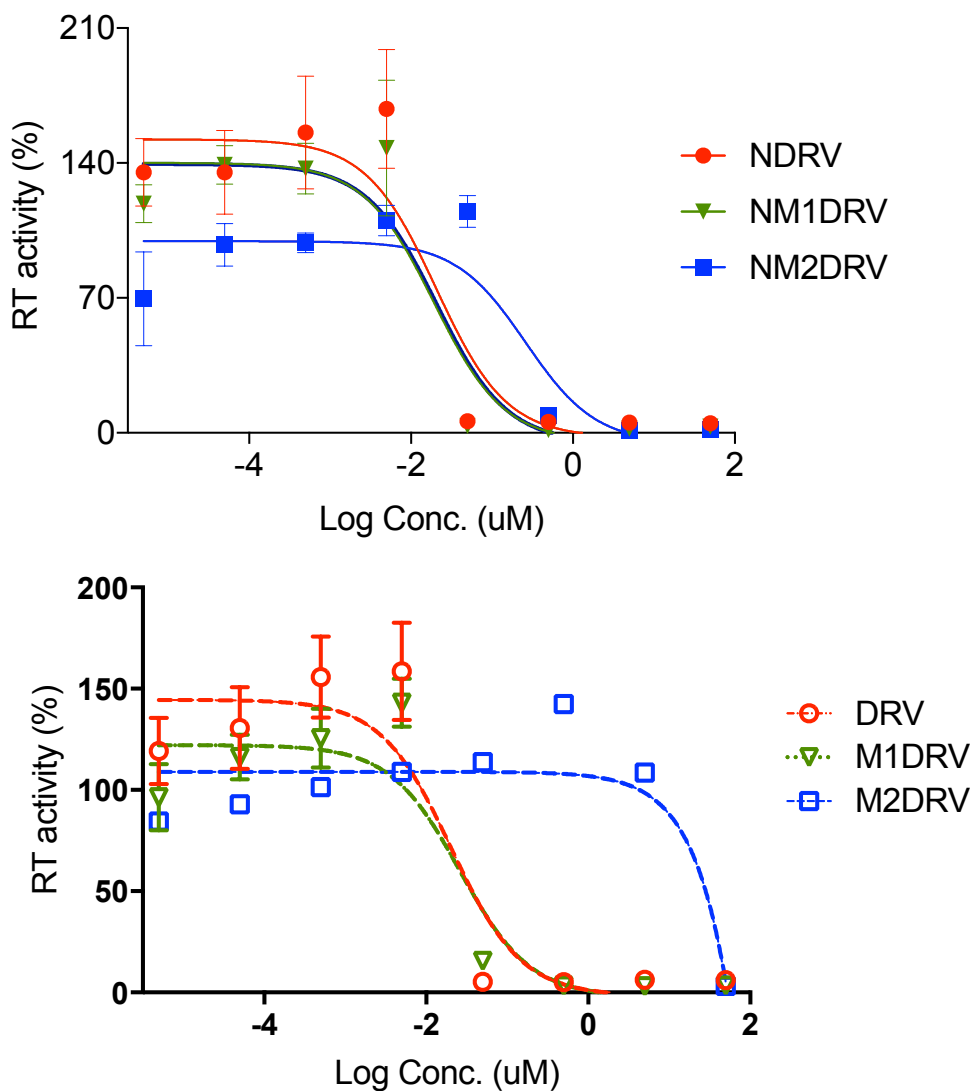
Figure 2. 27 Antiviral activities against HIV-1 were determined in MDM

Antiviral activities against HIV-1 were determined in MDM. EC_{50} determination was performed using non-nanoformulated (DRV, M1DRV, and M2DRV) and formulated (NDRV, NM1DRV, NM2DRV) compounds. Drugs were diluted in media at concentrations ranging from 0.005 nM-50 µM in tenfold dilution increments and cells were treated with the different concentrations for 60 min and replaced with drug-containing HIV-1$_{ADA}$ media at a multiplicity of infection (MOI) of 0.1. After 4 hours, infection medium was removed, and the cells were incubated an additional 10 days in the presence of the same concentration of drug prior to infection. Half media changes were done every other day. After 10 days of infection, culture media was collected for measures of HIV-1 reverse transcriptase (RT) activity. Data are expressed as mean ± SEM for n=3 samples per group.
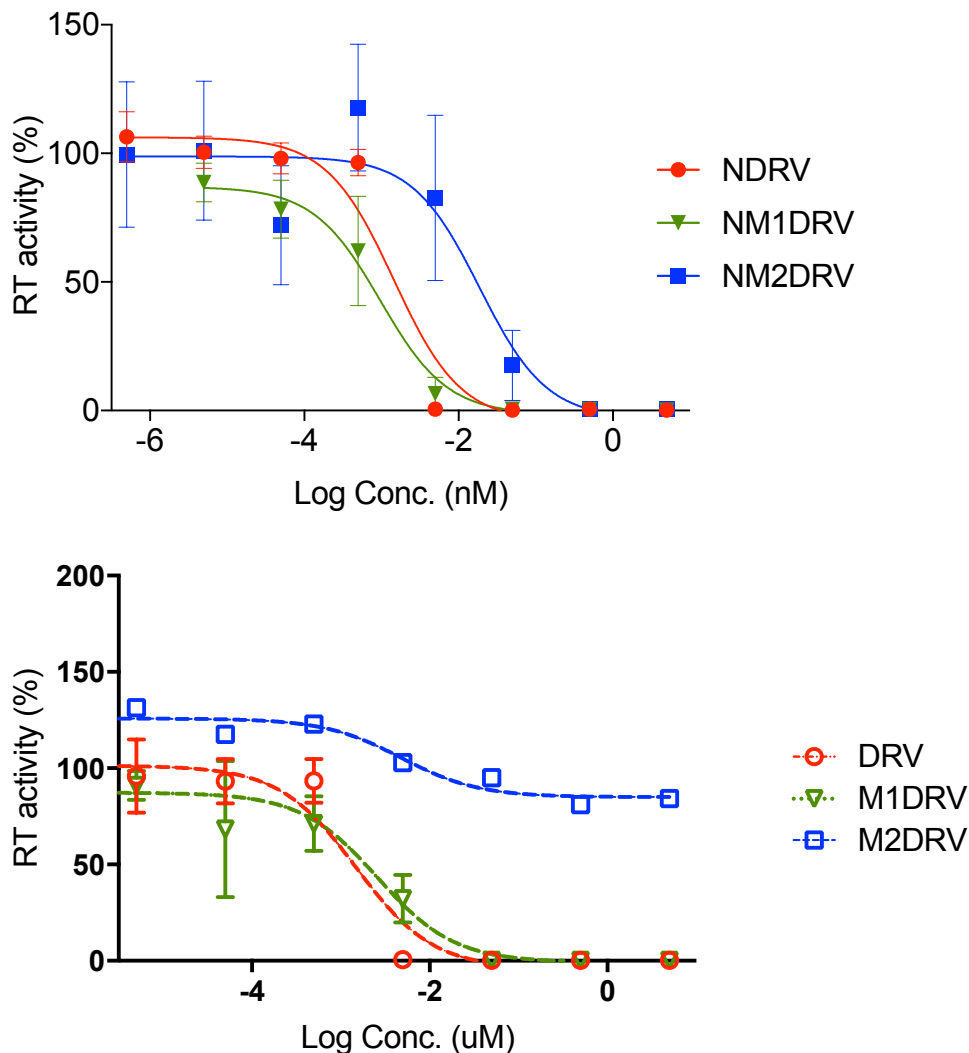
Figure 2. 28 Antiviral activities against HIV-1 were determined in CEM-SS CD4+ T cells

Antiviral activities against HIV-1 were determined in CEM CD4+ T cells. EC_{50} tests were performed using non-nanoformulated (DRV, M1DRV, and M2DRV) and formulated (NDRV, NM1DRV, NM2DRV) compounds. Drugs were diluted in media at concentrations ranging from 0.0005 nM-5 µM in tenfold dilution increments and cells were treated with the different concentrations for 60 min and replaced with drug-containing HIV-1$_{NL4-3-eGFP}$ media at a multiplicity of infection (MOI) of 0.1 by spin-inoculation followed by incubation for 2 hours. Cells were kept at 37°C in a 5% CO_2 incubator for 12 hours, after which media containing drug and FBS was added. Twenty-four hours post infection, all cells were washed twice with PBS to remove extracellular virus and drug-containing media was replaced with medium containing the same drug concentration prior to infection. Every other day, cells were centrifuged at 650 x g and resuspended in fresh drug-containing medium. After 10 days of infection, culture media was collected for measures of HIV-1 reverse transcriptase (RT) activity. Ten days post HIV-1 challenge; supernatants were collected for RT activity measurements. Antiretorviral activities were further confirmed using flow. Data are expressed as mean ± SEM for n=3 samples per group.
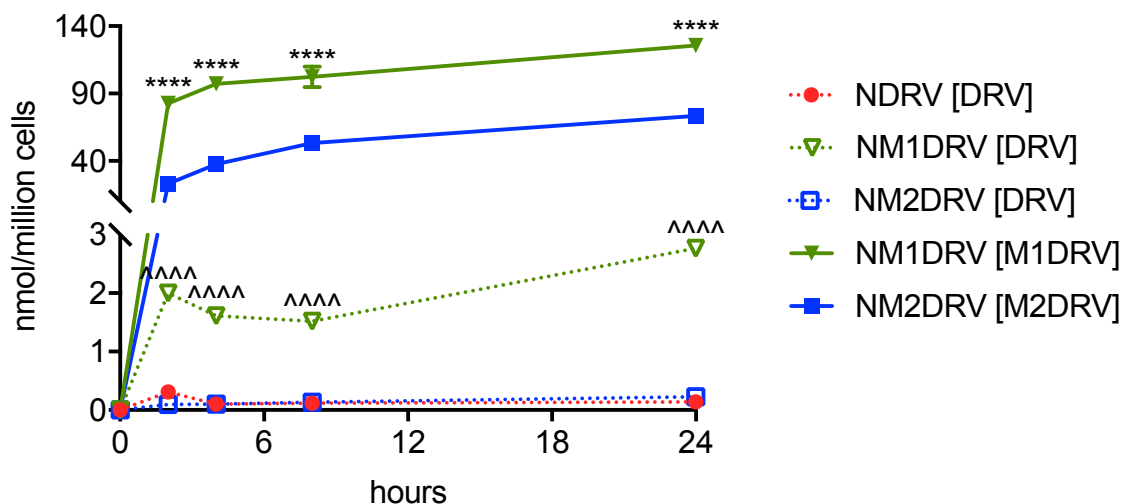
Figure 2. 29 Uptake of NDRV, NM1DRV and NM2DRV in MDM

Uptake of NDRV, NM1DRV and NM2DRV. Drug uptake studies in MDM demonstrated high intracellular drug levels for NM1DRV and NM2DRV treatments compared to undetectable levels for NDRV. MDM were cultured on 12-well culture plates and treated with media containing 100µM of NDRV, NM1DRV or NM2DRV. At 2, 4 and 8 hours post treatment, media was removed and adherent cells were washed twice with PBS then scraped into 1mL PBS. Cells were counted and pelleted by centrifugation at 956 x g for 8 minutes. The cell pellets were reconstituted and sonicated in 100 µL methanol for 5 minutes followed by centrifugation at 20,817 x g for 5 min and quantified using HPLC. Data are expressed as mean ± SEM for n=3 samples per group. ^^^^P<0.0001 for NDRV vs. NM1DRV, parent drug quantitation and ****P<0.0001 for NM1DRV vs. NM2DRV, quantitation of prodrugs
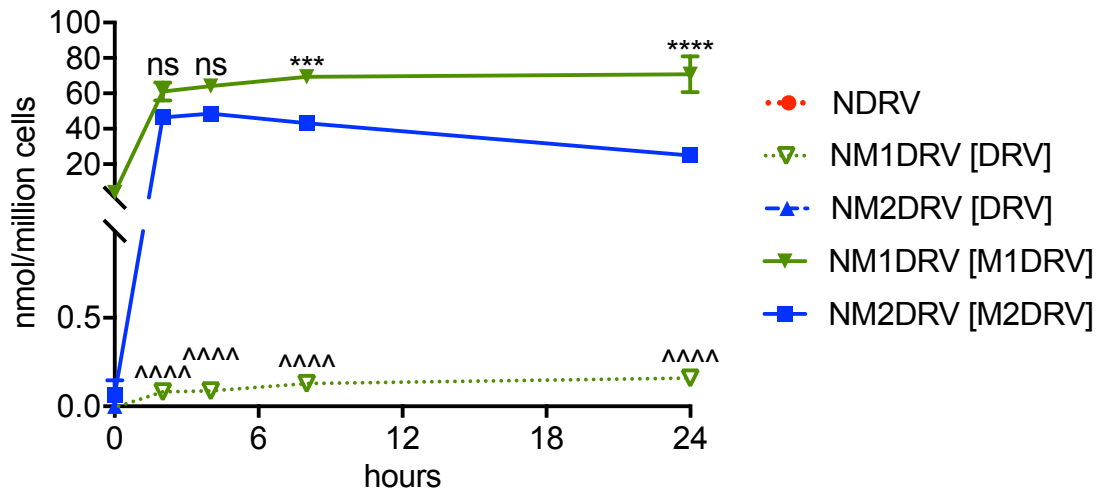
Figure 2. 30 Uptake of NDRV, NM1DRV and NM2DRV in CEM-SS CD4 T cells

Uptake of NDRV, NM1DRV and NM2DRV. Drug uptake studies in CEM-SS CD4+ T cells demonstrated high intracellular drug levels for NM1DRV and NM2DRV treatments compared to undetectable levels for NDRV. The cells were plated on to poly-L-lysine pre-coated cell culture plates that make it possible for these cells to adhere. At 2, 4 and 8 hours post treatment, media was removed and adherent cells were washed twice with PBS then scraped into 1mL PBS. Cells were counted and pelleted by centrifugation at 956 x g for 8 minutes. The cell pellets were reconstituted and sonicated in 100 µL methanol for 5 minutes followed by centrifugation at 20,817 x g for 5 min and quantified using HPLC. Data are expressed as mean ± SEM for n=3 samples per group. ^^^^P<0.0001 for NDRV vs. NM1DRV, parent drug quantitation and ****P<0.0001, ***P=0.0007 for NM1DRV vs. NM2DRV, quantitation of prodrugs.
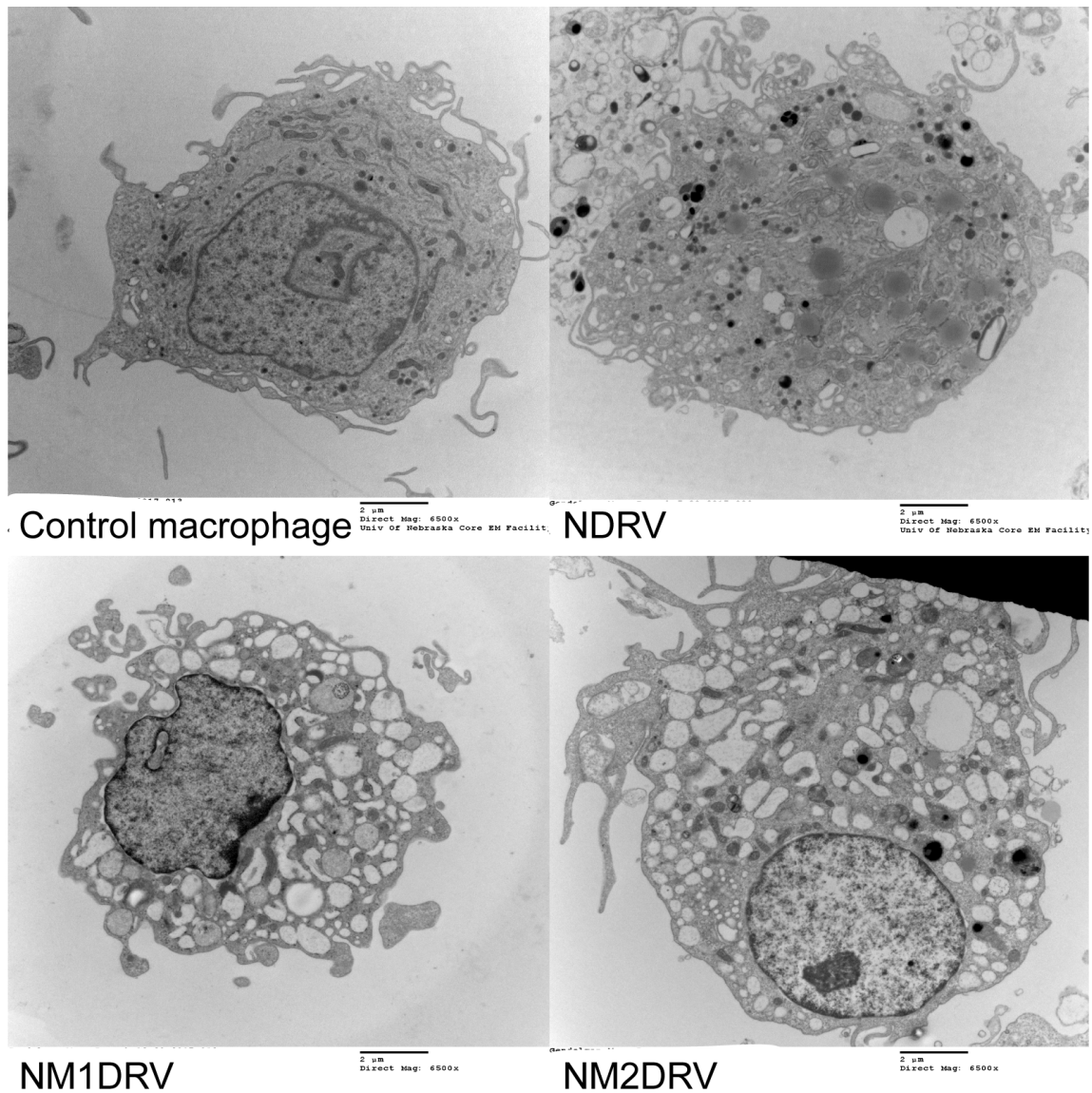
Control macrophage | NDRV

NM1DRV | NM2DRV

Figure 2. 31 TEM image of MDM loaded with NDRV, NM1DRV, and NM2DRV.

Transmission electron microscopy (TEM) was used to image the morphology of MDM-loaded with the different drug nanoparticles. Cells were loaded with the different nanoparticles for 4 hours then washed twice with PBS. Cells were collected in PBS, centrifuged, fixed in 2% paraformaldehyde (PFA) and kept at 4°C until TEM processing.
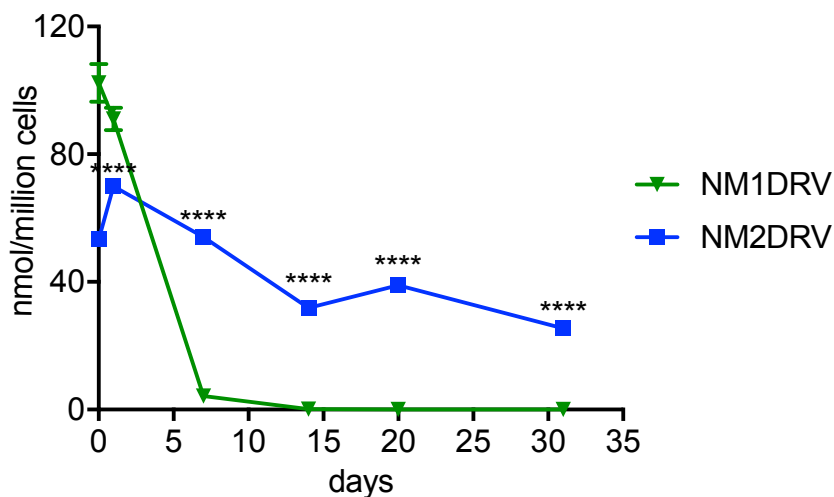
Figure 2. 32 Drug retention in MDM

NM1DRV and NM2DRV were retained in MDM for 14 and 31 days, respectively, while NDRV was washed out within hours. For drug retention studies, MDM were treated for 8 hours then washed with PBS and maintained with half-media changes every other day until collection days. Intracellular and supernatant drug content were analyzed using HPLC. Data are expressed as mean ± SEM for n=3 samples per group. ****P<0.0001 for NM1DRV vs. NM2DRV.

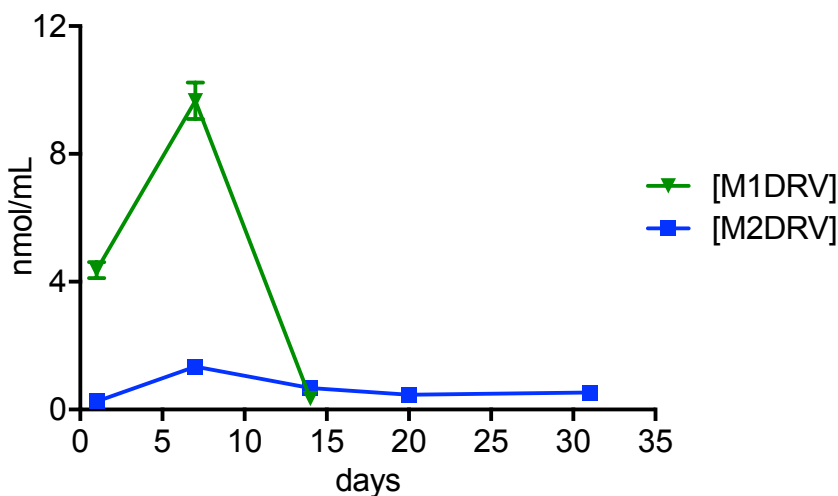
Figure 2. 33 Drug release from MDM

Drug release from MDM after a single treatment with 100 µM of drug. NM1DRV and NM2DRV exhibited sustained release of drug into culture media. Data are expressed as mean ± SEM for n=3 samples per group.
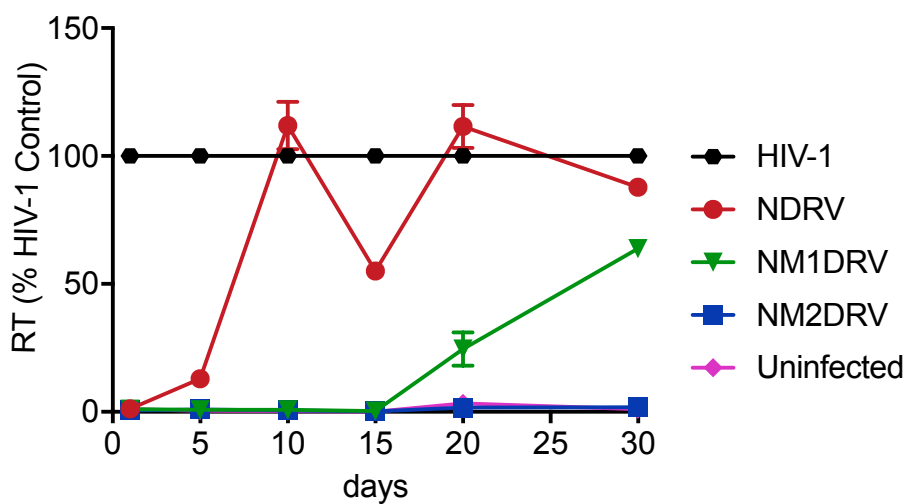
Figure 2. 34 Antiretroviral activity in MDM

Antiretroviral activities in MDM after a single treatment with 100 µM of drug determined by RT assay. To assess long-term antiretroviral efficacy, MDM were treated for 8 hours with 100 µM NDRV, NM1DRV or NM2DRV as previously described for uptake studies. After treatment, cells were washed twice with PBS and cultured in fresh media without drug followed by half-media changes every other day. At 5-day intervals from days 1 to 30 after treatment, cells were challenged with HIV-1$_{ADA}$ at a MOI of 0.1 for 16 hours. HIV-1$_{ADA}$ media was then replaced with fresh media without drug. Ten days after viral challenge culture media were analyzed for RT activity. Data are expressed as mean ± SEM for n=3 samples per group.

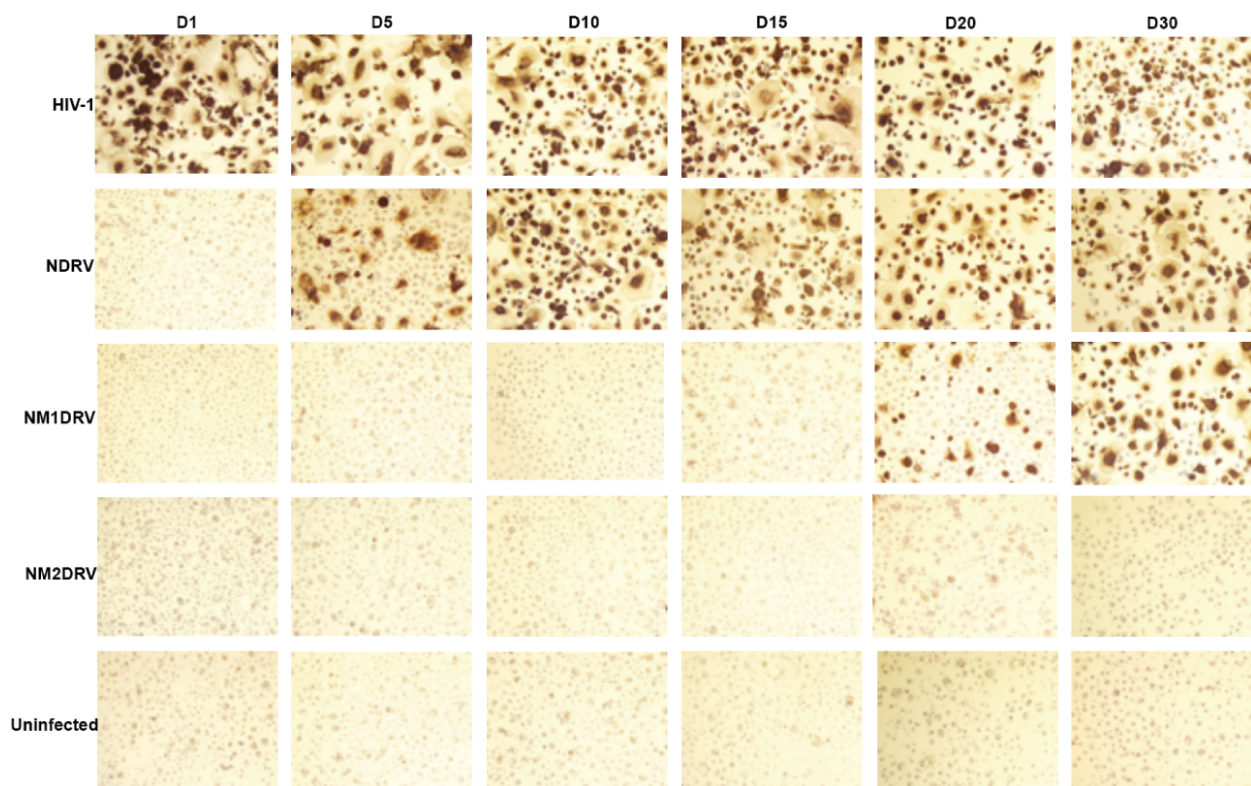**Figure 2. 35 Antiretroviral activity studies in MDM**

Antiretroviral activity studies in MDM after a single treatment with 100 µM of drug assayed by HIV-1p24 antigen staining. Adherent MDM were fixed with 2% PFA and assessed for HIV-1p24. NM2DRV formulation demonstrated long-term viral suppression for a period of 30 days compared to viral breakthrough within 15 days and one day for NM1DRV and NDRV, respectively.
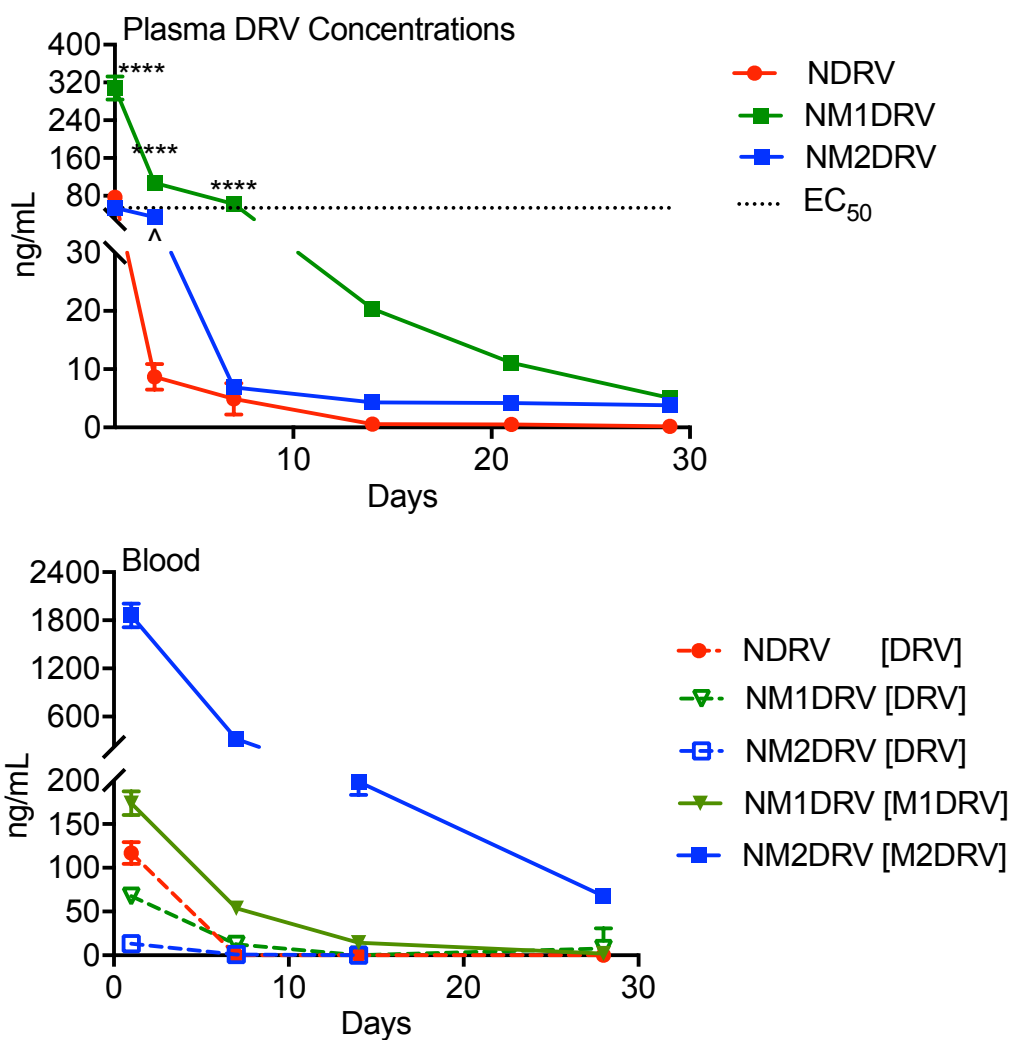
Figure 2. 36 Pharmacokinetics in mice

1-month pharmacokinetics in BALB/cJ mice - 50 mg/kg DRV equivalents. Plasma and blood DRV, M1DRV and M2DRV levels. Mice were injected intramuscularly with 40 uL of 50 mg/lg DRV equivalents for all three different nanoformulations. Blood and plasma samples were collected at different time points. DRV plasma levels remains over EC_{50} for a week after once treatment NM1DRV. Data are expressed as mean ± SEM for n=5 samples per group. ****$P < 0.0001$ for NM1DRV vs. NM2DRV and ^$P = 0.0165$ for NM2DRV vs. NDRV.
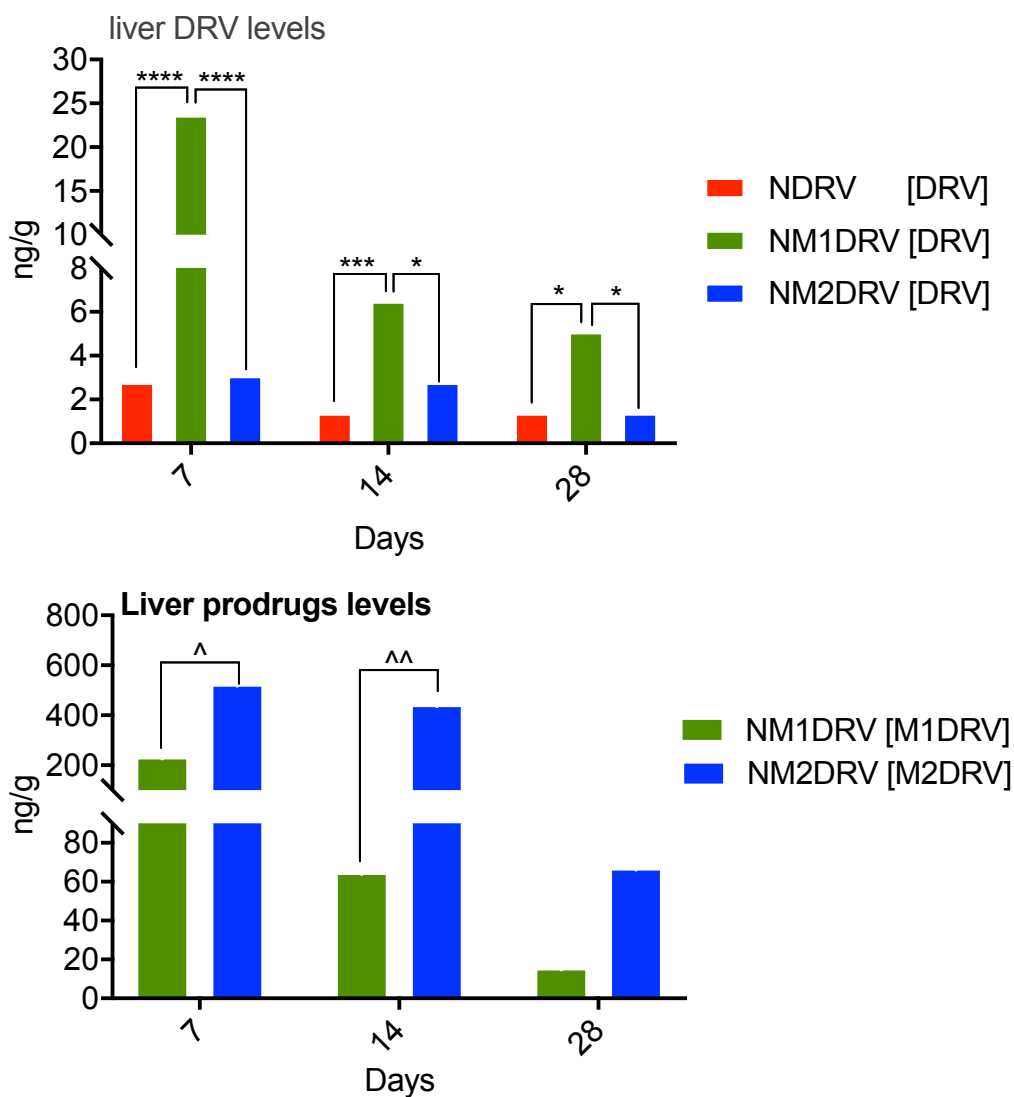
Figure 2. 37 Liver drug levels

1-month biodistribution in BALB/cJ mice - 50 mg/kg DRV equivalents. DRV and prodrugs levels in livers on days 7, 14, and 28 post NDRV, NM1DRV or NM2DRV treatments. DRV cleaving from NM1DRV is highest at day 7 compared to all other treatments and the different time points. High prodrug levels are detected at the different time points for both prodrug nanoformulations. Data are expressed as mean ± SEM for n=5 samples per group. ****P < 0.0001, ***P = 0.0004, and *P = 0.0104 for DRV levels in liver. ^^P = 0.0055 and ^P = 0.0347 for liver prodrug levels in NM1DRV vs. NM2DRV.

Figure 2. 38 Spleen and lymph nodes prodrug levels
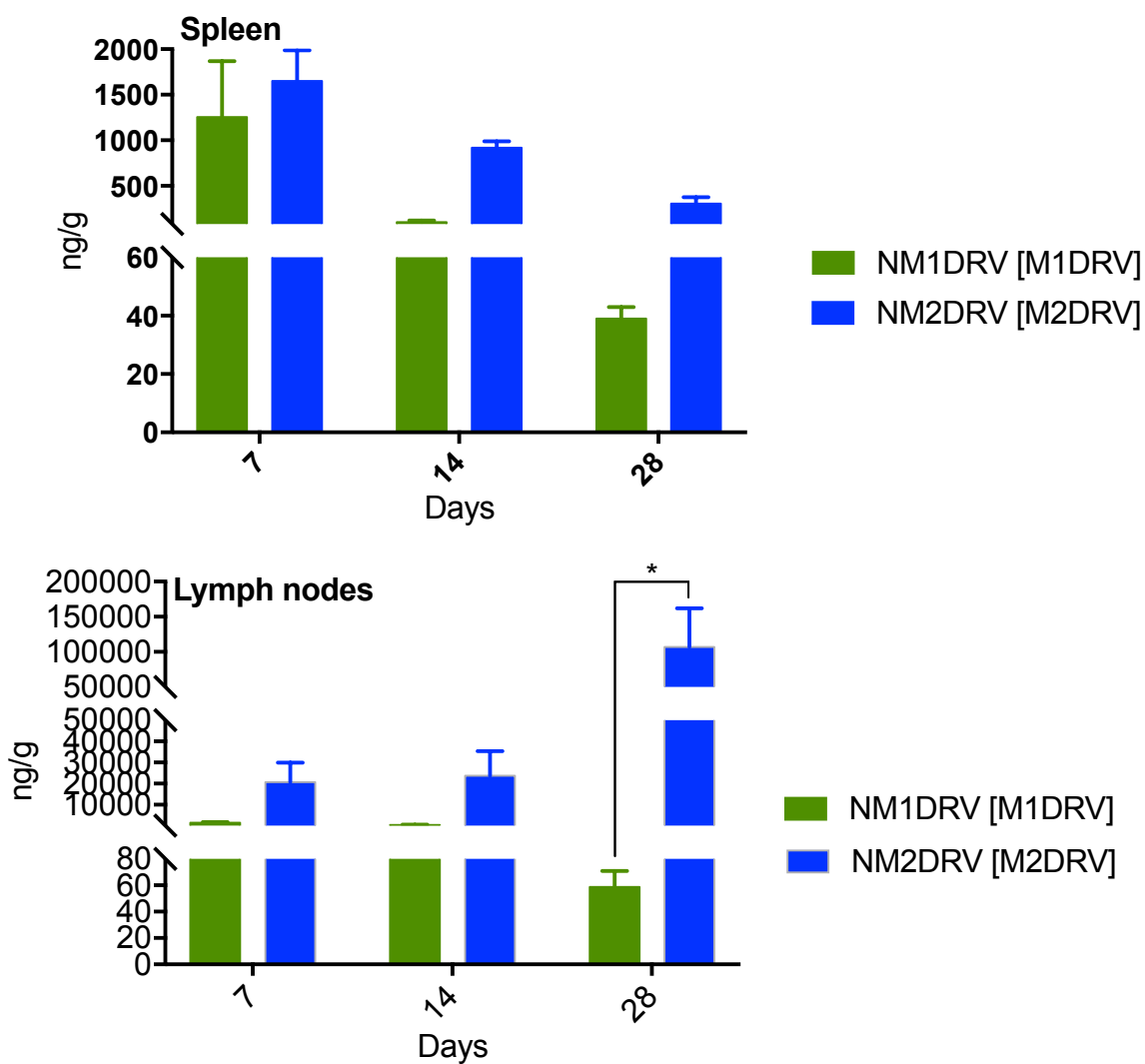
1-month biodistribution in BALB/cJ mice - 50 mg/kg DRV equivalents. High prodrug levels are detected at the different time points for both prodrug nanoformulations in spleens and lymph nodes. No DRV cleaved from the prodrugs is detected in these tissues over the different time points. Data are expressed as mean ± SEM for n=5 samples per group. *P = 0.0100 for NM2DRV vs. NM1DRV.

Figure 2. 39 RTV-boost Pharmacokinetics in PXR/CAR/CYP3A4/7 tADMET

RTV-boost pharmacokinetics in PXR/CAR/CYP3A4/7 tADMET. DRV and M1DRV levels in plasma and blood, respectively. Mice were administered 50 mg/kg DRV-equivalent dose of NM1DRV intramuscularly. RTV-boosted groups were given an RTV nanoformulation (NRTV) IM boost injections on days 0, 7 and 14 of the study. Plasma and blood samples were collected in heparinized tubes on days 1, 7, 14 and 21. Plasma and blood samples were analyzed by LC-MS/MS to determine parent and prodrug levels as well as the effect of the boost on drugs' bioavailability. RTV boosting effect was only significant one day post injections. Data are expressed as mean ± SEM for n=5 samples per group. **P = 0.0016 for DRV levels from NM1DRV/r vs. NM1DRV in control mice and ^^^P = 0.0009 for DRV levels from NM1DRV/r vs. NM1DRV in tADMETs.
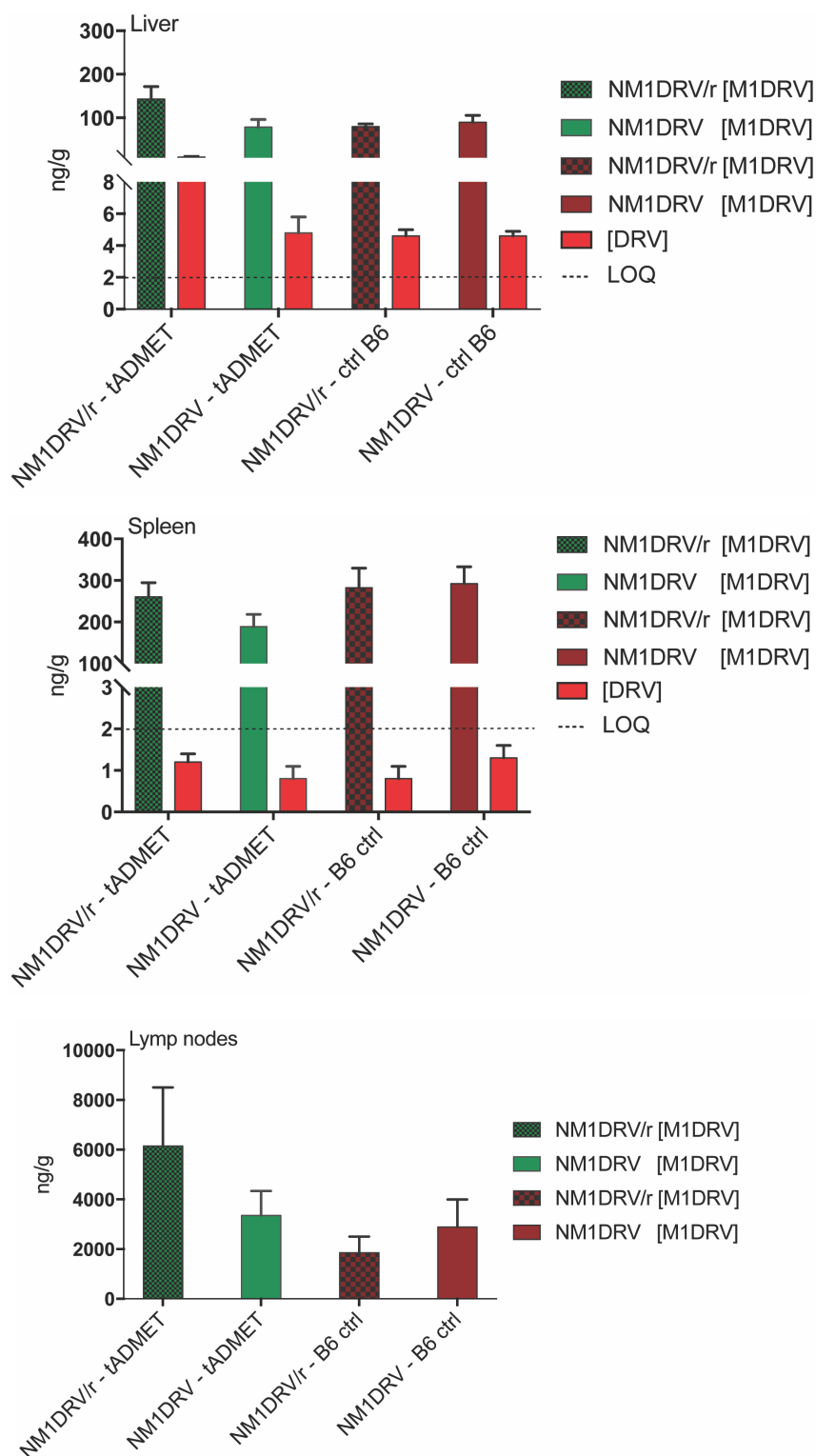
Figure 2. 40 Tissue drug levels in PXR/CAR/CYP3A4/7 tADMET

RTV-boost biodistribution in PXR/CAR/CYP3A4/7 tADMET. DRV and M1DRV drug levels the different tissues. In the humanized mice model, DRV is finally detected in the spleens of the mice, not only the livers. Data are expressed as mean ± SEM for n=5 samples per group
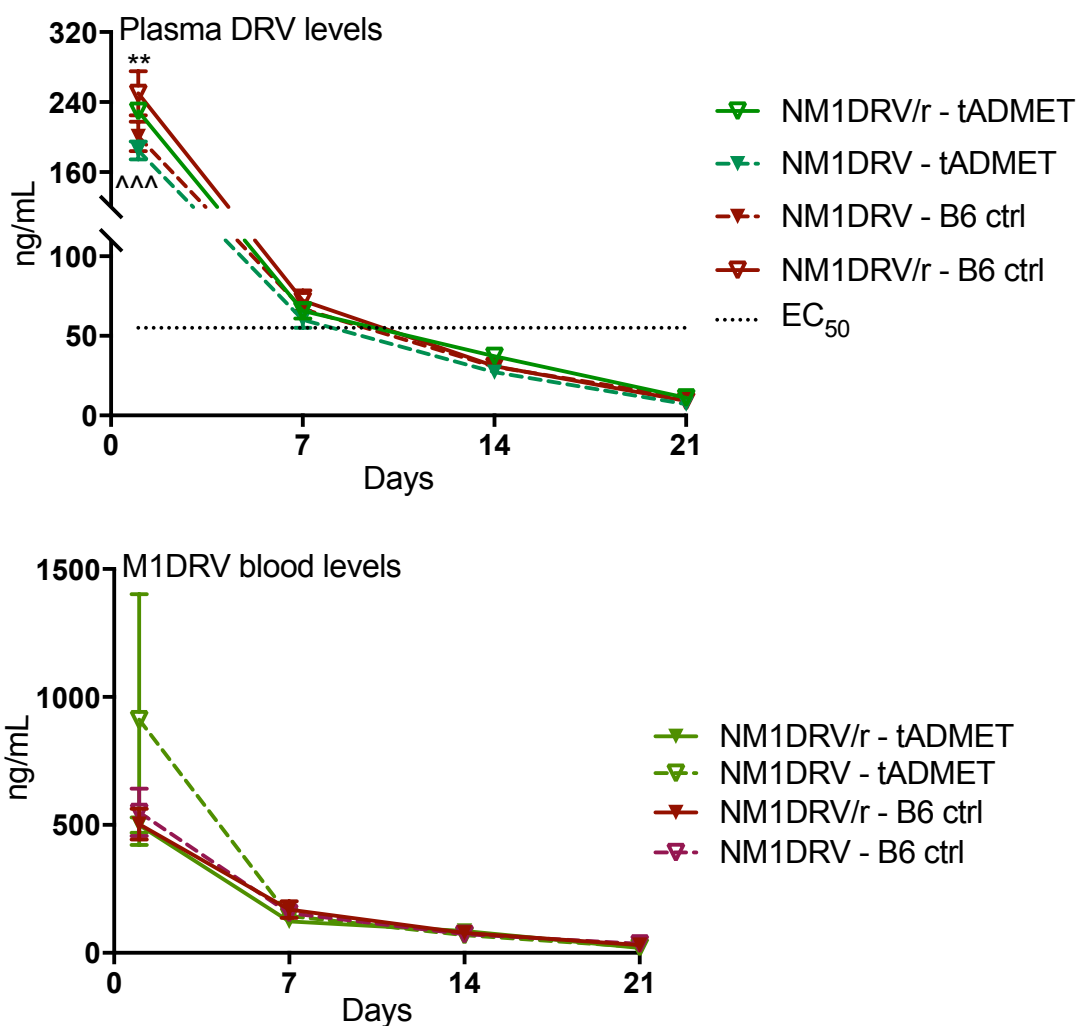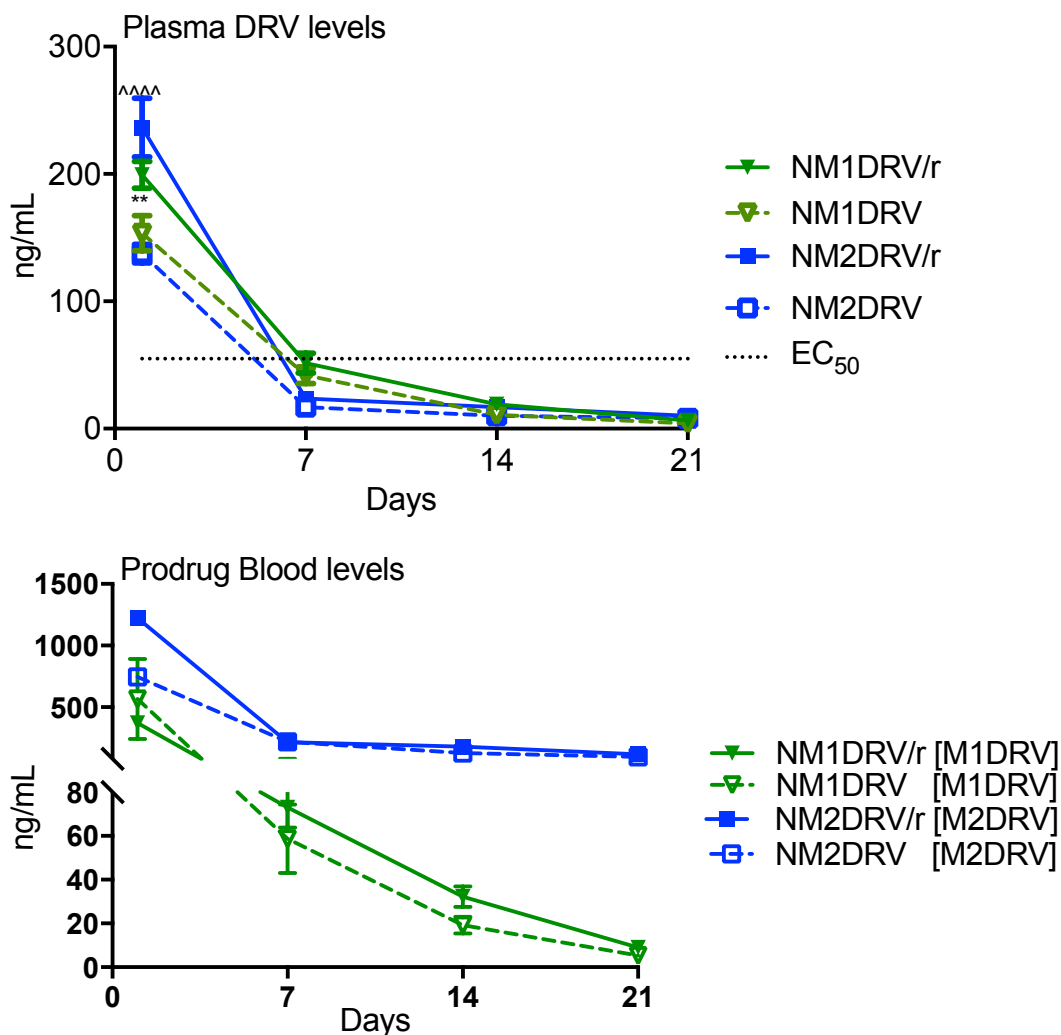
Figure 2. 41 RTV-boost Pharmacokinetics in PXR/CAR/CYP3A/NOG

RTV-boost pharmacokinetics in PXR/CAR/CYP3A/NOG. DRV levels in plasma. M1DRV and M2DRV levels in blood. Mice were administered 50 mg/kg DRV-equivalent dose of NM1DRV or NM2DRV intramuscularly. RTV-boosted groups were given an RTV nanoformulation (NRTV) IM boost injections on days 0, 7 and 14 of the study. Similar to the BALB/cJ PK studies, plasma and blood samples were collected in heparinized tubes on days 1, 7, 14 and 21. Plasma and blood samples were analyzed by LC-MS/MS to determine parent and prodrug levels as well as the effect of the boost on drugs' bioavailability. RTV boosting effect was only significant one day post injections. Data are expressed as mean ± SEM for n=5 samples per group. ^^^^$P < 0.0001$ for NM2DRV/r vs. NM2DRV and **$P = 0.0028$ for NM1DRV/r vs. NM1DRV.
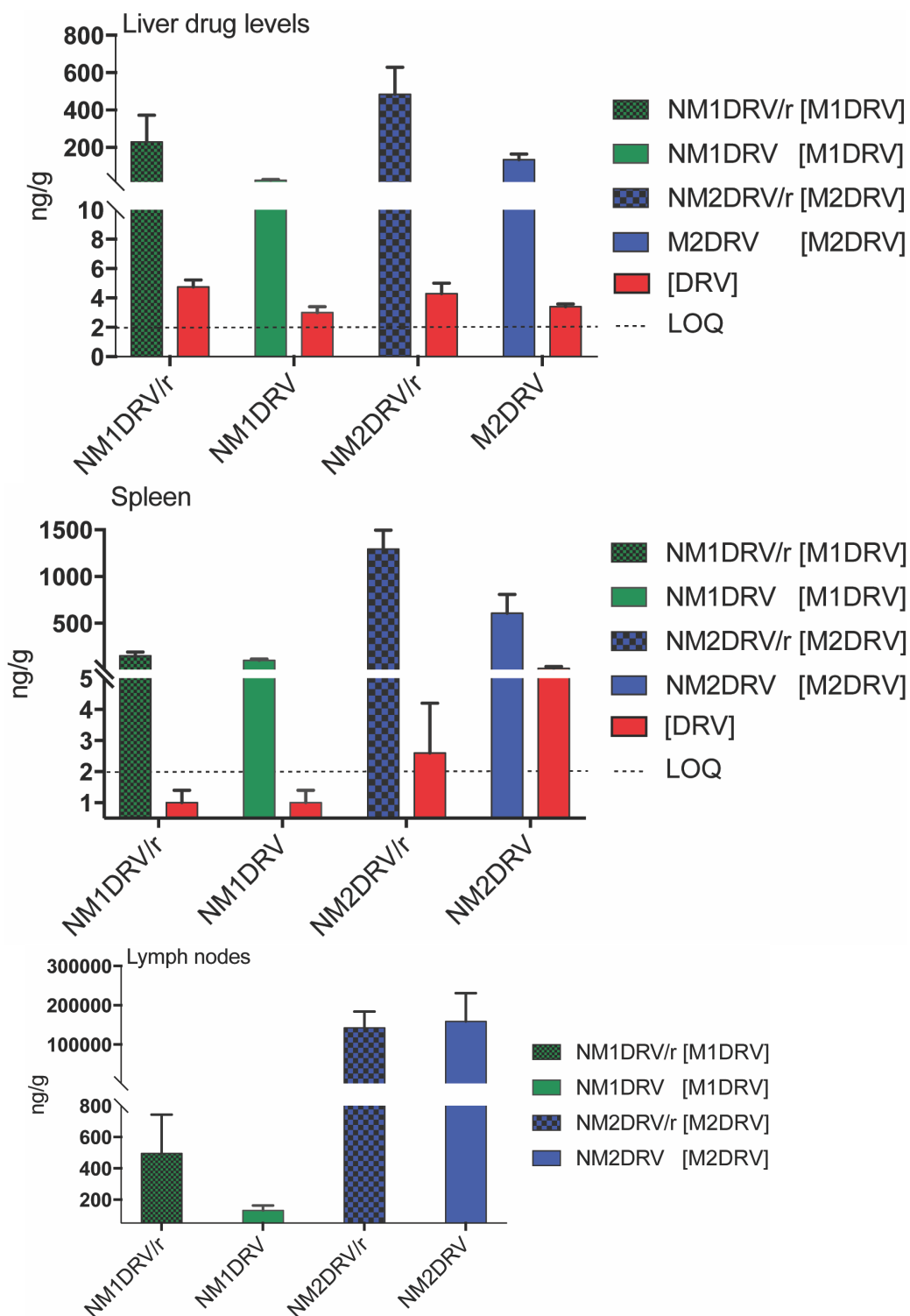
Figure 2. 42 Tissue drug levels in PXR/CAR/CYP3A/NOG

RTV-boost biodistribution in PXR/CAR/CYP3A/NOG. DRV, M1DRV and M2DRV levels in liver, spleen, and lymph nodes. In the humanized mice model, DRV is finally detected in the spleens of the mice, not only the livers especially in the case of NM2DRV. Data are expressed as mean ± SEM for n=5 samples per group.
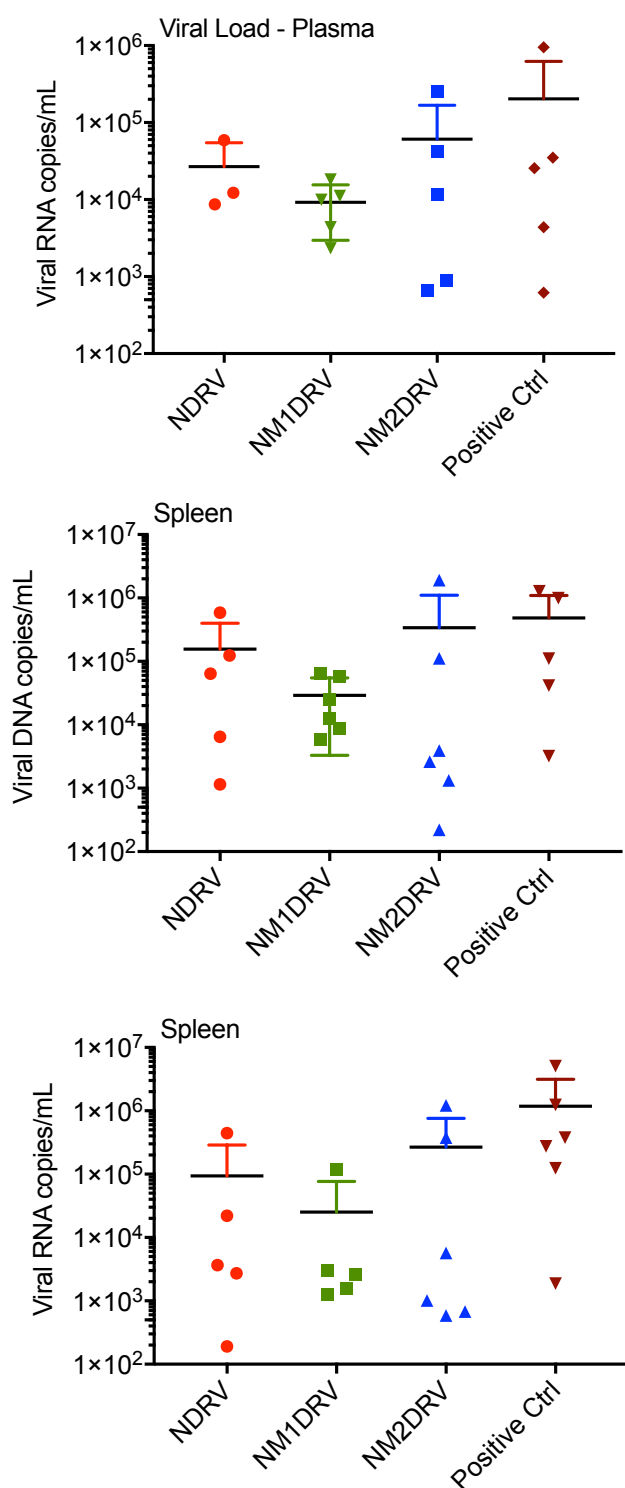
Figure 2. 43 Plasma viral loads

PrEP Pharmacodynamics in CD34+ NSG mice – 50 mg/kg DRV equivalents. Viral breakthrough was measured in all treatments as confirmed by plasma viral load as well as HIV-1 gag RNA and DNA copies in spleen.
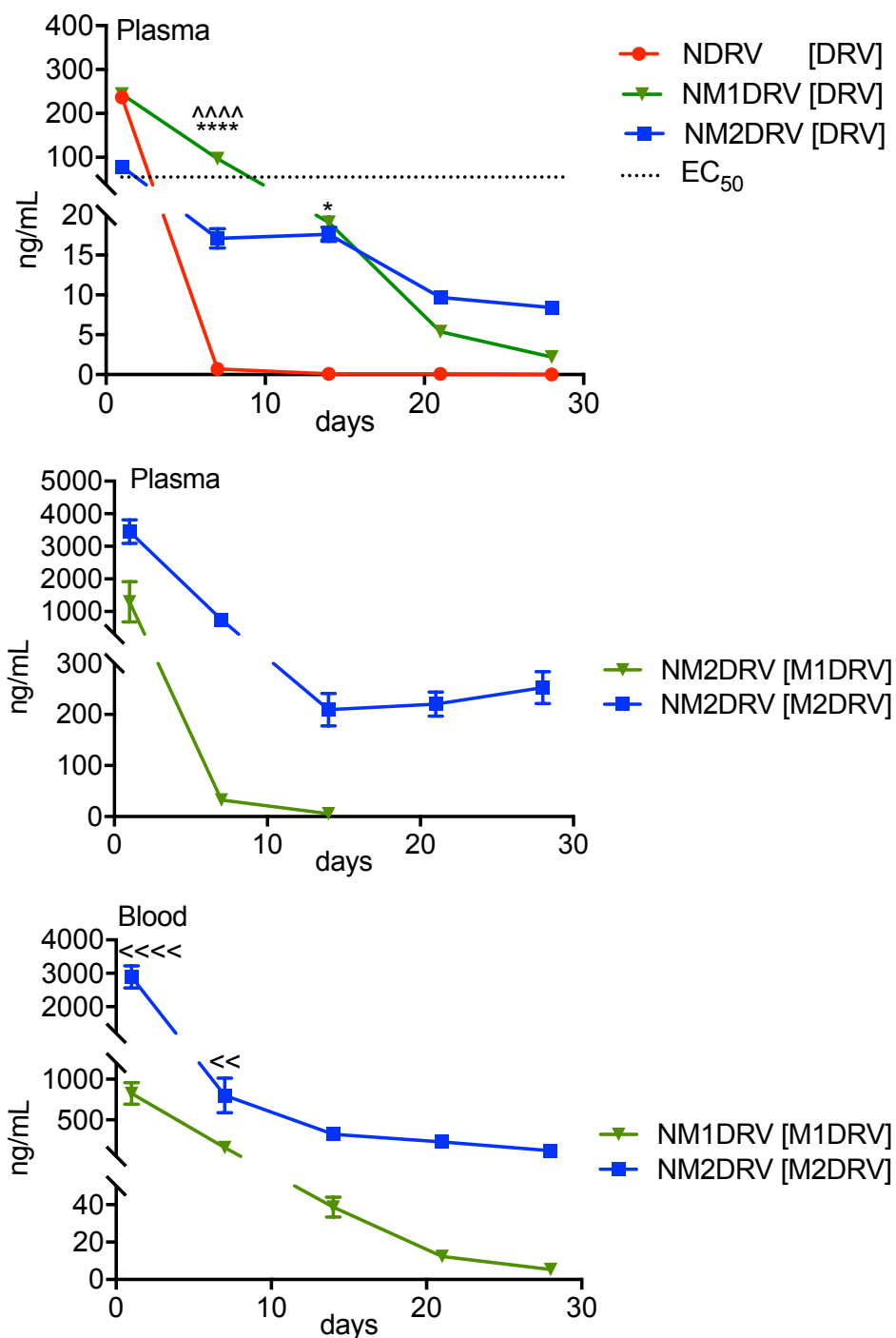
Figure 2. 44 DRV plasma levels (100 mg/kg eq.)

Pharmacokinetics in BALB/cJ mice after once IM 100 mg/kg DRV equivalents. Plasma DRV levels demonstrating sustained drug release for NM1DRV and NM2DRV formulations. High prodrug levels are detected in plasma and blood of these mice on day 28 especially for NM2DRV. Data are expressed as mean ± SEM for n=5 mice per group. ****P < 0.0001 and *P = 0.0438 for DRV levels from NM1DRV vs. NM2DRV, ^^^^P < 0.0001 for DRV levels from NM1DRV vs. NDRV, and <<<<P < 0.0001 and <<P = 0.0085 for prodrug levels from NM2DRV vs. NM1DRV.
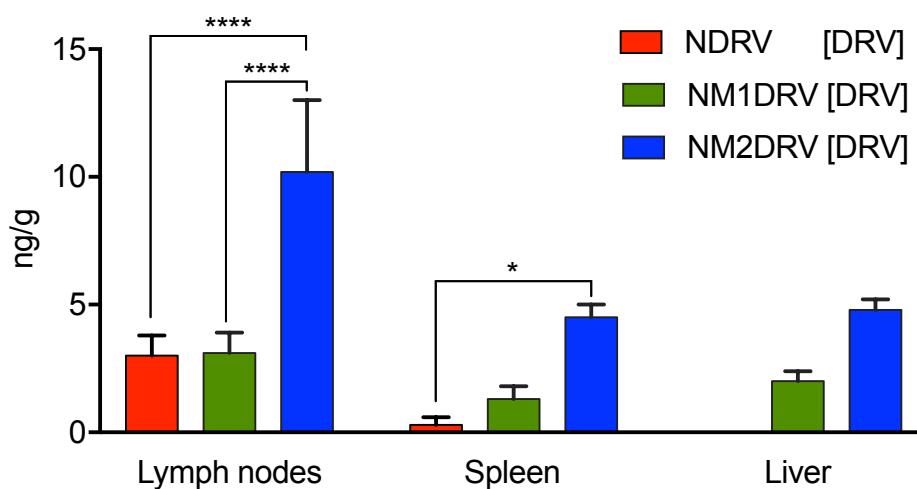
Figure 2. 45 Tissue DRV concentrations at day 28.

Pharmacokinetics in BALB/cJ mice -100 mg/kg DRV equivalents. DRV levels are detected in lymph nodes, spleen, and liver with the higher dose. Higher DRV is detected from NM2DRV on day 28 based only on the raw numbers. Data are expressed as mean ± SEM for n=5 mice per group. ****$P < 0.0001$ and *$P = 0.0237$ for DRV in tissues.
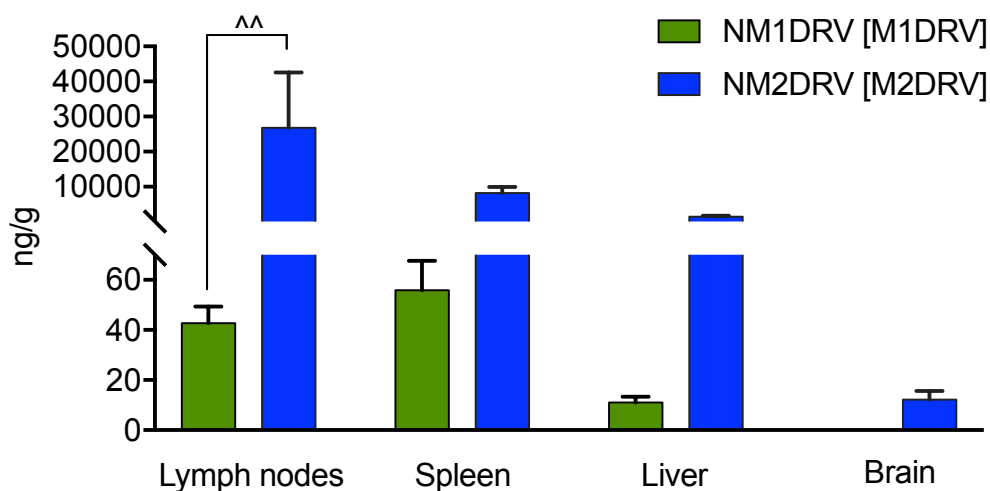
Figure 2. 46 Tissue M1DRV and M2DRV concentrations at day 28.

Pharmacokinetics in BALB/cJ mice -100 mg/kg DRV equivalents. Prodrug levels in the lymph nodes, spleen, liver, and brain demonstrating high prodrug concentrations for NM2DRV compared to NM1DRV treatment. Data are expressed as mean ± SEM for n=5 mice per group. ^^$P = .0074$ for prodrug levels in NM2DRV vs. NM1DRV.
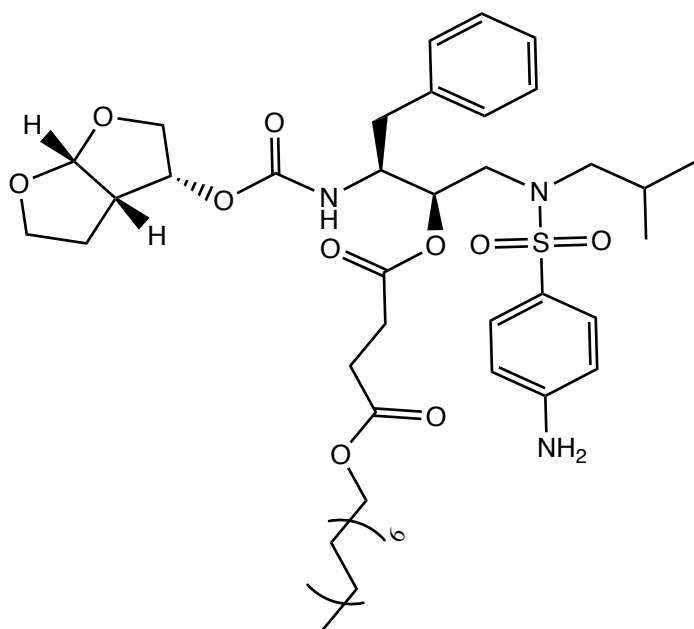
Figure 2. 47 Structure of M3DRV

M3DRV was synthesized by the modification of the hydroxyl group of DRV to a 14-carbon fatty acid chain attached to a succinate linker.
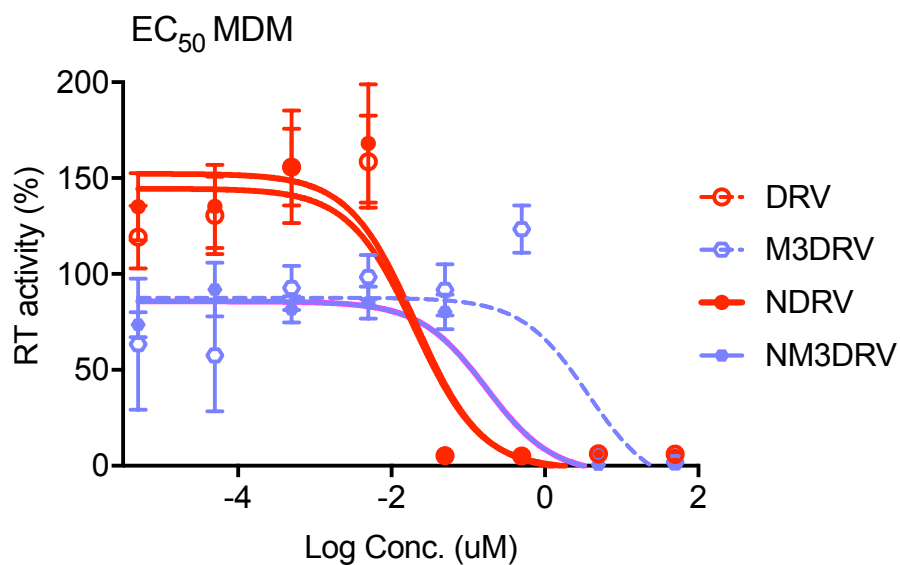
Figure 2. 48 M3DRV Antiviral activities against HIV-1 in MDM

EC_{50} was determined in macrophages for free drugs and their nanoformulations; DRV, M3DRV, NDRV and NM3DRV. Drugs were diluted in media at concentrations ranging from 0.005 nM-50 µM in tenfold dilution increments and cells were treated with the different concentrations for 60 min and replaced with drug-containing HIV-1$_{ADA}$ media at a multiplicity of infection (MOI) of 0.1. After 4 hours, infection medium was removed, and the cells were incubated an additional 10 days in the presence of the same concentration of drug prior to infection. Half media changes were done every other day. After 10 days of infection, culture media was collected for measures of HIV-1 reverse transcriptase (RT) activity. Data are expressed as mean ± SEM for n=3 samples per group.

Figure 2. 49 M3DRV Antiviral activities against HIV-1 in CEM-SS CD4 T cells

EC_{50} was determined in CEM-SS CD4 T cells for free drugs and their nanoformulations; DRV, M3DRV, NDRV and NM3DRV. Drugs were diluted in media at concentrations ranging from 0.0005 nM-5 µM in tenfold dilution increments and cells were treated with the different concentrations for 60 min and replaced with drug-containing HIV-1$_{NL4-3-eGFP}$ media at a multiplicity of infection (MOI) of 0.1 by spin-inoculation followed by incubation for 2 hours. Cells were kept at 37°C in a 5% CO_2 incubator for 12 hours, after which media containing drug and FBS was added. Twenty-four hours post infection, all cells were washed twice with PBS to remove extracellular virus and drug-containing media was replaced with medium containing the same drug concentration prior to infection. Every other day, cells were centrifuged at 650 x g and resuspended in fresh drug-containing medium. After 10 days of infection, culture media was collected for measures of HIV-1 reverse transcriptase (RT) activity. Ten days post HIV-1 challenge; supernatants were collected for RT activity measurements. Data are expressed as mean ± SEM for n=3 samples per group.
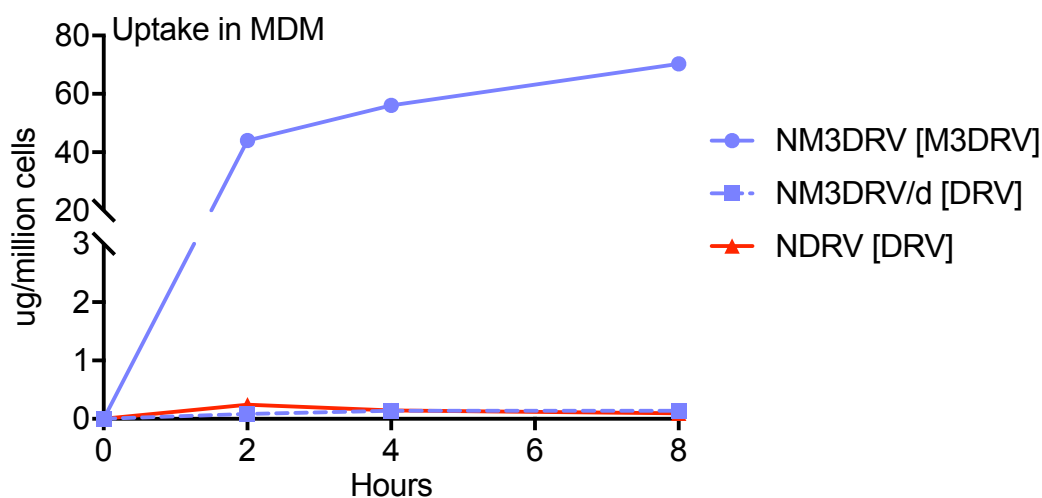
Figure 2. 50 NM3DRV uptake in MDM

High uptake of M3DRV was detected in macrophages treated with NM3DRV (100 uM). MDM were cultured on 12-well culture plates and treated with media containing 100µM of NDRV or NM3DRV. At 2, 4 and 8 hours post treatment, media was removed and adherent cells were washed twice with PBS then scraped into 1mL PBS. Cells were counted and pelleted by centrifugation at 956 x g for 8 minutes. The cell pellets were reconstituted and sonicated in 100 µL methanol for 5 minutes followed by centrifugation at 20,817 x g for 5 min and quantified using HPLC. Data are expressed as mean ± SEM for n=3 samples per group.
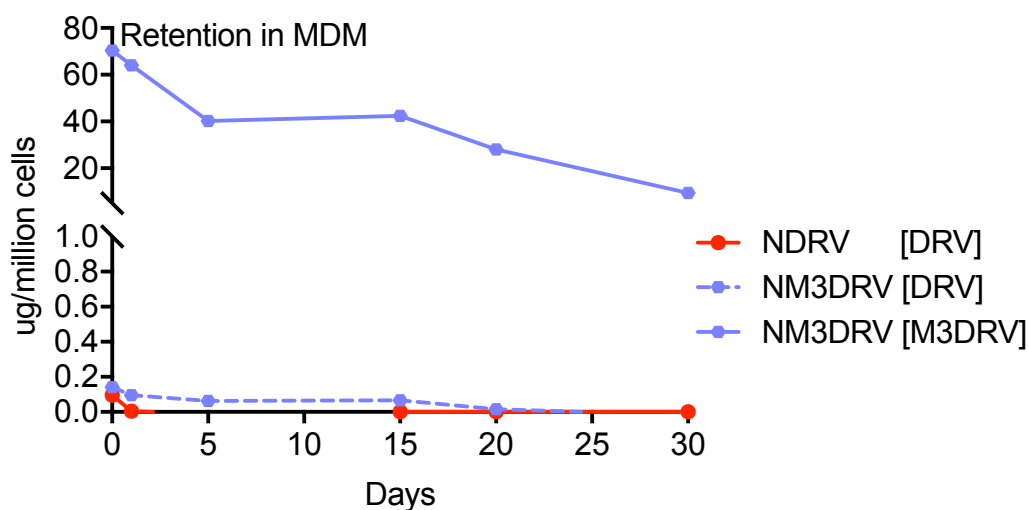
Figure 2. 51 NM3DRV retention in MDM for a month

M3DRV was retained in cells for 30 days compared to no detectable levels of DRV from NDRV treatment.For drug retention studies, MDM were treated for 8 hours then washed with PBS and maintained with half-media changes every other day until collection days. Intracellular and supernatant drug content were analyzed using HPLC. Data are expressed as mean ± SEM for n=3 samples per group.
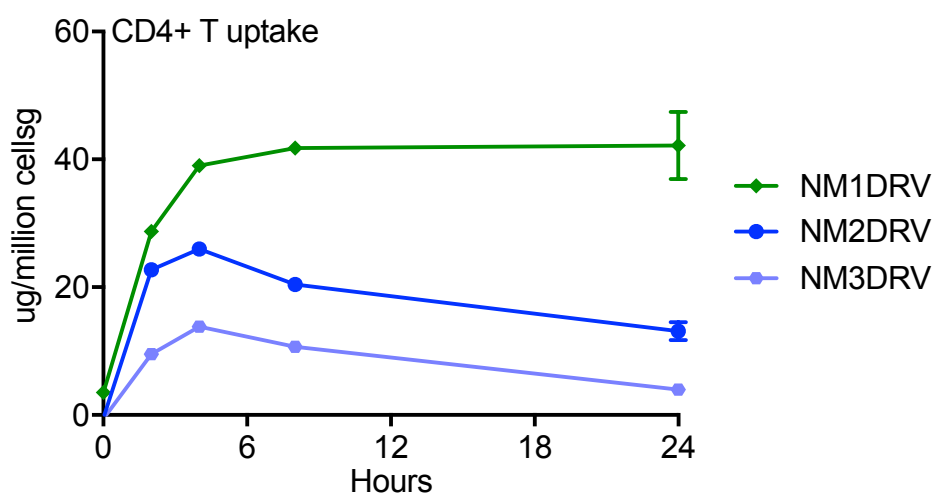
Figure 2. 52 NM3DRV uptake in CEM-SS CD4 T cells

Uptake of M3DRV in T cells was lower than uptake of M1DRV or M2DRV. The cells were plated on to poly-L-lysine pre-coated cell culture plates that make it possible for these cells to adhere. At 2, 4 and 8 hours post treatment, media was removed and adherent cells were washed twice with PBS then scraped into 1mL PBS. Cells were counted and pelleted by centrifugation at 956 x g for 8 minutes. The cell pellets were reconstituted and sonicated in 100 µL methanol for 5 minutes followed by centrifugation at 20,817 x g for 5 min and quantified using HPLC. Data are expressed as mean ± SEM for n=3 samples per group.
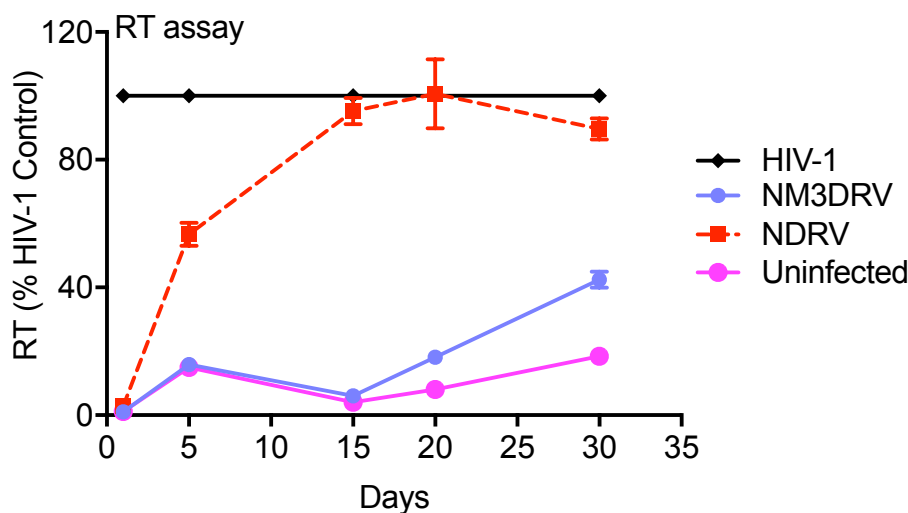
Figure 2. 53 NM3DRV antiretroviral activity in MDM

Antiretroviral activities in MDM after a single treatment with 100 µM of drug determined by RT assay. To assess long-term antiretroviral efficacy, MDM were treated for 8 hours with 100 µM NDRV, NM1DRV or NM2DRV as previously described for uptake studies. After treatment, cells were washed twice with PBS and cultured in fresh media without drug followed by half-media changes every other day. At 5-day intervals from days 1 to 30 after treatment, cells were challenged with HIV-1$_{ADA}$ at a MOI of 0.1 for 16 hours. HIV-1$_{ADA}$ media was then replaced with fresh media without drug. Ten days after viral challenge culture media were analyzed for RT activity. Data are expressed as mean ± SEM for n=3 samples per group.

Figure 2. 54 NM3DRV Pharmacokinetics in BALB/cJ mice

PK of NM3DRV in BALB/cJ mice - 100 mg/kg DRV equivalents. Plasma DRV levels from NM3DRV were consistently low (below 15 ng/mL) until day 28. Mice were injected intramuscularly with 40 uL of 50 mg/lg DRV equivalents for both drug nanoformulations. Blood and plasma samples were collected at different time points. Data are expressed as mean ± SEM for n=5 samples per group.
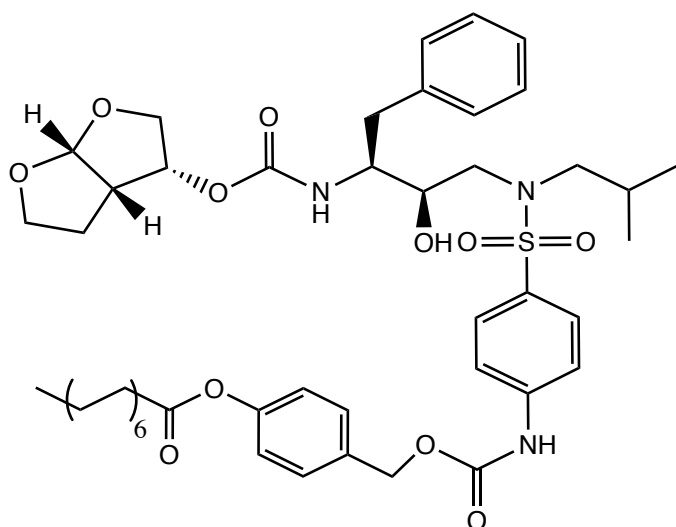
Figure 2. 55 NM4DRV structure

M4DRV was synthesized using a 14-carbon fatty acid chain with a phenyl linker through a carbamate bond.
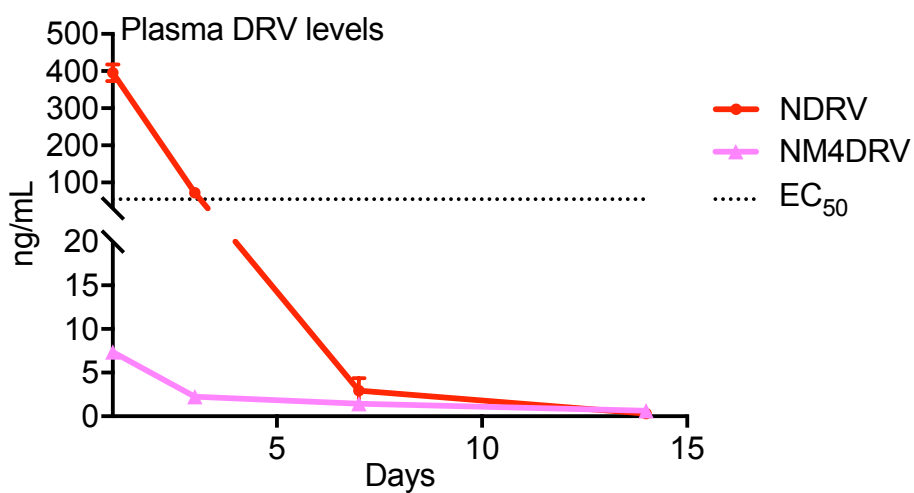
Figure 2. 56 NM4DRV Pharmacokinetics in BALB/cJ mice

PK of NM3DRV in BALB/cJ mice - 100 mg/kg DRV equivalents. Plasma DRV levels from NM3DRV were consistently low (below 15 ng/mL) until day 28. Mice were injected intramuscularly with 40 uL of 50 mg/lg DRV equivalents for both drug nanoformulations. Blood and plasma samples were collected at different time points. Data are expressed as mean ± SEM for n=5 samples per group.

Chapter 3: Development of Long-Acting Lamivudine

Abstract

Combination antiretroviral therapy (cART) has improved the quality and longevity of life for those living with HIV/AIDS. Despite the measured advances in clinical care, limitations in drug pharmacokinetics, bioavailability and inherent toxicities have often paralleled patient regimen adherence. The emergence of antiretroviral resistant viral strains has further limited long-term therapeutic success. We posit that the pharmacological limitations are superseded by LASER ART to improve cell and tissues drug delivery. To this end, we synthesized hydrophobic prodrug of lamivudine (S3TC). This was prepared by covalent linkage of an 18-carbon chain hydrophobic fatty acid to the parent compound by hydrolyzable ester bonds. Stable poloxamer 407 coated prodrug nanoformulations were produced by high pressure homogenization. Myristoylated lamivudine control prodrug formulation (NM3TC) uptake was 0.48 ug/million cells and undetected after 8 hours while prodrug formulation (NS3TC) was 19.17 ug/million cells at 8 hour time point and detected after 24 hours at concentrations of 27.09 ug/million cells. Of significance, nanoformulated S3TC exhibited improved pharmacokinetics of the native drug following a single intramuscular administration into mice. Specifically, plasma lamivudine concentration was detected in the prodrug treatment arm through day 14 following a single dose of 45 mg/kg. In contrast, native 3TC was below the limit of detection at day one post dosing. This project aims to improve the chemical and polymer chemistry for producing modified 3TC (S3TC), which is used to manufacture drug formulations with optimal properties of cell entry, stability, slow release and pharmacokinetic profiles by a spectrum of pharmaceutical approaches. Ultimately, we seek a modified antiretroviral 3TC to combine with other long lasting effective ARTs to achieve improved distribution and slow drug dissolution with limited to no toxicity for long-term treatment of HIV/AIDS patients.

Introduction

Human immunodeficiency virus infects its host integrating its DNA to the host and establishes cellular and tissue reservoirs allowing for it to persist and chronically inhabit its host. Therefore, HIV patients are burdened by strict drug adherence on daily basis to control and suppress viral replication in addition to other anti-inflammatory drugs needed to suppress inflammation associated with over activated macrophages releasing proinflammatory cytokines to combat viral replication. Therefore, development of long-acting antiretroviral (ART) drugs is essential to improve patient adherence and lifestyle. Nanoformulating ARTs into long-acting therapies have great potentials to improve patients' health due to their capability of lowering drug toxicities that often accompany daily dosage of ART combinations while sustaining viral suppression[159, 179]. Lamivudine (3TC), a pyrimidine analog/nucleotide reverse transcriptase inhibitor (NRTI), is used in treatment against HIV-1, HIV2 and Hepatitis B virus[180]. 3TC along with other NRTIs enters the cells by binding at high affinity to the organic cation transporters OCT1, OCT2, and OCT3 that are expressed on CD4+ T cells which are the main targets for HIV-1[181]. Inside cells, 3TC is first phosphorylated to its active metabolites, 3TC triphosphate, before it is capable of competing with deoxycytidine triphosphate (dCTP). Triphosphorylated 3TC incorporates itself in the viral DNA inhibiting the viral reverse transcriptase by chain termination[182, 183] and prevents the virus from replicating and proliferating. Studies are conflicted on whether triphosphorylated 3TC causes toxicities to the host DNA[180, 182]. The half-life of the 3TC triphosphate in HIV-1-infected peripheral blood lymphocytes ranges from 10.5 to 15.5 hours[184]. Prodrug strategies are currently used in many contraceptives as well as antipsychotics where limitations such as short half-lives and solubility can be avoided and whereby the modification can improve the performance of the drug[83]. The prodrug, an inactive bioreversible derivative of the parent drug, evades the disadvantages that accompany many native drugs such as short half-

life, hydrophilicity, and high toxicity[77, 83]. Our laboratory has been working extensively on nanoformulations for various ARTs to achieve long-acting effective ART formulations[150, 154]. In addition to nanoformulations, various prodrugs of many antiretroviral therapies were developed to achieve LASER ARTs such as prodrugs of abacavir (ABC) and 3TC[79, 80]. Modifications of ABC and 3TC to MABC and M3TC, respectively, yielded improvements in their half-lives, cell permeability, lower toxicities and antiretroviral activity. Initial modification to 3TC was achieved by conjugating a 14 carbon fatty acid chain through an ester bond yielding the myristoylated-3TC (M3TC)[79]. The modification improved the hydrophilic nature of the drug, increasing its half-life from hours for the parent 3TC to days for M3TC. Once inside the macrophages, M3TC is released from the encapsulating polymer and is cleaved by esterases reverting back to 3TC whereby the pharmacological effect of the drug takes place upon its phosphorylation. The modification is suggested to have improved protein binding to the prodrug which leads to sustained drug levels compared to the parent drug which is thought to be cleared out of the system at a faster rate based on pharmacokinetic studies[79]. Building on this successful modification, further improvements can be achieved by the conjugation of a longer fatty acid chain to 3TC, which further increased the drug's half-life enabling higher uptake in cells and sustained antiretroviral activities. Herein, we describe the synthesis, in vitro, and pilot PK study of the newly synthesized S3TC, stearolyated-3TC (S3TC).

Experimental Section

Reagents

Lamivudine was purchased from Boc Sciences (Shirley, NY). Anhydrous pyridine, dichloromethane (CH_2Cl_2), dimethyl sulfoxide (DMSO), *N,N*-dimethylformamide (DMF), deuterated chloroform ($CDCl_3$), diethyl ether, tetrahydrofuran (THF), fmoc N-hydroxysuccinimide ester, fmoc chloride, chlorotrimethylsilane (TMSCl), diethylamine (DEA), pluronic F127 (P407), 4-dimethylaminopyridine (DMAP), stearoyl chloride,

myristoyl chloride, paraformaldehyde (PFA), dichloromethane, methanol, ciprofloxacin and 3-(4,5-dimethylthiazol-2-yl)-2,5-diphenyltetrazolium bromide (MTT) were purchased from Sigma-Aldrich (St. Louis, MO). LC-MS grade methanol, acetonitrile, cell culture grade water (endotoxin-free), gentamicin and bovine serum albumin (BSA) were purchased from Fisher Scientific (Hampton, NH). CCK-8 was purchased from Dojindo Molecular Technologies, Inc, Rockville, MD, USA. Palladium, 10% on activated carbon, was purchased from STREM Inc. (Newburyport, MA). All chemical synthesis reactions were performed under a dry argon atmosphere. Flash column chromatography was performed on 32-63 μm flash silica gels from SiliCycle Inc. (Quebec, Canada). Reactions were monitored by thin-layered chromatography on precoated silica plates (250 μm, F-254 from SiliCycle Inc.). The compounds were visualized by UV fluorescence or stained with potassium permanganate. Heat-inactivated pooled human serum was purchased from Innovative Biologics (Herndon, VA). Dulbecco's Modification of Eagle's Medium (DMEM) was purchased from Corning Life Sciences (Tewksbury, MA).

Methods

Synthesis and characterization of hydrophobic 3TC prodrug (S3TC)
S3TC was synthesized in three steps. 3TC (2 g, 8.724 mmol, 1 equivalent) was first dried from pyridine prior to amine-protection reaction. 3TC was then suspended in anhydrous pyridine and cooled to 0°C. To the suspension, TMSCl (2.77 mL, 21.81 mmol, 2.5 equivalents) was added drop-wise and left to react for 30 minutes to protect the hydroxyl group followed by slow addition of Fmoc N-hydroxysuccinimide ester (3.53 g, 10.47 mmol, 1.2 equivalents) under cooling conditions to protect the amine group on 3TC. For the Fmoc-protection reaction, Fmoc-chloride and Fmoc N-hydroxysuccinimide ester was used interchangeably. The reaction was stirred for 48hrs under an argon atmosphere. . After completion, the reaction was quenched with water and ammonium hydroxide (NH_4OH) to hydrolyze the TMS group. The resulting product, Fmoc-3TC, was

purified using silica column chromatography eluting with 95%DCM:05%MeOH. The purified product was then concentrated and lyophilized before proceeding to the fatty acid conjugation step. To derivatize the hydroxyl group, Fmoc-3TC was dissolved in benzene and cooled to 0°C followed by addition of 1.3 equivalents of 4-dimethylaminopyridine (DMAP). Two equivalents of stearoyl chloride were then added and to the mixture and the reaction vessel was gradually warmed to 45°C for 24hr under argon. Upon reaction completion, the mixture was concentrated and subjected to column chromatography purification eluting with 95%DCM:05%MeOH to yield Fmoc-S3TC. The Fmoc group was then cleaved using DEA in DCM to yield the final compound, S3TC that was then purified using 98%DCM:02%MeOH and 95%DCM:05%MeOH. The fractions containing the desired product were combined, concentrated and precipitated from ether to give S3TC as a colorless powder. The final product and intermediates were characterized by NMR spectroscopy. M3TC[79] was also synthesized using the same protocol for S3TC synthesis substituting stearoyl chloride with myristoyl chloride. S3TC and M3TC successful syntheses were confirmed by NMR, FTIR, and MS. ^{1}H NMR where the different characterizations confirmed conjugation of the fatty acid by reflecting the linker's hydrogen peaks as well as the missing alcohol peak due to the ester bond formation. FTIR showed additional vibrational bands reflecting the symmetrical and asymmetrical C-H chemical stretches resulting from the conjugation of the fatty acid chain. Additionally mass spectrometry infusions reflected the expected molecular.

Development and Characterization of NS3TC

S3TC is formulated following established protocols from our laboratory[154]. Briefly, S3TC (1% w/v) was premixed in a 0.5% w/v P407 solution dispersed in 10 mM Hepes buffer for 16h at room temperature. The premix suspension is homogenized using a high-pressure homogenizer (Avestin EmulsiFlex-C3; Avestin Inc, Ottawa, ON, Canada) at a pressure range 15,000 – 20,000 psi at 0°C until desired size is achieved. Particles will

be characterized using dynamic light scattering (DLS) on a Malvern Nano-ZS (Worcestershire, UK) to determine size, PDI, and zeta potential. Drug loading in the nanoformulation was measured using Waters Alliance e2695 HPLC Separations Module. For pharmacokinetic study, NS3TC was subjected to centrifugal concentration to remove excess polymer and buffer and achieve low injection volumes. NS3TC was first centrifuged for 5 min at 5000 x g, the supernatant was transferred to a new centrifuge tube and the pellet is saved. The supernatant was centrifuged for 20 min at 20,000 x g. The supernatant was discarded and the pellet saved. Both pellets were resuspended in 500 µL of PBS and the sample quantified for drug content using HPLC.

Cytotoxicity and cell viability
Monocytes-derived macrophages assays were used to evaluate the NS3TC compared to NM3TC. Cytotoxicity of each formulation was evaluated using the cell counting kit-8 (CCK-8) (Dojindo Molecular Technologies, Inc, Rockville, MD, USA). Human monocytes were isolated and cultured for 7-10 days in 96-well culture plates (80,000 cells/well) with Dulbecco's Modified Eagles Media (DMEM) supplemented with 10% heat-inactivated pooled human serum, 1,000 U/ml of macrophage colony stimulating factor, 1% glutamine, 10 µg/mL ciprofloxacin, and 50 µg/mL gentamicin in a 37°C in a 5% CO_2 incubator[148-150]. A stock solution of each drug nanoformulation was serially diluted in DMEM to produce drug concentrations ranging from 100-400 µM and the cells were incubated 24 hours. After incubation in 37°C for 24 hours, 10 µL of the kit was added to each well; drug treated and untreated cells as well as drugs in media were included. Incubate plates at 37°C in a 5% CO_2 for 1-4 hours. Finally, absorbance measured at 450 nm on a SpectraMax M3 plate reader with SoftMax Pro 6.2 software (San Jose, CA). Percent of survival rate was calculated by this equation (($A_{sample}-A_{blank\ media}$)/($A_{control\ cells}-A_{blank\ media}$)) X 100.

MDM drug uptake and retention

MDM were cultured on 12-well culture plates and treated with media containing 100µM

of NS3TC or NM3TC[148-150]. At different time points; 2, 4, 8 and 24 hours post treatment,

media was removed and adherent cells were washed twice with PBS then scraped into

1mL PBS. Cells were counted on an Invitrogen Countess Automated Cell Counter

(Carlsbad, CA), pelleted by centrifugation at 3000 x rpm for 8 minutes. The cell pellets

were reconstituted and sonicated in 100 µL methanol for 5 minutes followed by

centrifugation at 14,000 x rpm for 5 min. Drug levels in each time point for each

treatment will be assayed using Waters Alliance e2695 HPLC Separations Module.

Antiretroviral effects of the different treatments were evaluated following well-established

protocols in our laboratory. Briefly, cells were first loaded with each drug formulation for

8hr. At different days post drug loading, cells were infected with HIV-1$_{ADA}$ for 16 hours.

After infection, virus media is removed and cells are washed twice with PBS and

incubated in media to maintain survival of cells. 10 days post infection, cell media were

collected at different time points to evaluate antiretroviral activity using reverse

transcriptase assay (RT assay) of the different treatments. Cells were fixed in 2% PFA

for p24 staining for further confirmation of RT results.

PK analysis of NS3TC

Mice were administered intramuscular injections (50 mg/kg) of NS3TC and NM3TC. The

two groups NS3TC and NM3TC were compared to each other to evaluate the effect of

drugs' increasing hydrophobicity. Each treatment was compared to show the effect of

nanoformulation on the control release of the drug and therefore its half-life. Plasma was

be collected from the mice at days 1, 3, 7, 10, 14, 21, and 28. Tissues (lung, liver,

spleen, gut, brain, lymph nodes and muscle injection sites) were collected to quantify

drug content and detect the drug peak of each treatment.

Results

Synthesis and characterization of prodrug, S3TC

S3TC was successfully synthesized by the conjugation of stearoyl chloride to Fmoc-

protected 3TC followed by the deprotection reaction to cleave the protecting group

(Figure 3.1). S3TC is an ester prodrug of 3TC that will be hydrolyzed once inside the cell

back to 3TC through the action of esterases. The drug is then further phosphorylated

into the active moiety (Figure 3.2). The final compound S3TC structure was verified

using ^{1}H NMR, FTIR, and MS. Broad peaks at 0.9 and 1.26 ppm correspond to the

terminal methyl and methylene protons of the fatty esters in the ^{1}H NMR spectra for

S3TC (Figure 3.3). Characterization of S3TC by Fourier transform infrared (FTIR)

spectroscopy showed absorption bands at 2917, 2915 and 2848 cm^{-1} representing

asymmetric and symmetric C-H stretches in the long chain fatty acids as well as 1760

cm^{-1} corresponding for the carbonyl stretches chemical stretch (Figure 3.4). Infusion of

the S3TC into a Waters Xevo TQ-S micro mass spectrometer showed the desired

molecular ion peaks at 496.72 [M+H] (Fig 3.5). As a control M3TC[79] was also

successfully synthesized and thoroughly characterized to be used as a control in

subsequent studies.

Nanoformulation of S3TC

S3TC was successfully nanoformulated (NS3TC) with P407 through top-down methods;

high pressure homogenization with a drug:polymer ration of 2:1 in 10 mM HEPES buffer.

As a control M3TC was also nanoformulated (NM3TC) following the same protocol[79].

Both drug nanoformulations had drug encapsulation efficiencies of 80% for NS3TC and

55% for NM3TC. NS3TC and NM3TC exhibited uniform particles sizes of 300.27 and

521.83 nm, PDI of 0.25 and 0.35, and charges of -6.48 and -17.97 mV, respectively.

Stability measurements of NS3TC showed the particles to be stable at room temperature

for the recorded observation period (Figure 3.6).

Cytotoxicity of NS3TC

Cytotoxicity of NS3TC in MDM was evaluated using cell counting kit-8 (CCK-8) and 3-(4,5-dimethylthiazol-2-yl)-2,5-diphenyltetrazolium bromide (MTT). Parallel cytotoxicity studies with NM3TC were used as a control. Treating with concentrations ranging from 50 to 400 uM showed no toxicity (Figure 3.7). Based on the viability studies, subsequent in vitro studies were done using 100 µM of both NS3TC and NM3TC.

Uptake of NS3TC

NS3TC showed improved and sustained uptake in MDM over NM3TC. At 2hr post treatments, concentration of M3TC peaked at 14.79 µg per million cells. However, by 4 and 8hr time points M3TC levels drop to 9.02 and 0.36 ug/million cells, respectively. M3TC concentrations were not detectable at 24hr time point. On the other hand, NS3TC treatment showed gradual increase in uptake over 24 hours period. S3TC concentration was 27.84 µg/million cells and increased gradually to 70.10 µg/million cells by 24 hours of uptake (Figure 3.8).

Retention of NS3TC

Loading MDMs with NS3TC or NM3TC (100 µM drug) for 8 hours revealed S3TC is retained longer inside cells and detected until day 11 at concentrations of 0.27 µg/million cells (Fig 3.9) compared to little or no retention of NM3TC as also suggested from previous uptake studies in MDM.

Antiretroviral effects of NS3TC

MDM loaded with NS3TC showed protection from HIV-1$_{ADA}$ for 15 days whereas NM3TC showed viral breakthrough by day 5 of the study as evident from the RT assay (Fig 3.10). This confirms that NS3TC showed better retention profiles inside MDM that paralleled by the antiretroviral efficacies against HIV-1.

Pilot pharmacokinetic study evaluation of NS3TC

To affirm that the modification improved bioavailability of the drug and its biodistribution

in tissues, BALB/cJ mice were administered a single intramuscular injection of 50 mg/kg

3TC equivalents of NM3TC or NS3TC. NS3TC showed superior PK profile compared to

NM3TC in terms of 3TC plasma levels (Fig 3.11). 3TC levels peaked for the NM3TC on

the first day with concentration of 245.87 ng/mL however, rapid decrease in 3TC

concentration was detected by day 4 where the 3TC concentration was only 24.20

ng/mL and continued to decrease to 1.23 ng/mL by 1 week. 3TC from NM3TC treatment

was undetectable for the rest of the study. On the other hand, NS3TC showed sustained

a gradual release of 3TC reflected in the concentrations detected at different time points;

116.86, 112.21, 33.81, 20.30, and 4.84 ng/mL on days 1, 4, 7, 10, and 14, respectively.

Discussion

NRTIs are considered a cornerstone in the treatment of HIV and hence are found in

most first line HIV regimens for adults and adolescents[97]. Optimal effective initial

regimens for majority of HIV-1 patients consist of triple ART therapy of two NRTIs and

an integrase inhibitor, NNRTI, or protease inhibitor[185]. Moreover, NRTIs are essential in

PrEP regimens because of their ability to inhibit viral reverse transcription into the DNA

hence eventually stopping the virus pre integration into the host DNA and therefore

these offer more protection than other ART drug classes such as protease inhibitors that

work post integration. Prevention of integration into host genome is generally the

preferred mode of action for PrEP regimens[177]. Based on the criteria for choosing PrEP

drugs, 3TC shows promising grounds. The NRTI drug is already being used in

developing countries and is cost effective. A study conducted in Rwanda and Uganda,

SIMBA, looking at the prophylaxis effects of 3TC in HIV-negative infants breast-feeding

from HIV-positive mothers showed protection effects with no infant infections[177]. Hence,

developing a long-acting 3TC represents a great advantage in the HIV current

treatments and future PrEP regimens. Daily dosage of ARTs frequently cause many side effects, thus long-acting injectables would greatly lower such toxicities and dramatically improve the lifestyle of patients by lessening the burden of daily pills and thus maintaining patient's privacy[77]. Recently, ViiV healthcare submitted an application to the FDA for monthly injectable of long-acting CAB and RPV. This would be the first long acting antiretroviral to be available for clinical use. CAB and RPV are characterized by certain physiochemical characteristics that make it possible for their use and development into long-acting therapeutics by nanoformulations[161, 162]. These characteristics include low aqueous solubility, high potency and long half-life due to their slow clearance. These characteristics enable formulation of these drugs as aqueous nanosuspensions. However, many of ART therapies do not conform to these criteria specifically NRTIs. Being an essential ART class for PrEP and HIV treatment, research on long-acting NRTIs is essential and would greatly benefit the HIV community and those at risk of infection. Therefore, in efforts to transform 3TC into a long-acting drug, we sought to transform it first into a water insoluble compound. Hence to nanoformulate 3TC, overcoming the hydrophilic nature of the drug becomes essential. We successfully synthesized a prodrug (S3TC) of 3TC increasing the hydrophobicity of the drug by the conjugation of an 18-carbon fatty acid chain on the hydroxyl end of the drug. The hydrophobic lipids are known to increase compound hydrophobicity, cell penetration and slow down drug clearance[142, 79]. We used NM3TC as a control. M3TC is an ester derivative of 3TC modified with a 14-carbon chain on the terminal alcohol and had previously shown superior in *in vitro* and *in vivo* characterization compared to free 3TC[79, 186]. Agarwal et al. previously synthesized a library of 3TC prodrugs where 3TC was modified with long-chain fatty acids on either the amine or hydroxyl group while protecting the other group not being modified[186]. Myristolyation of 3TC by modification of the alcohol (5'-O-derivative) showed dramatic increase in Log P of the drug from 0.06 to

5.79 for 3TC and myristolyated-3TC, respectively[186]. Effect of modification was drastic in efficacy studies against X4- and R5-tropic viruses. Myristolyated-3TC showed increase in potency, decrease in EC_{50} values from 32.7 and 11.4 uM for 3TC to 0.5 and 0.2 uM for myristolyated-3TC (M3TC) in X4- and R5-tropic viruses, respectively. Moreover, M3TC was shown to have lower IC_{50} and IC_{90} values than 3TC when tested against various resistant viruses. To this end, we sought to make further improvements on M3TC by making a more hydrophobic 3TC prodrug (S3TC) with longer half-life to eventually achieve more effective drug levels. The hydrophobic moiety modification increases the hydrophobicity of the parent drug leading to higher protein binding which in turn extends the drugs circulation time in blood thereby facilitating intracellular and tissue redistribution[79]. Moreover, to our knowledge, an aqueous nanosuspension of stearoylated 3TC prodrug (a stearoyl modification to 5' hydroxyl of 3TC) has not been previously explored. Theoretically, the hydrophobic modification is reversibly hydrolyzed by esterases present in plasma, cells and tissues yielding the parent drug that undergoes intracellular triphosphorylation by kinases to exert antiretroviral effects[79, 186] (Fig 3.2). Based on previous studies, we posit that the log P and intracellular uptake of S3TC would be greater than that of the parent drug. Consequently, enhancements in intracellular delivery and activation of the prodrug would lead to improved efficacy compared to 3TC.

Nanoformulating ARTs showed promising advantages in many studies done in our lab[77, 79, 80, 149, 150, 154] as well as pharmaceutical companies such as GSK and Janssen as discussed previously with their CAB LA and RPV LA[74]. Nanoformulations slows down the release of the drugs leading to lowering frequent dosing. Ideally, using different polymers to coat the drugs also lowers the possible drug toxicities and allows a more efficient drug penetration into cells when compared to free drugs[77, 150, 154]. Building on this and previous work in our laboratory, nanoformulation of S3TC (NS3TC) improved

the long-acting effect of the drug by controlled release from the polymer encapsulating it as well as lowering drug toxicities. Characterization of the nanoparticles confirmed stability and uniformity of the particles. From bench to patient's bedside, nanoformulation stability is a critical factor for future use of these nanoformulation in clinical settings. Since HIV-1 infects and replicate in T cells as well as macrophages hence representing major viral cellular reservoirs[172, 187] it is essential for NS3TC to be able to be taken up, retained, and effective inside these cells. For proof-of-concept we tested NS3TC in MDMs. Uptake of NM3TC peaked at 2hr post treatment and rapidly decreased until it reached undetectable levels. On the other hand, uptake of NS3TC showed sustained and gradual increase inside MDMs. This was also paralleled by high retention compared to M3TC. The superior uptake and retention profiles of NS3TC were reflected in the antiretroviral assay where protection against virus onset was extended 10 days beyond NM3TC. NM3TC showed viral breakthrough by day 5, which reflects the long-acting activity of NS3TC. The advantage of using macrophages lies in more than them being viral reservoirs. Our laboratory has previously shown that drug depots form at the injection sites in mice treated with prodrug nanoformulations[75] and notably macrophages, as major phagocytic cells, infiltrate in the injection site and phagocytose these formulations[188] followed by their migration to local lymph nodes. Additionally, since HIV is characterized by chronic inflammation and immune system activation, we posit that these macrophages would travel where the chemokine gradient attractants and ongoing viral replication are. Therefore it is significant that NS3TC is taken up and retained in macrophages at higher concentrations than NM3TC.

Moreover to test if the improved in vitro characterization is also reflected in vivo, NS3TC was tested in BALB/cJ mice in a pilot pharmacokinetic study to test bioavailability of the drug in plasma as well as its tissue distribution. Compared to NM3TC, 3TC levels from NS3TC were detectable up until 14 days post injection whereas 3TC from NM3TC was

not detected beyond 1 week after the intramuscular injection. This confirms the long-acting advantage of NS3TC over NM3TC. Further analysis will look into tissue-drug biodistribution. Guo et al. showed that targeting of NM3TC using folic acid (FA) targeted polymer to nanoformulate M3TC improved its pharmacokinetics profiles[79]. FA-targeted NM3TC provided better 3TC plasma drug levels by more than 2-fold compared to 3TC levels from NM3TC. Moreover, 3TC levels in liver, spleen, and lymph nodes showed 2-fold increases in the FA-NM3TC treatment arm over NM3TC[79]. Folic acid receptor on macrophages are able to internalize FA-tagged molecules and drugs as it was shown in FA-drugs targeted to folate receptor expressing cancerous cells[189]. Moreover, ongoing human clinical trials to investigate the advantage of folate-conjugated drugs confirm the significance of targeted therapies. FA targeting on the macrophage has been exploited for treatment of rheumatoid arthritis, an autoimmune disease, where activated macrophages contribute to disease pathogenesis hence targeting therapeutics to these macrophages in the arthritic joints would be most effective while avoiding toxicity in normal tissues[190]. Therefore, future studies will explore FA-targeting of NS3TC to improve the *in vitro* and *in vivo* profiles while lowering toxicities to other cells and tissues. Future studies on 3TC will include the development of a di-3TC prodrug formulation that is essentially consisting of two 3TC molecules conjugated by a linker through ester bonds (Fig 3.11). Different length linkers may be explored to achieve the optimum yet slow release of the drug in vivo.

Figures
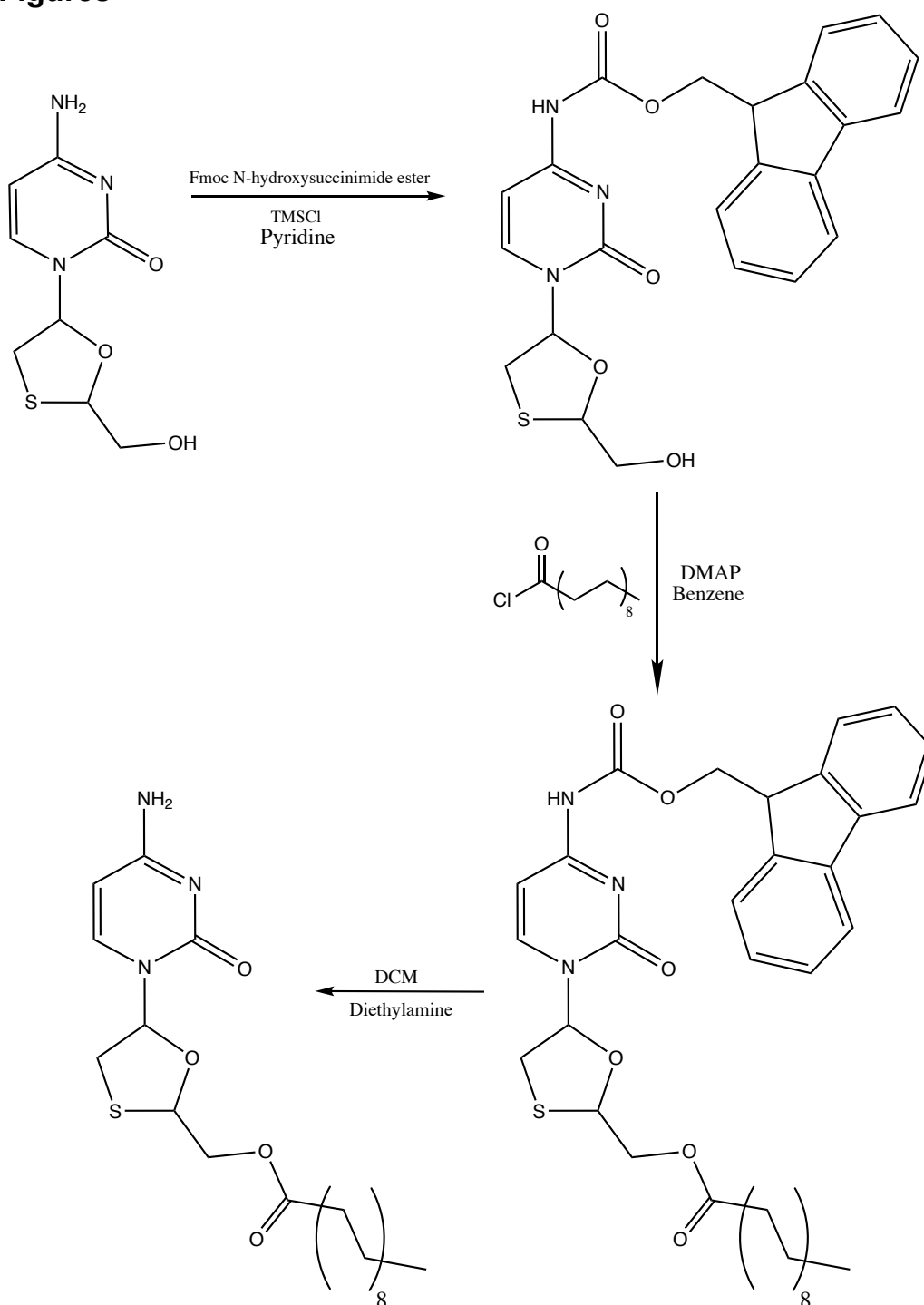
Figure 3. 1 Synthesis scheme of S3TC

3TC is first protected with an Fmoc group to shield the amine group prior fatty acid conjugation yielding into Fmoc-3TC. Fmoc-3TC is then reacted with stearoyl chloride (18 carbon fatty acid chain) to produce Fmoc-S3TC. The protecting group is eventually cleaved in a deprotection reaction to yield the final product, S3TC.
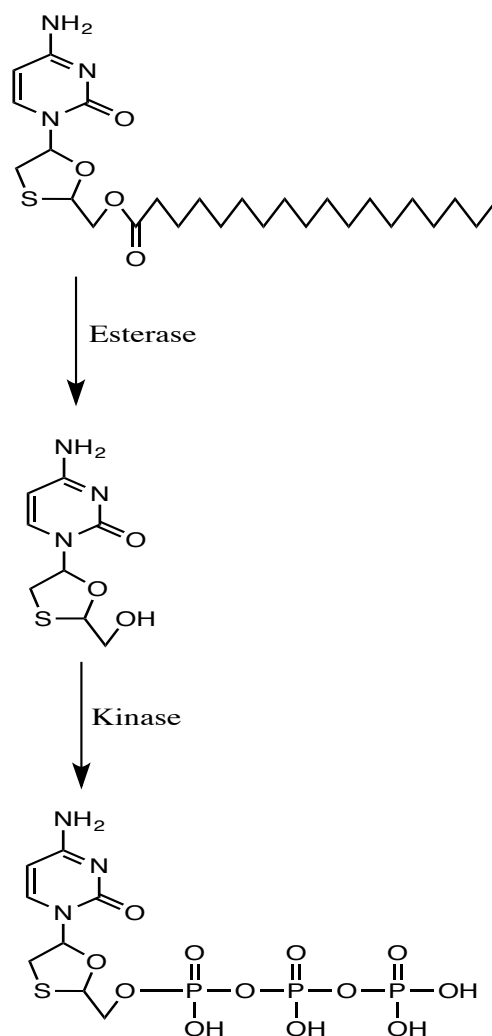
Figure 3. 2 Proposed mechanism of S3TC hydrolysis and activation

Once inside cells, various esterases can hydrolyze the ester bond on S3TC reverting it back to 3TC. Different kinases then can activate the parent drug into its active moiety – a triphosphate 3TC, this can induce antiretroviral activities in the form of chain elongation termination halting the viral cycle.
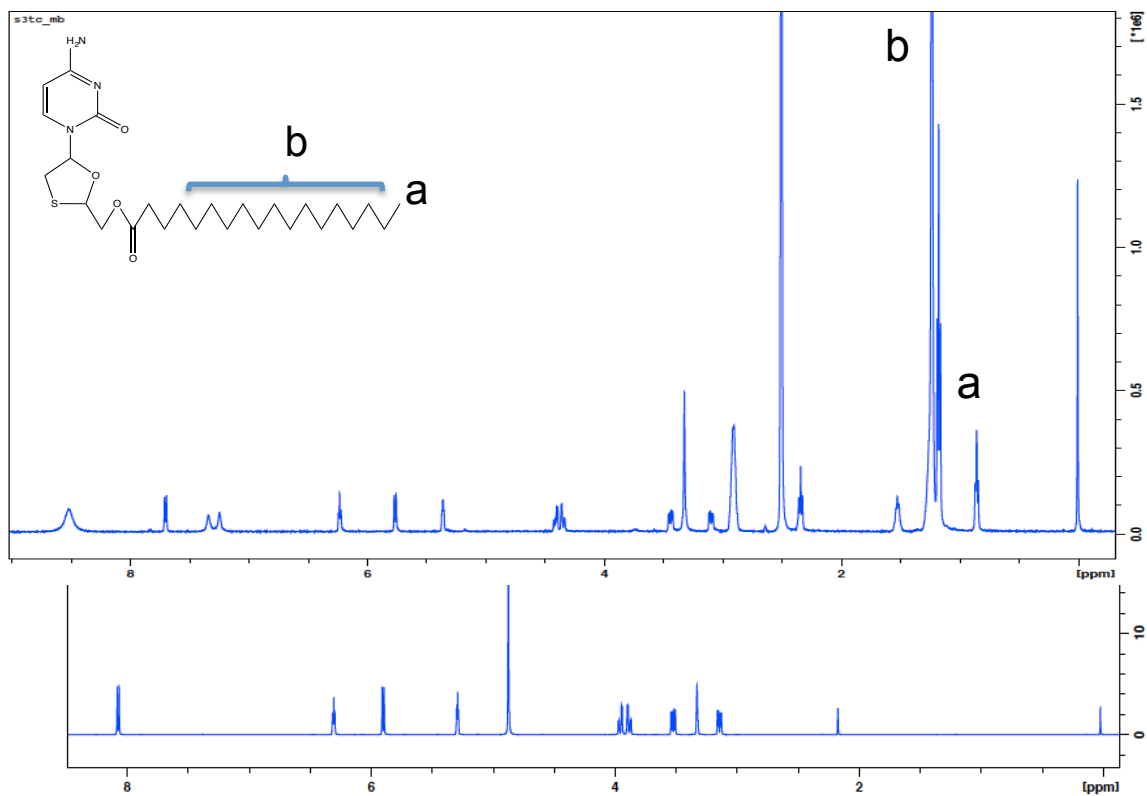
Figure 3. 3 ^{1}H NMR characterization of S3TC

NMR spectrum of S3TC reflecting the additional terminal methyl (0.9 ppm) and methylene protons (1.26 ppm) of the fatty esters. Lower panel reflects ^{1}H NMR of 3TC.
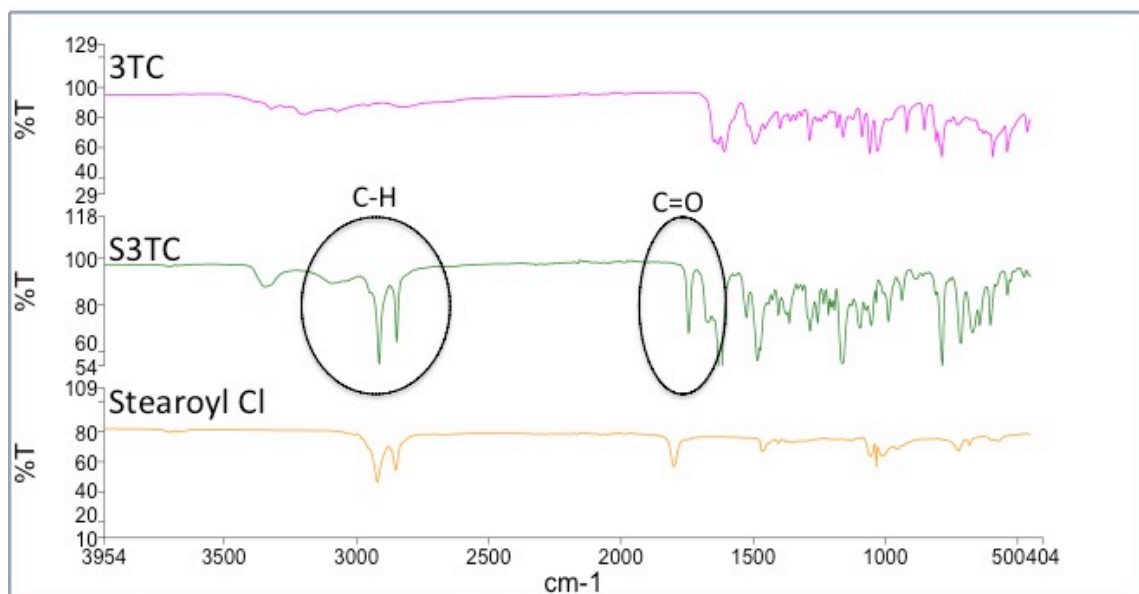
Figure 3. 4 FTIR characterization of S3TC

Spectrum for S3TC reflects absorption bands at 2917 and 2848 cm^{-1} representing asymmetric and symmetric C-H stretches in the long chain fatty acid. Additionally, absorption band at 1690 cm^{-1} represents the carbonyl chemical stretch resulting from the conjugation and addition of the carbonyl group from the fatty acid.
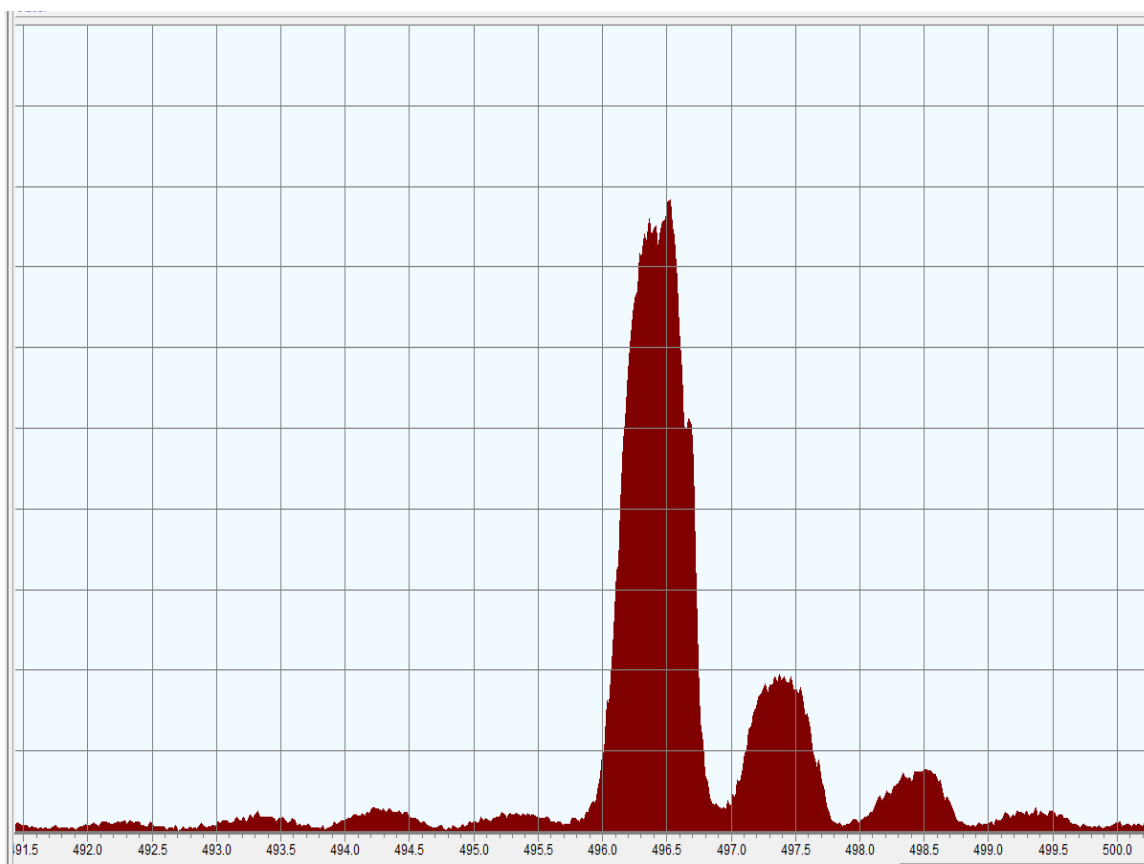
Figure 3. 5 Characterization of S3TC

Infusion into a Waters Xevo TQ-S micro mass spectrometer confirmed the desired molecular ion peaks at 496.72 [M+H] as well as smaller peaks resulting from the addition of other hydrogen isotopes.
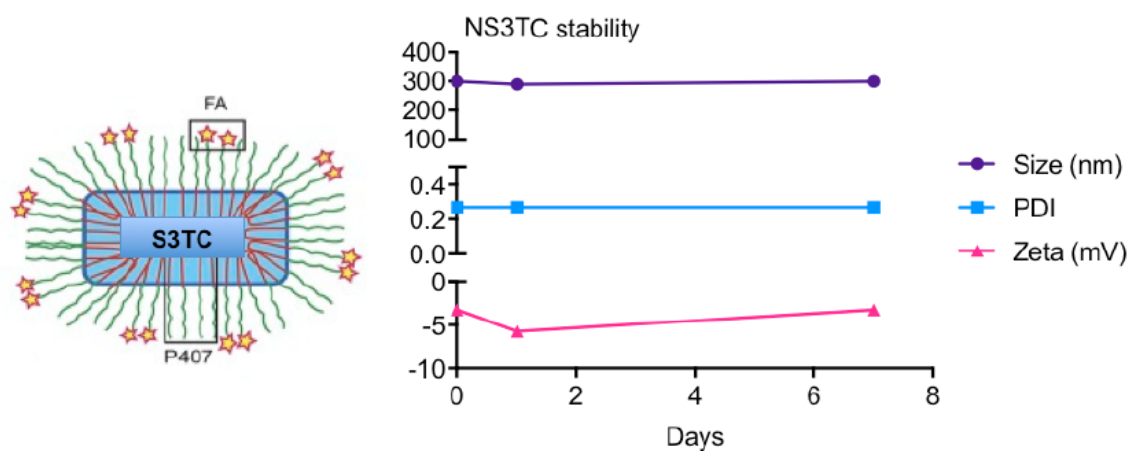
Figure 3. 6 Nanoformulating S3TC and stability measurements

S3TC is encapsulated in P407 through high pressure homogenization to yield NS3TC. NS3TC was prepared in HEPES buffer (10 mM) using 2:1 drug to polymer ratio. The formulation was premixed overnight and subjected to high pressure homogenization (C3 Avestin) applying 15,000 – 20,000 psi. Size of particles was monitored using dynamic light scattering (DLS).
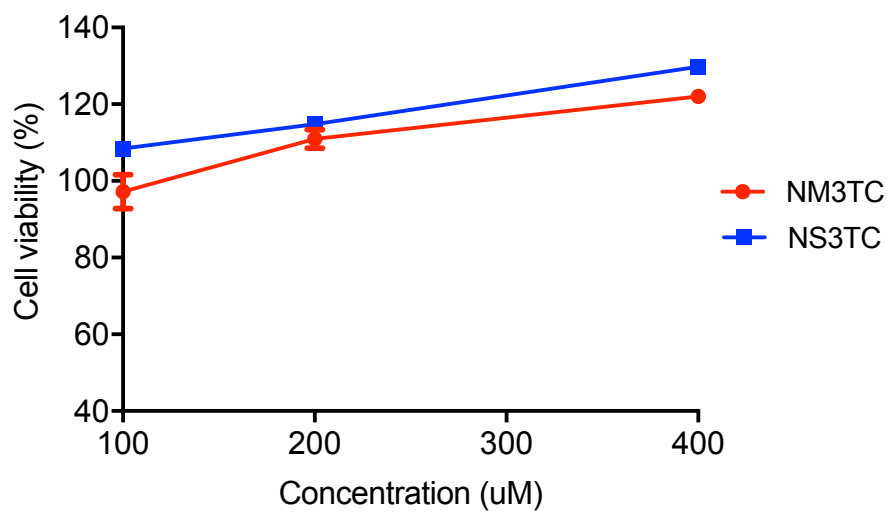
Figure 3. 7 Cytotoxicity assay of NS3TC and NM3TC in MDM

Cytotoxicity of NM3TC and NS3TC was assayed by MTT in MDM. A stock solution of each drug nanoformulation was serially diluted in DMEM to produce drug concentrations ranging from 100-400 µM. Cells were treated for 24 hours, washed and incubated with 200 µL/well 3-(4,5-dimethylthiazol-2-yl)-2,5-diphenyltetrazolium bromide (MTT) solution (5 mg/mL) for 45 minutes. Upon MTT removal, 200 µL/well of DMSO was added and absorbance measured at 490 nm on a SpectraMax M3 plate reader. Data are expressed as mean ± SEM for n=3 samples per group.
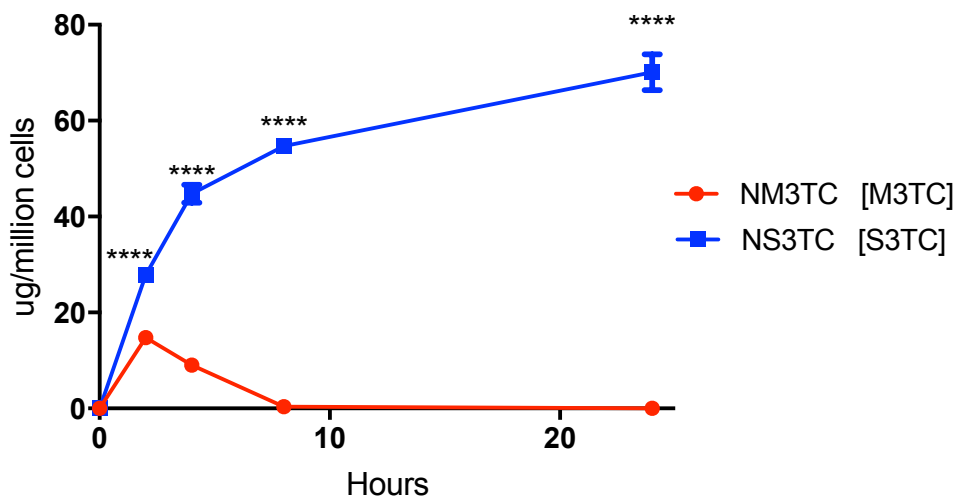
Figure 3. 8 Uptake of NS3TC in MDM

S3TC uptake levels are dramatically higher than M3TC drug levels inside MDM after one treatment of 100 µM drug. MDM were cultured on 12-well culture plates and treated with media containing 100µM of NDRV, NM1DRV or NM2DRV. At 2, 4 and 8 hours post treatment, media was removed and adherent cells were washed twice with PBS then scraped into 1mL PBS. Cells were counted and pelleted by centrifugation at 956 x g for 8 minutes. The cell pellets were reconstituted and sonicated in 100 µL methanol for 5 minutes followed by centrifugation at 20,817 x g for 5 min and quantified using HPLC. Data are expressed as mean ± SEM for n=3 samples per group. ****P < 0.0001 for NS3TC vs. NM3TC.
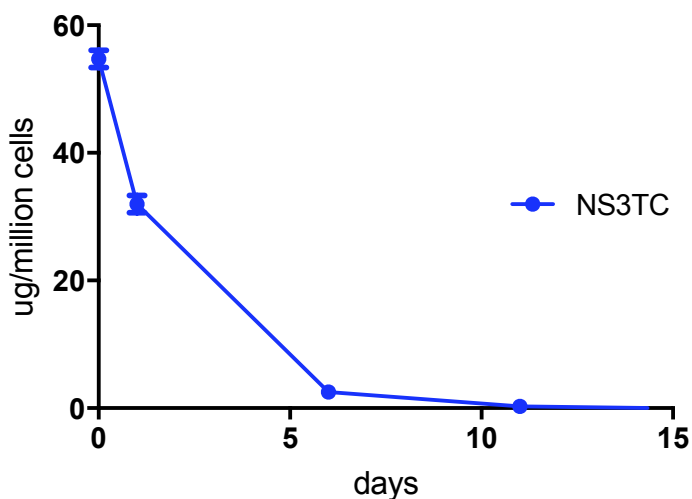
Figure 3. 9 Retention of S3TC in MDM

For S3TC retention studies, MDM were treated for 8 hours with 100 uM of NS3TC then washed with PBS and maintained with half-media changes every other day until collection days. Intracellular and supernatant drug content were analyzed using HPLC. Data are expressed as mean ± SEM for n=3 samples per group.
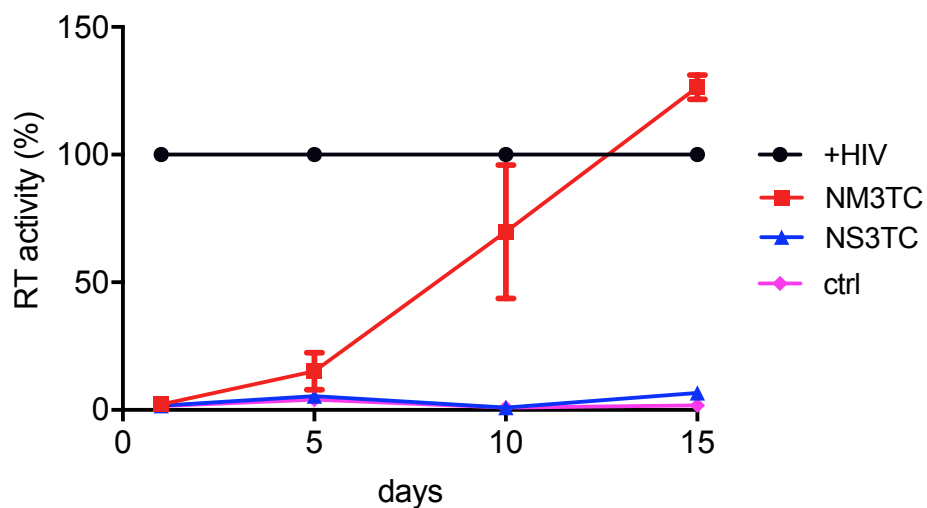
Figure 3. 10 Antiretroviral activity of NS3TC

Antiretroviral activities in MDM after a single treatment with 100 µM of drug determined by RT assay. To assess long-term antiretroviral efficacy, MDM were treated for 8 hours with 100 µM of NM3TC or NS3TC. After treatment, cells were washed twice with PBS and cultured in fresh media without drug followed by half-media changes every other day. At 5-day intervals from days 1 to 30 after treatment, cells were challenged with HIV-1$_{ADA}$ at a MOI of 0.1 for 16 hours. HIV-1$_{ADA}$ media was then replaced with fresh media without drug. Ten days after viral challenge culture media were analyzed for RT activity. Data are expressed as mean ± SEM for n=3 samples per group.
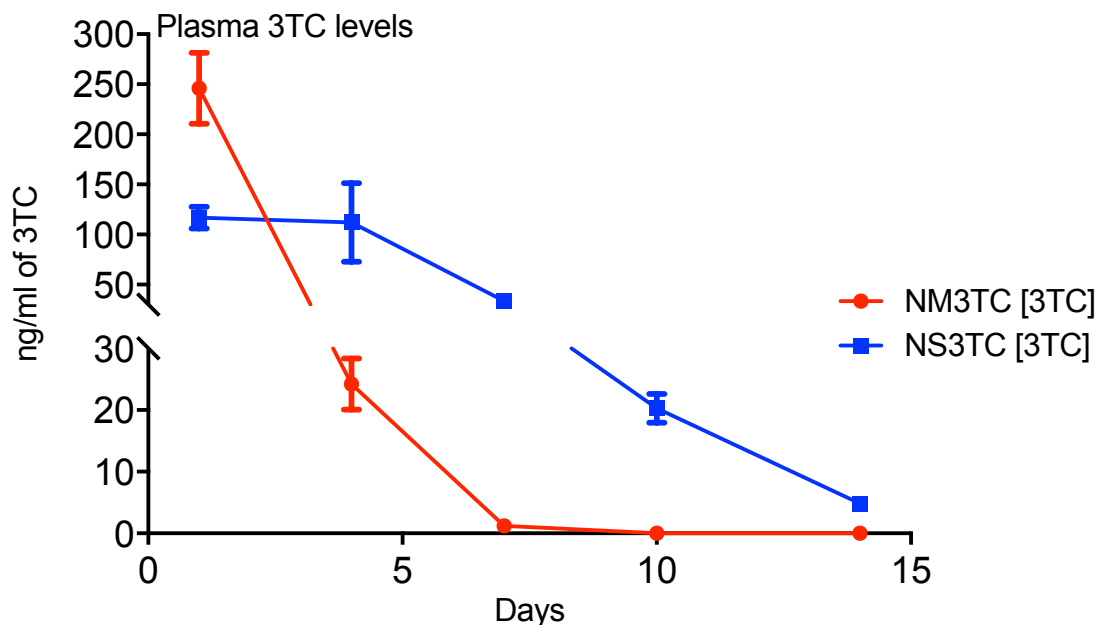
Figure 3. 11 Pharmacokinetics of NS3TC

Pharmacokinetics in BALB/cJ mice using 50 mg/kg 3TC equivalents. Mice were injected intramuscularly with 40 uL of 50 mg/lg 3TC equivalents for both NM3TC and NS3TC. Plasma samples were collected at different time points. Data are expressed as mean ± SEM for n=5 samples per group.
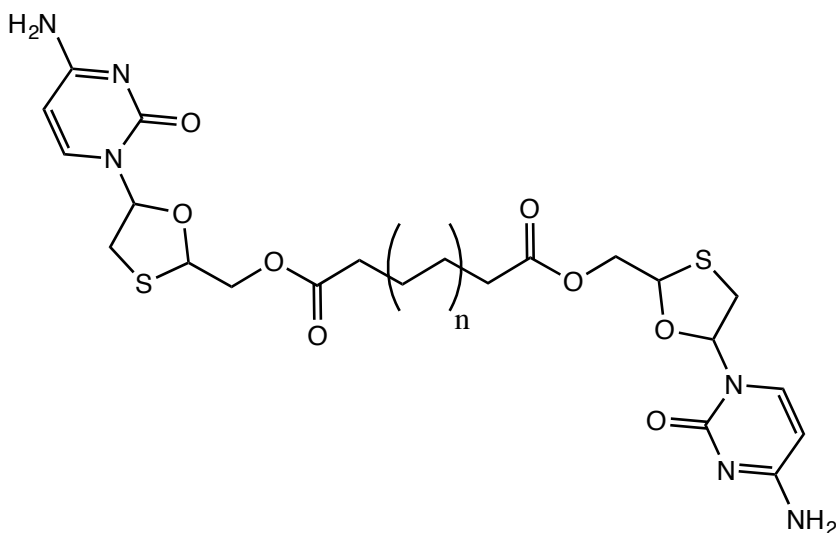
Figure 3. 12 Di-3TC molecule

Future direction for 3TC prodrug design.

Chapter 4: Conclusions and Future Studies

Prodrug strategies proved to be essential for antipsychotic and contraceptive[84, 191] drug regimens and are soon going to play critical roles in HIV-1 therapeutics to transform the daily regimens into long-acting drugs. Prodrugs are capable of altering drug tissue distribution, efficacy and improve toxicity profiles[83]. Currently, CAB LA and RPV LA of GSK and Janssen are taking the lead when it comes to long-acting HIV-1 treatments[76, 159]. These drugs, however, possess unique innate characteristics like poor water solubility and high potency that allow them to be nanoformulated and used as long-acting regimens. In order to apply the same characteristics with many other HIV drugs, poor physiochemical characteristics of the drugs need to be overcome to efficiently nanoformulate the drugs. This is where prodrug strategies play a major role in the transformation of most HIV-1 drugs into long-acting slow effective release drugs[77]. Prodrugs of DRV, M1DRV and M2DRV, showed superior uptake and retention in macrophages and T cells, known cellular reservoirs of HIV-1. In addition, antiretroviral efficacies of these drugs were comparable to the parent drug or maintained in the nanomolar range for M1DRV and M2DRV, respectively. *In vivo* studies in mice revealed DRV prodrug nanoformulations, NM1DRV and NM2DRV, showed better pharmacokinetics than the nanoformulated native drug. Limitation of the DRV prodrug, however, lies in the levels of DRV cleaving from the prodrugs *in vitro* and *in vivo*. Although, DRV cleaving from both prodrugs *in vitro* is not detected except for NM1DRV, this could be a limitation in the HPLC detection method hence there is a need for more sensitive HPLC methods to ensure whether the problem lies in detection limitation or hydrolytic stability of the drugs. Long-term efficacy studies in cells showed that the prodrugs' nanoformulation were able to protect the cells for up to 15 and 30 days for NM1DRV and NM2DRV, respectively. These studies paralleled the retention studies that

showed prodrugs within cells for 15 and 30 days for NM1DRV and NM2DRV, respectively. The long-term antiretroviral efficacy studies can be explained by the *in vitro* antiviral activity of DRV where the EC_{50} ranges between 1-5 nmol/L and EC_{90} from 2.7-12 nmol/L in HIV-1/2 infected cells such as MT-4, PBMCs, and macrophages [89]. Hence this protection could mean cleavage of the prodrugs are taking place but in very small concentrations that are not detected by the current HPLC methods. An additional limitation along the same lines is the low therapeutic DRV levels detected in mice plasma after once intramuscular injection of 100 mg/kg DRV equivalents for the prodrugs. NM1DRV treatment outperformed NM2DRV in terms of plasma DRV levels above the EC_{50} of the drug (55 ng/mL). DRV cleaving from NM1DRV remained above the EC_{50} of DRV for 1-week post-injection and dropped below 10 ng/mL by 28 days post-injections. DRV cleaving from NM2DRV remained above EC_{50} only at days 1 and 3 and rapidly decreased below 55 ng/mL reaching similar DRV levels as NM1DRV by day 28 days. However it is important to note that the mice were not dosed with an equivalent dose to the human dose. DRV is dosed in humans either 600 mg twice a day or 800 mg once daily. Using the once/daily dose of 800 mg to calculate a mouse dose would yield a dose around 164 mg/kg based on allometric scaling considering the body surface area[192]. The highest dose we used for our PK studies was 100 mg/kg to avoid possible toxicities in mice. Therefore, to further confirm our results, repeating PK studies in rats or mice at an equivalent dose to humans becomes essential to better understand the pharmacokinetics of the DRV prodrugs and to rule out possible dosing discrepancies.

Pharmacodynamics (PD) will be explored to assess the antiretroviral efficacy of NM1DRV and NM2DRV in post infection studies in humanized mice. Previous pharmacodynamics study did not show a protective effect from NM1DRV or NM2DRV compared to control infected and uninfected treatments. This observation could be due to the dose used (50 mg/kg), which is not high enough of a dose compared to the human

dose equivalence. Additionally, the PrEP PD study design is not ideal for protease inhibitors. Protease inhibitors are least preferred when considering PrEP regimens as their mode of function is post-integration of HIV into host genome. PrEP studies depends more on the prevention of integration of the proviral DNA into host genome[177]. Additionally, future PD studies will include combinational LA therapy that might include dual therapy along with long-acting NRTI or integrase inhibitors such as M3TC or MDTG[78, 79]. Moreover, toxicity studies in animals will be performed to ensure the prodrugs safety profiles. Liver enzymes such as alanine aminotransferase, alkaline phosphatase, and aspartate aminotransferase will be measured to ensure the health of the animals. Moreover, studies will be performed to measure the different lipids levels and their precursors since changes in lipids are common with the administration of many protease inhibitors[121].

Future studies involving DRV may include the synthesis of less stable drugs that can be cleaved easily by esterases *in vivo*. In our *in vivo* studies, we were able to detect dramatically high concentrations of prodrugs in plasma, blood and tissues for both prodrugs and specifically for M2DRV. The accumulation of the prodrugs may indicate that the prodrugs are not easily accessed by the esterases hence failing to be activated and released as the active molecule, DRV. Therefore future DRV prodrugs syntheses may include different linkers between the fatty acid and DRV to aid in propelling the fatty acid away. Previously, we synthesized M3DRV prodrug. The prodrug consisted of a hydroxy modification that consisted of a linker between a 14-carbon fatty acid chain and the DRV. The linker was conjugated to the fatty acid and the drug through ester bonds. However *in vitro* and *in vivo* cleavage of the drug was not improved over that of previous drugs formulations especially *in vivo*, where cleavage profiles were far less superior than with M2DRV, a hydroxyl-modified-DRV. This could have resulted from two different aspects. Modification to the internal hydroxyl of protease inhibitors had previously shown

the prodrugs to be more stable and have a longer hydrolysis half time[126, 127]. Additionally, the linker used in M3DRV was a short alkyl succinic linker that may have failed to propyl the fatty acid out of the drug. This modification may have caused folding of the drug concealing the ester group and avoiding activation by esterases. To overcome this in future studies we can try using bulky groups containing phenyl linkers between the fatty acid chain and the drug such as animoacyl phosphorocholoridates linkers shown to yield effective results in NRTI ProTides[86]. Previous attempts to improve protease inhibitors through modifications yielded fosamprenavir, a phosphate ester prodrug of amprenavir, structurally similar to darunavir[125]. The phosphate modification increased solubility of amprenavir and rendered it impermeable through cells. Fosamprenavir maintained elevated plasma amprenavir levels where the modification was readily reversible by the action of alkaline phosphatases[125]. The prodrug offered an advantage in oral administration regardless of food intake, which did not affect the absorption of amprenavir when administered as fosamprenavir tablets (regular oral amprenavir regimens are taken with food). Hence using aminoacyl phosphorocholoridates linkers would avoid the solubility increase for future DRV prodrugs by the conjugation of long-chain fatty acids and shielding the polar groups on the phosphates. Additionally future modifications would target the amine of the aniline to ensure the synthesis of a prodrug with comparable or better EC_{50} values than DRV as seen with M1DRV. M2DRV and M3DRV showed decrease in potency as reflected in their increased EC_{50} values (Chapter 2).

In vivo studies in mice using 100 mg/kg DRV equivalents of M2DRV showed prodrug detected in the brain of NM2DRV treated mice. This is significant because previously no drug was detected in these tissues. This could be due to the increased lipophilicity of M2DRV as compared to M1DRV and DRV. Further studies on protease inhibitors had shown that the difluorid-nation of the bis-THF moiety on DRV and its analogues can

increase drug permeability through the blood brain barrier [193, 194]. Ghosh et al showed that difluorination modification of the bis-THF moiety on DRV and its analogue (TMC-126) lead to increaseed drug lipophilicity and improved concentrations permeable in an in vitro model of the blood brain barrier. The modified drugs were more lipophilic and showed comparable or superior EC_{50} than DRV[193]. The modifications led to strong interactions between the fluorides with the carbonyl oxygen of Gly48 on the protease flap which further increased binding affinity to the substrate[193]. Hence for future directions, fluoridation of the DRV prodrugs may be explored to improve targeting and permeating into the brain for treatment of HIV-1-associated neurocognitive disorders (HAND). This would require the initial synthesis and fluoridination of DRV to incorporate these modifications[193]. Additionally, similar *in vitro* assays to determine blood brain barrier permeability of these drugs will be explored as well as binding assay and X-ray structures to determine their inherent binding to the proteases. In addition future optimization of drug nanoformulations is needed to ensure the hydrophobic drugs are efficiently encapsulated in stable formulations that are capable of slow release of the drugs.

3TC modification into S3TC yielded more promising data than the previously published M3TC[79], however further studies are needed to fully confirm S3TC efficacy and superiority to M3TC. These studies include formulation optimization as well as longer stability assays to ensure the best formulation for the drug. Efficacy studies will also be performed comparing S3TC to the efficacy of M3TC and 3TC. Moreover, uptake and retention studies will be repeated in macrophages and T cells to evaluate the intracellular levels of triphosphorylated levels of 3TC hydrolyzed from S3TC using Sep-Pak QMA cartridges and published processing methods[86]. Prodrug cleavage and hydrolysis will be evaluated in different plasmas where prodrug levels will be measured and monitored over 24 hours. Additional PK studies will be also performed to further

determine S3TC biodistribution in tissues as well as the triphosphorylated-3TC levels in plasma, blood and tissues. Finally PrEP PD study will be performed to determine the antiretroviral efficacy in vivo. Moreover, a PD study that includes NM1DRV or NM2DRV administered with NS3TC will be explored to evaluate the antiretroviral efficacies of combinational long-acting therapy. Current studies confirmed the non inferiority of a dual therapy that includes lamivudine and boosted DRV compared to triple therapy that includes RTV-boosted darunavir and 2 nucleotides; tenofovir disoproxil fumarate and emtricitabine or abacavir and lamivudine[102]. Additionally, exploring the different animal models to select the most suitable model for testing of ester prodrugs is essential to rule out discrepancies resulting from species differences in esterase actions/expressions as well as P450 drug metabolism[195, 196].

To better target these long-acting nanoformulations, future studies will explore targeting schemes to specifically target these drugs to macrophages, the cells that come in contact with the injectable drug nanoformulations first to ensure the drug formulations are not cleared out of the system quickly leading to a prolonged slow sustained release in circulation and tissues. This would better harness the macrophage carriage system as a depot and disseminator of antiretroviral therapy (ART). Targeting could be done by exploiting the C-type lectin receptor (CTLR)[197] to permit nanoformulated antiretroviral drug particle recognition and uptake into monocyte-macrophages. CTLR signaling is coordinated with other innate receptors to facilitate immunity to infection. Thus, the advantage of targeting schemes rests in its utility to combat a spectrum of microbial infections by facilitating intracellular immunization where the pathogen can replicate/reside[198]. Use of pathogen-associated molecular patterns (PAMP) for drug carriage can accelerate phagocytosis. CD206 is a type I transmembrane c-type lectin receptor that recognizes D-mannose, N-acetyl-D-glucosamine, and L-fucose[199] hence by modifying different poloxamers with these ligands we theoretically can increase drug

nanoformulation binding and uptake while enhancing innate immunity for microbial clearance. Many studies showed increased selective targeting with mannose-decorated drug carriers into CD206-expressing macrophages and dendritic cells; MR$^+$ cells[200-211]. Specifically, Stahl and his colleagues found that receptor mediated mannose glycoconjugates were endocytosed by alveolar macrophages where uptake of mannose ligands was time and concentration dependent[202]. Moreover, receptor blocking studies on MDM using soluble mannan or mannose-BSA to block the mannose receptors decreased phagocytosis of certain virulent *Mycobacterium tuberculosis* strains such as Erdman *M. tuberculosis* and H37Rv[212]. Another study reported that mannosylation of solid lipid nanoparticles (SLN) increased targeting of rifampicin (RIF) into alveolar macrophages by 2-fold (80%) compared to free drug (20%) and non-mannosylated SLN (40%)[213]. Different lengths of fatty acids conjugated to mannose ligands to achieve optimized hydrophobic/lipophilic balance to stabilize the particles therefore the ligands had bi-functional values in being a functionalizing agents and surfactants. Mannoslyated-SLNs RIF improved retention of the drug inside the cells. Notably, the longer hydrophobic chain used for functionalization showed slower release, *in vitro*, in comparison to free RIF and the shorter hydrophobic functionalized ligands-SLN[213]. In a different study, mannosylated lipid emulsions were more rapidly cleared and eliminated from the blood circulation accumulating into the liver compared to lower-mannose content nonmannosylated emulsions showing high drug-tissue distribution[214]. Amphotericin B (AB) or paromomycin-loaded mannosylated chitosan nanoparticles better targeted the drugs to the macrophages where *Leshmania* protozoans reside (obligate intracellular parasites) and showed increases in drug delivery compared to un-targeted particles[215, 216]. Additionally, thioalkylated mannnose-decorated dendrimers were found to be effective antigen-presenting cell-selective carriers; thus targeting the siRNAs to RAW264.7 mouse macrophage cells[203] and providing further proof that

mannose-decorated particles have better selectivity to MR^{+} cells. Targeting the dendritic cell receptor, DEC-205, a type I cell-surface protein C-type multilectin[217], using targeted nanoparticles encapsulating an antigenic peptide (melanoma associated) yielded both increased internalization and higher cross-presentation efficacy of the antigen compared to the untargeted nanoparticles[218]. In a similar experiment, treating dendritic cells with mannosylated antigens resulted in a more selective targeting followed by a higher presentation efficacy compared to the non-mannosylated antigens[219]. Our laboratory previously demonstrated increased uptake of ART nanoparticles that are folic acid-decorated polymer via folic acid receptor-mediated endocytosis compared to the unmodified polymer[79, 150, 154]. Collectively, these discoveries pave highly promising grounds for targeting schemes to specifically deliver ART nanoformulations to cells. In addition to folic acid targeting, CD206 targeting will be explored by first synthesizing a spectrum of mannose ligands. Successfully synthesized and characterized mannose ligands will be moved forward in decoration of different polymers, specifically P407, since many studies in our laboratory utilized this polymer for formulation of different ART drug classes and proved to be compatible with the majority of drug formulations. Mannose-decorated P407 will be used for ART nanoformulations to eventually target nanoparticles to mannose receptors on the macrophages/CD206^{+} cells being treated where they would be eventually internalized.

Prior studies to target mannose-decorated nanocarriers to macrophages had explored variant mannose densities and linkers to achieve highest uptake and targeting[200, 201]. D-mannose along with different peptide spacers, carbon chains, phenyl, PEGs, or biphenyl linkers are used to synthesize different spectrum of mannose ligands with different conformations and mannose densities. In a series of organic chemistry reactions starting with a D-mannose (mannospyranose) and reacting it to different linkers; biphenol linker, phenyl linker, GABA/lysine-GABA spacers, yielded final protected ligands. The protected

ligand can later be deprotected to react with the amine group of the amine-terminated polymer. Refer to Figure 4.1 for a scheme of different mannose ligands (1,2,3 & 4). Characterization of the ligand will be done through nuclear magnetic resonance (NMR) along with Fourier transform infrared spectroscopy (FTIR). One limitation in the characterization of these modified P407 structures is that ^{1}H NMR characterization will show chemical shifts around 3.1 – 4 ppm which masks and overlaps with the mannose peaks representing a problem in quantification of the mannose densities on the modified polymer. To overcome this, a fluorine tag [4-Azido-2,3,5,6-tetrafluorobenzoic acid][220] may be used to tag the structures of mannose to shift their signals downfield on the NMR spectra around 237 ppm which would provide tremendous clarity in viewing the mannose peaks as well as quantification of mannose ligand densities that are found on each polymer sample.

The developed ligands will vary from the mannose densities on each ligand to the spacer/linker length that will ensure the ligand is well positioned on the polymer and propelled out to maximize ligand-receptor interaction. The ligand-modified polymers generated will produce ART nanoparticles characterized by size, shape, polydispersity index and charge. The developed particles will be screened in macrophages to targeting advantage on uptake, retention, release, and eventually antiretroviral activities. It is essential to ensure that the targeting schemes do not interfere with the long-term antiretroviral activities of the drugs. Therefore targeted and untargeted drug nanoformulations will be tested in parallel studies to ensure the targeted nanoparticles retain their efficacy against the virus. Moreover, targeting and trafficking of these mannose-modified systems to the cells can be tracked by antibodies to the different markers of endosomal compartments[79]. In addition, tagging the finalized targeting system with a dye would also facilitate tracking the systemic trafficking by fluorescence microscopy in the absence and presence of fluorescent probes for specific endocytotic

markers. The mannose-targeting schemes will be compared to the folic acid targeting schemes for effect on targeting efficacy and exploring the possibility of combining different targeting schemes. Folate and CD206 receptors will be assayed for by flow cytometry in the cells/cell lines that will be used to test the targeting schemes. Antiretroviral targeting using the mannosylation schemes has not been explored enough however some studies reported promising results by targeting of lamivudine using mannosylated-poly propyleneimine dendrimers to efficiently target MT2 cells where uptake of these particles was improved as well as its anti-retroviral activities against HIV-1 compared to untargeted dendrimers or free lamivudine[221]. Using these targeting schemes to target our prodrug nanoformulations may lead to higher uptake inside the cells leading to higher retention hence the targeting schemes were shown to lead to slower release outside the cells. This may be reflected in pharmacokinetics studies where the macrophages would uptake targeted prodrug nanoparticles more efficiently from the injection site.

154

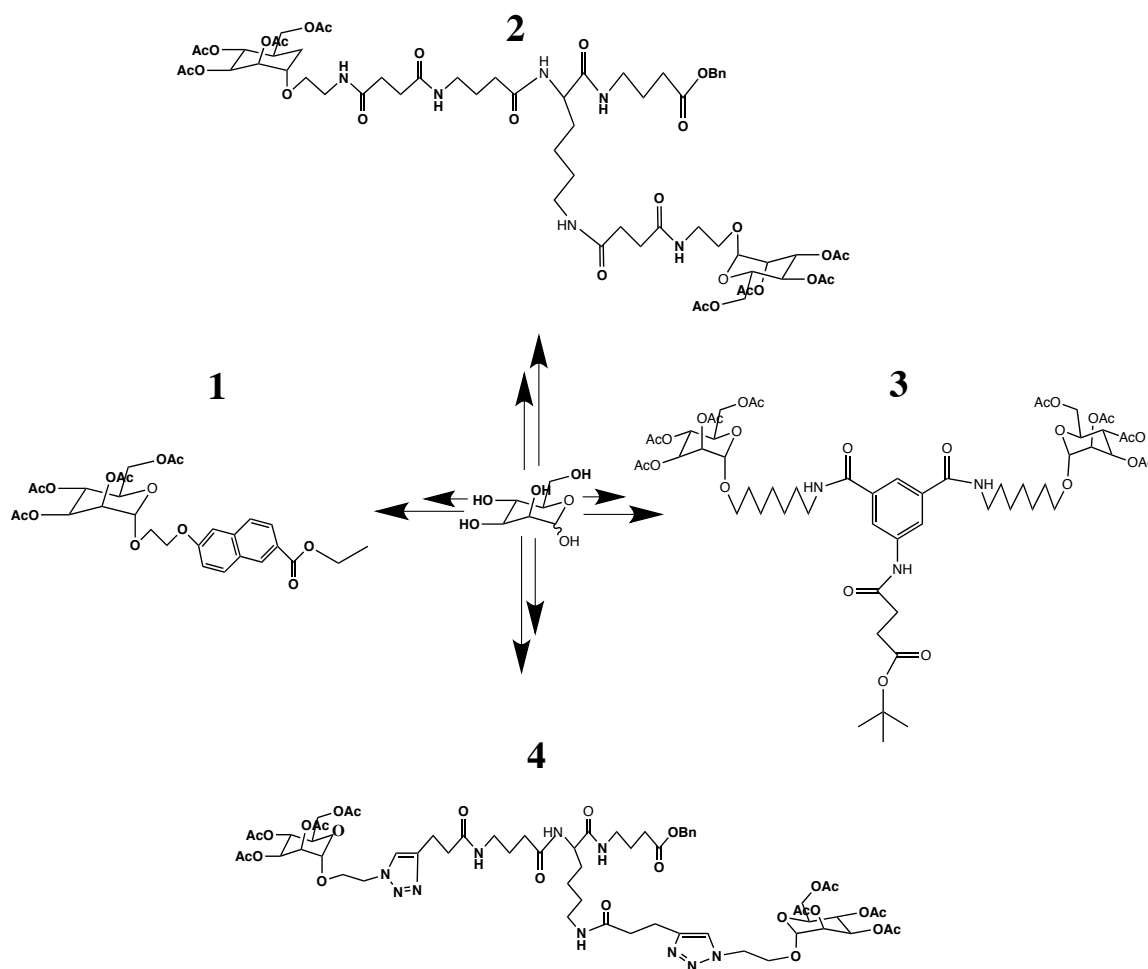# Figures

Figure 4. 1 Mannosylated ligands for targeting schemes

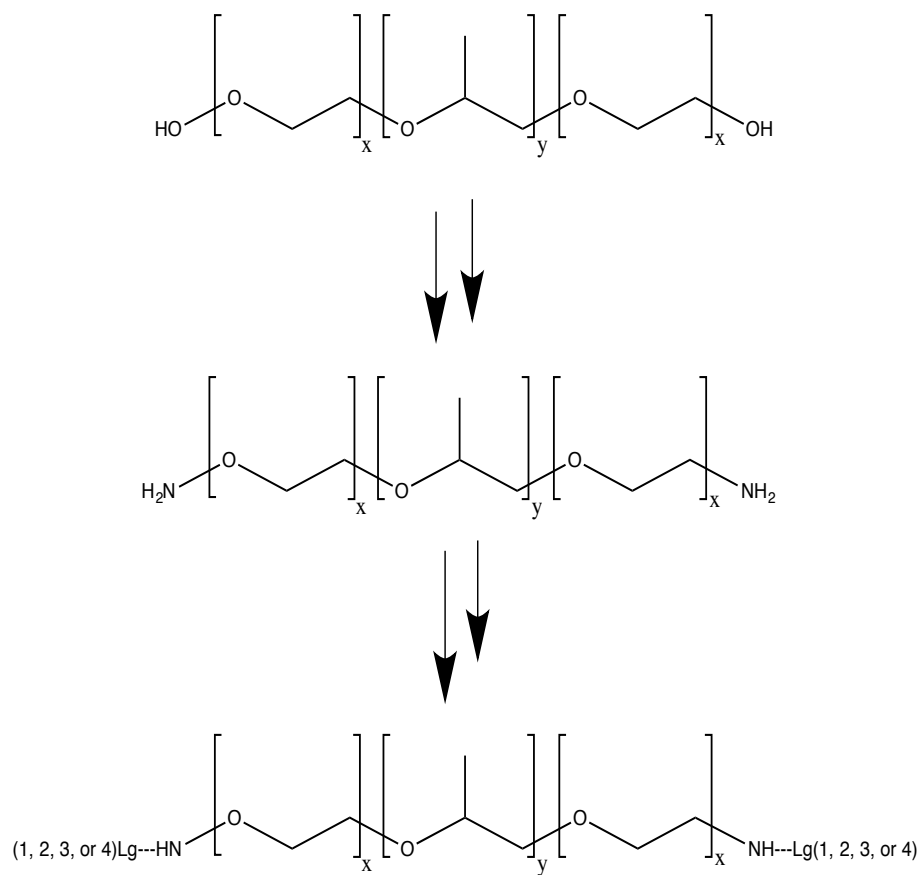Different mannose ligands synthesized/in progress starting from D-mannospyranose.

Figure 4. 2 Polymer decoration with mannosylated ligands from Figure 4.1

References

1. Chang CC, Crane M, Zhou J, Mina M, Post JJ, Cameron BA, et al. HIV and co-infections. Immunol Rev 2013; 254:114-42.
2. Stahl RE, Friedman-Kien A, Zolla-Pazner S. AIDS: a medical conundrum. J Cutan Pathol 1983; 10:550-8.
3. Sonderup MW, Wainwright HC. Human Immunodeficiency Virus Infection, Antiretroviral Therapy, and Liver Pathology. Gastroenterol Clin North Am 2017; 46:327-43.
4. Waymack JR, Sundareshan V. Acquired Immune Deficiency Syndrome (AIDS). In: StatPearls. Treasure Island (FL): StatPearls Publishing
   StatPearls Publishing LLC.; 2019.
5. Justiz Vaillant AA, Gulick PG. HIV Disease. In: StatPearls. Treasure Island (FL): StatPearls Publishing
   StatPearls Publishing LLC.; 2019.
6. Barre-Sinoussi F, Ross AL, Delfraissy JF. Past, present and future: 30 years of HIV research. Nat Rev Microbiol 2013; 11:877-83.
7. Downie JC, Howard R, Bowcock B, Cunningham AL. HIV-1 antibody testing strategy: evaluation of ELISA screening and western blot profiles in a mixed low risk/high risk patient population. J Virol Methods 1989; 26:291-303.
8. Selvaraj JR, Sudharshan S, Therese LK, Janani MK, Selvamuthu P, Rewri P, et al. Real-time polymerase chain reaction for diagnosis and management of HIV-induced uveitis. Indian J Ophthalmol 2018; 66:1634-6.
9. Stevenson M. HIV-1 pathogenesis. Nat Med 2003; 9:853-60.
10. Hutter G, Nowak D, Mossner M, Ganepola S, Mussig A, Allers K, et al. Long-term control of HIV by CCR5 Delta32/Delta32 stem-cell transplantation. N Engl J Med 2009; 360:692-8.
11. Fanales-Belasio E, Raimondo M, Suligoi B, Butto S. HIV virology and pathogenetic mechanisms of infection: a brief overview. Ann Ist Super Sanita 2010; 46:5-14.
12. Vogt VM. Retroviral Virions and Genomes. In: Coffin JM, Hughes SH, Varmus HE, eds. Retroviruses. Cold Spring Harbor (NY): Cold Spring Harbor Laboratory Press
    Cold Spring Harbor Laboratory Press.; 1997.
13. Khoury G, Darcis G, Lee MY, Bouchat S, Van Driessche B, Purcell DFJ, et al. The Molecular Biology of HIV Latency. Adv Exp Med Biol 2018; 1075:187-212.
14. Engelman A, Cherepanov P. The structural biology of HIV-1: mechanistic and therapeutic insights. Nat Rev Microbiol 2012; 10:279-90.
15. Merk A, Subramaniam S. HIV-1 envelope glycoprotein structure. Curr Opin Struct Biol 2013; 23:268-76.
16. Wilen CB, Tilton JC, Doms RW. HIV: cell binding and entry. Cold Spring Harb Perspect Med 2012; 2.
17. Goodsell DS. Illustrations of the HIV life cycle. Curr Top Microbiol Immunol 2015; 389:243-52.
18. Adamson CS, Freed EO. Human immunodeficiency virus type 1 assembly, release, and maturation. Adv Pharmacol 2007; 55:347-87.

19. Ganser-Pornillos BK, Yeager M, Sundquist WI. The structural biology of HIV assembly. Curr Opin Struct Biol 2008; 18:203-17.

20. Freed EO. HIV-1 assembly, release and maturation. Nat Rev Microbiol 2015; 13:484-96.

21. Lehmann M, Nikolic DS, Piguet V. How HIV-1 takes advantage of the cytoskeleton during replication and cell-to-cell transmission. Viruses 2011; 3:1757-76.

22. Gao Y, McKay PF, Mann JFS. Advances in HIV-1 Vaccine Development. Viruses 2018; 10.

23. Silvin A, Manel N. Innate immune sensing of HIV infection. Curr Opin Immunol 2015; 32:54-60.

24. Doitsh G, Galloway NL, Geng X, Yang Z, Monroe KM, Zepeda O, et al. Cell death by pyroptosis drives CD4 T-cell depletion in HIV-1 infection. Nature 2014; 505:509-14.

25. Hu J, Gardner MB, Miller CJ. Simian immunodeficiency virus rapidly penetrates the cervicovaginal mucosa after intravaginal inoculation and infects intraepithelial dendritic cells. J Virol 2000; 74:6087-95.

26. Ballweber L, Robinson B, Kreger A, Fialkow M, Lentz G, McElrath MJ, et al. Vaginal langerhans cells nonproductively transporting HIV-1 mediate infection of T cells. J Virol 2011; 85:13443-7.

27. Rodriguez-Garcia M, Shen Z, Barr FD, Boesch AW, Ackerman ME, Kappes JC, et al. Dendritic cells from the human female reproductive tract rapidly capture and respond to HIV. Mucosal Immunol 2017; 10:531-44.

28. Liu C, Perilla JR, Ning J, Lu M, Hou G, Ramalho R, et al. Cyclophilin A stabilizes the HIV-1 capsid through a novel non-canonical binding site. Nat Commun 2016; 7:10714.

29. Alter G, Heckerman D, Schneidewind A, Fadda L, Kadie CM, Carlson JM, et al. HIV-1 adaptation to NK-cell-mediated immune pressure. Nature 2011; 476:96-100.

30. Donahue DA, Wainberg MA. Cellular and molecular mechanisms involved in the establishment of HIV-1 latency. Retrovirology 2013; 10:11.

31. Peretz Y, Cameron C, Sekaly RP. Dissecting the HIV-specific immune response: a systems biology approach. Curr Opin HIV AIDS 2012; 7:17-23.

32. Perno CF. The discovery and development of HIV therapy: the new challenges. Ann Ist Super Sanita 2011; 47:41-3.

33. Brock JB, Henderson H. Antiretroviral Therapy. J Miss State Med Assoc 2015; 56:166, 71-2.

34. Poorolajal J, Hooshmand E, Mahjub H, Esmailnasab N, Jenabi E. Survival rate of AIDS disease and mortality in HIV-infected patients: a meta-analysis. Public Health 2016; 139:3-12.

35. Bangsberg DR, Acosta EP, Gupta R, Guzman D, Riley ED, Harrigan PR, et al. Adherence-resistance relationships for protease and non-nucleoside reverse transcriptase inhibitors explained by virological fitness. Aids 2006; 20:223-31.

36. Abdool Karim Q, Abdool Karim SS, Frohlich JA, Grobler AC, Baxter C, Mansoor LE, et al. Effectiveness and safety of tenofovir gel, an antiretroviral

microbicide, for the prevention of HIV infection in women. Science 2010; 329:1168-74.

37. Grant RM, Lama JR, Anderson PL, McMahan V, Liu AY, Vargas L, et al. Preexposure chemoprophylaxis for HIV prevention in men who have sex with men. N Engl J Med 2010; 363:2587-99.

38. Myers JE, Sepkowitz KA. A pill for HIV prevention: deja vu all over again? Clin Infect Dis 2013; 56:1604-12.

39. Cohen MS, Chen YQ, McCauley M, Gamble T, Hosseinipour MC, Kumarasamy N, et al. Prevention of HIV-1 infection with early antiretroviral therapy. N Engl J Med 2011; 365:493-505.

40. Baeten JM, Donnell D, Ndase P, Mugo NR, Campbell JD, Wangisi J, et al. Antiretroviral prophylaxis for HIV prevention in heterosexual men and women. N Engl J Med 2012; 367:399-410.

41. Thigpen MC, Kebaabetswe PM, Paxton LA, Smith DK, Rose CE, Segolodi TM, et al. Antiretroviral preexposure prophylaxis for heterosexual HIV transmission in Botswana. N Engl J Med 2012; 367:423-34.

42. Desai M, Field N, Grant R, McCormack S. Recent advances in pre-exposure prophylaxis for HIV. Bmj 2017; 359:j5011.

43. Flash C, Landovitz R, Giler RM, Ng L, Magnuson D, Wooley SB, et al. Two years of Truvada for pre-exposure prophylaxis utilization in the US. J Int AIDS Soc 2014; 17:19730.

44. Payne S. Chapter 6 - Immunity and Resistance to Viruses. In: Payne S, ed. Viruses: Academic Press; 2017: 61-71.

45. Keller MA, Stiehm ER. Passive immunity in prevention and treatment of infectious diseases. Clin Microbiol Rev 2000; 13:602-14.

46. Sok D, Burton DR. Recent progress in broadly neutralizing antibodies to HIV. Nat Immunol 2018; 19:1179-88.

47. Corti D, Lanzavecchia A. Broadly neutralizing antiviral antibodies. Annu Rev Immunol 2013; 31:705-42.

48. Gruell H, Klein F. Antibody-mediated prevention and treatment of HIV-1 infection. Retrovirology 2018; 15:73.

49. Mikell I, Sather DN, Kalams SA, Altfeld M, Alter G, Stamatatos L. Characteristics of the earliest cross-neutralizing antibody response to HIV-1. PLoS Pathog 2011; 7:e1001251.

50. Ferrari G, Haynes BF, Koenig S, Nordstrom JL, Margolis DM, Tomaras GD. Envelope-specific antibodies and antibody-derived molecules for treating and curing HIV infection. Nat Rev Drug Discov 2016; 15:823-34.

51. Ahmed Y, Tian M, Gao YJAR, Therapy. Development of an anti-HIV vaccine eliciting broadly neutralizing antibodies. 2017; 14:50.

52. Schoofs T, Barnes CO, Suh-Toma N, Golijanin J, Schommers P, Gruell H, et al. Broad and Potent Neutralizing Antibodies Recognize the Silent Face of the HIV Envelope. Immunity 2019; 50:1513-29.e9.

53. Bonsignori M, Wiehe K, Grimm SK, Lynch R, Yang G, Kozink DM, et al. An autoreactive antibody from an SLE/HIV-1 individual broadly neutralizes HIV-1. J Clin Invest 2014; 124:1835-43.

54. Haynes BF, Bradley T. Broadly Neutralizing Antibodies and the Development of Vaccines. Jama 2015; 313:2419-20.

55. Escolano A, Gristick HB, Abernathy ME, Merkenschlager J, Gautam R, Oliveira TY, et al. Immunization expands B cells specific to HIV-1 V3 glycan in mice and macaques. Nature 2019.

56. Subbaraman H, Schanz M, Trkola AJR. Broadly neutralizing antibodies: What is needed to move from a rare event in HIV-1 infection to vaccine efficacy? 2018; 15:52.

57. Shingai M, Nishimura Y, Klein F, Mouquet H, Donau OK, Plishka R, et al. Antibody-mediated immunotherapy of macaques chronically infected with SHIV suppresses viraemia. Nature 2013; 503:277-80.

58. Gautam R, Nishimura Y, Gaughan N, Gazumyan A, Schoofs T, Buckler-White A, et al. A single injection of crystallizable fragment domain-modified antibodies elicits durable protection from SHIV infection. Nat Med 2018; 24:610-6.

59. Xu L, Pegu A, Rao E, Doria-Rose N, Beninga J, McKee K, et al. Trispecific broadly neutralizing HIV antibodies mediate potent SHIV protection in macaques. Science 2017; 358:85-90.

60. Gaudinski MR, Coates EE, Houser KV, Chen GL, Yamshchikov G, Saunders JG, et al. Safety and pharmacokinetics of the Fc-modified HIV-1 human monoclonal antibody VRC01LS: A Phase 1 open-label clinical trial in healthy adults. PLoS Med 2018; 15:e1002493.

61. Caskey M, Schoofs T, Gruell H, Settler A, Karagounis T, Kreider EF, et al. Antibody 10-1074 suppresses viremia in HIV-1-infected individuals. Nat Med 2017; 23:185-91.

62. Scheid JF, Horwitz JA, Bar-On Y, Kreider EF, Lu CL, Lorenzi JC, et al. HIV-1 antibody 3BNC117 suppresses viral rebound in humans during treatment interruption. Nature 2016; 535:556-60.

63. Mendoza P, Gruell H, Nogueira L, Pai JA, Butler AL, Millard K, et al. Combination therapy with anti-HIV-1 antibodies maintains viral suppression. Nature 2018; 561:479-84.

64. Dey AK, Cupo A, Ozorowski G, Sharma VK, Behrens AJ, Go EP, et al. cGMP production and analysis of BG505 SOSIP.664, an extensively glycosylated, trimeric HIV-1 envelope glycoprotein vaccine candidate. Biotechnol Bioeng 2018; 115:885-99.

65. Cao S, Woodrow KA. Nanotechnology approaches to eradicating HIV reservoirs. Eur J Pharm Biopharm 2018.

66. Saez-Cirion A, Bacchus C, Hocqueloux L, Avettand-Fenoel V, Girault I, Lecuroux C, et al. Post-treatment HIV-1 controllers with a long-term virological remission after the interruption of early initiated antiretroviral therapy ANRS VISCONTI Study. PLoS Pathog 2013; 9:e1003211.

67. Luzuriaga K, Gay H, Ziemniak C, Sanborn KB, Somasundaran M, Rainwater-Lovett K, et al. Viremic relapse after HIV-1 remission in a perinatally infected child. N Engl J Med 2015; 372:786-8.

68. Margolis DM, Garcia JV, Hazuda DJ, Haynes BF. Latency reversal and viral clearance to cure HIV-1. 2016; 353:aaf6517.

69.   Rasmussen TA, Lewin SR. Shocking HIV out of hiding: where are we with clinical trials of latency reversing agents? Curr Opin HIV AIDS 2016; 11:394-401.

70.   Panfil AR, London JA, Green PL, Yoder KE. CRISPR/Cas9 Genome Editing to Disable the Latent HIV-1 Provirus. Front Microbiol 2018; 9:3107.

71.   Halper-Stromberg A, Lu CL, Klein F, Horwitz JA, Bournazos S, Nogueira L, et al. Broadly neutralizing antibodies and viral inducers decrease rebound from HIV-1 latent reservoirs in humanized mice. Cell 2014; 158:989-99.

72.   Borducchi EN, Liu J, Nkolola JP, Cadena AM, Yu WH, Fischinger S, et al. Antibody and TLR7 agonist delay viral rebound in SHIV-infected monkeys. Nature 2018; 563:360-4.

73.   Dash PK, Kaminski R, Bella R, Su H, Mathews S, Ahooyi TM, et al. Sequential LASER ART and CRISPR Treatments Eliminate HIV-1 in a Subset of Infected Humanized Mice. Nature Communications 2019; 10:2753-.

74.   Margolis DA, Gonzalez-Garcia J, Stellbrink HJ, Eron JJ, Yazdanpanah Y, Podzamczer D, et al. Long-acting intramuscular cabotegravir and rilpivirine in adults with HIV-1 infection (LATTE-2): 96-week results of a randomised, open-label, phase 2b, non-inferiority trial. Lancet 2017; 390:1499-510.

75.   Zhou T, Su H, Dash P, Lin Z, Dyavar Shetty BL, Kocher T, et al. Creation of a nanoformulated cabotegravir prodrug with improved antiretroviral profiles. Biomaterials 2018; 151:53-65.

76.   Andrews CD, Heneine W. Cabotegravir long-acting for HIV-1 prevention. Curr Opin HIV AIDS 2015; 10:258-63.

77.   Edagwa B, McMillan J, Sillman B, Gendelman HE. Long-acting slow effective release antiretroviral therapy. Expert Opin Drug Deliv 2017; 14:1281-91.

78.   Sillman B, Bade AN, Dash PK, Bhargavan B, Kocher T, Mathews S, et al. Creation of a long-acting nanoformulated dolutegravir. Nat Commun 2018; 9:443.

79.   Guo D, Zhou T, Arainga M, Palandri D, Gautam N, Bronich T, et al. Creation of a Long-Acting Nanoformulated 2',3'-Dideoxy-3'-Thiacytidine. J Acquir Immune Defic Syndr 2017; 74:e75-e83.

80.   Singh D, McMillan J, Hilaire J, Gautam N, Palandri D, Alnouti Y, et al. Development and characterization of a long-acting nanoformulated abacavir prodrug. Nanomedicine (Lond) 2016; 11:1913-27.

81.   Lin SJ, Vavasour I, Kosaka B, Li DKB, Traboulsee A, MacKay A, et al. Education, and the balance between dynamic and stationary functional connectivity jointly support executive functions in relapsing-remitting multiple sclerosis. Hum Brain Mapp 2018.

82.   Ibrahim IM, Bade AN, Lin Z, Soni D, Wojtkiewicz M, Shetty BLD, et al. Synthesis and characterization of a long-acting emtricitabine prodrug nanoformulation International Journal of Nanomedicine 2019; 14:6231-47.

83.   Huttunen KM, Raunio H, Rautio J. Prodrugs--from serendipity to rational design. Pharmacol Rev 2011; 63:750-71.

84.   Park EJ, Amatya S, Kim MS, Park JH, Seol E, Lee H, et al. Long-acting injectable formulations of antipsychotic drugs for the treatment of schizophrenia. Arch Pharm Res 2013; 36:651-9.

85. Andrews CD, Spreen WR, Mohri H, Moss L, Ford S, Gettie A, et al. Long-acting integrase inhibitor protects macaques from intrarectal simian/human immunodeficiency virus. Science 2014; 343:1151-4.

86. Lin Z, Gautam N, Alnouti Y, McMillan J, Bade AN, Gendelman HE, et al. ProTide generated long-acting abacavir nanoformulations. Chem Commun (Camb) 2018; 54:8371-4.

87. Gendelman HE, McMillan J, Bade AN, Edagwa B, Kevadiya BD. The Promise of Long-Acting Antiretroviral Therapies: From Need to Manufacture. Trends Microbiol 2019; 27:593-606.

88. Brown K, Stewart L, Whitcomb J, Yang D, Nettles RE, Lathouwers E. Prevalence of darunavir resistance in the United States from 2010 to 2017. AIDS Res Hum Retroviruses 2018.

89. Fenton C, Perry CM. Darunavir: in the treatment of HIV-1 infection. Drugs 2007; 67:2791-801.

90. Sherer R. Darunavir in the treatment of HIV-1 infection: a viewpoint by Renslow Sherer. Drugs 2007; 67:2802-3.

91. Holodniy M. Darunavir in the treatment of HIV-1 infection: a viewpoint by Mark Holodniy. Drugs 2007; 67:2803.

92. Tomaka FL, Kakuda TN, Brochot A, Hoetelmans RMW, Van De Casteele T, Vangeneugden T. Pharmacokinetics and pharmacodynamics of boosted once-daily darunavir. Journal of Antimicrobial Chemotherapy 2014; 69:2591-605.

93. Mallolas J. Darunavir Stands Up as Preferred HIV Protease Inhibitor. AIDS Rev 2017; 19:105-12.

94. Back D, Sekar V, Hoetelmans RM. Darunavir: pharmacokinetics and drug interactions. Antivir Ther 2008; 13:1-13.

95. Vermeir M, Lachau-Durand S, Mannens G, Cuyckens F, van Hoof B, Raoof A. Absorption, metabolism, and excretion of darunavir, a new protease inhibitor, administered alone and with low-dose ritonavir in healthy subjects. Drug Metab Dispos 2009; 37:809-20.

96. Spagnuolo V, Castagna A, Lazzarin A. Darunavir for the treatment of HIV infection. Expert Opin Pharmacother 2018; 19:1149-63.

97. Mbuagbaw L, Mursleen S, Irlam JH, Spaulding AB, Rutherford GW, Siegfried N. Efavirenz or nevirapine in three-drug combination therapy with two nucleoside or nucleotide-reverse transcriptase inhibitors for initial treatment of HIV infection in antiretroviral-naive individuals. Cochrane Database Syst Rev 2016; 12:Cd004246.

98. Hayashi H, Takamune N, Nirasawa T, Aoki M, Morishita Y, Das D, et al. Dimerization of HIV-1 protease occurs through two steps relating to the mechanism of protease dimerization inhibition by darunavir. Proc Natl Acad Sci U S A 2014; 111:12234-9.

99. Zhang Y, Chang YC, Louis JM, Wang YF, Harrison RW, Weber IT. Structures of darunavir-resistant HIV-1 protease mutant reveal atypical binding of darunavir to wide open flaps. ACS Chem Biol 2014; 9:1351-8.

100. Violari A, Bologna R, Kumarasamy N, Pilotto JH, Hendrickx A, Kakuda TN, et al. Safety and efficacy of darunavir/ritonavir in treatment-experienced

pediatric patients: week 48 results of the ARIEL trial. Pediatr Infect Dis J 2015; 34:e132-7.

101. Brogan AJ, Davis AE, Goodwin B. Short-term cost analysis of raltegravir versus atazanavir + ritonavir or darunavir + ritonavir for treatment-naive adults with HIV-1 infection in the United States. PLoS One 2018; 13:e0203293.

102. Pulido F, Ribera E, Lagarde M, Perez-Valero I, Palacios R, Iribarren JA, et al. Dual Therapy With Darunavir and Ritonavir Plus Lamivudine vs Triple Therapy With Darunavir and Ritonavir Plus Tenofovir Disoproxil Fumarate and Emtricitabine or Abacavir and Lamivudine for Maintenance of Human Immunodeficiency Virus Type 1 Viral Suppression: Randomized, Open-Label, Noninferiority DUAL-GESIDA 8014-RIS-EST45 Trial. Clin Infect Dis 2017; 65:2112-8.

103. Deeks ED. Darunavir/Cobicistat/Emtricitabine/Tenofovir Alafenamide: A Review in HIV-1 Infection. Drugs 2018; 78:1013-24.

104. Krauss J, Bracher F. Pharmacokinetic Enhancers (Boosters)-Escort for Drugs against Degrading Enzymes and Beyond. Sci Pharm 2018; 86.

105. Tseng A, Hughes CA, Wu J, Seet J, Phillips EJ. Cobicistat Versus Ritonavir: Similar Pharmacokinetic Enhancers But Some Important Differences. Ann Pharmacother 2017; 51:1008-22.

106. Desai J, Thakkar H. Darunavir-Loaded Lipid Nanoparticles for Targeting to HIV Reservoirs. AAPS PharmSciTech 2018; 19:648-60.

107. Yoganathan K, Roberts B, Heatley MK. Life-threatening digoxin toxicity due to drug-drug interactions in an HIV-positive man. Int J STD AIDS 2017; 28:297-301.

108. Khatri A, Dutta S, Wang H, Podsadecki T, Trinh R, Awni W, et al. Evaluation of Drug-Drug Interactions Between Hepatitis C Antiviral Agents Ombitasvir, Paritaprevir/Ritonavir, and Dasabuvir and HIV-1 Protease Inhibitors. Clin Infect Dis 2016; 62:972-9.

109. Tempestilli M, Fabbri G, Mastrorosa I, Timelli L, Notari S, Bellagamba R, et al. Plasma trough concentrations of antiretrovirals in HIV-infected persons treated with direct-acting antiviral agents for hepatitis C in the real world. J Antimicrob Chemother 2018; 73:160-4.

110. Kiser JJ, Lu D, Rosenkranz SL, Morse GD, DiFrancesco R, Sherman KE, et al. Boceprevir and Antiretroviral Pharmacokinetic Interactions in HIV/HCV Co-infected Persons: AIDS Clinical Trials Group Study A5309s. Drugs R D 2017; 17:557-67.

111. Hulskotte EG, Feng HP, Xuan F, van Zutven MG, Treitel MA, Hughes EA, et al. Pharmacokinetic interactions between the hepatitis C virus protease inhibitor boceprevir and ritonavir-boosted HIV-1 protease inhibitors atazanavir, darunavir, and lopinavir. Clin Infect Dis 2013; 56:718-26.

112. Feng HP, Caro L, Fandozzi C, Chu X, Guo Z, Talaty J, et al. Pharmacokinetic Interactions Between the HCV Inhibitors Elbasvir and Grazoprevir and HIV Protease Inhibitors Ritonavir, Atazanavir, Lopinavir, or Darunavir in Healthy Participants. Antimicrob Agents Chemother 2019.

113. Dickinson L, Winston A, Boffito M, Khoo S, Back D, Siccardi M. Simulation of the impact of rifampicin on once-daily darunavir/ritonavir pharmacokinetics and dose adjustment strategies: a population pharmacokinetic approach. J Antimicrob Chemother 2016; 71:1041-5.

114. Holmstock N, Gonzalez FJ, Baes M, Annaert P, Augustijns P. PXR/CYP3A4-humanized mice for studying drug-drug interactions involving intestinal P-glycoprotein. Mol Pharm 2013; 10:1056-62.

115. Midde NM, Gong Y, Cory TJ, Li J, Meibohm B, Li W, et al. Influence of Ethanol on Darunavir Hepatic Clearance and Intracellular PK/PD in HIV-Infected Monocytes, and CYP3A4-Darunavir Interactions Using Inhibition and in Silico Binding Studies. Pharm Res 2017; 34:1925-33.

116. Marzolini C, Back D, Gibbons S, Khoo S. Cobicistat versus ritonavir boosting and differences in the drug–drug interaction profiles with co-medications. Journal of Antimicrobial Chemotherapy 2016; 71:1755-8.

117. Makaram N, Russell CD, Roberts SB, Stevens J, Macpherson G. Exogenous steroid-induced hypoadrenalism in a person living with HIV caused by a drug-drug interaction between cobicistat and intrabursal triamcinolone. BMJ Case Rep 2018; 11.

118. Inugala S, Eedara BB, Sunkavalli S, Dhurke R, Kandadi P, Jukanti R, et al. Solid self-nanoemulsifying drug delivery system (S-SNEDDS) of darunavir for improved dissolution and oral bioavailability: In vitro and in vivo evaluation. Eur J Pharm Sci 2015; 74:1-10.

119. Smith K, Gomes D, Nixon D, Fulco PP. The use of unboosted darunavir in the setting of ritonavir intolerance: three case reports. Int J Clin Pharmacol Ther 2016; 54:52-7.

120. Hostetler KY, Richman DD, Forssen EA, Selk L, Basava R, Gardner MF, et al. Phospholipid prodrug inhibitors of the HIV protease. Antiviral activity and pharmacokinetics in rats. Biochem Pharmacol 1994; 48:1399-404.

121. Subbaiah MAM, Meanwell NA, Kadow JF. Design strategies in the prodrugs of HIV-1 protease inhibitors to improve the pharmaceutical properties. Eur J Med Chem 2017; 139:865-83.

122. Gaucher B, Rouquayrol M, Roche D, Greiner J, Aubertin AM, Vierling P. Prodrugs of HIV protease inhibitors-saquinavir, indinavir and nelfinavir-derived from diglycerides or amino acids: synthesis, stability and anti-HIV activity. Org Biomol Chem 2004; 2:345-57.

123. Vierling P, Greiner J. Prodrugs of HIV protease inhibitors. Curr Pharm Des 2003; 9:1755-70.

124. Chong KT, Ruwart MJ, Hinshaw RR, Wilkinson KF, Rush BD, Yancey MF, et al. Peptidomimetic HIV protease inhibitors: phosphate prodrugs with improved biological activities. J Med Chem 1993; 36:2575-7.

125. Wire MB, Shelton MJ, Studenberg S. Fosamprenavir : clinical pharmacokinetics and drug interactions of the amprenavir prodrug. Clin Pharmacokinet 2006; 45:137-68.

126. Rouquayrol M, Gaucher B, Greiner J, Aubertin AM, Vierling P, Guedj R. Synthesis and anti-HIV activity of glucose-containing prodrugs derived from saquinavir, indinavir and nelfinavir. Carbohydr Res 2001; 336:161-80.

127. Farese-Di Giorgio A, Rouquayrol M, Greiner J, Aubertin AM, Vierling P, Guedj R. Synthesis and anti-HIV activity of prodrugs derived from saquinavir and indinavir. Antivir Chem Chemother 2000; 11:97-110.

128. Abah IO, Ncube NB, Bradley HA, AgbaJi OO, Kanki P. Antiretroviral Therapy-associated Adverse Drug Reactions and their Effects on Virologic Failure- A Retrospective Cohort Study in Nigeria. Curr HIV Res 2019.

129. Dona D, Mozzo E, Luise D, Lundin R, Padoan A, Rampon O, et al. Impact of HIV-1 Infection and Antiretroviral Therapy on Bone Homeostasis and Mineral Density in Vertically Infected Patients. J Osteoporos 2019; 2019:1279318.

130. Giacomelli A, Riva A, Falvella FS, Oreni ML, Cattaneo D, Cheli S, et al. Clinical and genetic factors associated with increased risk of severe liver toxicity in a monocentric cohort of HIV positive patients receiving nevirapine-based antiretroviral therapy. BMC Infect Dis 2018; 18:556.

131. Fogarty L, Roter D, Larson S, Burke J, Gillespie J, Levy R. Patient adherence to HIV medication regimens: a review of published and abstract reports. Patient Educ Couns 2002; 46:93-108.

132. Motumma A, Negesa L, Hunduma G, Abdeta T. Prevalence and associated factors of common mental disorders among adult patients attending HIV follow up service in Harar town, Eastern Ethiopia: a cross-sectional study. BMC Psychol 2019; 7:11.

133. Chen J, Zhang M, Shang M, Yang W, Wang Z, Shang H. Research on the treatment effects and drug resistances of long-term second-line antiretroviral therapy among HIV-infected patients from Henan Province in China. BMC Infect Dis 2018; 18:571.

134. Ong EL. Common AIDS-associated opportunistic infections. Clin Med (Lond) 2008; 8:539-43.

135. Zhang C, Li X, Liu Y, Qiao S, Chen Y, Zhou Y, et al. Co-infections of tuberculosis, hepatitis B or C viruses in a cohort of people living with HIV/AIDS in China: predictors and sequelae. AIDS Care 2017; 29:974-7.

136. Kaufman AS, Morrison A. Patterns of non-adherence to oral antiretroviral medication: frequencies of consecutively missed doses. Patient Prefer Adherence 2019; 13:389-94.

137. Fauci AS, Redfield RR, Sigounas G, Weahkee MD, Giroir BP. Ending the HIV Epidemic: A Plan for the United States. Jama 2019.

138. Rutherford GW, Anglemyer A. Is 90-90-90 achievable? Lancet HIV 2017; 4:e193-e4.

139. Granich R, Williams B, Montaner J, Zuniga JM. 90-90-90 and ending AIDS: necessary and feasible. Lancet 2017; 390:341-3.

140. Spreen WR, Margolis DA, Pottage JC, Jr. Long-acting injectable antiretrovirals for HIV treatment and prevention. Curr Opin HIV AIDS 2013; 8:565-71.

141. Williams J, Sayles HR, Meza JL, Sayre P, Sandkovsky U, Gendelman HE, et al. Long-acting parenteral nanoformulated antiretroviral therapy: interest and attitudes of HIV-infected patients. Nanomedicine (Lond) 2013; 8:1807-13.

142. Remenar JF. Making the leap from daily oral dosing to long-acting injectables: lessons from the antipsychotics. Mol Pharm 2014; 11:1739-49.

143. Spreen W, Williams P, Margolis D, Ford SL, Crauwels H, Lou Y, et al. Pharmacokinetics, safety, and tolerability with repeat doses of GSK1265744 and rilpivirine (TMC278) long-acting nanosuspensions in healthy adults. J Acquir Immune Defic Syndr 2014; 67:487-92.

144. McMillan J, Szlachetka A, Slack L, Sillman B, Lamberty B, Morsey B, et al. Pharmacokinetics of a Long-Acting Nanoformulated Dolutegravir Prodrug in Rhesus Macaques. Antimicrob Agents Chemother 2018; 62.

145. Subbaiah MAM, Meanwell NA, Kadow JF, Subramani L, Annadurai M, Ramar T, et al. Coupling of an Acyl Migration Prodrug Strategy with Bio-activation To Improve Oral Delivery of the HIV-1 Protease Inhibitor Atazanavir. J Med Chem 2018; 61:4176-88.

146. Sanrame CN, Remenar JF, Blumberg LC, Waters J, Dean RL, Dong N, et al. Prodrugs of pioglitazone for extended-release (XR) injectable formulations. Mol Pharm 2014; 11:3617-23.

147. Gendelman HE, Orenstein JM, Martin MA, Ferrua C, Mitra R, Phipps T, et al. Efficient isolation and propagation of human immunodeficiency virus on recombinant colony-stimulating factor 1-treated monocytes. J Exp Med 1988; 167:1428-41.

148. Balkundi S, Nowacek AS, Veerubhotla RS, Chen H, Martinez-Skinner A, Roy U, et al. Comparative manufacture and cell-based delivery of antiretroviral nanoformulations. Int J Nanomedicine 2011; 6:3393-404.

149. Nowacek AS, Balkundi S, McMillan J, Roy U, Martinez-Skinner A, Mosley RL, et al. Analyses of nanoformulated antiretroviral drug charge, size, shape and content for uptake, drug release and antiviral activities in human monocyte-derived macrophages. J Control Release 2011; 150:204-11.

150. Puligujja P, Balkundi SS, Kendrick LM, Baldridge HM, Hilaire JR, Bade AN, et al. Pharmacodynamics of long-acting folic acid-receptor targeted ritonavir-boosted atazanavir nanoformulations. Biomaterials 2015; 41:141-50.

151. Foley GE, Lazarus H, Farber S, Uzman BG, Boone BA, McCarthy RE. Continuous culture of human lymphoblasts from peripheral blood of a child with acute leukemia. 1965; 18:522-9.

152. NARA PL, HATCH WC, DUNLOP NM, ROBEY WG, ARTHUR LO, GONDA MA, et al. Simple, Rapid, Quantitative, Syncytium-Forming Microassay for the Detection of Human Immunodeficiency Virus Neutralizing Antibody. 1987; 3:283-302.

153. McMillan JM, Cobb DA, Lin Z, Banoub MG, Dagur RS, Branch Woods AA, et al. Antiretroviral Drug Metabolism in Humanized PXR-CAR-CYP3A-NOG Mice. J Pharmacol Exp Ther 2018; 365:272-80.

154. Puligujja P, McMillan J, Kendrick L, Li T, Balkundi S, Smith N, et al. Macrophage folate receptor-targeted antiretroviral therapy facilitates drug entry, retention, antiretroviral activities and biodistribution for reduction of human immunodeficiency virus infections. Nanomedicine 2013; 9:1263-73.

155. Kadiu I, Nowacek A, McMillan J, Gendelman HE. Macrophage endocytic trafficking of antiretroviral nanoparticles. Nanomedicine (Lond) 2011; 6:975-94.

156. Handschin C, Meyer UA. Induction of drug metabolism: the role of nuclear receptors. Pharmacol Rev 2003; 55:649-73.
157. Willson TM, Kliewer SA. PXR, CAR and drug metabolism. Nat Rev Drug Discov 2002; 1:259-66.
158. Este JA, Cihlar T. Current status and challenges of antiretroviral research and therapy. Antiviral Res 2010; 85:25-33.
159. Jackson A, McGowan I. Long-acting rilpivirine for HIV prevention. Curr Opin HIV AIDS 2015; 10:253-7.
160. van 't Klooster G, Hoeben E, Borghys H, Looszova A, Bouche MP, van Velsen F, et al. Pharmacokinetics and disposition of rilpivirine (TMC278) nanosuspension as a long-acting injectable antiretroviral formulation. Antimicrob Agents Chemother 2010; 54:2042-50.
161. Williams PE, Crauwels HM, Basstanie ED. Formulation and pharmacology of long-acting rilpivirine. Curr Opin HIV AIDS 2015; 10:233-8.
162. Trezza C, Ford SL, Spreen W, Pan R, Piscitelli S. Formulation and pharmacology of long-acting cabotegravir. Curr Opin HIV AIDS 2015; 10:239-45.
163. Hickey MB, Merisko-Liversidge E, Remenar JF, Namchuk M. Delivery of long-acting injectable antivirals: best approaches and recent advances. Curr Opin Infect Dis 2015; 28:603-10.
164. Markowitz M, Frank I, Grant RM, Mayer KH, Elion R, Goldstein D, et al. Safety and tolerability of long-acting cabotegravir injections in HIV-uninfected men (ECLAIR): a multicentre, double-blind, randomised, placebo-controlled, phase 2a trial. Lancet HIV 2017; 4:e331-e40.
165. Desai J, Thakkar H. Effect of particle size on oral bioavailability of darunavir-loaded solid lipid nanoparticles. J Microencapsul 2016; 33:669-78.
166. Duan J, Freeling JP, Koehn J, Shu C, Ho RJ. Evaluation of atazanavir and darunavir interactions with lipids for developing pH-responsive anti-HIV drug combination nanoparticles. J Pharm Sci 2014; 103:2520-9.
167. Zhou T, Lin Z, Puligujja P, Palandri D, Hilaire J, Arainga M, et al. Optimizing the preparation and stability of decorated antiretroviral drug nanocrystals. Nanomedicine (Lond) 2018; 13:871-85.
168. Rautio J, Kumpulainen H, Heimbach T, Oliyai R, Oh D, Jarvinen T, et al. Prodrugs: design and clinical applications. Nat Rev Drug Discov 2008; 7:255-70.
169. Rautio J, Meanwell NA, Di L, Hageman MJ. The expanding role of prodrugs in contemporary drug design and development. Nat Rev Drug Discov 2018.
170. Pantaleo G, Graziosi C, Demarest JF, Butini L, Montroni M, Fox CH, et al. HIV infection is active and progressive in lymphoid tissue during the clinically latent stage of disease [see comments]. Nature 1993; 362:355-8.
171. Embretson J, Zupancic M, Ribas JL, Burke A, Racz P, Tenner-Racz K, et al. Massive covert infection of helper T lymphocytes and macrophages by HIV during the incubation period of AIDS [see comments]. Nature 1993; 362:359-62.
172. Arainga M, Edagwa B, Mosley RL, Poluektova LY, Gorantla S, Gendelman HE. A mature macrophage is a principal HIV-1 cellular reservoir in humanized

mice after treatment with long acting antiretroviral therapy. Retrovirology 2017; 14:17.

173. Gnanadhas DP, Dash PK, Sillman B, Bade AN, Lin Z, Palandri DL, et al. Autophagy facilitates macrophage depots of sustained-release nanoformulated antiretroviral drugs. J Clin Invest 2017; 127:857-73.

174. Thomas MB, Gnanadhas DP, Dash PK, Machhi J, Lin Z, McMillan J, et al. Modulating cellular autophagy for controlled antiretroviral drug release. Nanomedicine (Lond) 2018.

175. Nowacek AS, Miller RL, McMillan J, Kanmogne G, Kanmogne M, Mosley RL, et al. NanoART synthesis, characterization, uptake, release and toxicology for human monocyte-macrophage drug delivery. Nanomedicine (Lond) 2009; 4:903-17.

176. Dou H, Destache CJ, Morehead JR, Mosley RL, Boska MD, Kingsley J, et al. Development of a macrophage-based nanoparticle platform for antiretroviral drug delivery. Blood 2006; 108:2827-35.

177. Derdelinckx I, Wainberg MA, Lange JM, Hill A, Halima Y, Boucher CA. Criteria for drugs used in pre-exposure prophylaxis trials against HIV infection. PLoS Med 2006; 3:e454.

178. Naswa S, Marfatia YS. Pre-exposure prophylaxis of HIV. Indian J Sex Transm Dis AIDS 2011; 32:1-8.

179. Gunawardana M, Remedios-Chan M, Miller CS, Fanter R, Yang F, Marzinke MA, et al. Pharmacokinetics of long-acting tenofovir alafenamide (GS-7340) subdermal implant for HIV prophylaxis. Antimicrob Agents Chemother 2015; 59:3913-9.

180. Coates JAV, Cammack N, Jenkinson HJ, Jowett AJ, Jowet MI, Pearson BA, et al. (-)-2'-Deoxy-3'-Thiacytidine Is a Potent, Highly Selective Inhibitor of Human Immunodeficiency Virus Type 1 and Type 2 Replication In Vitro. ANTIMICROBIAL AGENTS AND CHEMOTHERAPY 1992; 36:733-9.

181. Minuesa G, Volk C, Molina-Arcas M, Gorboulev V, Erkizia I, Arndt P, et al. Transport of Lamivudine [(-)- -L-2',3'-Dideoxy-3'-thiacytidine] and High-Affinity Interaction of Nucleoside Reverse Transcriptase Inhibitors with Human Organic Cation Transporters 1, 2, and 3. Journal of Pharmacology and Experimental Therapeutics 2009; 329:252-61.

182. Hart GJ, Orr DC, Penn CR, Figueiredo HT, Gray NM, Boehme RE, et al. Effects of (-)-2'-deoxy-3'-thiacytidine (3TC) 5'-triphosphate on human immunodeficiency virus reverse transcriptase and mammalian DNA polymerases alpha, beta, and gamma. Antimicrobial agents and chemotherapy 1992; 36:1688-94.

183. Zhou Z, Rodman JH, Flynn PM, Robbins BL, Wilcox CK, D'Argenio DZ. Model for intracellular Lamivudine metabolism in peripheral blood mononuclear cells ex vivo and in human immunodeficiency virus type 1-infected adolescents. Antimicrobial agents and chemotherapy 2006; 50:2686-94.

184. Cammack N, Rouse P, Marr CL, Reid PJ, Boehme RE, Coates JA, et al. Cellular metabolism of (-) enantiomeric 2'-deoxy-3'-thiacytidine. Biochemical pharmacology 1992; 43:2059-64.

185. Gunthard HF, Saag MS, Benson CA, del Rio C, Eron JJ, Gallant JE, et al. Antiretroviral Drugs for Treatment and Prevention of HIV Infection in Adults: 2016 Recommendations of the International Antiviral Society-USA Panel. Jama 2016; 316:191-210.

186. Agarwal HK, Chhikara BS, Hanley MJ, Ye G, Doncel GF, Parang K. Synthesis and biological evaluation of fatty acyl ester derivatives of (-)-2′,3′-dideoxy-3′-thiacytidine. Journal of Medicinal Chemistry 2012.

187. Embretson J, Zupancic M, Ribas JL, Burke A, Racz P, Tenner-Racz K, et al. Massive covert infection of helper T lymphocytes and macrophages by HIV during the incubation period of AIDS. Nature 1993; 362:359-62.

188. Chamanza R, Darville N, van Heerden M, De Jonghe S. Comparison of the Local Tolerability to 5 Long-acting Drug Nanosuspensions with Different Stabilizing Excipients, Following a Single Intramuscular Administration in the Rat. Toxicol Pathol 2018; 46:85-100.

189. Xia W, Hilgenbrink AR, Matteson EL, Lockwood MB, Cheng JX, Low PS. A functional folate receptor is induced during macrophage activation and can be used to target drugs to activated macrophages. Blood 2009; 113:438-46.

190. Paulos CM, Turk MJ, Breur GJ, Low PS. Folate receptor-mediated targeting of therapeutic and imaging agents to activated macrophages in rheumatoid arthritis. Adv Drug Deliv Rev 2004; 56:1205-17.

191. Grubb G. Long-acting steroid contraceptive technology. Health Sex 1991; 2:1-5, 7, 16.

192. Nair AB, Jacob S. A simple practice guide for dose conversion between animals and human. J Basic Clin Pharm 2016; 7:27-31.

193. Ghosh AK, Yashchuk S, Mizuno A, Chakraborty N, Agniswamy J, Wang YF, et al. Design of gem-difluoro-bis-tetrahydrofuran as P2 ligand for HIV-1 protease inhibitors to improve brain penetration: synthesis, X-ray studies, and biological evaluation. ChemMedChem 2015; 10:107-15.

194. Yang YY, Meng WD, Qing FL. Synthesis of 2',3'-dideoxy-6',6'-difluorocarbocyclic nucleosides. Org Lett 2004; 6:4257-9.

195. Bahar FG, Ohura K, Ogihara T, Imai T. Species difference of esterase expression and hydrolase activity in plasma. J Pharm Sci 2012; 101:3979-88.

196. Martignoni M, Groothuis GM, de Kanter R. Species differences between mouse, rat, dog, monkey and human CYP-mediated drug metabolism, inhibition and induction. Expert Opin Drug Metab Toxicol 2006; 2:875-94.

197. Zelensky AN, Gready JE. The C-type lectin-like domain superfamily. The FEBS journal 2005; 272:6179-217.

198. Kerrigan AM, Brown GD. C-type lectins and phagocytosis. Immunobiology 2009; 214:562-75.

199. Martinez-Pomares L. The mannose receptor. Journal of leukocyte biology 2012; 92:1177-86.

200. Chen P, Zhang X, Jia L, Prud'homme RK, Szekely Z, Sinko PJ. Optimal structural design of mannosylated nanocarriers for macrophage targeting. Journal of controlled release : official journal of the Controlled Release Society 2014; 194:341-9.

201. Martínez-Avila O, Hijazi K, Marradi M, Clavel C, Campion C, Kelly C, et al. Gold manno-glyconanoparticles: multivalent systems to block HIV-1 gp120 binding to the lectin DC-SIGN. Chemistry (Weinheim an der Bergstrasse, Germany) 2009; 15:9874-88.
202. Stahl P, Schlesinger PH, Sigardson E, Rodman JS, Lee YC. Receptor-mediated pinocytosis of mannose glycoconjugates by macrophages: Characterization and evidence for receptor recycling. Cell 1980; 19:207-15.
203. Zhu L, Chen L, Cao Q-R, Chen D, Cui J. Preparation and evaluation of mannose receptor mediated macrophage targeting delivery system. Journal of controlled release : official journal of the Controlled Release Society 2011; 152 Suppl:e190-1.
204. Vieira ACC, Chaves LL, Pinheiro M, Lima SAC, Ferreira D, Sarmento B, et al. Mannosylated solid lipid nanoparticles for the selective delivery of rifampicin to macrophages. Artif Cells Nanomed Biotechnol 2018; 46:653-63.
205. Rezaei M, Hosseini SN, Khavari-Nejad RA, Najafi F, Mahdavi M. HBs antigen and mannose loading on the surface of iron oxide nanoparticles in order to immuno-targeting: fabrication, characterization, cellular and humoral immunoassay. Artif Cells Nanomed Biotechnol 2019; 47:1543-58.
206. Maretti E, Costantino L, Rustichelli C, Leo E, Croce MA, Buttini F, et al. Surface engineering of Solid Lipid Nanoparticle assemblies by methyl alpha-d-mannopyranoside for the active targeting to macrophages in anti-tuberculosis inhalation therapy. Int J Pharm 2017; 528:440-51.
207. Hasegawa U, Inubushi R, Uyama H, Uematsu T, Kuwabata S, van der Vlies AJ. Mannose-displaying fluorescent framboidal nanoparticles containing phenylboronic acid groups as a potential drug carrier for macrophage targeting. Colloids Surf B Biointerfaces 2015; 136:1174-81.
208. Oh B, Lee CH. Development of Man-rGO for Targeted Eradication of Macrophage Ablation. Mol Pharm 2015; 12:3226-36.
209. Tiwari S, Chaturvedi AP, Tripathi YB, Mishra B. Macrophage-specific targeting of isoniazid through mannosylated gelatin microspheres. AAPS PharmSciTech 2011; 12:900-8.
210. Irache JM, Salman HH, Gamazo C, Espuelas S. Mannose-targeted systems for the delivery of therapeutics. Expert Opin Drug Deliv 2008; 5:703-24.
211. Chono S. [Development of drug delivery systems for targeting to macrophages]. Yakugaku Zasshi 2007; 127:1419-30.
212. Schlesinger LS. Macrophage phagocytosis of virulent but not attenuated strains of Mycobacterium tuberculosis is mediated by mannose receptors in addition to complement receptors. Journal of immunology (Baltimore, Md. : 1950) 1993; 150:2920-30.
213. Maretti E, Costantino L, Buttini F, Rustichelli C, Leo E, Truzzi E, et al. Newly synthesized surfactants for surface mannosylation of respirable SLN assemblies to target macrophages in tuberculosis therapy. Drug Deliv Transl Res 2019; 9:298-310.
214. Yeeprae W, Kawakami S, Yamashita F, Hashida M. Effect of mannose density on mannose receptor-mediated cellular uptake of mannosylated O/W

emulsions by macrophages. Journal of controlled release : official journal of the Controlled Release Society 2006; 114:193-201.

215. Asthana S, Gupta PK, Jaiswal AK, Dube A, Chourasia MK. Overexpressed Macrophage Mannose Receptor Targeted Nanocapsules- Mediated Cargo Delivery Approach for Eradication of Resident Parasite: In Vitro and In Vivo Studies. Pharmaceutical research 2015; 32:2663-77.

216. Esfandiari F, Motazedian MH, Asgari Q, Morowvat MH, Molaei M, Heli H. Paromomycin-loaded mannosylated chitosan nanoparticles: Synthesis, characterization and targeted drug delivery against leishmaniasis. Acta Trop 2019:105072.

217. Gliddon DR, Hope JC, Brooke GP, Howard CJ. DEC-205 expression on migrating dendritic cells in afferent lymph. Immunology 2004; 111:262-72.

218. Saluja SS, Hanlon DJ, Sharp FA, Hong E, Khalil D, Robinson E, et al. Targeting human dendritic cells via DEC-205 using PLGA nanoparticles leads to enhanced cross-presentation of a melanoma-associated antigen. International journal of nanomedicine 2014; 9:5231-46.

219. Tan MC, Mommaas AM, Drijfhout JW, Jordens R, Onderwater JJ, Verwoerd D, et al. Mannose receptor-mediated uptake of antigens strongly enhances HLA class II-restricted antigen presentation by cultured dendritic cells. European journal of immunology 1997; 27:2426-35.

220. Kong N, Zhou J, Park J, Xie S, Ramström O, Yan M. Quantitative Fluorine NMR To Determine Carbohydrate Density on Glyconanomaterials Synthesized from Perfluorophenyl Azide-Functionalized Silica Nanoparticles by Click Reaction. 2015.

221. Dutta T, Jain NK. Targeting potential and anti-HIV activity of lamivudine loaded mannosylated poly (propyleneimine) dendrimer. Biochim Biophys Acta 2007; 1770:681-6.